Voraussetzungen für die Bildung von Skarnen im Erzgebirge und deren Metallogenese mit Schwerpunkt auf der Vererzung des Geyer-Reviers

Dissertation
der Mathematisch-Naturwissenschaftlichen Fakultät
der Eberhard Karls Universität Tübingen
zur Erlangung des Grades eines
Doktors der Naturwissenschaften
(Dr. rer. nat.)

vorgelegt von
MSc Nicolas Meyer
aus Ilmenau

Tübingen
2025

Gedruckt mit Genehmigung der Mathematisch-Naturwissenschaftlichen Fakultät der Eberhard Karls Universität Tübingen.

Tag der mündlichen Qualifikation:	19.05.2025
Dekan:	Prof. Dr. Thilo Stehle
1. Berichterstatter/-in:	Prof. Dr. Gregor Markl
2. Berichterstatter/-in:	Prof. Dr. Jochen Kolb

Inhalt

Danksagung

Allen voran danke ich Prof. Dr. Gregor Markl für die Vergabe des Promotionsthemas, das damit verbundene Vertrauen und die finanzielle Unterstützung. Besonderer Dank gilt ihm auch für die hilfreichen Ideen, Anregungen und Kommentare, deren Umsetzungen in den Publikationen wiederzufinden sind, sowie die zahlreichen produktiven Diskussionen, vor allem in Hinblick auf die Gliederung widerspenstiger Textabschnitte der Manuskripte. Außerdem möchte ich ihm meinen Respekt für das effektive und schnelle Bearbeiten und Korrigieren von Texten oder Revisionen sowie die pragmatische Handhabung bei Meinungsverschiedenheiten zwischen Koautoren zollen.
Großer Dank gilt auch Prof. Dr. Mathias Burisch für die intensive Betreuung während der gesamten Promotionszeit. Er hat es ermöglicht, dass diese Arbeit als Alternative zu dem nicht durchführbaren, ursprünglichen Projekt zustande kam. Außerdem hat er unermüdlich Probenmaterial zusammengetragen sowie die Beprobung des nicht-öffentlichen Teils der Lagerstätte Ehrenfriedersdorf arrangiert. Insbesondere sein Wissen zu Skarnen und zum Erzgebirge sowie die kritische Begutachtung der Entwürfe meiner Manuskripte und die zahllosen hilfreichen Hinweise und Denkanstöße haben einen bedeutsamen Anteil an dieser Arbeit.
Prof. Dr. Gutzmer sei an dieser Stelle für seine kompetente Beratung und zielstrebige Überarbeitung der Manuskripte gedankt. Seine Konzeptionen sind bedeutender Bestandteil der Veröffentlichungen. Außerdem ermöglichte auch er die Probenahme an den Kernen und übernahm finanziell die Präparation eines großen Teils der Dünnschliffe dieser Arbeit.
Des Weiteren danke ich Prof. Dr. Jochen Kolb herzlich dafür, dass er sich bereit erklärt hat, die Arbeit als externer Gutachter zu bewerten.
Darüber hinaus bedanke ich mich bei Dr. Axel Gerdes, Dr. Joachim Krausen, Dr. Jens Geier, Henning Scheibert und allen bereits genannten Mitautoren für die produktive Zusammenarbeit bei der Präparation der Manuskripte.
PD Dr. Thomas Wenzel und Dr. Sebastian Staude gebührt großer Dank für die Unterstützung an der Mikrosonde. Durch ihre Einweisung und das in mich gesetzte Vertrauen, dieses Gerät selbstständig zu bedienen, habe ich mein jetziges Wissen über Elektronenstrahlmikroanalytik erworben.
Bei PD Dr. Michael Marks möchte ich mich für die hilfreichen und motivierenden Gespräche bedanken.
Weiterhin bedanke ich mich bei Dr. Manuel Scharrer, der mir vor allem in der Anfangsphase der Promotion Wege zu Lösungen aufzeigte und immer ein offenes Ohr für Probleme hatte. Seine unverwüstliche frohe und freundliche Art gepaart mit Zielstrebigkeit und Wissen haben mich tief beeindruckt und in meiner Laufbahn inspiriert. In diesem Zuge möchte ich mich auch bei Dr. Thomas Binder bedanken. Er half mir bei der Auswertung chemischer Daten und korrigierte präzise und detailverliebt die Entwürfe meiner Manuskripte. Auch war er für jede Art von Diskussion bereit und motivierte mich während der Promotion. Besonderer Dank gilt meinen Kollegen und Freunden sowie noch nicht genannten aktuellen und ehemaligen Mitgliedern der Arbeitsgruppe Andreja Ladišić, Fabian Schmitt, Dominic Raisch, Lukas Mössinger, Pascal Löschner, Aylin Polat, PD Dr. Benjamin Walter, Gabriele Stoschek, Dr. Simon Braunger, Dr. Dominik Gudelius und Dr. Johannes Giebel für die vielen Gespräche und Diskussionen – auch abseits der Geologie.
Für das stetige Anspornen, die vorliegende Arbeit zu vollenden, gilt mein herzlicher Dank Sebastian Riekehr, Martin Becke, Sebastian Pahn und Felix Schneider
Weiterhin gebührt meiner gesamten Familie besonders meinen Eltern Ralf Meyer und Solveig Rebel und meinen künftigen Schwiegereltern Werner und Claudia Schlosser besonderer Dank, die mich immer in meinen Entscheidungen unterstützt und mir finanziell unter die Arme griffen.
Zum Ende richte ich meinen allerherzlichsten Dank an meine Verlobte Marie Schlosser. Ohne sie wäre weder diese Arbeit noch meine gesamte wissenschaftliche Laufbahn auf diese Weise möglich gewesen. Für deine immerwährende Unterstützung, Geduld, dein Vermögen, mich wieder auf den richtigen Weg zu führen und deine unglaublich starke Art achte und liebe ich dich.

Zusammenfassung

Skarne kommen in allen Regionen des Erzgebirges vor, wobei sich vererzte Systeme auf die Lagerstättenreviere von Aue-Schwarzenberg und Geyer-Ehrenfriedersdorf konzentrieren, jedoch auch isoliert bei Oelsnitz, Berggießhübel oder Zobes vorkommen. Die niedriggradigen, aber großvolumigen Skarne im Erzgebirge stellen eine noch wenig erschlossene Rohstoffquelle für Zinn, Wolfram, Indium und andere kritische Elemente innerhalb der Europäischen Union dar. Anatomie, Mineralogie und Metallogenie der Skarne sind von einer Vielzahl von Faktoren abhängig. Ein wesentliches Kriterium sind die Ausgangsgesteine, die im Erzgebirge einen unterschiedlichen Grad der Metamorphose erfahren haben. In Kalzitischen Marmoren tritt eine umfangreiche Verskarnung auf, bei welcher eine Abfolge von proximalem Granat über intermediären Pyroxen zu distalem Wollastonit ausgebildet ist. magnesiumreiche Paragenesen sind mit Dolomitmarmor assoziiert, in welchem sich bevorzugt magnetitreiche Zonen entwickelten. Komplex aufgebaute Skarne sind an basische Vulkanite, mergelige Metasedimentite und Wechsellagerungen zwischen karbonatischen und silikatischen Edukten gebunden. Die Bildungstiefe der Verskarnung hat Auswirkungen auf die Größe der Systeme: In sprödhaften Zonen kann die Porosität und Permeabilität eines Gesteins größer sein als in duktilen Bereichen, was direkten Einfluss auf die Fluidzirkulation und die Ausdehnung der Reaktionsfront hat. Dies führt zu gesteins- und fluidgepufferten Entstehungsbedingungen, die wiederum Mineralogie und Mineralchemie bedingen. Eine große Bedeutung hat auch das Vorhandensein von Wegsamkeiten für Fluide. Besonders die Präsenz überregionaler Störungen kann die Größe und die Mehrphasigkeit eines Systems beeinflussen. Jedoch sind auch kleinere Störungen im Zuge der retrograden Alteration wichtig, die es ermöglichen, dass Fluide trotz geschlossenen Porenraums weiterhin mit dem umgebenden Gestein reagieren können. Ein weiterer struktureller Faktor ist die Morphologie der Intrusionen, die für die Verskarnung verantwortlich sind. Vererzte Skarne sind an Granithochlagen gebunden oder kommen in einer gewissen Distanz zu der Intrusion vor. Alle derzeit bekannten wirtschaftlich relevanten Skarne im Erzgebirge stehen mit post-kollisionalem Magmatismus im Nachgang der variszischen Orogenese in Zusammenhang. Dieser wird durch S- und A-Typ-Granite geprägt, die unter anderem anhand ihres Fluor- und Phosphorgehalts unterschieden werden. Wolframhaltige Skarne treten sowohl in der

Nähe von Graniten mit niedrigem als auch mit hohem Fluorgehalt auf, während Zinn vor allem mit fluorreichen, leukokraten Graniten assoziiert ist. Zwei Perioden magmatischer Aktivität nach der variszischen Orogenese sind im Erzgebirge dokumentiert. Eine erste Phase brachte die großvolumigen Batholithe hervor (spätvariszisch), die nachträglich von kleinräumigeren Granitstöcken abgelöst wurden (postvariszisch). Simultan zu diesen magmatischen Zyklen entstanden auch die mehrphasigen Skarnsysteme. Geochronologische Daten zur Zinnmineralisation zeigen, dass die jüngste Phase des Magmatismus die produktivsten Erzkörper hervorbrachte. Obwohl die dominierenden Wertmetalle in einzelnen Systemen variieren, können sie im Wesentlichen als Wolfram- (Zobes), Wolfram-Zinn- (Globenstein), Zinn- (Ehrenfriedersdorf), Zinn-Zink- (Geyer) und Zink-Zinn-Skarne (Waschleithe) klassifiziert werden.
Das Revier von Geyer ist eine Blaupause für viele dieser Erkenntnisse. Hier zeigt sich die Ausbildung einer skarnoiden Alteration um 325 Millionen Jahre im Zusammenhang mit der Intrusion des Ehrenfriedersdorf-Plutons. Diese Phase weist weder eigenständige Zinnminerale auf, noch sind die Kalksilikatminerale an Zinn oder anderen Wertelementen angereichert. Die Verskarnung fand bei circa 450 °C in einer kontaktmetamorphen, gesteinsgepufferten Umgebung statt. Elemente wurden dabei hauptsächlich von Porenfluiden transportiert und die chemische Signatur der Skarnminerale vom Ausgangsgestein diktiert. Die nachfolgende metasomatische Verskarnung, die etwa 15–20 Millionen Jahre später erfolgte, umfasst eine pro- und eine retrograde Phase jeweils mit signifikanter Zinnvererzung. In der frühen Phase, die bei Temperaturen von circa 350 °C ablief, oszillierten fluid- und gesteinsgepufferte Bedingungen. In einer fluidreichen Umgebung bauen Kalksilikatminerale Elemente nicht gemäß ihres mineralspezifischen Verteilungskoeffizienten ein, sondern übernehmen die Signatur des Fluids. Dieses weist auch Charakteristika einer Phasenseparation auf. In der retrograden Phase werden zinnhaltige von nominell zinnfreien Mineralen verdrängt, was zu einer Freisetzung des Zinns und anschließenden Ausfällung von Kassiterit führt. Diese skarngebundene Zinnvererzung erfolgte gleichzeitig mit Greisenbildung im nahegelegenen Geyersberg sowie in den die Metasedimentite durchschneidenden Gängen, die beide Kassiteritführend sind. Somit ist die Zinnvererzung im Revier Geyer auf ein magmatisch-hydrothermales Event zurückzuführen.

Abstract

Skarns in the Erzgebirge are widespread, with mineralized systems concentrated in the districts of Aue-Schwarzenberg and Geyer-Ehrenfriedersdorf, but also present as isolated occurrences such as Oelsnitz, Berggießhübel, and Zobes. As low-grade but high-tonnage resources, these skarns represent an underexplored source of tin, tungsten, indium, and other critical elements within the European Union. Anatomy, mineralogy, and metallogeny of these skarns are governed by a variety of factors. One fundamental criterion is the nature of the protoliths, which underwent varying degrees of metamorphism in the Erzgebirge. Extensive skarn formation occurs in calcitic marbles, where a sequential transition from proximal garnet to intermediate pyroxene and distal wollastonite is observed. Magnesium-rich parageneses are associated with dolomitic marbles, preferentially hosting magnetite-rich zones. More complex skarns are linked to mafic volcanic rocks, marly metasediments, and alternating sequences of carbonate and silicate lithologies.

The depth of skarn formation has a direct impact on the size of these systems: in brittle domains, rock porosity and permeability can be increased compared to ductile environments, directly influencing fluid circulation and the extent of the reaction front. This results in both rock-buffered and fluid-buffered formation conditions, which in turn affect mineralogy and mineral chemistry. A similar interrelation concerns the presence of fluid pathways. In particular, large-scale regional faults can influence the size and multiphase nature of a system. However, smaller faults play a crucial role during retrograde alteration, allowing continuous interaction between fluids and host rock despite limited pore volume. Another controlling structural factor is the topography of the causative intrusions. Mineralized skarns are associated with granite highs or occur at a certain distance from the intrusion. All currently known economically significant skarns in the Erzgebirge are linked to magmatism following the Variscan orogeny. These intrusions are S- and A-type peraluminous granites, distinguished by their fluorine and phosphorus content as well as the presence of lithium-bearing micas. Tungsten-bearing skarns occur in association with both low- and high-fluorine granites, whereas tin mineralization is predominantly linked to highly evolved leucocratic granites.

Two cycles of post-Variscan magmatic activity are documented in the Erzgebirge. The first phase generated large-volume batholiths, which were subsequently intruded by smaller granite stocks. Simultaneously, multiphase skarn systems developed in

response to these magmatic cycles. Geochronological data on tin mineralization indicates that the youngest phase of magmatism generated the most productive ore bodies. While the dominant economic metals vary among individual systems, they can generally be classified as tungsten skarns (Zobes), tungsten-tin skarns (Globenstein), tin skarns (Ehrenfriedersdorf), tin-zinc skarns (Geyer), and zinc-tin skarns (Waschleithe).

The Geyer district serves as a case study for many of the interpretations. A skarnoid alteration phase developed around 325 Ma ago in connection with the intrusion of the Ehrenfriedersdorf pluton. In this phase, neither discrete tin minerals were formed, nor were the calc-silicate minerals enriched with tin or other critical elements. The skarn formation occurred at approximately 450 °C under contact metamorphic, rock-buffered conditions, element transport being primarily controlled by pore fluids. The geochemical signature of skarn minerals is dictated by the composition of the precursor rocks.

The subsequent metasomatic phase, which occurred approximately 15–20 Ma later, exhibited both a prograde and retrograde stage, both characterized by significant tin mineralization. In the early phase at around 350 °C, alternating fluid- and rock-buffered conditions influenced the mineral chemistry. Under fluid-rich conditions, calc-silicate minerals did not incorporate elements according to their partition coefficients but rather reflected the composition of the hydrothermal fluid, which also exhibited characteristics indicative of phase separation. During the retrograde phase, tin-bearing minerals replaced nominally tin-free phases due to the cooling of the system and the ingress of meteoric water, resulting in the release of tin and the additional precipitation of cassiterite. This skarn-hosted tin mineralization occurred simultaneously with greisen alteration at the nearby Geyersberg as well as in pneumatolytic veins cutting through the surrounding metasediments. Therefore, the tin mineralization in the Geyer district can be attributed to one single magmatic-hydrothermal event.

Liste der Publikationen der Dissertation

Die vorgelegte Dissertation befasst sich mit folgenden Publikationen. Die Tabellen dokumentieren die Anteile der Autoren an der jeweiligen Arbeit.

Arbeit 1

Meyer N, Markl G, Gerdes A, Gutzmer J, Burisch M (2024) Timing and origin of skarn-, greisen-, and vein-hosted tin mineralization at Geyer, Erzgebirge (Germany). Miner Deposita, *59*(1), 1–22. https://doi.org/10.1007/s00126-023-01194-8
Status: akzeptiert und veröffentlicht

Autor	*Wissenschaftliche Konzeption [%]*	*Datengenerierung [%]*	*Analyse und Interpretation [%]*	*Verfassen des Textes [%]*
Meyer, N.	30	65	50	60
Markl, G.	20	0	10	10
Gerdes, A.	0	15	0	0
Gutzmer, J.	20	0	10	10
Burisch, M.	30	20	30	20

Arbeit 2

Meyer N, Burisch M, Gutzmer J, Krause J, Scheibert H, Markl G (2025) Mineral chemistry of the Geyer SW tin skarn deposit: understanding variable fluid/rock ratios and metal fluxes. Miner Deposita 60, 85–111. https://doi.org/10.1007/s00126-024-01297-w
Status: akzeptiert und veröffentlicht

Autor	*Wissenschaftliche Konzeption [%]*	*Datengenerierung [%]*	*Analyse und Interpretation [%]*	*Verfassen des Textes [%]*
Meyer, N.	55	80	65	70
Burisch, M.	15	0	10	10
Gutzmer, J.	10	0	10	10
Krause, J.	0	10	0	0
Scheibert, H.	0	10	0	0
Markl, G.	20	0	15	10

Arbeit 3

Meyer N, Burisch M, Gutzmer J, Geier J, Gerdes A, Markl G (submitted) W-Sn-Zn±In skarn deposits in the Erzgebirge/Krušné hory metallogenic province (Germany and Czech Republic).

Status: eingereicht

Autor	*Wissenschaftliche Konzeption [%]*	*Datengenerierung [%]*	*Analyse und Interpretation [%]*	*Verfassen des Textes [%]*
Meyer, N.	60	80	60	60
Burisch, M.	15	5	20	20
Gutzmer, J.	15	0	10	10
Geier, J.	0	10	0	0
Gerdes, A.	0	5	0	0
Markl, G.	10	0	10	10

1. Einleitung

Das Erzgebirge (tschechisch: Krušné hory) bildet eine natürliche Grenze zwischen der Tschechischen Republik und Deutschland und ist bereits seit der Bronzezeit Ziel von Bergbautätigkeiten (Tolksdorf et al. 2020). Bis ins Mittelalter stellten Eisen, Zinn und später maßgeblich Silber wichtige Güter dar, die zum Reichtum des Erzgebirges beitrugen. Heutzutage ist Zinn nach wie vor ein wichtiger Rohstoff, jedoch stehen zudem weitere strategisch wichtige und kritische Elemente wie Wolfram, Indium und Lithium im Fokus von Exploration und Bergbau.

Diese wichtigen Metalle sind beispielsweise in den Skarn-Lagerstätten des Erzgebirges anzutreffen. Tatsächlich beherbergen die derzeit bekannten dortigen Skarne eines der größten Vorkommen von Zinn, Wolfram und Indium (sowie Zink, Eisen und Fluorit) in der Europäischen Union. Elsner (2014) berichtete beispielsweise von geschätzten Ressourcen von 337 kt Zinn, 344 kt Zink, 44,5 kt Wolfram und 1,2 kt Indium in den Skarnen des deutschen Teils des Erzgebirges. Trotz abbauwürdiger Metallgehalte (Elsner 2014) wurden die Skarne aufgrund ihrer komplexen und feinkörnigen Verwachsung (Hösel et al. 1996; 2003; Kern et al. 2019; Schuppan und Hiller 2012) nie im industriellen Maßstab abgebaut. Jüngste Pilotversuche haben jedoch eine erfolgreiche Aufbereitung demonstriert, was zu einem Wiederaufleben von Exploration und Forschung zur Vererzungen in Skarnen des Erzgebirges geführt hat (Saxore GmbH 2019). Dabei sind nicht alle Teile der Skarnsysteme von gleichem ökonomischem Wert, da auch vollkommen taube Abschnitte auftreten. Außerdem wurde in der Vergangenheit gezeigt, dass bereits frühgebildete Kalksilikatminerale Zinn enthalten können, was jedoch in nachfolgenden Aufbereitungsprozessen nicht ausbringbar ist (Einaudi et al. 1981; Kwak 1987; Meinert 1995). Weitaus aussichtsreicher sind späte Skarnparagenesen, da dort beispielsweise Zinn in Form von Kassiterit vorkommt, welcher wirtschaftlich gewinnbar ist (Bauer et al. 2019; Kern et al. 2019). Um die ergiebigen Bereiche eines Systems zu finden, müssen Explorationsvektoren auf mehreren Skalen definiert werden. Dabei helfen regionale Arbeiten, um allgemeine Voraussetzungen zu etablieren, sowie Detailstudien einzelner Vorkommen, um die Prozesse und Interaktionen während der Verskarnung zu verstehen.

Detaillierte Forschung zu Skarnen begann im Zusammenhang mit den Zinn-, Wolfram-, und Uran-Erkundungsprogrammen der Nachkriegszeit in der ehemaligen Deutschen Demokratischen Republik (DDR) und in der Tschechoslowakei. Diese

brachten umfangreiche Erkenntnisse zu Mineralogie und Geometrie skarngebundener Mineralisationen (Bolduan 1963; Hoth und Lorenz 1966; Kühne et al. 1972; Legler 1985; Legler und Baumann 1983; Makarevič et al. 1976; Pfeiffer und Schützel 1969; Štemprok 1967). Jedoch sind diese Arbeiten meistens beschreibender Natur und liefern nur begrenzte Informationen zur Genese der Skarne. Der Forschungsreichtum dieser Ära wurde in mehreren Monografien festgehalten, die einen Überblick über die Lagerstätten im Erzgebirge geben (Hiller und Schuppan 2008; 2016; Hösel 1994; Hösel et al. 1996; Schuppan und Hiller 2012).
Das wirtschaftliche und wissenschaftliche Interesse an Skarn-Mineralisationen des Erzgebirges ließ nach dem Zusammenbruch der Bergbauindustrie im Jahr 1990 abrupt nach, erlebte jedoch in den letzten 15 Jahren ein Wiederaufleben, angeregt durch erneute Explorationsaktivitäten. Neuere Untersuchungen zu den Skarnen im Erzgebirge konzentrierten sich auf die Petrologie und Mineralchemie (Bauer et al. 2019; Brosig et al. 2020; Kern et al. 2019; Lefebvre et al. 2019; Meyer et al. 2024; 2025; Reinhardt et al. 2021), die Geochronologie von Granat und Kassiterit in Verbindung mit Skarnen (Burisch et al. 2019; Meyer et al. 2024; Reinhardt et al. 2022) sowie auf die Mikrothermometrie (Korges et al. 2020; Meyer et al. 2024; Reinhardt et al. 2021).
Obwohl die meisten dieser jüngeren Studien Einblicke in die Zusammensetzung, Bildungsbedingungen und Metallgehalte der Skarne im Erzgebirge lieferten, konzentrierten sie sich in der Regel auf eine oder wenige Vorkommen. Angesichts der Fülle dieser historischen und aktuellen Daten lassen sich allgemeine Voraussetzungen für Skarnbildung im Erzgebirge ableiten sowie die Bedingungen, die zu einer signifikanten Vererzung von Skarnen führten, destillieren.

1.1 Modelle für die Skarnbildung

Skarne sind global auftretende Gesteinstypen, die in zahlreichen geologischen Umgebungen fast jeden Alters vorkommen (Einaudi et al. 1981). Sie bilden weltweit wichtige Lagerstätten, in denen Kupfer, Eisen, Wolfram, Molybdän, Gold und andere Wertelemente und Rohstoffe gefördert werden (Meinert et al. 2005). Die Mineralogie von Skarnen wird in der Regel von Kalksilikatmineralen wie solchen der Granat- und Pyroxengruppe dominiert. Obwohl die meisten Skarne in karbonatführenden Lithologien vorkommen, können sie sich in nahezu jedem Gesteinstyp bilden, darunter

Pelite, Sandsteine, Granite oder Basalte (Meinert et al. 2005). Sie können während einer Regional- oder Kontaktmetamorphose sowie durch eine Vielzahl von metasomatischen Prozessen entstehen, bei denen Fluide magmatischen, metamorphen, meteorischen und/oder marinen Ursprungs beteiligt sein können (Meinert et al. 2005). Mineralisierte Skarne stehen jedoch meist im Zusammenhang mit der Intrusion magmatischer Körper oder mit weitreichender Fluidzirkulation entlang von Störungen oder Scherzonen und sind an das Vorhandensein von karbonatischen Lithologien gebunden (Einaudi et al. 1981). Ist das Ausgangsgestein hauptsächlich dolomitisch, spricht man von Magnesia-Skarnen, bei kalzitischem Edukt von Kalk-Skarnen (Meinert et al. 2005). Eine weitere Einteilung beispielsweise als Wolfram-, Zinn- oder Blei-Zink-Skarn erfolgt nach den vorherrschenden Wertelementen (Einaudi et al. 1981; Meinert 1992). Zudem werden Skarne entsprechend ihrer räumlichen Position in Bezug auf Intrusion und Umgebungsgestein klassifiziert: Endoskarne kommen innerhalb des ursächlichen magmatischen Körpers vor, während Exoskarne im Umgebungsgestein auftreten (Kwak 1987; Meinert 1992).

Genetisch betrachtet gehen drei Haupttypen aus Verskarnungen hervor: Reaktionsskarne, Skarnoide und metasomatische Skarne. Reaktionsskarne entstehen in chemisch kontrastierenden Lithologien, zum Beispiel am Kontakt zwischen karbonatischen und pelitischen Gesteinen aufgrund von Temperaturerhöhung und damit erhöhten Diffusionsraten von Elementen (Meinert et al. 2005). Skarnoide bilden das genetische Bindeglied zwischen Reaktionsskarnen und metasomatischen Skarnen, gekennzeichnet durch eine Erhaltung der texturellen Merkmale der (meta-)sedimentären Protolithe. Skarnoide, zum Teil auch bimetasomatische Skarne genannt (Kwak 1987), entstehen durch Austauschreaktionen auf lokaler Ebene zwischen chemisch kontrastierenden Lithologien und der zusätzlichen Zufuhr externer (hydrothermaler) Fluide während der (kontakt)metamorphen Überprägung des Umgebungsgesteins in Folge einer Intrusion (Meinert et al. 2005). Daher wird die chemische Zusammensetzung von Skarnoiden hauptsächlich durch die Signatur des Wirtsgesteins bestimmt („gesteinsgepuffert“), obwohl externe Komponenten lokal in höheren Mengen vorhanden sein können (Jamtveit und Hervig 1994). Eine ausgeprägte retrograde Überprägung der prograden Skarnoide ist nur in Ausnahmen der Fall (Kwak 1987).

In einer fluidgepufferten Umgebung führt der großräumige Austausch von Elementen durch zirkulierende Fluide zur Bildung von metasomatischen Skarnen, bei denen die

Fluidzusammensetzung sowohl die resultierende Paragenese als auch die Mineralchemie der Skarn- und Erzminerale bestimmt (Einaudi et al. 1981; Jamtveit et al. 1993; Meinert 1992). Texturelle und strukturelle Merkmale der Protolithe werden durch die metasomatische Verskarnung weitestgehend überprägt. Die prograde Phase metasomatischer Skarne ist durch überwiegend wasserfreie Kalksilikatminerale gekennzeichnet, die eine typische Zonierung von Granat > Klinopyroxen nahe der Fluidquelle über Klinopyroxen > Granat im intermediären Bereich bis zu wollastonitreichen Paragenesen an der Reaktionsfront zu den Karbonaten ausbilden (Meinert et al. 2005). Während der retrograden Phase überwiegen wasserhaltige Minerale wie Epidot oder Amphibol, die bisher unverändertes Umgebungsgestein sowie die prograden Skarne entlang von fokussierten Wegsamkeiten überprägen können (Einaudi et al. 1981). Der Großteil der Erzminerale fällt typischerweise während dieser Phase aus (Kwak 1987). Das Erzgebirge beherbergt eine Vielzahl von Skarnsystemen, welche verschiedene Stadien der Alteration sowie Unterschiede im Metallinventar aufweisen, was es zu einem der vielfältigsten Untersuchungsgebiete hinsichtlich der petrogenetischen Prozesse während der Skarnbildung macht.

1.2 Geologie des Erzgebirges

Das Erzgebirge bildet den nördlichen Teil des Böhmischen Massivs und gehört innerhalb des variszischen Orogens zum Saxothuringikum (Kossmat 1927). Es bildet ein etwa 140 km × 80 km großes Erosionsfenster, welches im Südosten durch den Eger-Graben, im Nordosten durch das Elbe-Lineament und im Nordwesten durch das Zentralsächsische Lineament begrenzt wird und graduell in das Fichtelgebirge im Südwesten übergeht (Franke and Żelaźniewicz 2023; Pälchen und Walter 2011).
Im Wesentlichen ist das Erzgebirge aus einer Abfolge metamorpher Decken aufgebaut, deren Ausgangsgesteine heterogene vulkanosedimentäre Abfolgen des Neoproterozoikums darstellen, die aus Grauwacken, Konglomeraten, Sandsteinen, Tonsteinen, Mergeln und Karbonatgesteinen sowie untergeordnet vulkanischen Gesteinen mit mafischer bis felsischer Zusammensetzung bestehen (Ondrus et al. 2003; Tichomirowa et al. 2012). Während der variszischen Orogenese wurden diese Gesteinseinheiten in unterschiedlichem Maße deformiert und metamorph überprägt. Die Metamorphose erreichte vor etwa 340 Millionen Jahren ihren Höhepunkt, gefolgt von einer rapiden Exhumierung des metamorphen Deckenstapels auf mittel- bis oberkrustale Niveaus (Kröner und Willner 1998). Während und nach diesem Prozess

kam es vor 330–310 Millionen Jahren zu spätvariszischem, diskontinuierlichem postkinematischem Magmatismus (Romer et al. 2007; Tichomirowa et al. 2019; 2022). Dieser wurde von einem postvarizischen felsischen Magmatismus abgelöst, von dem heute vulkanische, subvulkanische und nur vereinzelt plutonische Gesteine aufgeschlossen sind. Diese Serie magmatischer Gesteine entstand zwischen 306 und 303 Millionen Jahren im westlichen und zwischen 301 und 296 Millionen Jahren im östlichen Teil des Erzgebirges (Tichomirowa et al. 2025). Diese permokarbonische Phase erhöhter magmatischer Aktivität ist mit greisen-, trum- und ganggebundenen Mineralisierungen (Leopardi et al. 2024a; Štemprok, 1967), Skarnen (Meyer et al. 2024; Reinhardt et al. 2022) sowie epithermalen Gangsystemen verbunden (Swinkels et al. 2021).

Der variszischen Orogenese folgend überwog bis zur Oberkreide Extensionstektonik, die zur Einsenkung epikontinentaler Becken führte. Mächtige Abfolgen von Sedimentgesteinen überdeckten in der Folge das metamorphe und magmatische Grundgebirge des Erzgebirges (Ziegler 1990). Während dieser Phase bildeten sich niedrigtemperierte hydrothermale Uran-, Bismut-, Kobalt-, und Silbervererzungen sowie Fluorit-Baryt-Mineralisierungen (Burisch et al. 2022; Romer und Cuney 2018). Schließlich führte die alpidische Tektonik zur Entstehung lokaler Rift-Systeme und Grabenstrukturen wie dem Eger-Graben, und die Gesteinseinheiten des Erzgebirges wurden exhumiert (Ziegler und Dèzes 2007). Diese Hebung wurde von alkalischem Vulkanismus begleitet, insbesondere innerhalb des Eger-Grabens und entlang der südlichen Grenze des Erzgebirges (Ulrych et al. 2011). Quarz-Eisen-Mangan-Gänge mit hohen Konzentrationen an Kobalt, Nickel und Lithium sind mit diesem geodynamischen Kontext assoziiert (Burisch et al. 2021) und stellen den jüngsten Mineralisierungszyklus im Erzgebirge dar.

1.3 Skarne des Erzgebirges

Skarne im Erzgebirge treten bevorzugt in metasedimentären Gesteinseinheiten auf und lassen sich genetisch in zwei Gruppen einteilen. Zum einen werden Skarne und Skarnoide zusammengefasst, die nicht mit Magmatismus assoziiert sind (Burisch et al. 2019; Reinhardt et al. 2022). Im Erzgebirge sind sie weitverbreitet und als „Erlan“ oder „Erlanfels“ bekannt. Diese Skarne waren in der Vergangenheit aufgrund ihres erhöhten Eisengehalts von wirtschaftlichem Interesse (Hoth et al. 2010). Ihre Genese und die Herkunft der hydrothermalen Fluide sind bisher nur unzureichend an wenigen

Vorkommen untersucht (Hiller und Schuppan 2012; Hösel 2003; Meyer et al. 2024; Schuppan und Hiller 2012). Die andere Gruppe umfasst Exoskarne, die direkt mit einer granitischen Intrusion zusammenhängen (Hösel 1994; Schuppan und Hiller 2012; Reinhardt et al. 2022; Weinhold 2002). Endoskarne sind aus keinem der Skarnsysteme bekannt, selbst dort nicht, wo Marmoreinheiten in direktem Kontakt mit granitischen Intrusionen stehen (Hösel et al. 1996; Schuppan and Hiller 2012).

Die östlichsten Skarne des Erzgebirges liegen im Berggießhübel-Gebiet innerhalb der Elbezone. Daran anschließend liegt am nördlichen Rand des Erzgebirges nahe der Gemeinde Großschirma eine 16 km lange und 1 km breite mylonitische Zone („Felsithorizont"), welche skarnartige Alterationen aufweist. Der zentrale Teil des Erzgebirges umfasst das Niederschmiedeberg- und Měděnec-System, in denen Skarne in hochmetamorphen Gneiseinheiten auftreten. Im Gegensatz dazu befinden sich die Skarne des Geyer-Ehrenfriedersdorf-Distrikts des zentralen Erzgebirges in niedrigmetamorphen Glimmerschiefern und Phylliten (Hösel 1994).

Im westlichen Erzgebirge sind die meisten Skarne im Aue-Schwarzenberg-Gebiet konzentriert. Diese treten hier um die Schwarzenberger Gneiskuppel auf und erstrecken sich südwärts bis nach Zlatý Kopec in der Tschechischen Republik. Diese Region beherbergt die ökonomisch interessanteste skarngebundene Mineralisierung, umfasst aber auch zahlreiche kleine und unwirtschaftliche Skarne. Auf der Westseite des Eibenstock-Nejdek-Massivs treten mineralisierte Kalksilikatgesteine im Zobes/Bergen-Gebiet sowie nahe Kraslice und Tisová auf. Im Vogtland sind bedeutende Skarnvorkommen nahe Oelsnitz und Tirpersdorf zu finden.

1.4 Voraussetzungen für Verskarnung und Vererzungen im Erzgebirge

Die Voraussetzungen für die Skarnbildung im Erzgebirge sind in einem Review zusammengefasst (Meyer et al. eingereicht) und werden in den nachfolgenden Abschnitten vorgestellt. Einen globalen Überblick zu Skarnen bieten die Arbeiten von Kwak (1987), Einaudi et al. (1981) und Meinert et al. (2005), deren Ergebnisse sich teilweise mit denen zu Skarnen des Erzgebirges decken. Skarnoide sind dabei in der Literatur uneindeutig und teilweise widersprüchlich definiert. Für das Erzgebirge wurde im Folgenden die Definition von Meinert (1992) und Kwak (1987) angewendet. Demnach weist dieser Gesteinstyp noch teilweise die Textur des Ausgangsgesteins und feinkörnige Verwachsungen auf und wird hauptsächlich von Klinopyroxen aufgebaut. Dieser kann sich mit feinen Bändern granatdominierter Bereiche abwechseln. Des Weiteren fand keine starke retrograde Alteration statt.

1.4.1 Reaktive Gesteine

Im Erzgebirge sind im Wesentlichen kalzitische und/oder dolomitische Marmore, mergelige Schiefer und Metavulkanite einer Verskarnung unterworfen. Marmor-Einheiten sind in den westlichen und zentralen Teilen des Erzgebirges am weitesten verbreitet, insbesondere in den Metasedimentiten der Přísečnice-, Klínovec-, Jáchymov- und Thum-Gruppe (Hösel 1994; 2003; Hösel et al. 1996; Hoth et al. 2010; Schuppan und Hiller 2012). Skarnoide bilden sich hauptsächlich innerhalb von unreinen Marmoren, Mergeln und an den Kontaktbereichen zwischen Marmor und klastischen Sedimentiten. Während alle zinnführenden Skarne diesen Übergang von skarnoiden zu metasomatischen Texturen an lithologischen Kontakten zeigen, gibt es auch Vertreter, bei denen Skarnoide in der gesamten Einheit dominieren (z. B. Zobes; Hiller und Schuppan 2012).

Je nach Zusammensetzung des (oft nicht erhaltenen) Ausgangsgesteins können sich Kalk-Skarne, Magnesia-Skarne oder Mischformen bilden. Forsteritreicher Olivin und Spinell finden sich ausschließlich in den selteneren Magnesia-Skarnen (z. B. Globenstein). Darüber tritt Ludwigit in diesen Lithologien auf, wenn borreiche Fluide in die Verskarnung involviert sind. Ein höherer Dolomitgehalt im Edukt begünstigt offenbar außerdem die Bildung von Magnetit (Burisch et al. 2023; Hösel et al. 2003; Meyer et al. 2024; Schuppan und Hiller 2016).

Kalk-Magnesia-Skarne sind die bedeutendsten Träger der Zinn-Wolfram-Zink-Vererzungen im Erzgebirge (z. B. Geyer, Tellerhäuser, Berggießhübel). Sie zeichnen sich durch Granat und Epidot aus, wobei die Menge an Granat mit steigendem Dolomitanteil im Ausgangsgestein abnimmt. Reine Kalk-Skarne enthalten überwiegend Wollastonit und untergeordnet Vesuvian, welcher mit Scheelit verwachsen sein kann. Häufiger sind mergelige Ausgangsgesteine, die zu Skarnen mit aluminiumreichen Mineralen führen (z. B. Ehrenfriedersdorf). Wenn die primären Karbonate nicht mehr vorhanden sind, erlaubt die beobachtete Mineralparagenese und -chemie der Skarne meist eine Rekonstruktion der Zusammensetzung des Edukts.

1.4.2 Bildungsbedingungen und Fluidmigration während der Verskarnung

In vielen Systemen wird die Durchflussmenge von Fluiden von der Porosität und Permeabilität der Rahmengesteine bestimmt, was direkte Auswirkungen auf die Größe

und Geometrie der metasomatisch überprägten Bereiche hat (Meinert et al. 2005). Initial weisen Marmore eine vernachlässigbare Porosität auf, welche während der prograden Verskarnung durch Mineralreaktionen zunimmt. Durch die erhöhte Porosität kann wiederum eine erhöhte Menge an Fluiden zirkulieren. Der Zufluss neuer Elemente und die metasomatische Reaktion von Mineralen während der folgenden Phasen können die Porosität wieder verringern, da voluminöse, wasserhaltige Mineralphasen gebildet werden. Dies ist vor allem während der retrograden Verskarnung der Fall. Welcher der Prozesse überwiegt, bestimmt den Umfang, in welchen die Marmore metasomatisch umgewandelt werden können (Dipple und Gerdes 1998). Während der retrograden Skarnalteration fallen Erzmineralen typischerweise entlang fokussierter Fluidbahnen wie Störungen und Gängen aus (Hösel et al. 1996; Kern et al. 2019; Korges et al. 2020; Meinert et al. 2005).
In tiefer situierten Systemen und in der Nähe zu Granitkontakten herrschen duktile Bedingungen vor, was die Entstehung wirkungsvoller Fluidwege verhinderte. Dies begünstigte die Bildung von nur selten mineralisierten Skarnoiden. In oberflächennahen Systemen dominiert hingegen spröde Deformation, die einen fokussierten Fluidfluss ermöglicht, welcher mit einer erhöhten Fluidfreisetzung aus dem Pluton einhergehen kann. Alle wirtschaftlich bedeutsamen Skarne des Erzgebirges zeigen Merkmale verstärkter Fluidzirkulation in oberflächennahen Stockwerken (z. B. Hämmerlein, Geyer).

1.4.3 Strukturgeologische Kontrolle

Die hohe Anzahl mineralisierter Skarne im Aue-Schwarzenberg-Gebiet hängt vermutlich mit der überregionalen Gera-Jáchymov-Störungszone und den parallel verlaufenden Verwerfungen zusammen. Diese NW-SE-orientierte Störungszone durchschneidet die metasedimentären Decken des Aue-Schwarzenberg-Gebiets und war prävariszisch (Romer et al. 2010) bis mindestens kretazisch aktiv (Guilcher et al. 2021; 2024). Obwohl detaillierte Untersuchungen fehlen, begünstigte sie wahrscheinlich den Aufstieg von Magmen und Fluiden. Wiederholte Reaktivierungen dieser langlebigen Störungszone könnten die Entstehung der beobachteten mehrphasigen Skarne des Aue-Schwarzenberg-Gebiets verursacht haben.
Ähnlich werden auch andere skarngebundene Vererzungen im Erzgebirge mit Störungszonen unterschiedlicher Ausmaße in Verbindung gebracht, beispielsweise die tiefgreifende Elbe-Störung (Berggießhübel) oder der Mylonithorizont bei

Großschirma (Hösel 1994; Hösel et al. 1997; Kuschka und Hahn 1996; Hiller und Schuppan 2008; Schuppan und Hiller 2012). Interessanterweise scheint die während der variszischen Orogenese aktive (Hösel 1994) Geyer-Schönfeld-Störung mit einem vertikalen Versatz von mindestens 100 m nur wenig Einfluss auf die Skarnbildung und Vererzung in dem Gebiet um Geyer gehabt zu haben.

Die Intrusion der drei Hauptbatholithe des Erzgebirges wurde vermutlich durch tiefreichende, prävariszische Schwäche- oder Störungszonen (ungefähr NW-SE verlaufend) kontrolliert, und auch kleinere Plutone zeigen eine enge räumliche Verbindung zu solchen Bruchzonen (Romer et al. 2010; 2022). In kleinerem Maßstab kontrollierten synplutonische Störungsnetzwerke im Dachbereich und in den umgebenden Wirtsgesteinen der Granite den Fluidfluss und die daraus resultierende Verskarnung (Hösel et al. 2003; Schuppan und Hiller 2012). Die Morphologie der Batholithe einschließlich ihrer Kuppeln könnte ebenfalls die Position und das Ausmaß der Mineralisierung beeinflusst haben. In Geyer-Ehrenfriedersdorf befinden sich alle ehemaligen Lagerstätten und aktuellen Explorationsziele einschließlich der Geyer-Skarne über Granitkuppeln (Brosig et al. 2020). Die hufeisenförmige Anordnung der Lagerstätten in diesem Gebiet folgt der darunterliegenden calderaartigen Morphologie des Granits.

1.4.4 Ursächliche Intrusionen für Skarn- und Erzbildung

Die derzeit ökonomisch relevanten Skarnsysteme sind ausnahmslos mit spät- bis postvariszischem Magmatismus assoziiert (Breiter et al. 1999; Förster et al. 1999; Romer et al. 2007; Tichomirowa et al. 2022). Zinn- und wolframakzentuierte Skarne sind in erster Linie mit peralumischen S- und A-Typ-Graniten verknüpft, die sich durch ihren erhöhten Fluor- und Phosphat-Gehalt sowie das Vorhandensein von lithiumhaltigem Glimmer auszeichnen (Casas-García et al. 2021; Förster et al. 1999). Obwohl Zinn und Wolfram häufig in einem gemeinsamen System vorkommen, sind sie räumlich und paragenetisch überwiegend voneinander getrennt. Wolframhaltige Skarne finden sich dabei sowohl in der Nähe von Graniten mit niedrigem (Zobes) als auch hohem Fluor-Gehalt (Globenstein), während Zinnmineralisationen in erster Linie mit stark entwickelten, leukokraten Graniten verbunden sind, die in hohe Krustenstockwerke intrudiert sind (Geyer, Berggießhübel, Oelsnitz). Zink-dominierte Skarne zeigen keine eindeutige Affinität zu einem bestimmten Granittyp.

Im Allgemeinen wird davon ausgegangen, dass Zinn während intensiver fraktionierter Kristallisation angereichert wird (Lehmann 2021), was durch Krustenverdickung und das Vorhandensein von Flussmitteln (z. B. Wasser, Fluor, Lithium) begünstigt wird. Die tiefkrustalen Protolithe, aus denen die granitischen Schmelzen stammen, könnten vor der Magmenbildung an diesen Komponenten angereichert worden sein (siehe Lehmann 1990; 2021). Im Erzgebirge sind zinnangereicherte Metasedimentite dokumentiert, die metamorphen Kassiterit enthalten (Weber et al. 2023). Ihre Relevanz für den Zinnreichtum des Erzgebirges ist jedoch noch unzureichend geklärt (Breiter 2012; Romer und Kroner 2016). Zumindest in einzelnen Lagerstätten könnte eine lokale Umverteilung aus diesen bereits mit Zinn angereicherten Metasedimentiten stattgefunden haben (Lefebvre et al. 2019), wenngleich die Mehrheit des skarngebundenen Zinns eindeutig durch magmatisch-hydrothermale Fluide zugeführt wurde (Burisch et al. 2019; Korges et al. 2020; Meyer et al. 2024; Reinhardt et al. 2021).

2. Das System Geyer als Fallbeispiel

Das Lagerstättengebiet von Geyer befindet sich im zentralen Teil des Erzgebirges und umfasst auf einer Fläche von etwa 5 km × 4 km historische Bergwerke wie Geyersberg, Kiesgrube und weitere unbedeutendere Abbaue sowie die Explorationsgebiete Geyer SW und Geyer NO (Hösel et al. 1996). Zwischen 1395 und 1913 erfolgte in diesem Gebiet Bergbau auf Zinn und Eisen, später auf Wolfram. Die Pinge (Binge) von Geyersberg zeugt noch heute von der intensiven Zinngewinnung. Nach dem Ende des Zweiten Weltkriegs wurde eine umfangreiche Explorationskampagne von der SDAG Wismut aufgelegt, welche die mineralisierten Skarne im Südwesten des Geyersbergs im Fokus hatte. Daraus resultierte ein Bohrprogramm mit 123 Bohrlöchern und 37 km Bohrkernmaterial (Hösel et al. 1996), was dieses Areal zu einem der bestuntersuchten des Erzgebirges macht. Die in den Jahren 2011 und 2012 vorgenommenen Bestätigungsbohrungen des Explorationsunternehmens Tin International bestätigten die vermuteten 44 kt Zinn, 57 kt Zink sowie 440 t Indium und 353 t Gallium (Elsner 2014; Hösel et al. 1996). Diese Zahlen belegen das erhebliche Potential dieser skarngebundenen Erze. Im Nordosten des Geyersbergs schließt sich das Lagerstättengebiet Ehrenfriedersdorf an, welches bis 1990 in Betrieb war und gang- und greisengebundenen Kassiterit förderte (Hösel 1994). Durch die hervorragende Daten- und Probengrundlage sowie das Vorhandensein unterschiedlicher Vererzungen über alle Entwicklungsstadien hinweg ist dieses Gebiet geeignet, Prozesse während der Genese der Skarne und der Vererzung nachzuvollziehen.

2.1 Geologischer Rahmen des Untersuchungsgebiets

Die geologischen Einheiten des Gebietes um Geyer werden von SW-NO-streichenden und nach Nordwesten einfallenden Schichten aufgebaut. Diese bestehen aus einer Abfolge kambrischer bis ordovizischer Phyllite, Glimmerschiefer und Paragneise der Jáchymov-Gruppe, in welche dolomitische und kalzitische Marmore eingeschaltet sind. In diesen metamorphen Gesteinseinheiten nahmen anschließend während der Hauptphase der variszischen Orogenese Granite Platz, welche das gesamte Gebiet unterlagern (Bolduan 1963; Tischendorf und Förster 1990; Tischendorf et al. 1965). Der Kontakt zwischen Intrusionen und Metasedimentiten verläuft nahezu horizontal in einer Tiefe von etwa 150–450 m, mit Ausnahme der diapierartigen Geyersberg-Intrusion, die in einem markanten Aufschluss im östlichen Teil des Gebiets ansteht. Die Flanken dieses Intrusivkörpers fallen bis in eine Tiefe von 180 m fast vertikal ab, bevor sie merklich abflachen (Hösel et al. 1996). Der Geyersberg selbst besteht im Wesentlichen aus zwei Intrusionstypen. Eine ältere granitische, fein- bis grobkörnige porphyrische Lithologie weist einen hohen Biotit-Anteil auf (Bolduan 1963) und ist nicht mit signifikanter Greisenalteration oder Zinnmineralisierung assoziiert (Hösel et al. 1996). Eine jüngere Intrusion durchschneidet die ältere und wird als äquigranularer, biotitarmer und topashaltiger Granit beschrieben (Bolduan 1963). Diese zweite Intrusion ist durch einen erhöhten Fluor-Gehalt charakterisiert und weist disseminierten Kassiterit sowie lithiumreichen Glimmer auf (Bolduan 1963). Beide Intrusionen wurden im Gebiet der Geyer-SW-Skarne bisher nicht datiert, jedoch weisen die Granite vom Sauberg und den Greifensteinen des benachbarten Ehrenfriedersdorf-Gebiets Intrusionsalter zwischen 324 ± 4 und 319,7 ± 3 Millionen Jahren und zwischen 323,9 ± 3 und 317,3 ± 2 Millionen Jahren auf (Romer et al. 2007). Die Intrusionstiefe wurde mithilfe von Schmelzeinschlüssen auf 2,5 bis 5 km bestimmt (Breiter et al. 1999).

Der Geyersberg mit der dazugehörigen „Binge“ war Hauptgegenstand des historischen Zinnabbaus. Hier war die Vererzung an pervasive Greisenbildung gebunden oder kam in pneumatolytischen Gängen vor (Hösel 1994; Hösel et al. 1996). Der Großteil des heutigen Zinn- (sowie Zink- und Indium-)Budgets bei Geyer SW ist mit Exoskarnen assoziiert, die hauptsächlich Marmor, aber auch mergeligen Glimmerschiefer und Phyllit ersetzen. Die meisten der durch Erkundungsbohrkerne von Geyer SW bekannten Marmoreinheiten sind von Skarnmetasomatose betroffen, wenngleich einige wenige Proben makroskopisch unveränderten Marmor aufweisen (Meyer et al. 2024).

Insgesamt sind drei parallel zur metamorphen Foliation mit einem Winkel von etwa 30–40° nach Nordwesten einfallende Skarneinheiten bekannt (Bolduan 1963; Hösel et al. 1996). Jeder dieser Skarne besteht aus mehreren Skarnlagern, die wahrscheinlich ehemalige Karbonatschichten innerhalb der heutigen Meta-Pelite repräsentieren (Hösel et al. 1996). Die untere Skarneinheit im Nordwesten enthält zwei Skarnlager, die über 3 km Länge verfolgt werden können und bis zum Granitkontakt in der Tiefe reichen, ohne dass Verskarnungen des Granits selbst dokumentiert wurden (Hösel et al. 1996). Das untere, 5–20 m mächtige Lager besteht aus zwei einzelnen Skarnkörpern und einem Erzkörper. Das obere 15–40 m mächtige Lager umfasst mehrere Skarn- und zwei Erzkörper. Die mittlere Skarneinheit hat eine Streichlänge von 1,5 km und keilt über dem Granitkontakt in einer Tiefe von etwa 180 m aus (Hösel et al. 1996). Sie zeichnet sich durch eine konstante Mächtigkeit von etwa 20 m aus und enthält mehrere einzelne Skarnkörper. Der untere Teil der mittleren Skarneinheit beherbergt nur einen Erzkörper.

Die obere Skarneinheit (im Südosten) im Glimmerschiefer kann lateral mehr als 3 km bis zum Granitkontakt verfolgt werden und besteht aus zwei Skarnlagern. Das untere Lager (Gesamtmächtigkeit von 7–25 m) besteht aus drei separaten Skarnkörpern und einem Erzkörper mit einer Mächtigkeit von 1–6 m. Das obere Lager hat eine nahezu konstante Mächtigkeit von 15–20 m mit mehreren lateral ausgerichteten linsenförmigen Skarnkörpern und einem separaten Erzkörper im unteren Teil. Im Distrikt wurden zusätzlich viele kleinere Skarnkörper identifiziert, die typischerweise nur geringe Mächtigkeiten aufweisen und keine signifikante Zinnmineralisierung enthalten. Hohe Gehalte an skarngebundenem, disseminiertem Kassiterit sind teilweise mit magnetitreichen Arealen verknüpft, die vor allem in einer Entfernung von 300–450 m zum Granitkontakt auftreten (Hösel et al. 1996).

2.2 Probenmaterial, Methoden und Zielsetzung

2.2.1 Petrographie, Uran-Blei-Geochronologie und Untersuchungen an Fluideinschlüssen

Sechs durch die SDAG Wismut und Tin International gewonnene Bohrkerne standen für eine Beprobung zur Verfügung. Der Zugang wurde vom Landesamt für Umwelt, Landwirtschaft und Geologie des Freistaates Sachsen gewährt. Um die genetischen Zusammenhänge der Skarnmineralisationen zu untersuchen, wurden 60 Proben mit Längen zwischen 5 und 20 cm aus den Bohrkernen entnommen. Das Hauptziel lag auf der Beprobung möglichst unterschiedlicher sowohl tauber als auch vererzter Mineralparagenesen aus verschiedenen Teufen, welche komplette prograde und retrograde Entwicklung der Skarne abbilden. Von den Bohrkernstücken wurden 84 polierte Dünnschliffe präpariert, die mittels petrographischer Mikroskopie eingehend untersucht wurden. Da Skarne häufig sehr feinkörnige Verwachsungen aufweisen, kam dabei neben Lichtmikroskopie auch Rasterelektronenmikroskopie zur Anwendung. Die Untersuchung von Fluideinschlüssen in Skarnen des Erzgebirges zur Bestimmung von Salinität (Abkühlexperimente) und Homogenisierungstemperaturen (Aufheizexperimente) erfolgte mithilfe 21 doppelseitig polierter neuer Dünnschliffe, womit die bisher unzureichende Datengrundlage deutlich erweitert und verbessert wurde. Damit lassen sich nun Rückschlüsse auf die Fluidcharakteristika sowie die

Bildungsbedingungen während der Evolution der Skarne ziehen. Um vorhandene Altersdaten von Skarnen des Erzgebirges zu ergänzen, präzisieren und evaluieren, wurden Granat in sechs und Kassiterit in drei Proben mittels ortsaufgelöster Massenspektrometrie mit induktiv gekoppeltem Plasma und Laserablation (LA-ICP-MS) basierend auf Uran-Blei-Geochronologie datiert.

2.2.2 Haupt-, Neben-, und Spurenelemente von Skarn- und Erzmineralen

Um die chemischen Veränderungen während der Entwicklung des Skarnsystems nachvollziehen zu können, wurde die Zusammensetzung ausgewählter Minerale in insgesamt 48 Proben mittels Elektronenstrahlmikroanalytik (ESMA) ortsaufgelöst bestimmt. Unter Einbeziehung der petrographischen Beobachtungen und der aus den Fluideinschlüssen abgeleiteten Bildungsbedingungen der Minerale ergibt sich ein umfassendes petrogenetisches Modell. Unterschiede im Spurenelementbudget während der Verskarnung wurden anschließend mithilfe der Ergebnisse aus der LA-ICP-MS herausgearbeitet. Damit kann die Verteilung der Wertelemente innerhalb einer Mineralassoziation und in unterschiedlichen paragenetischen Stadien der Verskarnung nachvollzogen werden. Unter anderem die Identifizierung von Änderungen in der Seltenerdverteilung der Minerale ermöglichte außerdem ein besseres Verständnis interner wie externer Prozessänderungen. Die Quantifizierung des Umfangs und des Verhältnisses gesteins- und fluidgepufferter Mineralreaktionen zeigt, auf welche Weise Anreicherungs- und Verarmungsprozesse beeinflusst werden.

2.3 Ergebnisse und Diskussion

Im nachfolgenden Kapitel werden die Ergebnisse der Untersuchungen des Geyer-Systems zusammengefasst und diskutiert (Meyer et al. 2024; 2025). Auf dieser Basis wird ein widerspruchsfreies genetisches Modell für die Skarn-Lagerstätte abgeleitet, welches eine skarnoide Alterationsphase und eine darauffolgende prograde sowie eine anschließende retrograde metasomatische Überprägung umfasst.

2.3.1 Skarnoide

Die erste Phase der Verskarnung tritt innerhalb metamorpher Mergel sowie an den lithologischen Kontakten zwischen klastischen Metasedimentiten und Marmoren auf. Diese Areale bestehen im Wesentlichen aus feinkörnigem, beigem bis hellgrünem Klinopyroxen zusammen mit hellrotem bis braunem Granat. Letzterer kann lokal eine Größe von mehreren Millimetern erreichen und ist durch eine Sektorzonierung gekennzeichnet. Hellroter, leistenförmiger Vesuvian kommt mit Granat vor und verdrängt diesen zuweilen, meist begleitet von Wollastonit, was sehr feinverwachsene Texturen hervorbringt. An der Reaktionsfront ist Wollastonit das dominante Skarnmineral. Zwischen Metapeliten und Marmor beziehungsweise Mergel tritt fahlgrüner Epidot auf. Idiomorpher Titanit ist regelmäßig in Granat eingeschlossen und bildet sich außerdem als Umwandlungsprodukt von Ilmenit und Rutil (aus dem metasedimentären Protolith). Genuine Zinnminerale oder Buntmetallsulfide sind während dieser Phase abwesend und eine deutliche retrograde Verskarnung ist nicht zu beobachten. Paragenesen, Texturen und Zonierungen definieren diese Gesteine als Skarnoide (Meinert et al. 2005) und die Farbe der Skarnminerale weist auf ein proximales Bildungsmilieu hin (Meinert 1992; Reinhardt et al. 2021).
Minerale dieser ersten Verskarnung sind meist aluminiumreich und besonders Granat und Vesuvian enthalten häufig größere Mengen Fluor. Pyroxen tritt in Form der Diopsid-Hedenbergit-Mischkristallreihe auf, wobei meist das Eisen-Endglied dominant ist. Titanit weist durch die gekoppelte Substitution von Titan und Sauerstoff (Deer et al. 2013) anormale Fluor- und Aluminiumgehalte auf. Die Neben- und Spurenelementanalysen ergaben zudem, dass die Kalksilikatminerale nur geringe Gehalte an Zinn und anderen Wertelementen aufweisen. Granat enthält maximal 300 µg/g Zinn, ebenso gering sind Wolfram-, Indium- und Zink-Konzentrationen. Jedoch enthalten Granat und Vesuvian mitunter vergleichsweise höhere Mengen von *High-field-strength*-Elementen (HFSE), darunter Zirkon und Titan. Chondritnormierte

Seltenerdmuster in Granat zeigen eine typische Verteilung mit einer Anreicherung der schweren gegenüber den leichten Seltenen Erden, was auf ein langsames Kristallwachstum hindeutet, bei welchem der Einbau von Spurenelementen durch die Kristallstruktur bestimmt wird (Røhr et al. 2007; Yang et al. 2013). Die Analysen zeigten darüber hinaus, dass Granat ausnahmslos eine negative Europium-Anomalie aufweist. Die niedrigen Gehalte von Zinn und Wolfram sowie die ihrem Verteilungskoeffizienten folgende Verteilung der Seltenen Erden in Granat weisen darauf hin, dass der Einfluss eines magmatisch-hydrothermalen Fluids nicht dominierte. Bei der Kontakt-metamorphose kam es anfangs vor allem zu einem Temperaturanstieg, der lediglich zu kleinräumigen Elementtransfers führte. Unter diesen Bedingungen verbesserten Porenfluide die lokale Mobilität bestimmter Elemente, was die Diffusionsraten während der Skarnbildung erhöhte (Gaspar et al. 2008; Jamtveit et al. 1993). Elemente wie Aluminium, Zirkon oder Titan wurden den Skarnen auf diese Weise aus dem metamorphen Protolith zugeführt (Corfu und Davis 1991; Jamtveit und Hervig 1994). Erst im weiteren Verlauf kamen dann auch magmatisch-hydrothermale Fluide hinzu. Dies zeigen die veränderten Seltenerdmuster und die erhöhten Eisengehalte der Minerale der späten skarnoiden Phase.

Dass kontaktmetamorphe Einflüsse zu Beginn der Verskarnung dominierten, wird durch Untersuchungen an Fluideinschlüssen in Mineralen dieser Phase unterstützt. Die Einschlüsse bestehen bei Raumtemperatur aus einer flüssigen und einer gasförmigen Phase und zeigen keine Anzeichen für Phasenseparation, was auf lithostatischen Druck während ihrer Bildung hindeutet (Driesner and Heinrich 2007; Korges et al. 2020). Fluide, die zu der ersten Verskarnung beigetragen haben, besitzen intermediäre Salinitäten von 7,1–11,0 % eq. w(NaCl) und ihre Homogenisierungs-temperaturen liegen nach der Korrektur des Druckes zwischen circa 445 und 470 °C, was auf den Austritt aus einer proximalen Intrusion ohne weitere Umwandlungen hinweist (Korges et al. 2020). Granat aus der ersten Mineralassoziation weist ein Uran-Blei-Alter von 322,4 ± 5,1 bzw. 322,1 ± 11.8 Millionen Jahren auf. Dementsprechend fand die Überprägung zeitgleich mit der Platznahme des nahegelegenen Greifenstein-Granits (324 ± 4 bzw. 320 ± 3 Ma; Romer et al. 2007) sowie der Intrusion des großvolumigen Eibenstock-Plutons (323–314 Ma; Förster et al. 2009; Kempe et al. 2004; Tichomirowa et al. 2019) statt.

2.3.2 Prograder Skarn

Die metasomatische Skarnphase führte zur Überprägung großer Teile der Marmore und griff auch auf die umgebenden Metapelite über, wobei auch Skarnoide der ersten Phase erfasst wurden, ohne dass die interne Textur der Protolithe erhalten blieb. Die progradan Skarne sind vielmehr von gleich- und grobkörniger Textur und enthalten deutlich mehr isometrischen Granat als die Skarnoide, wobei dunkel gefärbter Klinopyroxen als weiterer Hauptbestandteil und langprismatischer, grüner Vesuvian hinzukommen. Letzterer verdrängt teilweise Vesuvian und Granat aus der skarnoiden Phase. Die erste eigenständige Zinnphase, das zinnhaltige Titanit-Analogon Malayait kommt mit Granat assoziiert in Form idiomorpher Prismen, aber auch als Verdrängungsprodukt von Titanit vor. Zwei Granat-Generationen können während der prograden Skarnphase anhand von Verdrängungstexturen unterschieden werden, wobei beide einen poikilitischen Kern aufweisen, der von einem oszillatorisch zonierten Rand umschlossen wird. Die frühere Generation ist von roter bis brauner Farbe, während der teilweise in Adern vorkommende, spätere Granat gelb bis kräftig grün gefärbt ist. Die ausgeprägt oszillierende Zonierung von Granat, Klinopyroxen und Vesuvian und das Verhältnis der Skarnminerale zueinander zeigen, dass es sich bei der zweiten Alterationsphase um eine metasomatische Verskarnung handelt.

Mineralchemisch weist die erste Granat-Generation große Parallelen mit Granat aus der vorangegangenen, skarnoiden Phase auf. Beide sind durch die Dominanz des Endglieds Grossular, niedrige Zinngehalte (< 0.09 Gew.-%) sowie vergleichsweise hohe Konzentrationen an HFSE gekennzeichnet. Die Signatur der Seltenen Erden weist auf ein Granatwachstum im Gleichgewicht mit kogenetischen Phasen, was auf eine gesteinsgepufferte Umgebung hinweist. Habitus und Zusammensetzung der folgenden Granat-Generation und der damit assoziierten Minerale ändern sich drastisch gegenüber der vorherigen. Stark zonierter Granat mit einer höheren Andradit-Komponente weist erhöhte Gehalte an Zinn (< 3,35 Gew.-%), Wolfram und Lithium auf, was auf eine fortschreitende Zunahme des Fluidflusses hindeutet, da diese Elemente typischerweise in einem magmatisch-hydrothermalen Fluid angereichert sind (Ayers und Eggler 1995; Bai und Koster van Groos 1999). Die erhöhten Gehalte der leichten Seltenen Erden, die Verarmung der schweren Seltenen Erden sowie eine deutlich positive Europium-Anomalie in Granat untermauern das Vorhandensein eines hydrothermalen Fluids (Douville et al. 1999; Wood 1990), welches nicht wesentlich mit dem Umgebungsgestein interagierte (Smith et al. 2004).

Wenngleich bekannt ist, dass skarnassoziierter, in einem fluidgepufferten Umfeld gebildeter Granat eine positive Europium-Anomalie aufweisen kann (Gaspar et al. 2008; Jamtveit and Hervig 1994; Park et al. 2017a; 2017b), wurde bisher keine beweiskräftige Erklärung für diese Tatsache gefunden. Kristallchemische Effekte können ausgeschlossen werden, da die andraditreichen Granate der skarnoiden Phase keine positive Anomalie zeigen. Stattdessen ist in diesem Stadium von einer positiven Europium-Anomalie im magmatisch-hydrothermalen Fluid auszugehen, die auf die vorherige Kristallisation von Mineralen mit einer negativen Europium-Anomalie zurückzuführen sein könnte (Breiter et al. 1999; Terekhov und Shcherbakova 2006). Alternativ ließe sich die positive Europium-Anomalie durch Ererbung in Folge der Auflösung von Plagioklas in den durchströmten Gesteinseinheiten erklären (Möller et al. 2021). Auch in Gesteinen der apikalen Bereiche der an Geyer SW angrenzenden Lagerstätte Ehrenfriedersdorf sowie in hochentwickelten, peralumischen Graniten in Frankreich, wurden positive Europium-Anomalien identifiziert (Lehmann und Seltmann 1995; Raimbault und Azencott 1987). Dies unterstützt einen genetischen Zusammenhang des Granats mit einem Fluid aus einer hochentwickelten magmatischen Quelle. Da diese spätere Generation ein untypisches (Spuren-)Elementmuster für Granat aufweist, ist ein fluidgepuffertes Bildungsmilieu wahrscheinlich, bei dem die Wachstumsrate der Minerale die Diffusionsrate der Fluide übersteigt (Gaspar et al. 2008; Jamtveit et al. 1993; Jamtveit und Hervig 1994). Diese migrieren vermehrt entlang von zusammenhängenden Porenräumen, Trümern oder gar Störungszonen (Gaspar et al. 2008; Jamtveit et al. 1993; Meinert 1992).

Das fluiddominierte System ging schließlich durch wieder zunehmend gesteinsgepufferte Bedingungen in eine intermediäre Phase über. Dies führte abermals zur Bildung einer neuen Granat-Generation mit poikilitischer Textur. Mineralchemisch äußert sich dies durch höhere Gehalte an immobilen Elementen (Aluminium, Titan und Zirkon) sowie eine weniger ausgeprägte Verarmung der schweren Seltenen Erden. Erhöhte Gehalte an Zinn, Wolfram und Indium im Granat belegen jedoch, dass während dieser Phase weiterhin ein magmatisches Fluid präsent war.

Die intermediäre Phase wurde von der fluiddominiertesten Stufe abgelöst. Andraditreicher Granat mit den höchsten Konzentrationen an Zinn (< 6,54 Gew.-%), Wolfram und Indium, einer ausgeprägten positiven Europium-Anomalie sowie hohen Gehalten an leichten und geringen Gehalte an schweren Seltenen Erden belegt die

fluiddominierte Natur dieser Episode (Gaspar et al. 2008; Jamtveit und Hervig 1994). Die im System höchsten Lanthan-Konzentrationen in Granat könnten mit höheren Fluid-Salinitäten zusammenhängen, da ein hoher Chlor-Gehalt die Löslichkeit von Lanthan erhöht (Allen und Seyfried 2005). Dies steht im Einklang mit Analysen von Fluideinschlüssen, die zum Teil auf hochsalinare Fluide (26,9–28,7 % eq. w($NaCl+CaCl_2$)) hinweisen und innerhalb derselben Einschlussbahn vorkommen wie Inklusionen, die nur aus einer Gasphase bestehen. Dies deutet auf die Entmischung eines hydrothermalen Fluids in höheren Krustenstockwerken bei hydrostatischem Drücken hin (Driesner und Heinrich 2007; Meinert et al. 2005).
Uran-Blei-Datierungen an Granat aus drei Proben dieser Alterationsphase ergaben ein Alter zwischen 307,3 ± 4,8 und 301,6 ± 5,0 Ma. Diese Alter sind deutlich jünger als die der skarnoiden Phase und bestätigen damit die paragenetischen Zusammenhänge. Als Fluidquellen für diese metasomatische Verskarnung kommen Subintrusionen infrage, die nach der Hauptphase des Magmatismus im Raum Geyer intrudierten (Bolduan 1963). Geochronologische Daten eine solche Spätphase, die diesen Zusammenhang bestätigen würden, sind für Geyer derzeit nicht verfügbar.

2.3.3 Retrograder Skarn

Diese Phase ist eng mit der metasomatischen progradén Verskarnung verknüpft und ihr Beginn wird durch das Auftreten von Magnetit sowie wasserhaltigen Mineralen markiert. Magnetit tritt in Form grobkörniger, unregelmäßiger Einschlüsse oder interstitiell auf und bildet sich nach Klinopyroxen und Granat aber vor Amphibol und Chlorit. Er kann mit schwammartig kristallisiertem Kassiterit verwachsen sein, der erstmals in der Mineralparagenese der Lagerstätte Geyer SW auftritt. Epidot bildet dunkelgrüne, prismatische Kristalle mit ausgeprägter Zonierung und tritt häufig linsenförmig oder glomerophyrisch gemeinsam mit Fluorit und gelegentlich Sphalerit auf. Die Häufigkeit von Epidot variiert stark, aber er ist sowohl in pyroxen- als auch in granatreichen Skarnlagern zu beobachten. Minerale der Amphibolgruppe treten als idiomorphe, oszillatorisch zonierte Kristalle auf und werden von Fluorit, Quarz und gelegentlich Sulfidmineralen wie Sphalerit, Chalkopyrit, Galenit und seltenem Stannit begleitet. Außerdem verdrängt Amphibol präferiert den zuvor gebildeten Klinopyroxen und tritt folglich häufiger in pyroxenreichen Skarnlagern auf. In der Spätphase der retrograden Alteration ist Chlorit das vorherrschende Skarnmineral und häufig in Trümern, Adern und deren Alterationsaureolen anzutreffen. Er wird von Amphibol, Kassiterit sowie Fluorit begleitet. Zum Ende der retrograden Verskarnung erfolgte die Bildung einer Mineralassoziation aus Quarz, Fluorit, Arsenopyrit, gelegentlich Prehnit und manganhaltigen Kalzit, welche einen Großteil der Kalksilikatminerale verdrängen kann.

Die präferentielle Kristallisation von Skarnmineralen in Adern sowie das weiterhin idiomorphe Wachstum und die Zonierung der Minerale weisen auf eine noch immer fluidgepufferte Umgebung hin, wenngleich im Stabilitätsbereich anderer Mineralphasen (Jamtveit and Hervig 1994; Meinert et al. 2005). Dies zeigt sich insbesondere an Epidot und frühem Amphibol, die jeweils eisenreich sind, einen hohen Zinngehalt (< 7,81 Gew.-% bzw. < 1,9 Gew.-%) und eine dem hydrothermalen Fluid und der letzten Granatgeneration ähnliche Verteilung der Seltenen Erden aufweisen (Douville et al. 1999; Wood 1990). Sowohl diese Granate als auch Amphibol und Epidot sind demnach aus demselben abkühlenden hydrothermalen Fluid ausgefallen (Hantsche et al. 2021). Ein weiteres Abkühlen des Systems belegt Chlorit, der neben prograden Mineralen auch zinnhaltigen Amphibol verdrängt (Meinert et al. 2005) und teilweise hohe Konzentrationen von Lithium, Bor und Zink besitzt, was auch für ihn auf Kristallisation in Gegenwart eines magmatisch-hydrothermalen Fluids hindeutet, selbst wenn ein Teil dieser Elemente von den Ausgangsmineralen ererbt sein könnte.

Obwohl Analysen von Fluideinschlüssen in Epidot oder Amphibol nicht möglich waren, ist ein kontinuierlicher Abkühlungstrend der hydrothermalen Fluide während der frühen retrograden Phase anhand der Chlorit-Bildungstemperaturen (210–350 °C; Cathelineau 1988) sowie der ermittelten Homogenisierungstemperaturen für Fluideinschlüsse in Kassiterit und Fluorit (255–340 °C) dokumentiert. Einschlüsse mit einer festen, flüssigen und gasförmigen Phase sowie einer hohen Salinität besitzen dabei die höheren Homogenisierungstemperaturen. Diese sind kogenetisch mit gasreichen Einschlüssen, was – wie im Falle der prograden Skarne – auf ein heterogenes Einschließen der Fluide und Phasenseparation hindeutet. Die abnehmende Salinität der Fluideinschlüsse zeigt, dass sich das hydrothermale Fluid zunehmend mit einem weniger salinaren und kühleren meteorischen Fluid mischte (Bertelli et al. 2009; Einaudi et al. 1981; Meinert et al. 2005).

Uran-Blei-Datierungen an Kassiterit der retrograden Phase ergeben ein Alter von 308,2 ± 2,9 Ma, welches mit dem Alter des Granats aus der prograden Phase überlappt und belegt, dass die beiden Prozesse zum gleichen magmatisch-hydrothermalen Ereignis gehören, welches nach der Hauptintrusionsphase der Plutone in diesem Teil des Erzgebirges stattfand (Romer et al. 2007).

2.3.4 Greisenalteration

Die Greisenalteration tritt hauptsächlich innerhalb der granitischen Intrusion bei Geyer auf (Endogreisen), erstreckt sich aber in Form pneumatolytischer Gänge auch in das metamorphe Umgebungsgestein (Exogreisen). Die Greisenalteration innerhalb des Granits ist hauptsächlich an Trümer (< 3 cm Mächtigkeit) und dichte Gangscharen (< 6 m Mächtigkeit) gebunden, welche ausgedehnte Alterationsaureolen erzeugen (Bolduan 1963; Hösel et al. 1996). Die Alterationsaureole ist in Abhängigkeit des von den 15 cm mächtigen Adern durchschlagenen Gesteins heterogen ausgebildet, reicht jedoch meist nicht weiter als 30 cm ins Nebengestein hinein (Bolduan 1963). Die typische Mineralassoziation der Greisen beinhaltet die pervasive Ersetzung magmatischen Feldspats, kommt aber auch als Gangfüllung vor und besteht hauptsächlich aus Quarz, Lithium-Glimmer und Topas. Kassiterit tritt entweder disseminiert in Dispersionshöfen oder in den Gängen in Form größerer Kristalle gemeinsam mit Fluorit und Apatit sowie geringen Mengen Wolframit, Molybdänit und Löllingit auf, die mit Arsenopyrit verwachsen sind. Kassiterit aus dieser Paragenese besitzt ein Uran-Blei-Alter zwischen 305,7 ± 2.8 und 306,6 ± 2.5 Ma. Die Greisenalteration fand damit eindeutig nach der Hauptintrusionsphase der bekannten Granite dieser Gegend statt (Romer et al. 2007), fällt jedoch in denselben Zeitraum wie die metasomatische pro- und retrograde Verskarnung.

2.3.5 Fluidsignatur und -quelle

Das Yttrium/Holmium-Verhältnis in Kalksilikatmineralen ist geeignet, die Quelle eines Fluids in einem System zu bestimmen (Chu et al. 2023). Weder die fraktionierte Kristallisation eines granitischen Magmas noch Modifikationen des Fluids wie Entmischung oder Abkühlung führen zu einer Fraktionierung zwischen Yttrium und Holmium (Bau und Dulski 1995). Schwankungen im Yttrium/Holmium-Verhältnis wurden daher mit der Verdünnung eines magmatisch-hydrothermalen Fluids durch meteorisches Wasser in Verbindung gebracht (Bau 1996).

Alle Granat- und Epidot-Generationen und die zinnhaltigen Minerale der Amphibolgruppe weisen über einen weiten Konzentrationsbereich hinweg konstante Yttrium/Holmium-Verhältnisse auf, weshalb all diese Minerale wahrscheinlich aus dem gleichen magmatischen Fluid ausfielen (Ayers und Eggler 1995; Bai und Koster van

Groos 1999; Bau 1996; Park et al. 2017b). Mit Sulfiden koexistierender Amphibol zeigt jedoch eine Abweichung von diesen Verhältnissen sowie niedrigere Zinngehalte, was auf den Zustrom von meteorischen Wässern hindeutet, im Einklang mit dem reichlichen Auftreten von Sulfiden in dieser Paragenese des retrograden Skarnsystems (Bau und Dulski 1995; Gao et al. 2020; Meinert et al. 2003; Öztürk et al. 2008). Alle späteren Phasen (Chlorit und Kassiterit) entstanden nach der Mischung von magmatischem und externem Fluid, was sich deutlich in der veränderten Yttrium/Holmium-Systematik von Kassiterit widerspiegelt.

2.3.6 Das Verhalten von Zinn während der Entwicklung des Systems

Kalksilikatminerale der Skarnoide des Geyer-Systems weisen nur sehr geringe Zinngehalte auf. Zudem enthält die Paragenese dieser ersten Verskarnungsphase keine genuinen Zinnminerale. Demnach haben die alterierten Ausgangsgesteine keine signifikant erhöhten Gehalte an Zinn aufgewiesen und die involvierten Fluide führten dem System kein Zinn zu. Umgekehrt enthalten die wichtigsten Skarnminerale der metasomatischen Phase (Malayait-Titanit, Granat, Vesuvian) erhebliche Mengen an Zinn, wobei Granat aufgrund seiner Häufigkeit und seiner hohen Zinngehalte als Hauptträger des Gesamtbudgets angesehen werden kann. Dieser beobachtete Anstieg der Zinn-Konzentrationen fällt offensichtlich mit dem Zutritt eines Fluids im Zuge der Skarnmineralbildung zusammen. Die mineralchemischen Daten zeigen eindeutig, dass der Zustrom von zinnhaltigen magmatisch-hydrothermalen Fluiden während der progradenVerskarnung anschließend stetig weiter zunahm. Dies führte zu allgemein steigenden Zinn-Konzentrationen in Kalksilikatmineralen und zur Bildung von Malayait.

Im Zuge der retrograden Verskarnung stellen Kassiterit, Epidot und Amphibol die Hauptträger von Zinn dar. Die Abkühlung des Systems, die durch Stabilisierung von Amphibol und Chlorit deutlich wird (Meinert 1992), sowie die Verdünnung des magmatischen Fluids mit externen Fluiden sind wahrscheinlich die Hauptgründe für die Ausfällung von Kassiterit und Sulfiden (Eadington and Kinealy 1983). Darüber hinaus führt die Ersetzung zinnhaltiger Kalksilikatminerale durch nominell zinnfreie Minerale zur zusätzlichen Freisetzung von Zinn und anschließenden Ausfällung von weiterem Kassiterit (Kwak 1987; Meinert et al. 2005). Ein ähnlicher Prozess der Fokussierung, Umverteilung und Wiederausfällung wird in Skarnsystemen auch für Indium vorgeschlagen (Bauer et al. 2019).

Die Mineralchemie aller in Geyer analysierten Silikate weist darauf hin, dass vierwertiges Zinn über isovalente Substitution (Titanit-Malayait; Deer et al. 2013) oder durch gekoppelte Substitution zweier dreiwertiger Kationen gemeinsam mit einem zweiwertigen Kation ins Kristallgitter eingebaut wurde, wie für Granat (Amthauer et al. 1976; Chen et al. 1992; Plimer 1984; Yu et al. 2020) und Epidot (Armbruster et al. 2006) demonstriert. Dies steht im Einklang mit jüngsten Experimenten (Chou et al. 2021; Schmidt 2018; Wang et al. 2021) sowie mit thermodynamischen Modellierungen (Liu et al. 2023), die zeigen, dass eine beträchtliche Menge Zinn in Form von Zinn(IV)-Komplexen transportiert werden kann. Die Annahme eines oxidierten Milieus zum Zeitpunkt der Kristallisation zinnhaltiger Kalksilikate wird durch die hohen Gehalte dreiwertigen Eisens in kogenetischen Mineralen wie Andradit und Epidot gestützt. Während der Entwicklung des Skarnsystems lassen sich zwei verschiedene Phasen der Zinn-Remobilisierung unterscheiden. Während der ersten überwiegend gesteinsgepufferten Phase ersetzte grossularreicher Granat die zinnhaltigen Kalksilikatminerale. Da Grossular gegenüber diesen weniger kompatibel für Zinn ist (Sonnet und Verkaeren 1989; Park et al. 2017b; Plimer 1984), bildet sich in der Folge Malayait, welcher bei relativ hohen Temperaturen und einer hohen Siliziumaktivität, wie zu dessen Bildung angenommen, gegenüber Kassiterit stabiler ist (Aleksandrov und Troneva 2007). Die zweite Remobilisierung von Zinn erfolgte während der Spätphase der retrograden Alteration, bei welcher ein Großteil der Kalksilikatminerale durch hydrothermalen Kalzit, Quarz und Prehnit ersetzt wurde. Während dieses Prozesses bilden sich auf Kosten des Kassiterits sekundäre Zinn-Minerale wie Stokesit ($CaSnSi_3O_9 \cdot 2H_2O$). Dies wurde auch in anderen Skarnsystemen wie Hämmerlein und Zlatý Kopec beschrieben (Kern et al. 2019; Pauliš et al. 2015).

2.4 Lagerstättenkundliches Modell

Die erste Phase der Verskarnung in Geyer ist gekennzeichnet durch das Auftreten von feinkörnigen Kalksilikatmineralen mit einer skarnoiden Textur (folgend den Argumenten von Meinert 1992). Die texturellen Eigenschaften der Ausgangsgesteine blieben erhalten und die Mineralneubildungen zeigen kaum chemische Zonierung. Die Entstehungszeit dieser ersten Skarne koinzidiert mit der Platznahme des spätvariszischen Ehrenfriedersdorf-Plutons, welcher das gesamte Lagerstättenrevier unterlagert (Bolduan 1963; Hösel et al. 1996). Die Skarnoide entstanden bei hohen Temperaturen unter lithostatischem Druck (Einaudi et al. 1981) in einer gesteinsgepufferten Umgebung (Gaspar et al. 2008; Jamtveit et al. 1993), mit Ausnahme der durch ein hydrothermales Fluid beeinflussten Spätphase dieser ersten Alteration.

Die zeitliche Lücke zwischen der skarnoiden und der metasomatischen Phase beträgt mehr als 15 Millionen Jahre und zeigt, dass diese beiden Alterationsprozesse genetisch getrennt voneinander abliefen. Dies bestätigt auch die um 100 °C niedrigere Temperatur während der metasomatischen Verskarnung, die in höheren Krustenstockwerken und unter hydrostatischen Bedingungen stattfand. Bei der ursächlichen Intrusion handelt es sich vermutlich um ein kleinvolumiges, hochentwickeltes granitisches Vorkommen, das im genetischen Zusammenhang mit postvariszischen, rhyolitischen Körpern stehen könnte, die im Lagerstättengebiet nachgewiesen sind und den Ehrenfriedersdorf-Batholith intrudierten (Bolduan 1963).

Die metasomatische Verskarnung entwickelt sich von einem nahezu geschlossenen System innerhalb eines gesteinsgepufferten Milieus hin zu einem offenen, fluiddominierten System. Wechsel zwischen fluid- und gesteinsgepufferten Bedingungen äußern sich in den unterschiedlichen Seltenerdmustern der Granat-Generationen sowie in deren Haupt- und Spurenelement-Konzentrationen. Diese zeigen ferner, dass mindestens zwei individuelle Fluid-Pulse auf die Mineralbildung während der prograden Metasomatose Einfluss nahmen.

Die retrograde Phase der zweiten Skarngeneration ist durch ein fluidgepuffertes Umfeld unter spröden, hydrostatischen Bedingungen charakterisiert. Ihr Beginn ist durch einen Wechsel der Silikat-Paragenese gekennzeichnet. Chlorit sowie späte Amphibole entwickelten sich in der Präsenz eines zunehmend kühleren magmatisch-hydrothermalen Fluids, welches womöglich mit meteorischen Wässern verdünnt worden ist. Das Auftreten von zinnreichen Kalksilikatmineralen inklusive Malayait während der metasomatischen Verskarnung sowie die Bildung von Kassiterit während der retrograden Skarnphase und der Greisenalteration sind zeitlich demselben magmatisch-hydrothermalen Ereignis zuzuordnen. Dieses ist mit post-kollisionalen, auch in anderen Teilen des Erzgebirges nachgewiesenen, kleinräumigen Intrusionen in der Spätphase der variszischen Orogenese in Verbindung zu bringen (Burisch et al. 2019; Hofmann et al. 2013; Kröner and Willner 1998; Leopardi et al. 2024a; Löcse et al.2023). Die zugehörigen Fluide verursachten den überwiegenden Teil der Zinnvererzung des Geyer-Systems.

3. Metallogenetische Implikationen

Diese Arbeit über das Geyer-System lässt sich in einen gemeinsamen Kontext mit den historischen und modernen Arbeiten über andere zinnhaltige Skarnsysteme im Erzgebirge stellen, sodass grundsätzliche Erkenntnisse zu den Entstehungsprozessen von Skarnlagerstätten gewonnen werden können. Dazu zählen Aussagen zur Zonierung der Wertmetalle innerhalb einer Lagerstätte oder eines gesamten Lagerstättenreviers und zu den Zeitpunkten von Verskarnung und Vererzung. Eine neue, allgemeingültige Klassifikation der Skarne des Erzgebirges kann anschließend wiederum mit zinnassoziierten Skarnen weltweit verglichen werden.

3.1 Zonierung der Skarne

Innerhalb eines Lagerstättendistrikts zeigen die Skarnsysteme des Erzgebirges eine ausgeprägte Zonierung von einer proximalen Wolfram-Zinn- über eine intermediäre Zinn-Zink(-Indium)- bis hin zu einer distalen Zink-Blei(-Zinn)-Dominanz. Die räumliche Zonierung innerhalb einer Lagerstätte wird durch die mehrphasige Natur der Skarne, variable Wirtsgesteinszusammensetzungen und Wechsel zwischen fluid- und gesteinsgepufferten Phasen während der Metasomatose verschleiert. Dennoch lassen sich unvererzte Skarnoide von mineralisierten Skarnsystemen anhand der Mineralchemie von prograd gebildeten Kalksilikatmineralen unterscheiden. Diese Unterscheidung ist bisher nur für das System Geyer in Gänze beschrieben worden; jedoch zeigen mineralchemische Daten von den Lagerstätten Hämmerlein (Korges et al. 2020; Lefebvre et al. 2019; Meyer et al. 2025) und Ehrenfriedersdorf (Meyer et al. eingereicht) ebenfalls eine bimodale Zinnverteilung, was zusammen mit petrographischen Beobachtungen (Meyer et al. eingereicht; Schuppan und Hiller 2012) auf eine unvererzte skarnoide Phase und eine nachfolgende metasomatische, zinnassoziierte Verskarnung hinweist.

Zusätzlich können weitere Eigenschaften von Skarnmineralen genutzt werden, um die räumliche Position einer Probe in Bezug auf die Entfernung zur Fluidquelle innerhalb eines Skarnsystems zu ermitteln. Beispielsweise ändert sich die Färbung von Klinopyroxen von blassbeige zu intensivgrün mit fortschreitender Entfernung zur Fluidquelle, während die Intensität der Färbung von Granat generell mit steigender Entfernung abnimmt (Kwak 1987; Meinert et al. 2005; Reinhardt et al. 2021).

Während der Platznahme eines Granits sind Verskarnung und Vererzung entkoppelte Prozesse, die von zwei Hauptvariablen abhängen: Temperatur und

Fluidzusammensetzung (Einaudi et al. 1981; Heinrich 1990; Kwak 1987; Meinert et al. 2005). Proximale Skarne entstehen zunächst durch temperaturbedingte Kontaktmetamorphose in unmittelbarer Nähe des Granits, während metasomatische Effekte durch magmatisch-hydrothermale Fluide in distalen Skarnen wirksamer sein können. An diese distalen Bereiche ist auch der Hauptteil der Vererzung gebunden, was auch mit den sich abkühlenden Fluiden abhängig ist (Audétat et al. 2000). Sowohl die granitische Intrusion als auch die assoziierten Fluide kühlen sukzessiv ab, wobei die frühe Hochtemperatur-Paragenese je nach Anzahl der Fluidpulse mehrphasig überprägt oder ersetzt wird. Regionale Exhumierung und der Rückzug der Kontaktaureole während der Skarn-Entwicklung können zur Überlagerung von mehreren Paragenesen in einem geologischen Körper, sodass an derselben Position innerhalb eines Skarns mehrere Generationen desselben Minerals mit unterschiedlichem Chemismus und Alter auftreten.

3.2 Zeitpunkt der Verskarnung und Vererzung

Die erste Phase der Skarn-Alteration im Erzgebirge umfasst (neben Reaktionsskarnen während der Metamorphose) Skarne und Skarnoide, die keine eindeutige räumliche oder genetische Verbindung zu granitischem Magmatismus aufweisen (Bubal und Dolejš 2013; Burisch et al. 2019). Diese Skarne weisen ein Bildungsalter auf, das mit dem Höhepunkt der regionalen Metamorphose und der anhaltenden Kollisionstektonik (343–331 Ma) übereinstimmt (Burisch et al. 2019). Diese Vorkommen sind in der Regel kleinräumig und enthalten hauptsächlich Eisen- und in geringerer Anzahl Kupfervererzungen (Hoth et al. 2010; Pauliš and Haake 1991; Starý et al. 2024). Dieses Stadium ist auch durch Granat-Alter der vererzten Skarne von Breitenbrunn und Globenstein im Aue-Schwarzenberg-Distrikt belegt (Reinhardt et al. 2022). Deren Texturen deuten auf eine Entstehung nach dem Höhepunkt der Metamorphose hin, obwohl potenziell ursächliche Intrusionen aus dieser Zeit in der Region nicht dokumentiert sind (Reinhardt et al. 2022). Dies deutet auf ein frühes hydrothermales Alterationsgeschehen im Erzgebirge mit Fluiden ohne magmatischen Ursprung hin. Skarne, die diese Alter zeigen, haben mehrere Alterationsphasen, die aus der Petrographie abgeleitet sind. Dadurch, dass diese Daten nicht synchronisiert sind, lässt sich keine genaue Zuordnung der Alteration mit dem Zeitpunkt der Vererzung ableiten.

Die zweite Generation von Skarnen und Skarnoiden enthält bedeutende Zinn-, Wolfram-, Zink- und Indium-Vorkommen (Burisch et al. 2019; Reinhardt et al. 2022) und steht im direkten Zusammenhang mit der post-kinematischen Tektonik in der Spätphase der variszischen Orogenese und dem dazugehörigen Magmatismus (330–295 Ma). Der frühere Abschnitt dieser Phase erfolgte zeitgleich mit der Intrusion der großvolumigen Batholithe im Erzgebirge (330–310 Ma; Förster et al. 1999; Tichomirowa und Leonhardt 2010; Tichomirowa et al. 2019) und umfasst unvererzte Skarnoide (Geyer, Ehrenfriedersdorf), scheelitführende Skarnoide (Zobes) sowie metasomatische Skarne, die eine Zink(-Zinn)-Vererzung aufweisen können. Dieser Zusammenhang ist sowohl für das zentrale (Geyer-Ehrenfriedersdorf) als auch das westliche Erzgebirge (Aue-Schwarzenberg-Distrikt; Burisch et al. 2019; Reinhardt et al. 2022) nachgewiesen. Die metasomatischen Skarnsysteme des Erzgebirges haben die frühe Bildung einer Skarnoid-Phase, die durch die darauffolgende prograde und retrograde Verskarnung überprägt wird, gemeinsam. Diese frühe Phase stellt ein eigenständiges Ereignis dar, an welches die metasomatische Phase direkt anschließen kann. In anderen Systemen besteht zwischen den beiden Prozessen ein zeitlicher Abstand von bis zu 15 Millionen Jahren (Geyer, Ehrenfriedersdorf, Tellerhäuser, Breitenbrunn). Die Skarne des Waschleithe-Vorkommens enthalten keine Skarnoide und stellen damit eine Ausnahme dar, die wahrscheinlich mit den sehr distalen Entstehungsbedingungen zusammenhängt.

Die jüngste Altersgruppe der Skarne im Erzgebirge weist Alter zwischen 310 und 295 Millionen Jahren auf. Die datierten Granat-Populationen zeigen durchweg metasomatische Texturen und treten in Proben des Geyer-Ehrenfriedersdorf-Distrikts sowie in den Skarnen von Oelsnitz und Berggießhübel auf (Burisch et al. 2019). Die entsprechenden Skarne entstanden eindeutig nach der Intrusion der Batholithe und stehen wahrscheinlich mit der postvariszischen magmatischen Aktivität in Verbindung, die sich in kleineren Intrusivkörpern manifestierte (Burisch et al 2019; Reinhardt et al. 2022). Tichomirowa et al. (2025) grenzen diese postvariszische magmatische Aktivität auf 301–296 Millionen Jahren im östlichen und auf 306–303 Millionen Jahren im westlichen Erzgebirge ein. Diese Alter stützen die Annahme eines genetischen Zusammenhangs zwischen Skarnalteration und magmatischer Aktivität in diesem Zeitraum (Hoffmann et al. 2013; Reinhardt et al. 2022; Tichomirowa et al. 2025), in welchen sich die Skarne von Geyer widerspruchsfrei einfügen. Zusätzlich kann dort die Erzbildung mit der metasomatischen Verskarnung korreliert werden, da alle

zinnangereicherten Paragenesen (zinnreiche Kalksilikatminerale sowie Kassiterit im Rahmen der retrograden Verskarnung, in pneumatolytischen Gängen und in Greisen) innerhalb derselben Altersspanne vorkommen. Dies konnte auch für das benachbarte Lagerstättenrevier Ehrenfriedersdorf gezeigt werden (Meyer et al. eingereicht). Diese beiden Skarnsysteme sind die ersten und einzigen im Erzgebirge, für welche die zeitlichen Zusammenhänge zwischen Alteration und Erzbildung geklärt sind.
Das große Altersspektrum und der Altersunterschied zwischen verschiedenen Granat-Generationen innerhalb derselben Lagerstätte im Aue-Schwarzenberg-Distrikt belegen, dass einige Skarne das Produkt mehrerer aufeinanderfolgender magmatisch-hydrothermaler Ereignisse sind. Die komplexe Altersverteilung könnte mit der überregionalen Gera-Jáchymov-Störungszone in Verbindung stehen. Zusätzliche ortsaufgelöste Datierungen von Erzmineralen wie Kassiterit sind erforderlich, um ein belastbares Rahmenwerk zu schaffen, damit der Zusammenhang zwischen Alterationen und Vererzungen besser aufgelöst werden kann, insbesondere in mehrphasigen Skarnsystemen.

3.3 Klassifikation der Skarne des Erzgebirges

Zinnreiche Skarne werden häufig in Wolfram-Zinn-, Zinn- oder Zinn-Zink±Blei±Indium±Silber-Skarne (polymetallische Skarne) eingeteilt. Diese Gruppen sind jedoch als Kontinuum zu betrachten (Einaudi et al. 1981; Kwak 1987; Meinert et al. 2005). Wolfram-Zinn-Skarne sind typischerweise mit kalkalkalischen, voluminösen Plutonen assoziiert, die von ausgedehnten Kontakt-Aureolen umgeben sind (Elongo et al. 2020; Ni et al. 2023). Die Verskarnung findet in tiefen Krustenstockwerken statt und führt zu proximalen Alterationszonen. Solche Skarne entwickeln sich ausschließlich als Exoskarne mit Scheelit als vorherrschendem Erzmineral und werden von Skarnoiden und Kalksilikat-Hornfelsen begleitet (Meinert et al. 2005). Zobes und das erste Alterationsstadium der Lagerstätte Globenstein zeigen Merkmale von proximalen Wolfram-Zinn-Skarnen, die tief und nahe der Intrusion entstanden. Allerdings wurden die primären Skarne in Globenstein später durch metasomatisch-hydrothermale Prozesse überprägt, was zu einer Umverteilung der Wertelemente führte (Hiller und Schuppan 2016; Hösel et al. 2003).
Zinn-Skarne, wie von Einaudi et al. (1981) definiert, sind hauptsächlich mit Graniten assoziiert, die aus krustalen Schmelzen hervorgingen (S- und A-Typ). Skarne dieses Typs sind durch Elemente wie Bor, Fluor, Lithium, Molybdän und/oder Wolfram sowie

durch das Vorkommen von Greisen in den Hochlagen der granitischen Intrusionen gekennzeichnet (Kwak 1987; Meinert et al. 2005). Die Platznahme der Granite und die damit verbundene Verskarnung erfolgen in flachen Krustenniveaus (Einaudi et al. 1981; Kwak 1987; Meinert et al. 2005). Zinn-Skarne besitzen eine große laterale Ausdehnung und zeigen eine starke strukturelle und tektonische Kontrolle. Kassiterit kristallisiert hauptsächlich während der retrograden Phase (Eadington und Kinealy 1983; Meinert et al. 2005). Die Skarne von Ehrenfriedersdorf und Geyer weisen Merkmale von Zinn-Skarnen auf und sind mit hochentwickelten, vergreisten Graniten assoziiert.

Zink-Skarne mit unterschiedlichen Anteilen von Zinn, Blei, Silber und anderen Metallen sind nicht an einen bestimmten Intrusionstyp gebunden und treten in verschiedenen geologischen Umgebungen auf (Meinert et al. 2005). Ein gemeinsames Merkmal dieser Skarne ist ihre distale Position in Bezug auf die Fluidquelle (Einaudi et al. 1981). Die Skarnalteration erfolgt entlang lithologischer Kontakte und/oder tektonischer Strukturen und wird von meteorischen Wässern beeinflusst (Einaudi et al. 1981). Die assoziierte Paragenese zeichnet sich durch Minerale mit eisen- und insbesondere manganreicher Zusammensetzung sowie durch eine starke retrograde Verskarnung aus. Diese späte Alterationsphase trägt wesentlich zur Bildung von Buntmetallsulfiden bei. Insbesondere in Systemen mit hochfraktionierten S- und A-Typ-Graniten kann Indium in bedeutenden Mengen in Sphalerit eingebaut werden (Schwarz-Schampera und Herzig 2000). Die Vorkommen von Waschleithe und Gelbe Birke im östlichen Erzgebirge sind distale polymetallische Skarne. Aufgrund der komplexen und mehrphasigen Natur sind einige andere Vorkommen schwer zu klassifizieren, da sie Merkmale mehrerer Skarntypen aufweisen. Die meisten davon können als intermediäre bis distale Zinn-Zink-Skarne eingestuft werden.

3.4 Vergleich mit anderen zinnführenden Skarnen

Skarnsysteme mit Zinn-Mineralisierung kommen weltweit in Zinn-Gürteln vor, unter anderem in Großbritannien (Cornwall und Devon), Malaysia, Australien, Kanada und China (Chang et al. 2019; Einaudi et al. 1981; Jackson et al. 1989; Kwak 1987; Layne und Spooner 1991; Ray 2013).

Die Skarne des Erzgebirges sind mit denen des Kornischen Erzreviers vergleichbar, dessen Vorkommen ebenfalls zur Gruppe der polyphasigen, intermediären bis distalen Zinn-Zink-Indium-Skarne gezählt werden können. Sie haben das variszische Alter, die tektono-metamorphe Entwicklung und die Intrusion hochdifferenzierter Zinn-Wolfram-Lithium-assoziierter Granite in metasedimentären Lithologien gemeinsam (Anderson et al. 2016; Jackson et al. 1989; Moscati und Neymark 2020; Shail und Leveridge 2009). Weiterhin zeigt die Verskarnung auffällige Parallelen, darunter die Bildung früher, nicht-mineralisierter Skarnoide in Folge einer Kontaktmetamorphose (lokal als „Calc-Flintas“ bekannt; Alderton und Jackson 1978; van Marcke de Lummen 1986) und die anschließende Überprägung durch metasomatische Skarne.

Die polymetallische metasomatische Skarnalteration in Cornwall und Devon erfolgte mehrphasig in Verbindung mit Granitintrusionen und zeigt eine Wolfram-Zinn-Arsen-Kupfer-Zink-Vererzung, die mit Greisen und pneumatolytischen Gängen assoziiert ist (Simons et al. 2017). Demnach weisen die Kornischen Skarne ein höheres Kupfer/Zink-Verhältnis auf als die Erzgebirgsskarne und enthalten mehr Bor und Beryllium als die fluordominierten Skarne in Deutschland und Tschechien. Diese Variationen reflektieren wahrscheinlich unterschiedliche geochemische Eigenschaften der ursächlichen Intrusionen und ihrer Quellen (Förster et al. 1999; Jackson et al. 1989; Štemprok 1995).

Weltweit sind zinndominierte Skarne mit S- und A-Typ-Graniten assoziiert, die in einem post-kollisionalen Umfeld entstanden sind (Aleksandrov 2010; Brown et al. 1984; Chen et al. 1992; Ray 2013). Die Intrusionen variieren in ihrer Zusammensetzung, sind jedoch typischerweise peralumisch, leukokrat und enthalten Lithium-Glimmer (Einaudi et al. 1981; Kwak 1987; Ray 2013).

In solchen geologischen Umfeldern tritt die Skarnalteration hauptsächlich in Form von Exoskarnen auf, während die Greisenalteration in kontaktnahen Bereichen des Granits dominiert (Einaudi et al. 1981; Aleksandrov 2010; Kwak und Askin 1981; Meinert 2005). In einigen Skarnsystemen wie Mt. Garnet, Lost River oder den JC-Tin-Skarnen bildete sich Kassiterit bereits in der progradem metasomatischen Entwicklungsphase. Eine solch frühe Kassiterit-Bildung tritt im Erzgebirge nur in bestimmten Bereichen des Hämmerlein-Skarns auf (Korges et al. 2020). Ein großer Teil des Zinns ist in Kalksilikatmineralen gebunden und damit nicht wirtschaftlich aufzubereiten. Erst die nachfolgende Verdrängung dieser Minerale durch nominell zinnfreie Phasen führt zur Freisetzung von Zinn und zur anschließenden Ausfällung von Kassiterit oder Stannit. Hinzu kommt Kassiterit, der direkt aus dem zinnhaltigen Fluid kristallisiert. Solch eine umfangreiche retrograde Alteration ist ein typisches Merkmal intermediärer bis distaler

Zinn-Skarne weltweit (Eadington und Kinealy 1983; Einaudi et al. 1981; Kern et al. 2019; Kwak 1987; Meinert et al. 2005; Ray et al. 2000).
Für die meisten zinnhaltigen Skarne in der Nanling-Region in Südchina wird eine enge Verbindung zwischen Zinn und Buntmetallen angenommen (Chang et al. 2019). Zinn- sowie Silber-Blei-Zink-Vererzungen bilden sich dort aus einem einzigen homogen zusammengesetzten Fluid, wobei die beobachtete Metallzonierung ausschließlich durch Abkühlung gesteuert wird (Li et al. 2022). Im Erzgebirge zeigt das Greisensystem von Sadisdorf eine ähnliche Signatur (Leopardi et al. 2024b), während ein solche homogenes Fluid für Skarne des Erzgebirges bisher nicht belegt ist.

4. Fazit

Skarngebundene, niedriggradige, aber großvolumige Rohstoffvorkommen im Erzgebirge stellen eine noch wenig erschlossene Quelle für Zinn, Wolfram, Indium und andere kritische Elemente innerhalb der Europäischen Union dar, welche zur Rohstoffsicherheit in Deutschland beitragen könnte. Ihre Petrogenese sowie die zeitliche und räumliche Affiliation zu den granitischen Intrusionen des Erzgebirges sind lange umstritten gewesen. Erst die Kombination von petrographischen Beobachtungen auf mehreren Skalen, ortsaufgelösten mineralchemischen Analysen, Untersuchungen von Fluideinschlüssen und Uran-Blei-Datierungen an Skarn- und Erzmineralen am Zinn-System Geyer führte zu einem umfassenden und widerspruchsfreien Lagerstättenmodell, das generalisiert auch auf andere zinnführende Skarnsysteme übertragen werden kann. Für Geyer konnte ein Zusammenhang zwischen der ersten Verskarnungsphase und der Intrusion des Ehrenfriedersdorf-Batholiths vor 320 Millionen Jahren gezeigt werden. Dabei entstanden bei Temperaturen von 450–470 °C in 2,5–4 km Tiefe unter lithostatischen Drücken in einem gesteinsgepufferten Milieu Skarnoide, die überwiegend kontaktmetamorph beeinflusst sind und keine Vererzungen oder erhöhten Gehalte an Zinn aufweisen. Der Großteil der Zinnvererzung ist jedoch mit einem deutlich jüngeren magmatisch-hydrothermalen Ereignis zwischen 308,2 ± 3,7 und 301,6 ± 5,0 Millionen Jahren assoziiert, bei welchem metasomatische Skarne mit einer prograden und einer retrograden Phase, Greisen sowie pneumatolytische Gänge entstanden. Die ersten Skarne bildeten sich bei circa 350 °C unter hydrostatischen Drücken in einer Tiefe von 1,5–2 km. Im weiteren Verlauf kühlten die hydrothermalen Fluide ab und unterliefen einer Phasenseparation. Anfangs war Zinn dabei noch in Kalksilikatmineralen gebunden, konnte jedoch durch spätere Überprägungen remobilisiert und als Kassiterit wiederausgefällt werden. Die retrograde Phase war durch einen hauptsächlich fluidgepufferten Charakter geprägt, was sich in aderförmigen Mineralparagenesen ausdrückt. Im Wesentlichen beeinflusste die unterschiedliche Pufferung die Textur sowie die chemische Zusammensetzung der Minerale. Änderungen im Verhältnis zwischen Gesteins- und Fluidpufferung waren dabei eine direkte Reaktion auf die diskontinuierlich aus der Intrusion ausgetretenen Fluidpulse. Die durchgängig hohen Konzentrationen von Zinn, Wolfram und Indium in Mineralen, die bei Dominanz von Fluidpufferung gebildet wurden, stützen die Annahme, dass diese Wertmetalle vom magmatisch-hydrothermalen Fluid eingebracht wurden, und sprechen gegen eine Remobilisierung aus den Metasedimentiten der Umgebung.

Diese Erkenntnisse lassen sich auf zahlreiche Skarnvorkommen des Erzgebirges und darüber hinaus übertragen. So ist eine bimodale Verteilung von unvererzten Skarnoiden und mineralisierten metasomatischen Skarnen im Erzgebirge üblich und in Cornwall wahrscheinlich. Ferner zeichnet sich ab, dass das Einbringen von Zinn in die Lagerstätten im Rahmen der Intrusion post-kollisionaler Granite erfolgt und nicht an großvolumige Batholithe gebunden ist.

Damit diese Annahmen und petrographischen Beobachtungen bestätigt werden können sind detaillierte Studien zur chemischen Zusammensetzung der Minerale sowie weitere Fluideinschlussuntersuchungen erforderlich. Zudem sind, präzise Altersdaten für andere Skarnsysteme unabdingbar, um zeitliche und genetische Aspekte der Alterationen und Vererzungen in Einklang zu bringen und um eine weitergehende Generalisierung des Modells vornehmen zu können.

Literaturverzeichnis

Alderton DHM, Jackson NJ (1978) Discordant calc-silicate bodies from the St. Just aureole, Cornwall. Mineral Mag 42:427–434. https://doi.org/10.1180/minmag.1978.042.324.03

Aleksandrov SM (2010) Skarn-greisen deposits of the lost river and mount ear ore field, Seward Peninsula, Alaska, United States. Geochem Int 48:1220-1236. https://doi.org/10.1134/S0016702910120062

Aleksandrov SM, Troneva MA (2007) Composition, mineral assemblages, and genesis of titanite and malayaite in skarns. Geochem Int 45:1012–1024. https://doi.org/10.1134/S0016702907100059

Amthauer G, Annersten H, Hafner SS (1976) The Mössbauer spectrum of ^{57}Fe in silicate garnets. Z Krist 143:14–55. https://doi.org/10.1524/zkri.1976.143.jg.14

Andersen JC, Stickland RJ, Rollinson GK, Shail RK (2016). Indium mineralisation in SW England: host parageneses and mineralogical relations. Ore Geol Rev 78:213-238. https://doi.org/10.1016/j.oregeorev.2016.02.019

Armbruster T, Bonazzi P, Akasaka M, Bermanec V, Chopin Ch, Gieré R, Heuss-Assbichler S, Liebscher A, Menchetti S, Pan Y, Pasero M (2006) Recommended nomenclature of epidote-group minerals. European Journal of Mineralogy 18 (5): 551–567. https://doi.org/10.1127/0935-1221/2006/0018-0551

Audétat A, Günther D, Heinrich CA (2000). Causes for large-scale metal zonation around mineralized plutons: Fluid inclusion LA-ICP-MS evidence from the Mole Granite, Australia. Econ Geol 95(8):1563-1581. https://doi.org/10.2113/gsecongeo.95.8.1563

Ayers JC, Eggler DH (1995) Partitioning of elements between silicate melt and H_2O-NaCl fluids at 1.5 and 2.0 GPa pressure: implications for mantle metasomatism. Geochim Cosmochim Acta 59:4237–4246. https://doi.org/10.1016/0016-7037(95)00244-T

Bai TB, Koster van Koster AF (1999) The distribution of Na, K, Rb, Sr, Al, Ge, Cu, W, Mo, La, and Ce between granitic melts and coexisting aqueous fluids. Geochim Cosmochim Acta 63:1117–1131. https:// doi.org/10.1016/S0016-7037(98)00284-1

Bauer ME, Seifert T, Burisch M, Krause J, Richter N, Gutzmer J (2019) Indium-bearing sulfides from the Hämmerlein skarn deposit, Erzgebirge, Germany: evidence for late-stage diffusion of indium into sphalerite. Miner Deposita 54:175–192. https://doi.org/10.1007/s00126-017-0773-1

Bau M (1996) Controls on the fractionation of isovalent trace elements in magmatic and aqueous systems: evidence from Y/Ho, Zr/Hf, and lanthanide tetrad effect. Contrib Mineral Petrol 123:323–333. https://doi.org/10.1007/s004100050159

Bau M, Dulski P (1995) Comparative study of yttrium and rare-earth element behaviour in fluorine-rich hydrothermal fluids. Contrib Mineral Petrol 119:213–223. https://doi.org/10.1007/ BF00307282

Bertelli M, Baker T, Cleverley JS, Ulrich T (2009) Geochemical modelling of a Zn–Pb skarn: constraints from LA–ICP–MS analysis of fluid inclusions. J Geochem Expl 102:13–26. https://doi.org/ 10.1016/j.gexplo.2008.11.015

Bolduan H (1963) Geologie und Genese der Zinn-Wolframlagerstätte Geyer (Erzgeb.). Freiberger Forsch-Hefte C 167:7–34.

Breiter K (2012) Nearly contemporaneous evolution of the A- and S-type fractionated granites in the Krušné hory/Erzgebirge Mts., Central Europe. Lithos 151:105–121. https://doi.org/10.1016/j.lithos.2011.09.022

Breiter K, Förster H-J, Seltmann R (1999) Variscan silicic magmatism and related tin-tungsten mineralization in the Erzgebirge-Slavkovský les metallogenic province. Miner Deposita 34:505–521. https://doi.org/ 10. 1007/ s0012 60050 217

Brosig A, Barth A, Knobloch A, Dickmayer E (2020) Rohstoffprognosen für Zinn, Wolfram, Fluss-und Schwerspat im Mittelerzgebirge. Bergbau in Sachsen, 19. Sächsisches Druck- und Verlagshaus GmbH, Dresden.

Brown WM, Kwak TAP, Askins PW (1984) Geology and geochemistry of a F-Sn-W skarn system—The Hole 16 deposit, Mt Garnet, North Queensland, Australia. Journal of the

Geological Society of Australia, 31(3):317-340. https://doi.org/10.1080/14400958408527934
Bubal J, Dolejš D (2013) Magnetite chemistry in skarns of the Bohemian Massif: evaluating competing effects of protolith inheritance, crystal chemistry, fluid composition and pressure-temperature conditions. Proceedings 12th SGA Biennial Meeting 1:264-267.
Burisch M, Gerdes A, Meinert LD, Albert R, Seifert T, Gutzmer J (2019) The essence of time – fertile skarn formation in the Variscan orogenic belt. Earth Planet Sci Lett 519:165–170. https://doi. org/10.1016/j.epsl.2019.05.015
Burisch M, Frenzel M, Seibel H, Gruber A, Oelze M, Pfänder JA, Sanchez-Garrido C, Gutzmer J (2021) Li-Co–Ni-Mn-(REE) veins of the Western Erzgebirge, Germany—a potential source of battery raw materials. Miner Deposita 56:1223-1238. https://doi.org/10.1007/s00126-021-01061-4
Burisch M, Markl G, and Gutzmer J (2022) Breakup with benefits-hydrothermal mineral systems related to the disintegration of a supercontinent: Earth and Planetary Science Letters 580:117373. https://doi.org/10.1016/j.epsl.2022.117373
Burisch M, Bussey SD, Landon N, Nasi C, Kakarieka A, Gerdes A, Albert R, Stein HJ, Gabites JA, Friedman RM (2023) Timing of magmatism and skarn formation at the Limon, Guajes, and Media Luna gold±copper skarn deposits at Morelos, Guerrero State, Mexico. Econ Geol 118:695-718. https://doi.org/10.5382/econgeo.4985
Casas-García R, Rapprich V, Repstock A, Magna T, Schulz B, Kochergina YVE, Breitkreuz C (2021) Crustal vs. mantle contributions in the Erzgebirge/Krušne hory Mts. magmatism: Implications for generation of zoned, A-type silicic rocks in the late-Variscan Altenberg-Teplice Caldera, Central Europe. Lithos. https://doi.org/10.1016/j.lithos.2021.106429
Cathelineau M (1988) Cation site occupancy in chlorites and illites as a function of temperature. Clay Miner 23(4):471–485. doi:10.1180/claymin.1988.023.4.13
Chang Z, Shu Q, Meinert LD (2019) Skarn deposits in China. In: Mineral deposits of China. 6: 189-234. https://doi.org/10.5382/SP.22.06
Chen J, Halls C, Stanley CJ (1992) Tin-bearing skarns of South China: geological setting and mineralogy. Ore Geol Rev 7:225–248. https://doi.org/10.1016/0169-1368(92)90006-7
Chou I-M, Wang R, Fang J (2021) In situ redox control and Raman spectroscopic characterisation of solutions below 300 °C. Geochem Persp Lett 1–5. https://doi.org/10.7185/geochemlet.213
Chu G, Chen H, Zhang S, Zhang Y, Cheng J (2023) Geochemistry and geochronology of multi-generation garnet: new insights on the genesis and fluid evolution of prograde skarn formation. Geosci Front 14:101495. https://doi.org/10.1016/j.gsf.2022.101495
Corfu F, Davis DW (1991) Comment on Archean hydrothermal zircon in the Abitibi greenstone belt: constraints on the timing of gold mineralization by Claoué-Long JC, King RW, Kerrich R Earth Planet Sci Lett 104:545–552. https://doi. org/10.1016/0012-821X(91)90229-B
Deer WA, Howie RA, Zussman J (2013) An introduction to the rockforming minerals. The Mineralogical Society, London.
Dipple GM, Gerdes ML, Lentz D (1998) Reaction-infiltration feedback and hydrodynamics at the skarn front. Mineralized intrusion-related skarn systems. Mineralogical Association of Canada Short Course 26:71-97.
Douville E, Bienvenu P, Charlou JL, Donval JP, Fouquet Y, Appriou P, Gamo T (1999) Yttrium and rare earth elements in fluids from various deep-sea hydrothermal systems. Geochim Cosmochim Acta 63:627–643. https://doi.org/10.1016/S0016-7037(99)00024-1
Driesner T, Heinrich CA (2007) The system H2O–NaCl. Part I: correlation formulae for phase relations in temperature–pressure– composition space from 0 to 1000 °C, 0 to 5000 bar, and 0 to 1 XNaCl. Geochim Cosmochim Acta 71:4880–4901. https://doi.org/10.1016/j.gca.2006.01.033

Eadington PJ, Kinealy K (1983) Some aspects of the hydrothermal reactions of tin during skarn formation. J Geol Soc Aust 30:461-471. https://doi.org/10.1080/00167618308729270
Einaudi MT, Meinert LD, Newberry RJ (1981) Skarn deposits: Economic Geology, 75. Anniversary Volume 317-391.
Elongo V, Lecumberri-Sanchez P, Legros H, Falck H, Adlakha E, Roy-Garand A (2020) Paragenetic constraints on the Cantung, Mactung and Lened tungsten skarn deposits, Canada: Implications for grade distribution. Ore Geol Rev 125:103677. https://doi.org/10.1016/j.oregeorev.2020.103677
Elsner H (2014) Zinn - Angebot und Nachfrage bis 2020, 2014th edn. DERA Rohstofnformationen, 20. DERA, Berlin.
Förster H-J, Tischendorf G, Trumbull RB, Gottesmann B (1999) Late-collisional granites in the Variscan Erzgebirge, Germany. J Petrol 40:1613–1645. https://doi.org/10.1093/petroj/40.11.1613
Förster HJ, Romer RL, Gottesmann B, Tischendorf G, Rhede D (2009) Are the granites of the Aue-Schwarzenberg Zone (Erzgebirge, Germany) a major source for metalliferous ore deposits? A geochemical, Sr-Nd-Pb isotopic, and geochronological study. N Jb Mineral Abh 186:163–184. https://doi.org/10.1127/0077-7757/2009/0138
Franke W, Żelaźniewicz A (2023) Variscan Evolution of the Bohemian Massif (Central Europe): fiction, facts and problems. Gondwana Res 124:351-377. https://doi.org/10.1016/j.gr.2023.06.012
Gao X, Yang L-Q, Yan H, Meng J-Y (2020) Ore-forming processes and mechanisms of the Hongshan Skarn Cu–Mo deposit, South-west China: insights from mineral chemistry, fluid inclusions, and stable isotopes. Ore Energy Resource Geol 4–5:100007. https:// doi.org/10.1016/j.oreoa.2020.100007
Gaspar M, Knaack C, Meinert LD, Moretti R (2008) REE in skarn systems: a LA-ICP-MS study of garnets from the Crown Jewel gold deposit. Geochim Cosmochim Acta 72:185–205. https://doi. org/10.1016/j.gca.2007.09.033
Guilcher M, Albert R, Gerdes A, Gutzmer J, Burisch M (2021) Timing of native metal-arsenide (Ag-Bi-Co-Ni-As±U) veins in continental rift zones – In situ U-Pb geochronology of carbonates from the Erzgebirge/Krušné Hory province. Chem Geol 584:120476. https://doi.org/10.1016/j.chemgeo.2021.120476
Guilcher M, Gutzmer J, Hiller A, Krause J, Blamey N, Härtel B, Burisch M (2024) The Origin of Native Metal-Arsenide Mineralization in the World-Class Schlema-Alberoda Uranium Deposit (Germany): Insights from Arsenide Compositions and Fluid Inclusion Characteristics. Econ Geol 119(6):1329-1354. https://doi.org/10.5382/econgeo.5090
Hantsche AL, Kouzmanov K, Milenkov G, Vezzoni S, Vassileva R, Dini A, Sheldrake T, Laurent O, Guillong M (2021) Metasomatism and cyclic skarn growth along lithological contacts: physical and geochemical evidence from a distal Pb-Zn skarn. Lithos 400–401. https://doi.org/10.1016/j.lithos.2021.106408
Heinrich CA (1990) The chemistry of hydrothermal tin(-tungsten) ore deposition. Econ Geol 85:457–481. https://doi.org/10.2113/gseco ngeo.85.3.457
Hiller A, Schuppan W (2008) Geologie und Uranbergbau im Revier Schlema-Alberoda. Bergbau in Sachsen, 14. Sächsisches Landesamt für Umwelt, Landwirtschaft und Geologie, Dresden. ISBN 978-3-9811421-3-6
Hiller A, Schuppan W (2016) Das Lagerstättengebiet Zobes-Bergen im Vogtland und benachbarte Uranvorkommen im Bereich des Bergener Granitmassivs. Bergbau in Sachsen, 18. Sächsisches Landesamt für Umwelt, Landwirtschaft und Geologie, Dresden. ISBN 978-3-9811421-5-0
Hofmann U, Breitkreuz C, Breiter K, Sergeev S, Stanek K, Tichomirowa M (2013) Carboniferous–Permian volcanic evolution in Central Europe—U/Pb ages of volcanic rocks in Saxony (Germany) and northern Bohemia (Czech Republic). Int J Earth Sci (Geol Rundsch) 102:73–99. https://doi.org/10.1007/s00531-012-0791-2
Hösel G (1994) Das Zinnerz-Lagerstättengebiet Ehrenfriedersdorf/ Erzgebirge. Bergbau in Sachsen, 1. Sächsisches Druck- und Verlagshaus GmbH, Dresden.

Hösel G (2003) Die polymetallische Skarnlagerstätte Pöhla-Globenstein. Bergbau in Sachsen, 8. Sächsisches Druck- und Verlagshaus GmbH, Dresden.
Hösel G, Fritsch E, Josiger U, Wolf P (1996) Das Lagerstättengebiet Geyer. Bergbau in Sachsen, 4. Sächsisches Druck- und Verlagshaus GmbH, Dresden.
Hoth K, Lorenz W (1966) Die skarnhöffigen Horizonte des westlichen Erzgebirges (Geologische Fragen der Skarnprognose im Erzgebirge - Teil 1). Geologie: Zeitschrift für das Gesamtgebiet der Geologischen Wissenschaften 15 (7):769–799.
Hoth K., Krutsky N, Schilka W, Schellenberg F (2010) Marmore im Erzgebirge. Bergbau in Sachsen, 16. Sächsisches Landesamt für Umwelt, Landwirtschaft und Geologie, Dresden
Jackson NJ, Willis-Richards J, Manning DA, Sams MS (1989) Evolution of the Cornubian ore field, Southwest England; Part II, Mineral deposits and ore-forming processes. Economic Geology, 84(5):1101-1133. https://doi.org/10.2113/gsecongeo.84.5.1101
Jamtveit B, Hervig RL (1994) Constraints on transport and kinetics in hydrothermal systems from zoned garnet crystals. Science 263:505–508. https://doi.org/10.1126/science.263.5146.505
Jamtveit B, Wogelius RA, Fraser DG (1993) Zonation patterns of skarn garnets: records of hydrothermal system evolution. Geology 21(2):113-116. https://doi.org/10.1130/0091-7613(1993)021%3C0113:ZPOSGR%3E2.3.CO;2
Kempe U, Bombach K, Matukov D, Schlothauer T, Hutschenreuter J, Wolf D, Sergeev S (2004) Pb/Pb and U/Pb zircon dating of sub-volcanic rhyolite as a time marker for Hercynian granite magmatism and Sn mineralisation in the Eibenstock granite, Erzgebirge, Germany: considering effects of zircon alteration. Miner Deposita 39:646–669. https://doi.org/10.1007/s00126-004-0435-y
Kern M, Kästner J, Tolosana-Delgado R, Jeske T, Gutzmer J (2019) The inherent link between ore formation and geometallurgy as documented by complex tin mineralization at the Hämmerlein deposit (Erzgebirge, Germany). Miner Deposita 54:683–698. https://doi.org/10.1007/s00126-018-0832-2
Korges M, Weis P, Lüders V, Laurent O (2020) Sequential evolution of Sn–Zn–In mineralization at the skarn-hosted Hämmerlein deposit, Erzgebirge, Germany, from fluid inclusions in ore and gangue minerals. Miner Deposita 55:937–952. https://doi.org/10.1007/ s00126-019-00905-4
Kossmat F (1927) Gliederung des varistischen Gebirgsbaues. Abh Sächs Geol L.-A. 1: 39
Kröner A, Willner AP (1998) Time of formation and peak of Variscan HP-HT metamorphism of quartz-feldspar rocks in the central Erzgebirge, Saxony, Germany. Contrib Mineral Petrol 132:1–20. https://doi.org/10.1007/s004100050401
Kühne R, Wasternack J, and Schulze H (1972) Fortschritte der Metallogenie im Erzgebirge: Postmagmatische Metasomatose im Endo-Exokontakt der jüngeren postkinematischen Granite des Erzgebirges: Geologie 21:494-520.
Kuschka E, Hahn W. (1996) Flußspatlagerstätten des SW-Vogtlandes: Schönbrunn, Bösenbrunn, Wiedersberg. Bergbau in Sachsen, 2. Sächsisches Druck- und Verlagshaus GmbH, Dresden
Kwak, TAP (1987) W-Sn skarn deposits and related metamorphic skarns and granitoids. Developments in Economic Geology, 24. Elsevier, Amsterdam, 451 pp. ISBN 0-444-42820-8
Kwak TAP, Askins PW (1981) Geology and genesis of the F-Sn-W (-Be-Zn) skarn (wrigglite) at Moina, Tasmania. Econ Geo 76(2):439-467. https://doi.org/10.2113/gsecongeo.76.2.439
Layne GD, Spooner ETC (1991) The JC tin skarn deposit, southern Yukon Territory; I, Geology, paragenesis, and fluid inclusion microthermometry. Econ Geol 86(1):29–47. https://doi.org/10.2113/gsecongeo.86.1.29
Legler C (1985) Die schichtgebundenen Mineralisationen des Erzgebirges. – Freiberger Forsch.-H., C 401, 93 S. Leipzig.
Lefebvre MG, Romer RL, Glodny J, Kroner U, Roscher M (2019) The Hämmerlein skarn-hosted polymetallic deposit and the Eibenstock granite associated greisen, western

Erzgebirge, Germany: two phases of mineralization—two Sn sources. Miner Deposita 54:193–216. https://doi.org/10.1007/s00126-018-0830-4
Legler C, Baumann L (1983) Bildungsmöglichkeiten kalksilikatischer Erzlagerstätten – ein Beitrag zur Skarnproblematik. – Z. geol. Wiss., 11: 1417-1442, Berlin.
Lehmann B (1990) Metallogeny of tin. Springer, p 211.
Lehmann B (2021) Formation of tin ore deposits: a reassessment. Lithos 402-403:105756. https://doi.org/10.1016/j.lithos.2020.105756
Lehmann B, Seltmann R (1995) Der Übergangsbereich Pegmatit-/ Aplit- in Hydrothermal-Systeme am Beispiel Ehrenfriedersdorf/ Erzgebirge: Abschlußbericht zum DFG-Projekt Le 578/7–1 und Se 594/3–1 (Scientific Technical Report; 95/20).
Leopardi D, Gerdes A, Albert R, Gutzmer J, Lehmann B, and Burisch M (2024a) LA-ICP-MS U-Pb cassiterite age data of the Sadisdorf deposit link Sn-Li-(W-Cu) mineralization in the eastern Erzgebirge to the collapse of the Altenberg-Teplice Caldera: Geochemistry, p. 126038. https://doi.org/10.1016/j.chemer.2023.126038
Leopardi D, Gutzmer J, Lehmann B, Burisch M (2024b) The Spatial and Temporal Evolution of the Sadisdorf Li-Sn-(W-Cu) Magmatic-Hydrothermal Greisen and Vein System, Eastern Erzgebirge, Germany. Econ Geol 119(4):771-803. https://doi.org/10.5382/econgeo.5077
Li YJ, Zhang RQ, Ji H, Wang C, Tan J, Wei JH (2022) Chemistry and U–Pb geochronology of cassiterite in the Xiasai deposit, central Yidun Terrane (SW China): Link between Sn and Ag–Pb–Zn mineralisation. Ore Geol Rev 149. https://doi.org/10.1016/j.oregeorev.2022.105106
Liu X, Yu P, Xiao C (2023) Tin transport and cassiterite precipitation from hydrothermal fluids. Geosci Front 14:101624. https://doi. org/10.1016/j.gsf.2023.101624
Löcse F, Schneider G, Linnemann U, Rößler R (2023) Carboniferous– Permian volcanic evolution in the mid-European Variscides: U-Pb LA-ICP-MS zircon ages, geochemical and petrographical constraints from the NW Saxonian Volcanic Basin (Germany). Z Dt Ges Geowiss 174:7–30. https://doi.org/10.1127/zdgg/2023/0359
Makarevič W, Fritsch E, Velickin W, Kargatev W, Ivanov I, Serov B, Nasarov WG, Lohrmann H (1976) Über die Ergebnisse der geologischen Erkundungsarbeiten im Bereich der Lagerstätte Geyer einschließlich der Vorratsberechnung auf Zinn mit Stand vom 1. Juli 1976. Internal report, SDAG Wismut Chemnitz.
van Marcke de Lummen G (1986) Tin-bearing epidote from skarn in the Land's End aureole, Cornwall, England. The Canadian Mineralogist:411–415.
Marks MAW, Coulson IM, Schilling J, Jacob DE, Schmitt AK, Markl G (2008) The effect of titanite and other HFSE-rich mineral (Ti-bearing andradite, zircon, eudialyte) fractionation on the geochemical evolution of silicate melts. Chem Geol 257:153–172. https://doi.org/10.1016/j.chemgeo.2008.09.002
McDonough WF, Sun SS (1995) The composition of the Earth. Chem Geol 120(3–4):223–253 McLennan SM (1989) Chap. 7. Rare Earth elements in sedimentary rocks. Influence of provenance and sedimentary processes. In: Lipin BR, McKay GA (Eds.) Geochemistry and Mineralogy of Rare Earth Elements. De Gruyter, 169–200.
Meinert LD (1992) Skarns and Skarn deposits. Geosci Can 19:145–162.
Meinert LD, Dipple GM, Nicolescu S (2005) World skarn deposits. In: Hedenquist JW, Thompson JFH, Goldfarb RJ, Richards JP (eds) One Hundredth Anniversary Volume. Society of Economic Geologists, pp 299–336.
Meyer N, Markl G, Gerdes A, Gutzmer J, Burisch M (2024) Timing and origin of skarn-, greisen-, and vein-hosted tin mineralization at Geyer, Erzgebirge (Germany). Miner Deposita 59:1-22. https://doi.org/10.1007/s00126-023-01194-8
Meyer N, Burisch M, Gutzmer J, Krause J, Scheibert H, Markl G (2025). Mineral chemistry of the Geyer SW tin skarn deposit: understanding variable fluid/rock ratios and metal fluxes. Miner Deposita, 1-27. https://doi.org/10.1007/s00126-024-01297-w
Möller P, Dulski P, de Lucia M (2021) REY patterns and their natural anomalies in Waters and Brines: the correlation of Gd and Y anomalies. Hydrology 8:116. https://doi.org/10.3390/hydrology8030116

Moscati RJ, Neymark LA (2020) U–Pb geochronology of tin deposits associated with the Cornubian Batholith of southwest England: Direct dating of cassiterite by in situ LA-ICPMS. Miner Deposita, 55(1):1-20. https://doi.org/10.1007/s00126-019-00870-y
Ni P, Pan JY, Han L, Cui JM, Gao Y, Fan MS, Li WS, Chi Z, Zhang KH, Cheng ZL, Liu YP. (2023) The tungsten and tin deposits in South China: temporal and spatial distribution, metallogenic models and prospecting directions. Ore Geol Rev 157:105453. https://doi.org/10.1016/j.oregeorev.2023.105453
Ondrus P, Veselovsky F, Gabasova A, Hlousek J, Srein V (2003) Geology and hydrothermal vein system of the Jachymov (Joachimsthal) ore district. J Geosci 48:3–18.
Öztürk YY, Helvacı C, Satır M (2008) The influence of meteoric water on skarn formation and late-stage hydrothermal alteration at the Evciler skarn occurrences, Kazdağ, NW Turkey. Ore Geol Rev 34:271–284. https://doi.org/10.1016/j.oregeorev.2008.01.001
Park C, Song Y, Kang IM, Shim J, Chung D, Park C-S (2017a) Metasomatic changes during periodic fluid flux recorded in grandite garnet from the Weondong W-skarn deposit, South Korea. Chem Geol 451:135–153. https://doi.org/10.1016/j.chemgeo.2017.01.011
Park C, Choi W, Kim H, Park MH, Kang I-M, Lee H-S, Song Y (2017b) Oscillatory zoning in Skarn Garnet: implications for tungsten ore exploration. Ore Geol Rev 89:1006–1018. https:// doi.org/10.1016/j.oregeorev.2017.08.003
Pälchen, W., Walter, H. (2008). Geologie von Sachsen. Schweizerbart, Stuttgart.
Pauliš P, Haake R (1991) Die Mineralien der Skarnlagerstätte Měděnec (Kupferberg) im Erzgebirge (ČSFR). Mineralien Welt 5:19-29.
Pauliš P, Vrtiška L, Sejkora J, Malíková R, Hloušek J, Dvořák Z, Gramblička R, Pour O, Ludvík, J (2015) Supergene mineralization of the skarn tin deposit Zlatý Kopec in the Krušné hory Mts. (Czech Republic). Bulletin Mineralogie Petrologie, 23(2):182-200.
Pfeiffer L, Schützel H (1969) Skarnparagenesen des Erzgebirges. – Freiberger Forsch.-H., C 266: 65-75, Leipzig.
Plimer IR (1984) Malayaite and tin-bearing silicates from a skarn at Doradilla via Bourke, New South Wales. Aust J Earth Sci 31:147–153. https://doi.org/10.1080/08120098408729286
Raimbault L, Azencott C (1987) Géochimie Des éléments majeurs et traces du granite a métaux rares de beauvoir (Sondage GPF, échassieres). Géologie de la France 2–3:189–198.
Ray, G. E. (2013). Skarns of the Canadian Cordillera: British Columbia Ministry of Energy and Mines. British Columbia Geological Survey Paper, 11, 112.
Reinhardt N, Frenzel M, Meinert LD, Gutzmer J, Kürschner T, Burisch M (2021) Mineralogy and fluid characteristics of the Waschleithe Zn skarn – a distal part of the Schwarzenberg mineral system, Erzgebirge Germany. Ore Geol Rev 131:104007. https://doi.org/ 10.1016/j.oregeorev.2021.104007
Reinhardt N, Gerdes A, Beranoaguirre A, Frenzel M, Meinert LD, Gutzmer J, Burisch M (2022) Timing of magmatic-hydrothermal activity in the Variscan orogenic belt: LA-ICP-MS U–Pb geochronology of skarn-related garnet from the Schwarzenberg District, Erzgebirge. Miner Deposita 57:1071–1087. https://doi.org/10. 1007/s00126-021-01084-x
Røhr TS, Austrheim H, Erambert M (2007) Stress-induced redistribution of yttrium and heavy rare-earth elements (HREE) in garnet during high-grade polymetamorphism. Amer Min 92:1276–1287. https://doi.org/10.2138/am.2007.2479
Romer RL, Kroner U (2016) Phanerozoic tin and tungsten mineralization—tectonic controls on the distribution of enriched protoliths and heat sources for crustal melting. Gondwana Res 31:60–95. https://doi.org/10.1016/j.gr.2015.11.002
Romer RL, Cuney M (2018) Phanerozoic uranium mineralization in Variscan Europe–more than 400 Ma of tectonic, supergene, and climate-controlled uranium redistribution. Ore Geol Rev 102:474-504. https://doi.org/10.1016/j.oregeorev.2018.09.013

Romer RL, Thomas R, Stein HJ, Rhede D (2007) Dating multiply overprinted Sn-mineralized granites—examples from the Erzgebirge, Germany. Miner Deposita 42:337–359. https://doi.org/10.1007/ s00126-006-0114-2
Romer RL, Förster HJ, Štemprok M (2010) Age constraints for the late-Variscan magmatism in the Altenberg-Teplice Caldera (Eastern Erzgebirge/Krusne hory). Neues Jahrbuch fur Mineralogie-Abhandlungen, 187(3):289. https://doi.org/10.1127/0077-7757/2010/0179
Romer RL, Förster HJ, Glodny J (2022) Role of fractional crystallization, fluid-melt separation, and alteration on the Li and B isotopic composition of a highly evolved composite granite pluton: The case of the Eibenstock granite, Erzgebirge, Germany. Lithos, 422:106722. https://doi.org/10.1016/j.lithos.2022.106722
Schmidt C (2018) Formation of hydrothermal tin deposits: Raman spectroscopic evidence for an important role of aqueous Sn(IV) species. Geochim Cosmochim Acta 220:499–511. https://doi.org/10.1016/j.gca.2017.10.011
Schuppan W, Hiller A (2012) Die Komplexlagerstätten Tellerhäuser und Hämmerlein: Uranbergbau und Zinnerkundung in der Grube Pöhla der SDAG Wismut. Bergbau in Sachsen, 17. Sächsisches Landesamt für Umwelt, Landwirtschaft und Geologie, Dresden.
Schwarz-Schampera U, Herzig PM (2000) Indium: geology, mineralogy and economics. Springer-Verlag, Berlin. https://doi.org/10.1002/9781118755341.ch9
Shail RK, Leveridge BE (2009) The Rhenohercynian passive margin of SW England: Development, inversion and extensional reactivation. Compt Rendus Geosci 341:140–155. https://doi.org/10.1016/j.crte.2008.11.002.
Simons B, Andersen JCØ, Shail RK, Jenner FE (2017) Fractionation of Li, Be, Ga, Nb, Ta, In, Sn, Sb, W and Bi in the paraluminous Early Permian Variscan granites of the Cornubian Batholith: precursor processes to magmatic-hydrothermal mineralization. Lithos 278:491–512. https://doi.org/10.1016/j.lithos.2017.02.007
Smith MP, Henderson P, Jeffries TE, Long J, Williams CT (2004) The Rare Earth elements and uranium in garnets from the Beinn an Dubhaich Aureole, Skye, Scotland, UK: constraints on processes in a dynamic Hydrothermal System. J Petrol 45:457–484. https://doi.org/10.1093/petrology/egg087
Sonnet PM, Verkaeren J (1989) Scheelite-, malayaite-, and axinite-bearing skarns from El Hammam, central Morocco. Econ Geol 84:575–590. https://doi.org/10.2113/gsecongeo.84.3.575
Starý J, Mašek D, Gabriel Z, Němec M, Hodková T, Novák J, Kavina P (2024) Mineral commodity summaries of the Czech Republic 2023. Statistical data to 2022. Czech Geological Survey. 2023 yearbook -1, Prag.
Štemprok M (1967) Genetische Probleme der Zinn-Wolfram-Vererzung im Erzgebirge: Mineralium Deposita, v. 2, p. 102-118. https://doi.org/10.1007/BF00206583
Štemprok M (1995) A comparison of the Krušné Hory-Erzgebirge (Czech Republic–Germany) and Cornish (UK) granites and their related mineralizations. Proc Ussher Soc 8:347-356.
Swinkels LJ, Schulz-Isenbeck J, Frenzel M, Gutzmer J, Burisch M (2021) Spatial and Temporal Evolution of the Freiberg Epithermal Ag-Pb-Zn District, Germany: Economic Geology, v. 116, p. 1649-1667. https://doi.org/10.5382/econgeo.4833
Terekhov EN, Shcherbakova TF (2006) Genesis of positive Eu anomalies in acid rocks from the Eastern Baltic Shield. Geochem Int 44:439–455. https://doi.org/10.1134/S0016702906050028
Tichomirowa M, Leonhardt D, (2010) New age determinations (Pb/Pb zircon evaporation, Rb/Sr) on the granites from Aue-Schwarzenberg and Eibenstock, Western Erzgebirge, Germany. Z. Geol. Wiss. 38 (2–3), 4, 99–123.
Tichomirowa M, Sergeev S, Berger H-J, Leonhardt D (2012) Inferring protoliths of high-grade metamorphic gneisses of the Erzgebirge using zirconology, geochemistry and comparison with lower-grade rocks from Lusatia (Saxothuringia, Germany). Contrib Mineral Petrol 164:375–396. https://doi.org/10.1007/ s00410-012-0742-8

Tichomirowa M, Käßner A, Sperner B, Lapp M, Leonhardt D, Linnemann U, Münker C, Ovtcharova M, Pfänder JA, Schaltegger U, Sergeev S, von Quadt A, Whitehouse M (2019) Dating multiply overprinted granites: the effect of protracted magmatism and fluid flow on dating systems (zircon U-Pb: SHRIMP/SIMS, LAICP-MS, CA-ID-TIMS; and Rb–Sr, Ar–Ar) – granites from the Western Erzgebirge (Bohemian Massif, Germany). Chem Geol 519:11–38. https://doi.org/10.1016/j.chemgeo.2019.04.024
Tichomirowa M, Käßner A, Repstock A, Weber S, Gerdes A, Whitehouse M (2022) New CA-ID-TIMS U–Pb zircon ages for the Altenberg–Teplice Volcanic Complex (ATVC) document discrete and coeval pulses of Variscan magmatic activity in the Eastern Erzgebirge (Eastern Variscan Belt): International Journal of Earth Sciences 111:1885-1908.
Tichomirowa M, Käßner A, Burisch M, Weber S, Lehmann U, Görz I (submitted) Non-synchronous pulses of (post-)Variscan magmatic activity in the Eastern and Western Erzgebirge (Eastern Variscan belt), and their relation to ore formation.
Tischendorf G, Förster H-J (1990) Acid magmatism and related metallogenesis in the Erzgebirge. Geol J 25:443–454. https://doi. org/10.1002/gj.3350250326
Tischendorf G, Wasternack J, Bolduan H, Bein E, Tischendorf G (1965) Zur Lage der Granitoberfäche im Erzgebirge und Vogtland mit Bemerkungen über ihre Bedeutung für die Verteilung der endogenen Lagerstätten. Z angew Geol 11(1965):410–423.
Tolksdorf JF, Hemker C, Schubert M (2020) Bronzezeitlicher Zinnseifenbergbau bei Schellerhau im östlichen Erzgebirge, Sachsen. Der Anschnitt, 71, 223-233.
Ulrych J, Dostal J, Adamovič J, Jelínek E, Špaček P, Hegner E, Balogh K (2011) Recurrent Cenozoic volcanic activity in the Bohemian Massif (Czech Republic): Lithos, v. 123, p. 133-144. https://doi.org/10.1016/j.lithos.2010.12.008
Wang T, She JX, Yin K, Wang K, Zhang Y, Lu X, Liu X, Li W (2021) Sn(II) chloride speciation and equilibrium Sn isotope fractionation under hydrothermal conditions: a first principles study. Geochim Cosmochim Acta 300:25–43. https://doi.org/10.1016/j. gca.2021.02.023
Weber S, Legler C, Kallmeier E, Schulz B, Burisch M (2023) Metamorphic origin of stratiform cassiterite mineralization in the Schwarzenberg-Aue district–Clues to the metamorphic history and pre-orogenic Sn enrichment of the Erzgebirge (Germany). Lithos, 454:107273. https://doi.org/10.1016/j.lithos.2023.107273
Weinhold G (2002) Die Zinnerz-Lagerstätte Altenberg/Osterzgebirge. Bergbau in Sachsen, 9. Sächsisches Landesamt für Umwelt, Landwirtschaft und Geologie, Dresden.
Wood SA (1990) The aqueous geochemistry of the rare-earth elements and Yttrium. Chem Geol 88:99–125. https://doi. org/10.1016/0009-2541(90)90106-H
Yang J, Peng J, Hu R, Bi X, Zhao J, Fu Y, Shen NP (2013) Garnet geochemistry of tungsten-mineralized Xihuashan granites in South China. Lithos 177:79–90. https://doi.org/10.1016/j. lithos.2013.06.008
Yu F, Shu Q, Niu X, Xing K, Li L, Lentz DR, Zeng Q, Yang W (2020) Composition of Garnet from the Xianghualing Skarn Sn Deposit, South China: its Petrogenetic significance and exploration potential. Minerals 10:456. https://doi.org/10.3390/min1005045
Ziegler PA (1990) Geological Atlas of Western and Central Europe: Den Haag, Netherlands, Shell Internat. Petroleum Maatschappij. ISBN 9066441259
Ziegler PA, Dèzes P (2007) Cenozoic uplift of Variscan Massifs in the Alpine foreland: Timing and controlling mechanisms: Global and Planetary change, v. 58, p. 237-269. https://doi.org/10.1016/j.gloplacha.2006.12.004

Anlage I

Arbeit 1

Akzeptierte Publikation

Mineralium Deposita (2024) 59:1–22
https://doi.org/10.1007/s00126-023-01194-8

ARTICLE

Timing and origin of skarn-, greisen-, and vein-hosted tin mineralization at Geyer, Erzgebirge (Germany)

Nicolas Meyer[1] · Gregor Markl[1] · Axel Gerdes[2,3] · Jens Gutzmer[4] · Mathias Burisch[4,5]

Received: 27 January 2023 / Accepted: 6 July 2023 / Published online: 1 August 2023

Abstract
This contribution presents new insights into the origin and age relationships of the Geyer tin deposit in the Erzgebirge, Germany. Tin mineralization occurs in skarns, greisen, and in cassiterite-bearing fluorite-quartz veins. Skarn alteration replaces marble layers of the Cambrian Jáchymov Group and occurs in two clearly distinct stages. The first skarn stage forms skarnoid textured assemblages of clinopyroxene, garnet, and wollastonite with no tin phases recognized. Garnet U-Pb ages of this skarn stage (~322 Ma) relate the earlier skarn stage to the emplacement of the Ehrenfriedersdorf granite (~324 to 317 Ma). The second stage of skarn alteration is marked by the occurrence of malayaite and cassiterite associated with garnet recording ages of 307 to 301 Ma. Greisen- and skarn-hosted cassiterite-bearing veins provide U-Pb ages in the range of 308 to 305 Ma, relating greisenization and vein formation to the same magmatic-hydrothermal event as the second skarn stage. This suggests that tin mineralization at Geyer is related to a distinctly younger magmatic-hydrothermal event, clearly postdating the Ehrenfriedersdorf granite, which was previously assumed as the source of the tin-rich fluids. Fluid inclusions show salinities in the range of 1.0 to 31.5 % eq. w($NaCl{\pm}CaCl_2$) and homogenization temperatures between 255 and 340 °C. Cassiterite-associated fluid inclusions show indications for heterogeneous entrapment and dilution of hydrothermal with meteoric fluids. Dilution of high-salinity fluids with low-salinity fluids and cooling of the system was probably a decisive process in the precipitation of cassiterite in the Geyer Sn system.

Keywords Magmatic-hydrothermal · LA-ICP-MS geochronology · Tin deposit · Garnet · Cassiterite

Introduction

The majority of global tin resources is hosted by various styles of magmatic-hydrothermal mineralization such as greisen, pegmatites, skarns, and veins related to highly evolved granitic systems (Breiter et al. 2017; Černý 1991; Chen et al. 1992; Jackson 1979; Lehmann 2021). In central Europe, tin systems are invariably related to late Paleozoic granites emplaced during the post-collisional stage of the Variscan orogeny (Förster et al. 1999). The Erzgebirge (Germany) is among Cornwall (UK), the Massif Central (France), the Iberian Massif (Spain/Portugal), and the Armorican Massif (France), one of Europe's prolific tin provinces (Lehmann 1990; Raimbault et al. 1995; Reinhardt et al. 2022; Romer and Kroner 2015, 2016). The Erzgebirge is host to polymetallic greisen-, skarn-, and vein-type deposits (Korges et al. 2020; Reinhardt et al. 2022; Swinkels et al. 2021), of which the known skarn deposits of the Erzgebirge, as a group, reflect the largest tin resource in Europe (Elsner 2014). In addition to Sn,

Editorial handling: B. Lehmann

Nicolas Meyer
nicolas.meyer@uni-tuebingen.de

Mathias Burisch
burisch@mines.edu

1 Fachbereich Geowissenschaften, Petrologie und Mineralische Rohstoffe, Eberhard Karls Universität Tübingen, Tübingen, Germany

2 Institut für Geowissenschaften, Goethe-Universität Frankfurt, Frankfurt, Germany

3 Frankfurt Isotope and Element Research Center (FIERCE), Goethe-Universität Frankfurt, Frankfurt, Germany

4 Institute Freiberg for Resource Technology, Helmholtz-Zentrum Dresden-Rossendorf, Freiberg, Germany

5 Mineral System Analysis Group, Department of Geology and Geological Engineering, Colorado School of Mines, Golden, CO, USA

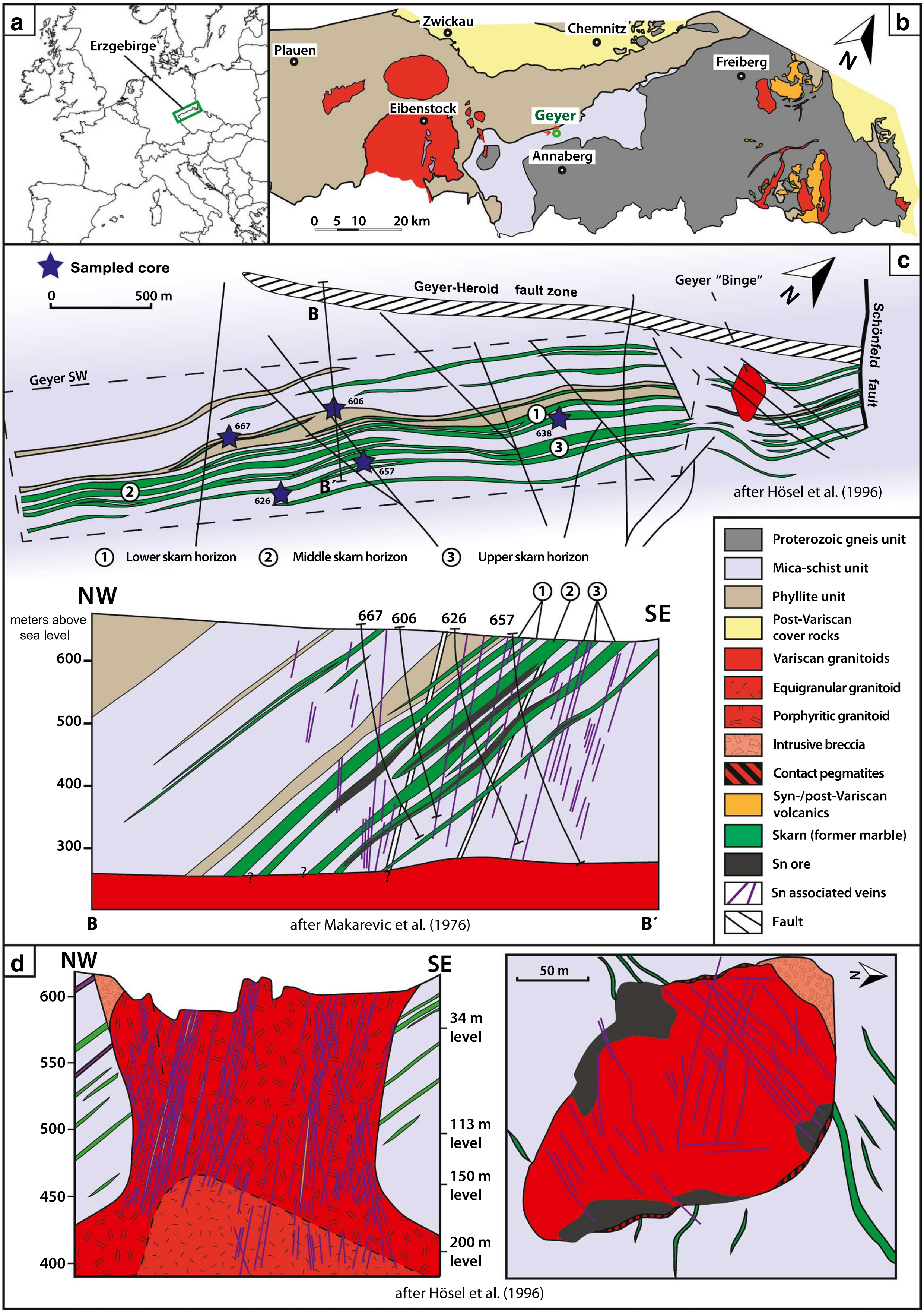

a
Erzgebirge
b
Zwickau
Chemnitz
Plauen
Freiberg
Eibenstock
Geyer
Annaberg
0 5 10 20 km
N
c
Sampled core
0 500 m
Geyer-Herold fault zone
Geyer "Binge"
Schönfeld fault
B
Geyer SW
606
667
638
657
626
B´
after Hösel et al. (1996)
1 Lower skarn horizon
2 Middle skarn horizon
3 Upper skarn horizon
NW
SE
meters above sea level
600
500
400
300
667 606 626 657
B
after Makarevic et al. (1976)
B´
Proterozoic gneis unit
Mica-schist unit
Phyllite unit
Post-Variscan cover rocks
Variscan granitoids
Equigranular granitoid
Porphyritic granitoid
Intrusive breccia
Contact pegmatites
Syn-/post-Variscan volcanics
Skarn (former marble)
Sn ore
Sn associated veins
Fault
d
NW
SE
600
550
500
450
400
34 m level
113 m level
150 m level
200 m level
50 m
N
after Hösel et al. (1996)

◂**Fig. 1** **a** Geographic overview map. **b** Simplified geological overview map of the Erzgebirge including the location of the Geyer system. **c** Geological map and cross-section of the study area. The skarn layers are orientated parallel to the foliation of the surrounding low- to medium-grade meta-sedimentary units, trending NE-SW. Skarns are delimited by the Schönfeld fault in the northeast. The cross-section shows that the skarns are underlain by a large-volume intrusion at depth, which has a sub-horizontal contact. The Geyersberg granite intrusive stock crops out in the north-east of the district (after Hösel et al. 1996). Skarn layers extend down-dip from the surface to the top of the underlying pluton with a dip of about 45° NW. Veins and faults intersect the skarn lenses (after Makarevič et al. 1976). **d** Geological cross-section and overview map of the Geyersberg area including the historic pit of the Geyer "Binge"

some of the skarns in the Erzgebirge also host significant resources of W, Zn, Fe, and In—in addition to Sn (Bauer et al. 2019; Hösel 1994; Hösel 2002; Lorenz and Hoth 1967; Reinhardt et al. 2021).

Despite their economic significance, detailed geological descriptions and geochemical data are for many occurrences limited to technical reports and resource estimates related to the tin exploration program of the former German Democratic Republic (GDR; 1945–1989). Consequently, most of the skarn systems in the Erzgebirge have not been subject of studies with modern geochemical methods, with the exception of a few recent studies that focused on the Hämmerlein (Bauer et al. 2019; Kern et al. 2019; Korges et al. 2020; Lefebvre et al. 2019) and Waschleithe deposits (Reinhardt et al. 2021), both located in the Schwarzenberg district in the western part of the Erzgebirge (Schuppan and Hiller 2012).

The Geyer mining district (~5 × 4 km) is also located in the western part of the Erzgebirge, ~25 km south of Chemnitz. Historic tin (and minor tungsten and iron) mining occurred between 1395 and 1913 in the Geyer area. After World War II, an extensive exploration campaign was carried out by the SDAG Wismut targeting skarn-hosted tin mineralization in the area south-west of the outcropping Geyersberg stock. This resulted in 123 boreholes with more than 37,000 m of recovered core material (Hösel et al. 1996). In 2011 and 2012, Tin International drilled four new confirmation boreholes in the Geyer SW area, which were used to constrain an indicated resource of 46 kt of tin at an average ore grade of 0.56% Sn (Elsner 2014). Toward the northeast, the Geyer skarn- and greisen-hosted deposit is separated by the NW–SE trending Geyer-Schönfeld fault system from the stockwork-hosted Ehrenfriedersdorf tin deposit (Hösel 1994). Th-U-Pb dating of uraninite in granites from the nearby Ehrenfriedersdorf district (Greifensteine and Sauberg) and U-Pb dating of apatite from granite (Sauberg) provide intrusion ages between 324 ± 4 and 319.7± 3 Ma, 323.9 ± 3, and 317.3 ± 2 Ma, respectively (Romer et al. 2007), whereas no geochronological data is available for the intrusions at Geyer. The intrusion depth is constrained by melt inclusion analyses to 2.5–4 km (Breiter et al. 1999).

The origin and timing of skarn-hosted tin mineralization were controversially debated (Lefebvre et al. 2019) until direct geochronological data (U-Pb ages of garnet using LA-ICP-MS) revealed the magmatic-hydrothermal origin of skarn formation in the Erzgebirge. On the scale of the Erzgebirge, skarn-related garnet ages range from 335 to 295 Ma (Burisch et al. 2019; Reinhardt et al. 2022), which coincide with late-collisional magmatic (335–310 Ma) and post-orogenic volcanic rock units (305–285 Ma; Luthardt et al. 2018; Romer et al. 2007; von Seckendorff et al. 2004) in the region. Cassiterite is the main tin ore mineral. In the Hämmerlein deposit, the most important tin skarn resource of the Erzgebirge, cassiterite is usually associated with chlorite-actinolite-quartz alteration that replaces early-stage skarn or occurs also as infill of veinlets cross-cutting the skarn bodies and surrounding host rocks (Kern et al. 2019). Conversely, cassiterite in greisen is associated with typical greisen minerals such as mica, quartz, fluorite, and topaz, which may occur as discrete veins or disseminations (Hösel et al. 1996). In this study, we present field and petrographic observations, *in situ* U-Pb dating, and fluid inclusion microthermometric data to constrain the timing and underlying processes of greisen and skarn alteration and related ore formation at the Geyer SW deposit.

Regional geology and skarn-related fluids

The Erzgebirge-Krušné hory is a ~160 × 35 km exposure of mainly metamorphic rocks belonging to the Bohemian Massif within the Saxothuringian zone of the European Variscan Belt (Förster et al. 1999). The Erzgebirge comprises various metamorphic nappes (Rötzler 1995; Willner et al. 1997) that underwent peak metamorphic conditions at ~340 Ma (Kröner and Willner 1998). These units include gneisses, mica schists, marbles, phyllites, and metavolcanic rocks (Fig. 1). Ondrus et al. (2003) and Tichomirowa et al. (2012) showed that the protoliths of these rocks are greywackes, conglomerates, granodiorites (gneiss units) or volcanic rocks, and marine sediments (mica schist and phyllite unit). After rapid uplift to middle and upper crustal levels (Schmädicke et al. 1995), the metamorphic units were intruded by highly evolved, late-orogenic peraluminous granites (335–310 Ma; Förster et al. 1999) accompanied by the emplacement of late- and post-collisional lamprophyric and rhyolitic dykes and other (sub)volcanic rocks (330–275 Ma; Bolduan 1963a; Hoffmann et al. 2013; Luthardt et al. 2018). The emplacement depths of late-orogenic granitic batholiths and stocks in the western part of the Erzgebirge have been constrained to 3–6 km using melt inclusion analyses (Breiter et al. 1999; Thomas and Klemm 1997).

The Erzgebirge hosts numerous hydrothermal skarn, greisen, and vein-type deposits genetically related to late- and post-collisional magmatism in the area (Burisch et al. 2019; Legler 1985; Swinkels et al. 2021; Tischendorf and Förster 1990; Zhang et al. 2017). U-Pb LA-ICP-MS data on cassiterite define a mineralization age of 326–320 Ma of the mineralization for the Ehrenfriedersdorf tin deposit (Zhang et al. 2017). These ages might be doubtful and are probably up to 8 Ma younger than reported (Zhang pers. comm.). Multimineral Rb-Sr geochronology on greisen and skarn samples from the Hämmerlein deposit indicates three age groups: ~340 Ma obtained from skarn associated white mica, K-feldspar, and fluorite, and ~320 Ma and 290 Ma from greisen-associated muscovite, apatite, and K-feldspar (Lefebvre et al. 2019). Re-Os dating of hydrothermal molybdenite from greisen of the Altenberg Sn-(W-Mo) complex reveals mineralization ages of 326–319 Ma (Romer et al. 2007). U-Pb LA-ICP-MS data of skarn-related garnet range from ~335–295 Ma (Burisch et al. 2019; Reinhardt et al. 2022) spanning a much broader range than greisen-related ages. Garnet ages related to skarns with significant metal endowment define at least two principal stages: an older group of skarns formed at ~325–313 Ma, which coincides with available greisen-related ages and late-collisional magmatism, whereas a younger skarn stage occurred at ~310–295 Ma, post-dating late-collisional intrusions, but coinciding with post-collisional volcanic activity (Burisch et al. 2019; Hoffmann et al. 2013; Löcse et al. 2023; Reinhardt et al. 2022).

Fluid inclusions in skarn-associated garnet and clinopyroxene from the Sn-Zn-In Hämmerlein deposit and from the Waschleithe Zn-skarn in the Schwarzenberg district show homogenization temperatures of 270–385 °C with salinities ranging from 0.3–3.8% eq. w(NaCl), while those in skarn-related fluorite has lower homogenization temperatures (210–225 °C), but higher salinities (~7.7% eq. w(NaCl); Korges et al. 2020; Reinhardt et al. 2021). Korges et al. (2020) recently reported fluid inclusions in skarn-hosted cassiterite from the Hämmerlein deposit with unusually high homogenization temperatures (500 °C) and high salinities (30–47% eq. w(NaCl)), whereas coexisting greisen-hosted fluid inclusions in cassiterite and quartz have lower formation temperatures (350–400 °C) and lower salinities (1.9–6.0% eq. w(NaCl); (Korges et al. 2020). Fluid inclusions in vein-hosted fluorite and greisen-hosted quartz have homogenization temperatures around 450 °C, with salinities of 11–14% eq. w(NaCl), and a second group has lower homogenization temperatures of 210 to 325 °C and salinities between 2.0 and 9.0% eq. w(NaCl) (Korges et al. 2020).

The Geyer district

The geological architecture of the Geyer district is dominated by SW-NE striking and NW dipping paragneisses, mica schists, and phyllites of the Cambrian Jáchymov Group, with intercalations of dolomitic to calcitic marbles and quartzites (Hösel 1994). This succession was metamorphosed at low- to medium-grade during the Variscan orogeny and later intruded by a composite intrusion present below the surface in the entire area (Bolduan 1963a; Hermann 1967; Hösel et al. 1996; Tischendorf et al. 1965; Tischendorf and Förster 1990). The contact between the granitoids and the metamorphic host rocks is almost horizontal (at a depth of ~150–450 m below surface level; see Fig. 1c), except for the stock-like Geyersberg intrusion, which forms a prominent outcrop in the eastern part of the district (Fig. 1d). The flanks of this intrusive stock dip almost vertically to a depth of 180 m, where they become significantly shallower (Fig. 1d). The Geyersberg composite stock consists mainly of two types of intrusions. An older granitic suite is with fine- to coarse-grained porphyritic texture and high biotite content (Bolduan 1963a). This older intrusion is not associated with significant greisen alteration nor Sn mineralization (Hösel et al. 1996). The younger main intrusive stage cross-cuts the older intrusion and is characterized as an equigranular, low-biotite topaz-bearing granite (Bolduan 1963a). This second intrusion contains up to 4 wt% fluorine and hosts abundant disseminated cassiterite and lithium-bearing mica (Bolduan 1963a, 1963b; Breiter et al. 1999; Hösel 1994; Hösel et al. 1996) and an intrusive breccia body. To greater depth (~450 m), the texture of the intrusive units merges into a fine-grained, porphyritic granite, which coincides with an increase of biotite and a decreasing topaz content (Hösel 1994). Rhyolitic dykes cross-cut the main intrusions (Bolduan 1963a; Hösel et al. 1996). "Stockscheider" pegmatites occur at the contact between the individual intrusions and at the contact with the surrounding metasedimentary units. Hornfels and mica schists with contact metamorphic biotite, cordierite, and andalusite are abundant in the contact aureole, which is developed to a distance of ~50 m away from the intrusive contact (Hösel et al. 1996).

Minor fluorite-quartz, fluorite-barite, native metal-arsenide, and Mn-Fe veins occur in the Geyer area (Bolduan 1963a). These mainly Mesozoic and Cenozoic veins are genetically unrelated to Sn mineralization (Burisch et al. 2021, 2022; Guilcher et al. 2021; Haschke et al. 2021; Kuschka 1994) and hence not discussed any further.

Geyer SW skarn

The majority of Sn mineralization at Geyer SW is hosted by exoskarns that mainly replaced marble but also mica schists in direct vicinity of the marble units (Fig. 1c). Most of the marble units intersected by exploration drill cores at Geyer SW are to some degree affected by skarn alteration, but there are a few drill cores (e.g., BZ 667/75 at 412.2-414.0 m) which intersect macroscopically unaltered marble. Three distinct skarn units (from NW to SE 1, 2, and 3; Fig. 1c) have been distinguished (Hösel et al. 1996) which are dipping to the NW with an angle of about 30–40°, parallel to the metamorphic layering. Each of these skarn units is composed of several skarn layers thought to represent former carbonate layers (Hösel et al. 1996) and forms laterally discontinuous lens-shaped ore bodies. The lower skarn unit contains two discrete skarn layers and can be traced over a strike length of 3 km and extends down to the granite surface at depth, without any recognition of endoskarn (Fig. 1c). The lower layer with a thickness of 5–20 m is composed of two individual skarn bodies and one ore body. The upper layer with a thickness of 15–40 m comprises several skarn bodies replacing marble and adjacent mica schists. Two discrete ore bodies have been recognized in the upper layer (see Fig. 1c). The middle skarn unit has a strike length of 1.5 km and pinches out at a depth of about ~180 m above the granite contact (Hösel et al. 1996). It is characterized by a constant thickness of about ~20 m and contains several individual skarn bodies (Fig. 1c). The lower part of the middle skarn unit hosts only one ore body.

The upper skarn unit can be traced over a lateral distance of more than 3 km. It extends down to the granite contact and contains two individual skarn layers. Similar to the lower skarn unit, no endoskarn is documented in association with this skarn unit. The lower layer (total thickness of 7–25 m) consists of three skarn bodies and one ore body with a thickness between 1 and 6 m, which are separated by unaltered mica schists. The upper layer is again separated from the other skarn layer by unaltered mica schists and has a constant thickness of 15–20 m with several laterally discontinuous lens-shaped skarn bodies and one discrete ore body in the lower part of this layer. Many smaller skarn bodies have been additionally identified in the district. These are typically of only minor thickness and do not host significant tin mineralization.

Skarn mineralogy at Geyer comprises clinopyroxene and garnet with minor wollastonite, epidote, vesuvianite, magnetite, and fluorite in highly variable modal abundances (Hösel et al. 1996). These mineral assemblages are overgrown or replaced by chlorite, actinolite, fluorite, and cassiterite as well as base metal sulfides. High grades of skarn-hosted disseminated cassiterite are intimately associated with magnetite-rich domains, which have been reported to be mainly present within a distance of 450–300 m distance to the granite contact (Hösel et al. 1996). The bulk of tin resources (~80%) is hosted by skarn affected by chlorite-actinolite alteration and by fluorite-quartz or fluorite-chlorite veins intersecting the skarns and metasedimentary units with a maximum thickness of 15 cm (Hösel et al. 1996).

Geyer Binge greisen

Most of the historic underground mining activity at Geyer focused on the “Binge,” the exposed Geyersberg granite (Fig. 1c and d), which forms a stock-like intrusive body with a diameter of around 230 m (Hoth and Wolf 1986). Greisen alteration and associated cassiterite mineralization predominantly develop along NE-SW and NW-SE striking, steeply and flat dipping veins that form a dense stockwork within the granite. These vein swarms consist of individual veins, ranging in length from 2 to 6 m, having a variable alteration halo (Hösel et al. 1996). Mineralogically, the alteration halo and veins mainly comprise topaz, lithium mica, and cassiterite (Bolduan 1963a). Most cassiterite is hosted by hydrothermal veins and related greisen alteration. Molybdenite and wolframite may also be recognized in some of these veins, but clearly predate cassiterite based on petrographic observations. A variety of hydrothermal veins cross-cut greisen alteration and cassiterite veins. They may comprise quartz, fluorite, hematite, and minor barite. They typically occur in different orientation or as the latest vein infill and are genetically unrelated, based on their mineralogy and cross-cutting relationships (Hösel 1994).

Sampling and methodology

A total of 60 samples from the Geyer mining district were collected from six drill cores from the Wismut SDAG and Tin International exploration campaigns. Access to drill cores was provided by the Geological Survey of the Free State of Saxony (LfULG). The sampling focused mainly on skarn bodies — both with and without significant tin mineralization — but also include some marble and mica-schist samples. 84 polished sections for petrographic investigations and 21 doubly polished sections for fluid inclusion analyses were prepared at the Helmholtz Institute for Resource Technology. Additionally, six garnet-rich samples and three cassiterite-rich samples were prepared as 1-inch epoxy rounds for LA-ICP-MS geochronology.

Petrography

Identification of minerals and examination of the textures were performed in transmitted and reflected light with a Leica DM750P light microscope and recorded with an Olympus single-lens reflex camera. This work was supported by scanning electron microscopy (SEM) performed on a Phenom XL SEM equipped with an energy dispersive X-ray spectrometer at the Geo- and Environmental Research Center (GUZ) of the University of Tübingen. Backscattered electron (BSE) images and qualitative mineral compositions were obtained with the SEM using a beam current of 15 nA and 15 kV acceleration voltage. Furthermore, cm-scale element maps were obtained by a microbeam XRF at the GUZ using a Bruker Tornado desktop unit equipped with a rhodium tube operating with 50 kV and 500 nA and two spectrometers. Element distribution maps were compiled using a 20 µm spot size on a 20 µm grid with dwell times of 10-16 milliseconds per pixel.

Fluid inclusion petrography and microthermometry

The fluid inclusion microthermometric measurements were carried out using a Leica light microscope equipped with a Linkam THMS 600 heating-freezing stage and a FLIR grasshopper3 USB camera at the GUZ Tübingen on doubly polished thick sections with a thickness of 150 µm. The classification of fluid inclusions into primary, secondary, and pseudosecondary inclusions follows the description of Roedder (1984). The stage was calibrated before and after each measurement campaign using synthetic fluid inclusion standards for the following phase transitions: melting temperature of ice (Tm_{ice}) and homogenization temperature (T_h) of pure H_2O and melting temperature of CO_2 (Tm_{CO2}) of H_2O-CO_2-standards. Tm_{ice} was used to calculate the salinity in the NaCl-H_2O system according to Steele-MacInnis et al. (2012). Melting temperature of halite (Tm_h), hydrohalite (Tm_{hh}), and Tm_{ice} were used to calculate salinities in the NaCl-$CaCl_2$-H_2O system after the spreadsheet of Steele-MacInnis et al. (2011). According to the classification criteria of Roedder (1984), fluid inclusions were classified as either primary, pseudosecondary, or clusters. Fluid inclusions with indications of metastability, post-entrapment modification, or leakage due to (micro)-fractures are excluded.

U-Pb LA-ICP-MS geochronology

Six samples with abundant garnet from the Geyer skarns and 3 cassiterite samples from greisen alteration and veins were selected for geochronology. The samples are from three drill cores and the scientific collection of Freiberg (Table 1). These samples cover textures and colors of skarn hosted garnet recognized in the exploration cores from Geyer SW; the garnets range from isometric, green garnet to anhedral garnet of red to beige color (Table 1 and ESM 1 and 2; Fig. 2). Samples selected for garnet U-Pb LA-ICP-MS geochronology exhibit a variable degree of retrograde overprint, with variable abundances of amphibole, chlorite, and fluorite. For U-Pb isotope analyses, samples with the lowest possible retrograde alteration and domains unaffected by retrograde overprint were selected to set the spots for LA-ICP-MS analysis. Cassiterite samples from veins contain fluorite and quartz; cassiterite from greisen samples is intergrown with quartz, sericite, and minor topaz. None of these samples exhibit hydrothermal overprint. Cassiterite crystals are euhedral and have a size up to 3 mm. In total, six skarn samples with abundant garnet and three cassiterite samples were cut to size and mounted in 1-inch epoxy rounds.

Uranium-Pb data were subsequently collected on a Thermo Scientific Element XR sector field ICP-MS coupled to a RESOlution (COMpex Pro 102) 193 nm ArF excimer laser equipped with a two-volume (Laurin Technic S155) ablation cell at the Frankfurt Isotope and Element Research Center (FIERCE), Goethe University Frankfurt (Germany) following the methodology of Burisch et al. (2019, 2022), Millonig et al. (2020), and Reinhardt et al. (2022). Measurement points for each polished section derive from a small area (<1 cm^2) and were set after careful screening before each analytical session to identify growth-zones with higher $^{238}U/^{206}Pb$ ratios and to avoid superficial exposure of mineral inclusions by monitoring trace element ratios during screening. Samples were then analyzed *in situ* in fully automated mode. During the measurements, the signals of ^{206}Pb, ^{207}Pb, ^{208}Pb, ^{232}Th, and ^{238}U were acquired by peak jumping in pulse counting mode with a total integration time of ~0.1 s, resulting in 360 mass scans. The raw data was corrected offline deploying an in-house Microsoft Excel spreadsheet program (Gerdes and Zeh 2006, 2009). Common Pb correction has not been applied to the data. Instead, U-Pb ages are calculated using linear regression in Tera-Wasserburg Concordia diagrams (Tera and Wasserburg 1972) since the ablated andradite-grossular and cassiterite incorporates a mixture of non-radiogenic and radiogenic Pb formed due to *in situ* decay of uranium. U-Pb dates are defined as the lower intercept of the regression line with the Concordia curve. Mali grandite (dated by ID-TIMS at 202.0 ± 1.2 Ma; Seman et al. 2017) and Swaziland cassiterite (3086 ± 3 Ma) were used as a primary reference material (RM), respectively. The age of Swaziland cassiterite was determined prior to this study using an approach similar to that described by Neymark et al. (2018). The $^{207}Pb/^{206}Pb$ ratio of multiple spot analyses on a single Swaziland cassiterite grain (1 × 0.6 cm) was NIST SRM612-mass bias corrected and yielded a weighted mean Pb/Pb age of 3086 ± 3 Ma. Excess of scatter on $^{207}Pb/^{206}Pb$ of NIST 612 (n = 20) for each session was around 0.14% (1 σ) and the mass bias varied from 0.7 to 0.4% between the different analytical sessions. Swaziland cassiterite typically yielded homogenous $^{206}Pb/^{238}U$ (e.g., 0.6141 ± 0.54%, 2 σ; n = 20) suggesting no disturbance of the U-Pb system. Therefore, the correction factor for $^{206}Pb/^{238}U$ was calculated using the percentage difference between the uncorrected $^{206}Pb/^{238}U$ age and the mass bias corrected $^{207}Pb/^{206}Pb$ of the Swaziland cassiterite. To verify the obtained $^{206}Pb/^{238}U$ fractionation correction, cassiterite from Pitkäranta (Neymark et al. 2018; Tapster and Bright 2020) and Ehrenfriedersdorf (inhouse RM) was measured as secondary quality control RM. Both RM yielded precise

Table 1 Description of samples and concentrations of U, Pb, and LA-ICP-MS U-Pb ages of garnet and cassiterite of the Geyer system

Sample number	Location	Description	U-Pb age (Ma)	MSWD	Initial $^{207}Pb/^{206}Pb$	U (µg/g)	Pb (µg/g)	*N*
GR1	Skarn SW Z626-96.5m	Green grt[1] with chl veins	301.6 ± 4.4 / 5.0	2.02	0.868	0.04–0.65	0.02–0.86	33
GR2	Skarn SW Z626-59m	Green grt[1] with pale green cpx	305.1 ± 3.0 / 3.9	1.22	0.880	0.01–0.36	0.01–0.09	25
GR4	Z626 85m	Pale red grt[1] with cpx and wo	322.4 ± 4.4 / 5.1	1.64	0.870	0.04–0.65	0.01–0.14	31
GR5	Z606 79.5m	Red grt[1] with red ves, wol	322.1 ± 10.7 / 11.8	11.38	0.865	0.01–1.8	0.05–0.39	27
GR6	Z626-45.6m	Pale green grt[1] with white cpx	307.3 ± 4.1 / 4.8	0.78	0.868	0.01–1.4	0.02–0.40	28
GR657	Z657-83.8m	cst[1] in fl-qz-vein	308.2 ± 1.9 / 3.7	0.81	0.868	1.4–16.5	0.08–1.2	35
60974	“Binge” Geyer	cst[1] with tpz and qtz in granite	305.7 ± 1.8 / 3.7	0.59	0.788	0.09–33.1	0.06–1.5	27
60973	“Binge” Geyer	cst[1] with tpz and qtz in granite	306.6 ± 1.5 / 3.5	0.84	0.788	1.4–14.2	1.4–14.1	33

[1]Analysed mineral; *MSWD*, mean square of weighted deviates; *N*, number of spot analyses; *grt*, garnet; *cpx*, clinopyroxene; *wo*, wollastonite; *ves*, vesuvianite; *chl*, chlorite; *cst*, cassiterite; *fl*, fluorite; *qz*, quartz; *tpz*, topaz

and reproducible (<1%) lower intercept ages during different analytical sessions (e.g., 1538.4 ± 6.7 and 1534.1 ± 6.4 Ma; 313.8 ± 2.1 and 314.1 ± 1.5 Ma, respectively). The perfect agreement of the Pitkäranta age with published ID-TIMS ages (1536.6 ± 1.0 Ma; Tapster and Bright 2020) also implies an accuracy of the applied method of better than 1%. Garnet RM Lake Jaco (dated by ID-TIMS by Seman et al. 2017), MaliGUF, and Ehrenfriedersdorf cassiterite (in-house reference materials) were employed as secondary quality control RM for garnet analyses. Primary and secondary RM were measured in duplicate after every 50 analyses of unknowns. All uncertainties are quoted at 2σ absolute and are quadratic additions of the within-run precision, counting statistics, background, excess of scatter (primary RM, NIST SRM-612), and excess of variance (Mali garnet and Swaziland cassiterite, respectively). Systematic uncertainties are reported as an expanded uncertainty, considering long-term reproducibility (0.8 %, 2σ) and decay constant uncertainties. A detailed description and location of drill core samples are summarized in ESM Table 2.

Results

In the following, mineralogical and petrographic investigations of host rocks, skarns, greisen alteration, and vein mineralization are presented. Macroscopic and microscopic observations (Figs. 3–6) were complemented by careful fluid

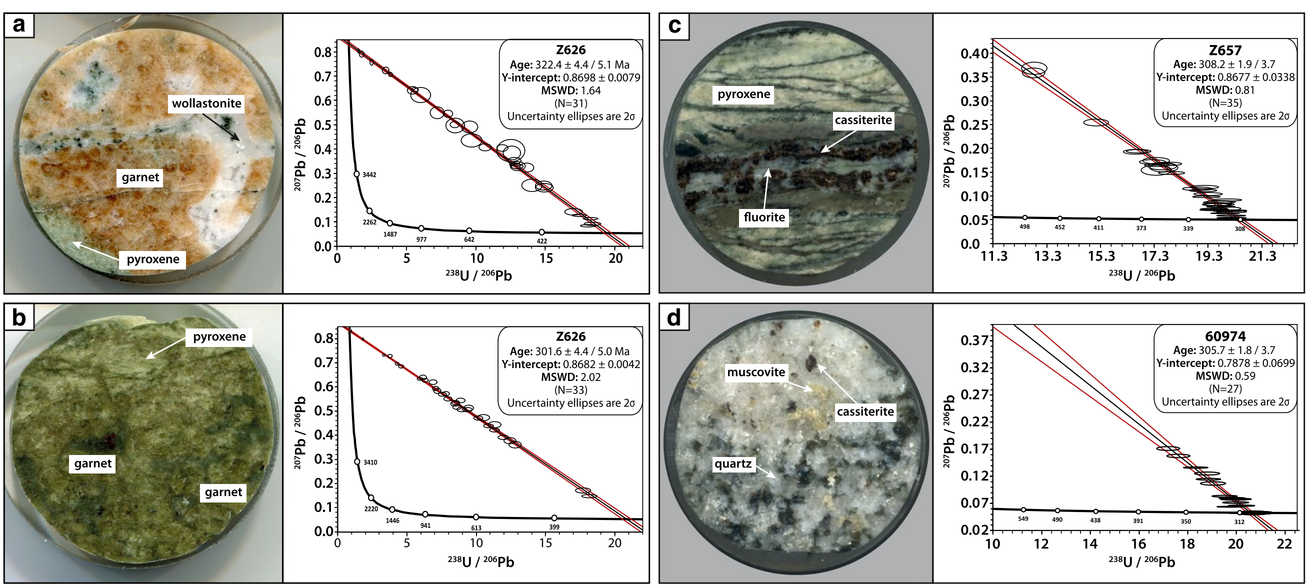

Fig. 2 Representative scans of age dated garnet and cassiterite with corresponding Tera-Wasserburg Concordia diagrams. Lower intercept ages are reported with internal/external uncertainties. **a** Pale red garnet of stage I with white wollastonite, **b** green garnet of stage II and clinopyroxene, **c** cassiterite-fluorite vein with chloritized alteration halo, and **d** greisenized granite with disseminated cassiterite

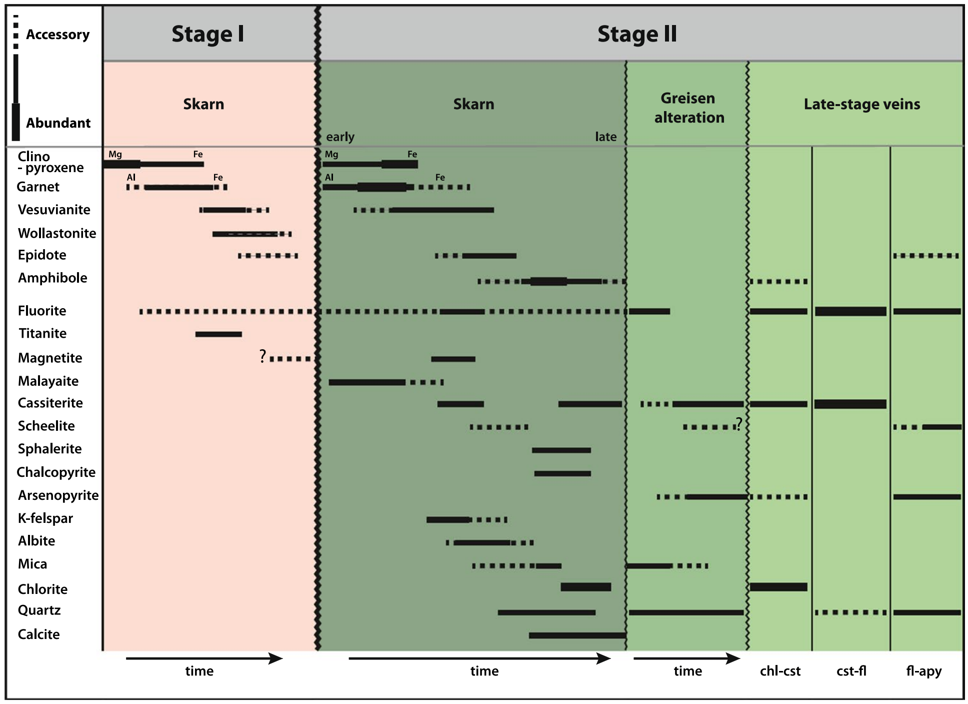

Fig. 3 Paragenetic sequence of skarn, greisen, and vein mineralization at Geyer, subdivided into two stages: stage I includes skarn stage I and stage II includes skarn stage II, greisen, and late-stage veins. Greisen and skarn alteration have the same paragenetic position but reflect spatial mineralogical variations that are controlled by protolith composition. Qualitative major element compositions of clinopyroxene and in garnet are indicated above the black bars

inclusion petrography (Fig. 7) and microthermometric analyses (Table 2). The complete background data set is provided in ESM Table 1. A selection of LA-ICP-MS U-Pb data are plotted in the Tera-Wasserburg diagram (Fig. 2), and a summary of geochronological data is provided in Table 1. LA-ICP-MS U-Pb background data is provided in ESM Table 2.

Host rock units

Mica schists

Mica schists are the most abundant rock unit in the Geyer area, containing biotite, muscovite, feldspar, garnet, rutile, and quartz as main components (Fig. 4a). On the m-scale, the mica schist composition is heterogeneous including garnet-bearing, graphite-bearing, and feldspar-rich layers (Fig. 5a). Apatite occurs locally as an accessory phase. Subordinate clinozoisite with an allanite component, zircon, but also sulfides like rammelsbergite, pyrite, and chalcopyrite may rarely occur. Mica shists can be overprinted by skarn alteration to some extent, with a gradual transition between both. These areas are characterized by a change toward green color due to the formation of clinopyroxene and chlorite.

Marble

Unaltered marble was only intersected in drill core BZ 667/75 at 412.2–414.0 m and is predominantly composed of anhedral calcite with an equigranular texture (Fig. 5b). Calcite crystals exhibit a size between 0.5 and 3.0 mm. Minor quartz (<0.2 mm), muscovite (<0.4 mm), and apatite (0.1–0.3 mm) occur as disseminations or as discrete bands, resulting in a weak metamorphic fabric. Furthermore, euhedral green metamorphic amphibole of (<2.0 mm) is recognized. This amphibole is distinctly different from skarn-related amphibole as it shows deformation features aligned with the metamorphic fabric of the surrounding mica schist. Thin veinlets are filled with chlorite, amphibole, or epidote together with chalcopyrite and sphalerite locally cross-cut the marble. In addition, progressive silicification of the marble is recognized close to the contact to the adjacent skarn.

Skarns

Mineral abundances and textures vary strongly across and within individual skarn bodies. Nevertheless, there are general similarities with respect to their petrographic and mineralogical composition, replacement textures, and cross-cutting relationships, which are summarized in a simplified paragenetic sequence (Fig. 3). Two types of skarn alteration can be distinguished based on their cross-cutting relationships, textures, and mineralogy: an early, pyroxene-dominated stage I skarn with fine-grained and Mg-richer minerals (Fig. 4a–c) is characterized by the preservation of the metamorphic fabric of the altered mica schist. Such texture is commonly referred to as a skarnoid skarn according to the terminology of Meinert et al. (2005). In the skarn I assemblages, no distinct tin phases or base metal sulfides are present. Younger garnet-pyroxene stage II skarn (Fig. 4d) is characterized by replacement textures that form euhedral minerals (Fig. 4d–f), which is consistent with metasomatic

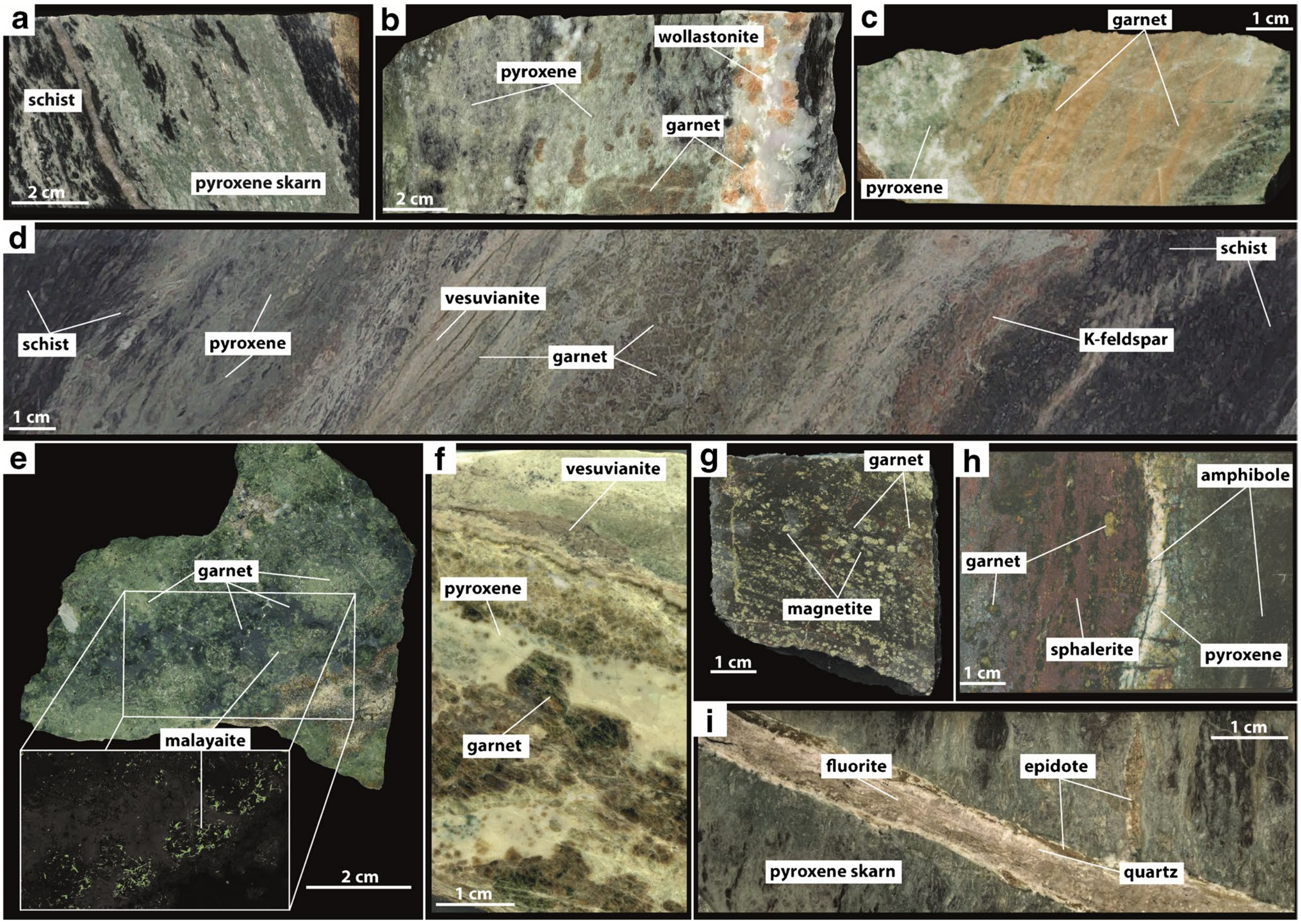

Fig. 4 Representative drill core intersections from Geyer. **a** Fine-grained pyroxene-dominated skarn of stage I skarn with mica-schist remnants (GM 10/60; 22.0–22.1 m). **b** Stage I skarn consisting of mainly anhedral clinopyroxene and garnet with some domains that contain euhedral garnet and wollastonite (BZ 667/75; 394.0–394.1 m). **c** Anhedral, very fine-grained red garnet intergrown with anhedral clinopyroxene of stage I skarn (BZ667/75; 190.6–190.7 m). **d** Complete intersection of a skarn lens with a fine-grained rim and isometric coarser-grained minerals in the center (Z626; 96.5–96.8 m). **e** Isometric skarn stage II with green garnet. The inlet shows the distribution of malayaite intergrown with garnet (GM 10/60; 29.8–30.2 m). **f** Coarse-grained euhedral garnet cogenetic with white clinopyroxene and a vesuvianite-rich domain of stage II skarn (Z626; 45.6–46.7 m). **g** Magnetite-rich skarn II with remnants of garnet (Z638; 80.2–80.3 m). **h** Amphibole and sphalerite-rich domains in skarn stage II with remnants of garnet and clinopyroxene (Y617; 116.4–116.8 m). **i** Fluorite-quartz-vein bordered by epidote cross-cutting a skarn layer (BZ667/75; 391.9–392.2 m)

skarn textures described by Meinert et al. (2005). Stage II skarn alteration is subdivided into (a) an early stage with garnet, clinopyroxene, vesuvianite, epidote, and other calc-silicate minerals (i.e., the prograde skarn evolution of Meinert et al. 2005) and (b) a late stage with amphibole, chlorite, and sulfide minerals (Fig. 4g and h) which would correspond to the retrograde skarn stage (Meinert et al. 2005). Since the euhedral vesuvianite is paragenetically coeval with garnet, it is ascribed to the early stage of skarn II formation.

Individual skarn layers typically exhibit a distinct geometry and may reach up to a few meters in thickness, but mostly do not exceed several tens of centimeters. Stage I skarn shows gradual transitions into the mica schists and often has irregularly-shaped patchy domains of unreplaced protolith (Fig. 4a). There seems to be no retrograde overprint associated with skarn stage I. Stage II skarn invariably occupies a central position of the individual skarn layers having thicknesses of 10 to 50 cm. Stage II skarn clearly replaces and postdates stage I skarn and even occurs as infill of fractures in skarn I. In contrast to skarn stage I, remnants of mica schist are rarely preserved in stage II skarns and the transition between skarn and metasedimentary rock is sharply defined. Vesuvianite-rich domains occur within garnet-skarn of both stages. Malayaite is the only distinct tin phase in the early phase of the second skarn alteration (cassiterite occurs later in the paragenetic sequence).

Lens-shaped domains and fractures filled with garnet, epidote, and vesuvianite, which have crystal sizes between tens of µm up to 3 cm, postdating the isometric stage II and the fine-crystalline stage I skarns, are interpreted as

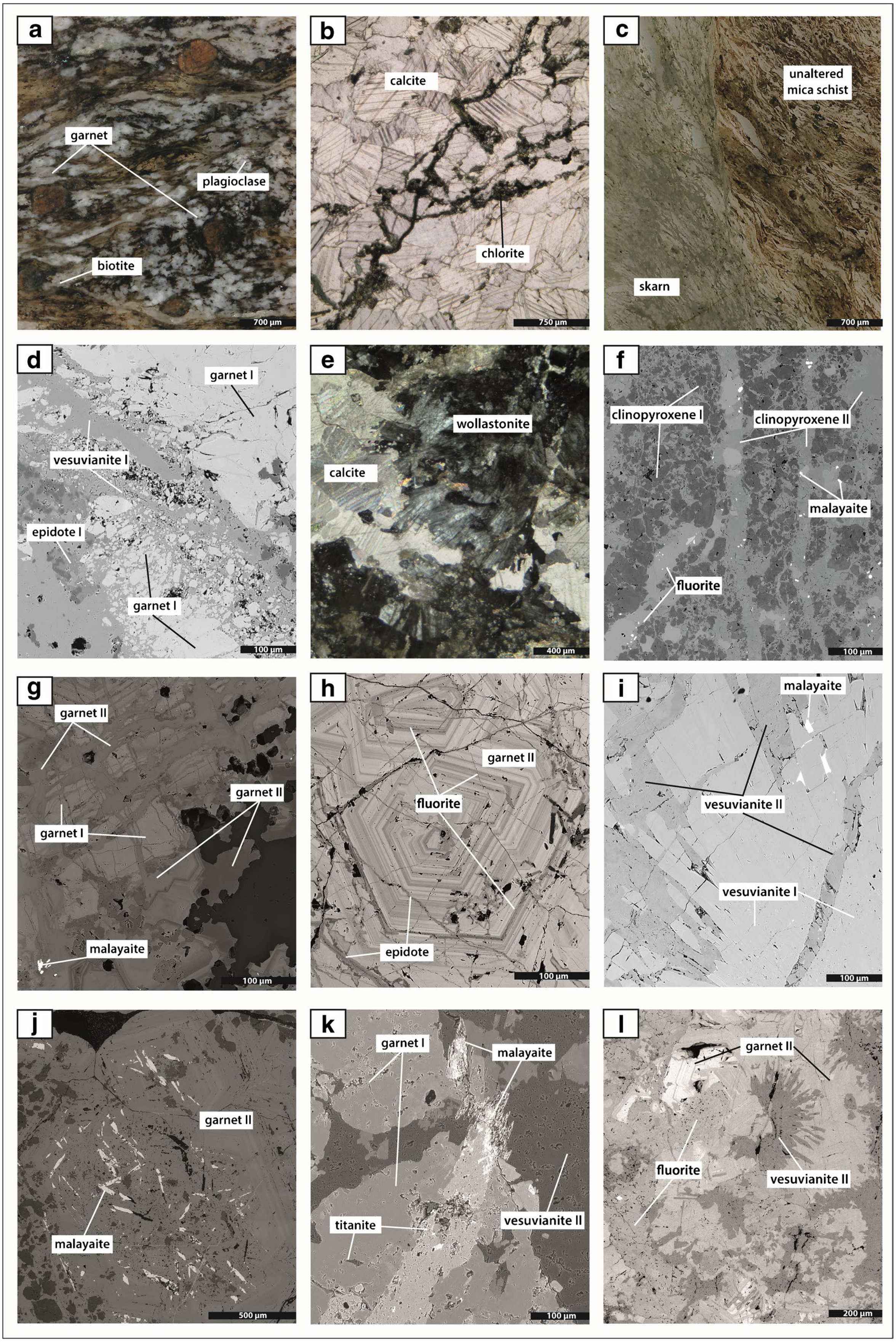
a
garnet
plagioclase
biotite
700 µm
b
calcite
chlorite
750 µm
c
unaltered
mica schist
skarn
700 µm
d
garnet I
vesuvianite I
epidote I
garnet I
100 µm
e
wollastonite
calcite
400 µm
f
clinopyroxene I
clinopyroxene II
malayaite
fluorite
100 µm
g
garnet II
garnet II
garnet I
malayaite
100 µm
h
garnet II
fluorite
epidote
100 µm
i
malayaite
vesuvianite II
vesuvianite I
100 µm
j
garnet II
malayaite
500 µm
k
garnet I
malayaite
titanite
vesuvianite II
100 µm
l
garnet II
fluorite
vesuvianite II
200 µm

◂**Fig. 5** Photomicrographs and backscattered electron microscopy images of characteristic minerals and textures of skarn and host rock. **a** Metamorphic texture of the metasedimentary host rock including mainly garnet, biotite, and quartz (GR-626-03b). **b** Subhedral calcite intersected by chlorite-filled veinlets (GR-667-11-03). **c** Contact between biotite schist and pyroxene skarn (GM-1-07B). **d** Garnet intersected by veins with vesuvianite and epidote infill (GR-667-10-02). **e** Grayish wollastonite replacing calcitic marble (GR-667-10-02). **f** Stage II clinopyroxene, malayaite, and fluorite replace clinopyroxene of skarn stage I (GR-626-06b). **g** Iron-rich garnet of skarn stage I is cross-cut by garnet with malayaite inclusions of skarn stage II (GR-626-04c). **h** Euhedral and zoned garnet of skarn stage II. Some of the growth zones are intergrown with coeval fluorite (GR-626-08a). **i** Vesuvianite of the first skarn stage, replaced, and cross-cut by vesuvianite II, which comprises malayaite inclusions (GR-667-16-03a). **j** Lath-shaped, euhedral malayaite enclosed by stage II garnet (GM-1-08c). **k** Lath-shaped titanite enclosed by garnet of skarn stage I. Both, titanite and garnet I, are intersected by vesuvianite; where titanite is in contact with vesuvianite it is replaced by malayaite (GR-667-1-01b). **l** Cogenetic garnet and vesuvianite of stage II replaced by fluorite (GR-626-04b)

transitional to later retrograde skarn textures and cassiterite-bearing veins. This late-stage alteration overprints both skarn stages and is characterized by the replacement of skarn minerals by amphibole, chlorite, quartz, and calcite. The alteration commonly centers on veinlets that cross-cut the skarn alteration; locally, the prograde skarn texture is almost completely replaced and only relicts are preserved. The thickness of these veinlets commonly does not exceed 5 cm, and their alteration halo shows minor chloritization of the adjacent host rock. These veins are mostly confined to skarns and can be traced only a few centimeters into the metasedimentary units. In association with chloritization and late-stage overprint of skarn assemblages, cassiterite is a common mineral and accounts for the majority of the tin mineralization within the Geyer skarns.

Stage I skarn

The skarnoid stage I skarns of the Geyer SW deposit occur as weakly delimited areas intercalated in the metasedimentary rocks and are composed predominantly of white to pale green, fine-crystalline clinopyroxene (Fig. 5d). Locally, euhedral brown to red garnet with sizes of up to several millimeters occurs as layers or aggregates that follow the metamorphic layering. This garnet is of the andradite-grossular series, shows only weak zonation and has abundant inclusions of pyroxene.

Pale red, lath-shaped vesuvianite accompanies pyroxene, garnet, and wollastonite. Commonly, vesuvianite and wollastonite replace garnet (Fig. 5d), which results in a very fine-grained texture. The skarn front (contact between skarn and marble) is marked by abundant wollastonite replacing calcite marble (Fig. 5e). Locally, euhedral, pale green epidote occurs at the contact between skarn and host rock. Titanite occurs regularly as euhedral minerals enclosed by garnet. Rutile and ilmenite of the metasedimentary rocks are replaced by titanite of the first skarn stage.

Fluorite is the most common non-silicate mineral in stage I skarn. It occurs throughout skarn I, comprising textures such as anhedral interstitial grains among clinopyroxene, infill between growth zones of garnet, and up to 0.6 mm large euhedral single grains coeval with vesuvianite.

Early skarn II stage

Stage II skarn contains significantly more garnet than stage I skarn, with clinopyroxene still being very abundant. This results in highly variable garnet/pyroxene ratios. In addition to the prominent vertical zoning within skarn layers (stage I at the margins and stage II in the center), skarn stage II also exhibits an internal mineralogical zoning. This zoning includes pyroxene- and vesuvianite-rich, fine-grained, massively textured rims almost without garnet. Toward the center of the skarn layers, the mineralogy becomes progressively coarser grained and enriched in garnet, with some garnet crystals reaching up to several centimeters size, whereas pyroxene crystals do not exceed a few millimeters in size (Fig. 4d). The metamorphic fabric of the host rocks is partly preserved in the pyroxene-vesuvianite rims of stage II skarn, whereas garnet-rich centers show an isometric texture without any remnant foliation. Almost monomineralic skarn layers consisting of vesuvianite or clinopyroxene and densely intergrown garnets are less affected by later replacement. Diopsidic to hedenbergitic clinopyroxene occurs as white to dark green acicular to columnar crystals (0.02 mm to 0.5 mm in length) that commonly form dense masses partly replacing stage I clinopyroxene (Fig. 5f). Stage II garnet belongs to the grossular-andradite solid solution series, which is highly variable with respect to size (µm- to cm-scale), color (red, beige, or green) and shape (euhedral and anhedral). This garnet generation truncates, cross-cuts, or overgrows previous garnet of skarn stage I (Fig. 5g).

Cores of garnet II form anhedral to euhedral crystals with more intense brown to reddish colors, weak growth zoning, and are optical anisotropic. The cores are commonly overgrown by rims of dark green to yellow garnet, exhibiting well defined growth zones and euhedral crystal shapes (Fig. 5h). Garnet II crystals may contain remnants of stage I garnet in their core.

Vesuvianite forms euhedral and lath-shaped crystals of reddish or greenish color, which are coeval to or postdate garnet II and which are commonly accompanied by fluorite. Vesuvianite of stage II fills fractures in and encloses vesuvianite I (Fig. 5i).

Malayaite, ($CaSnO[SiO_4]$), is the first tin-bearing mineral in the entire paragenetic sequence. It forms euhedral, lath-shaped crystals (<1 mm) that are intimately associated with

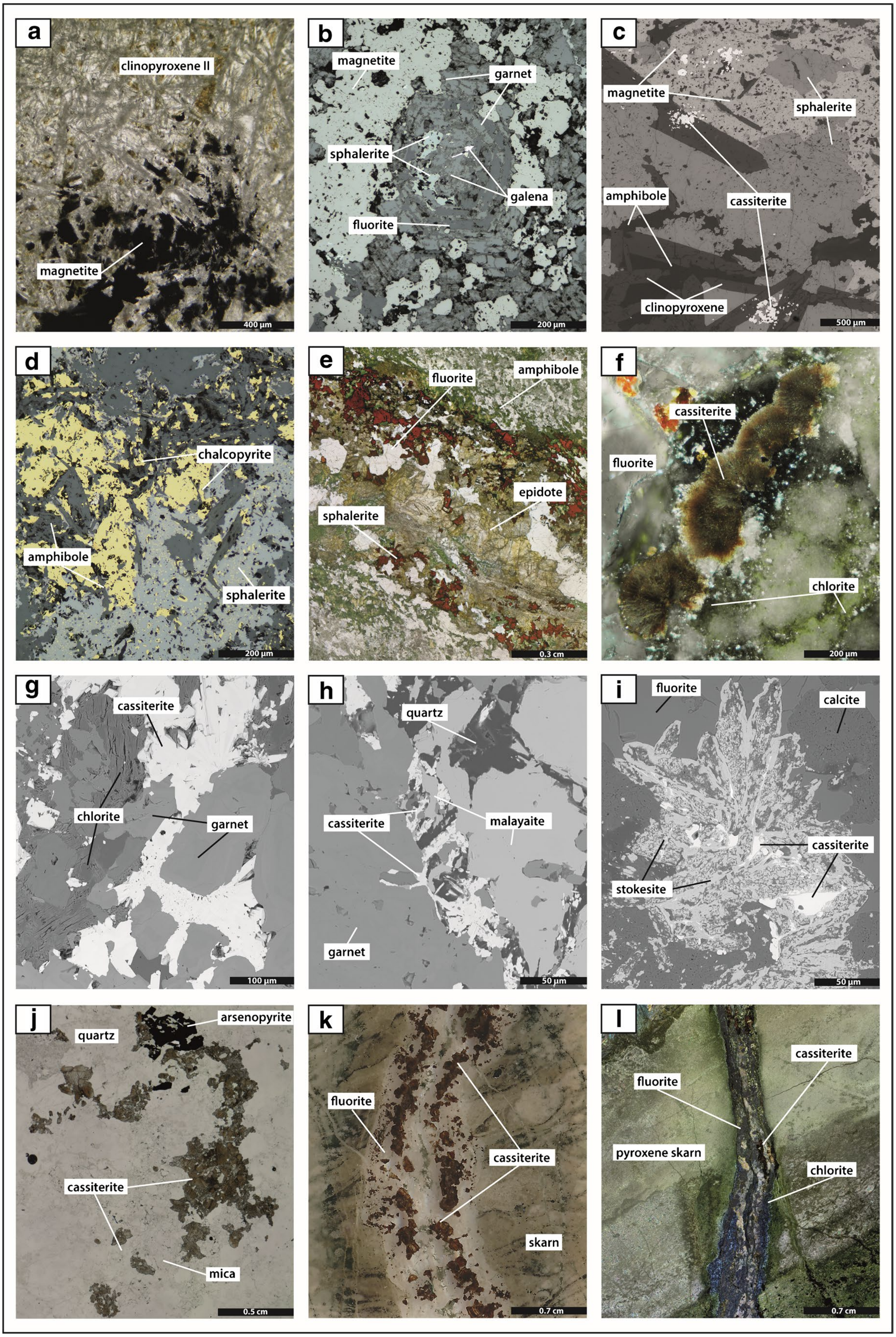
a
clinopyroxene II
magnetite
400 µm
b
magnetite
garnet
sphalerite
galena
fluorite
200 µm
c
magnetite
sphalerite
amphibole
cassiterite
clinopyroxene
500 µm
d
chalcopyrite
amphibole
sphalerite
200 µm
e
fluorite
amphibole
epidote
sphalerite
0.3 cm
f
cassiterite
fluorite
chlorite
200 µm
g
cassiterite
chlorite
garnet
100 µm
h
quartz
cassiterite
malayaite
garnet
50 µm
i
fluorite
calcite
cassiterite
stokesite
50 µm
j
quartz
arsenopyrite
cassiterite
mica
0.5 cm
k
fluorite
cassiterite
skarn
0.7 cm
l
cassiterite
fluorite
pyroxene skarn
chlorite
0.7 cm

◂**Fig. 6** Photomicrographs and backscattered electron microscopy images of common ore minerals and mineral textures. **a** Euhedral, diopside-rich clinopyroxene replaced by magnetite (GR-626-06c). **b** Magnetite, sphalerite, and minor galena replace garnet (GR-638-03a). **c** Euhedral clinopyroxene overgrown and partially replaced by magnetite, cassiterite, sphalerite, and amphibole (GR-626-06a). **d** Amphibole intergrown with chalcopyrite, sphalerite, and minor galena (GR-638-04a). **e** Epidote and amphibole accompanied by sphalerite and fluorite (GR-606-02a). **f** Anhedral to acicular wood-tin, fluorite, and chlorite in the late stage of skarn II alteration (GR-606-02a). **g** Cassiterite and chlorite fill fractures in garnet (GR-626-05a). **h** Malayaite enclosed by garnet is replaced by cassiterite and quartz (GM-1-08a). **i** Cassiterite replaced by stokesite and manganiferous calcite (GR-638-03c). **j** Greisenized granite with disseminated cassiterite (GR-R-148b). **k** Skarn cross-cut by a cassiterite fluorite and quartz vein (GR-657-02a). **l** Chlorite-fluorite-cassiterite vein cross-cuts pyroxene-skarn (GR-657-04a)

pyroxene, vesuvianite, and cores of grossular-rich garnet II (Fig. 5f, i, and j). Malayaite often replaces titanite (Fig. 5k) and occurs as lath-shaped, euhedral crystals enclosed by garnet and vesuvianite or occurs along growth zones of garnet. Early-stage skarn minerals are replaced by plagioclase and K-feldspar, at the end of the early skarn stage II. They are in turn overgrown by sericite, calcite, fluorite, and quartz (Fig. 5l).

Late-stage skarn II alteration

The transition to the late-stage phase of skarn II alteration (which affects both stage I and II skarns) is marked by the occurrence of magnetite, hydrous calc-silicates like epidote and amphibole as well as chlorite, minor base metal sulfides, and cassiterite. Magnetite occurs as coarse, crystalline, irregular pods, or interstitial grains enclosed by pyroxene (Fig. 6a). It is partially altered to hematite. It postdates clinopyroxene and garnet but predates amphibole and chlorite (Fig. 6b and c). Magnetite can be intergrown with spongy cassiterite, marking the first occurrence of this mineral in the mineral assemblage of the Geyer SW deposit and a variety of sulfide minerals like sphalerite, chalcopyrite, and galena. The latter, though, appear to be paragenetically younger than magnetite and associated cassiterite (Fig. 6d). Epidote forms dark green, prismatic crystals that exhibit distinct zoning. Epidote commonly occurs as lens-shaped to roundish aggregates together with fluorite and sometimes sphalerite (Fig. 6e). Modal abundances of epidote are highly variable, but it is usually present in both pyroxene-rich and garnet-rich skarn layers. Sphalerite, usually with chalcopyrite inclusions and coeval with independent chalcopyrite grains, is present as coarse-crystalline aggregates. Galena is almost invariably enclosed as anhedral inclusions in the other sulfides. Euhedral, greenish to black amphibole (<2 mm) is accompanied by fluorite, quartz, occasionally sulfide minerals, and acicular cassiterite (i.e., wood tin; Fig. 6f). Fine-grained green amphibole, however, occurs in pyroxene-dominated skarn and replaces clinopyroxene along veins and fractures. Euhedral cassiterite accompanied by chlorite and quartz fills fractures in garnet, vesuvianite, and clinopyroxene (Fig. 6g). There is evidence that cassiterite replaces malayaite (Fig. 6h). Minor amounts of fluorite and manganiferous hydrothermal calcite are the last minerals in the paragenetic sequence of skarn alteration. Calcite pseudomorphs after clinopyroxene are a characteristic feature of this stage, whereas garnets enclosing clinopyroxene remain unaffected by the replacement. In addition, Mn-calcite overgrows cassiterite; scarce stokesite (a rare Ca-Sn-hydrosilicate) is in close association with calcite (Fig. 6i).

Greisen alteration

Greisen alteration occurs mainly within the granitic intrusion at Geyer (endogreisen), but also extends into the metamorphic host rock (exogreisen). Greisen alteration at Geyer is mainly related to veins (<3 cm thickness) and dense stockwork zones (<6 m thickness) that result in extensive alteration zones. Greisen mineral association comprises mainly quartz, Li-mica, and topaz that replace igneous feldspar and mica, but also occur as vein infill. Cassiterite accompanies greisen minerals and occurs as disseminated grains in the alteration halos and in the veins (Fig. 6j). Sizes of cassiterite crystals are generally larger in veins than in pervasively altered areas. In addition, fluorite and apatite occur within veins. Minor wolframite, molybdenite, and loellingite intergrown with arsenopyrite were recognized.

Late-stage veins

Abundant veinlets, which range in thickness between 0.5 mm and 5 cm, cross-cut metasedimentary and skarn units (Fig. 4i). Veins of this type can be traced in drill cores over a length of up to 300 m. The mineralogy of the veins includes variable abundances of chlorite, quartz, fluorite, cassiterite, and arsenopyrite. Based on the predominant vein minerals, three different associations are observed: (a) chlorite-cassiterite, (b) fluorite-cassiterite, and (c) fluorite-quartz veins. Chlorite-cassiterite veins, which are typically accompanied by an alteration halo that reaches about five times the vein thickness, mainly occur within skarn units but may extend up to several centimeters into the metasedimentary units. They postdate skarn I and the early stage of skarn II and contain aggregates of euhedral chlorite (<200 μm), accompanied by subhedral fluorite crystals (<400 μm). Cassiterite occurs as euhedral zoned crystals with sizes <5 mm (Fig. 6k) and as massive dark brown aggregates interstitial between chlorite grains in the alteration halo (Fig. 6l). Locally, euhedral arsenopyrite is present together with anhedral quartz between fluorite and chlorite minerals. Fluorite-cassiterite

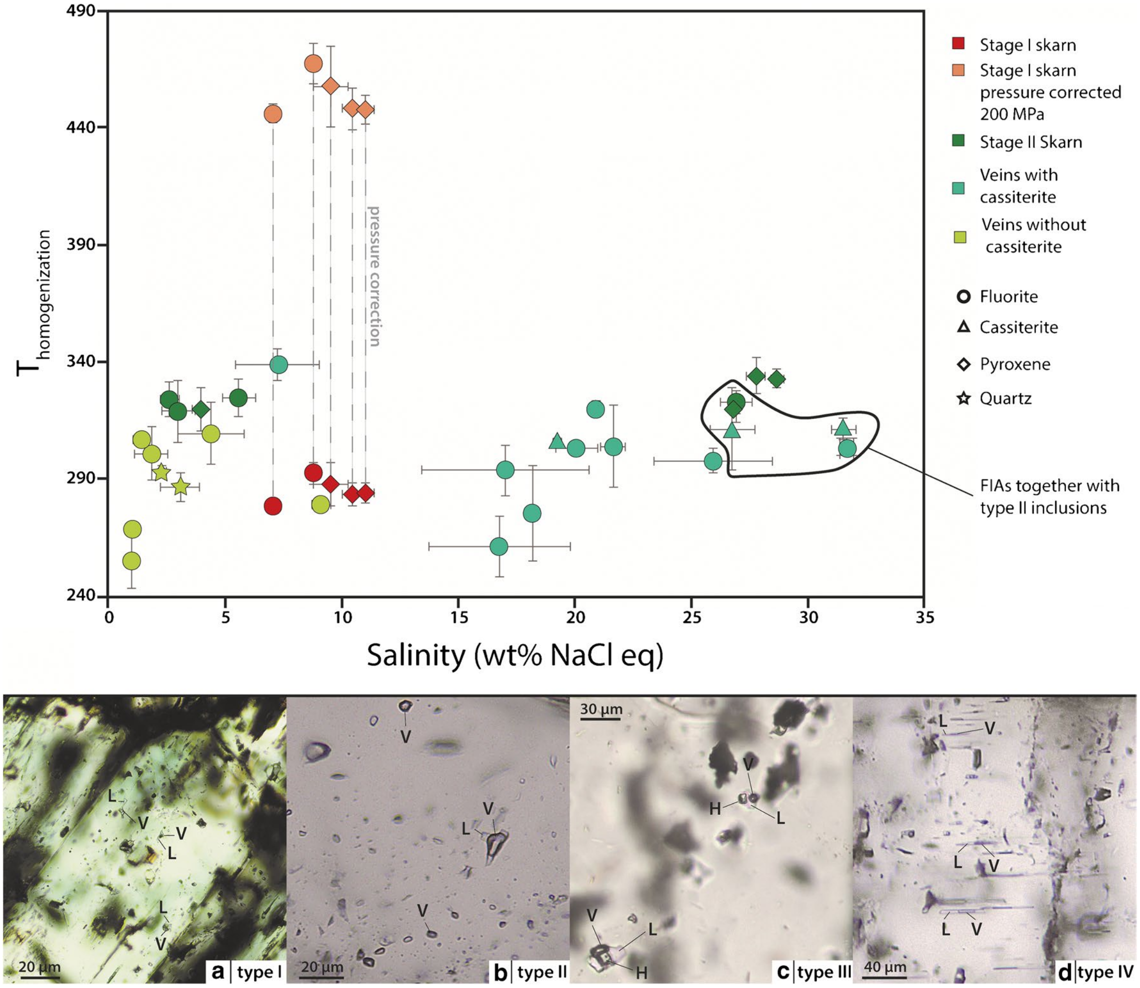

Fig. 7 Salinity (NaCl±$CaCl_2$) versus homogenization temperature in °C of analyzed fluid inclusion assemblages (FIAs). Data points show the average values of measured FIAs with corresponding error bars delineate the range of FIAs. FIAs are categorized according to the host mineral and the respective alteration stage. FIAs of stage I are pressure corrected assuming 200 MPa as formation pressure. **a** Type I liquid-rich two-phase primary fluid inclusions in green clinopyroxene. **b** Type II vapor-dominant fluid inclusions in fluorite. **c** Type III liquid-rich multiphase fluid inclusions in a pseudosecondary trail hosted by fluorite. **d** Type IV two-phase fluid inclusions in primary trails hosted by fluorite from a vein

Table 2 Summary of the microthermometric data of analyzed fluid inclusion assemblages from the Geyer system

Alteration stage	Host mineral	Fluid inclusion type	Petrography of fluid inclusion	# of FIAs	# fluid inclusions	Tm(ice) (°C) min/avg/max	Th (°C) uncorrected min/avg/max	Th (°C) P-corrected min/avg/max	Salinity in wt. % eq. (Nacl ± $CaCl_2$)
Stage I skarn[1]	cpx	Type I-L	ps	5	25	-7.4/-6.2/-4.4	279/285/293	447/ 454/468	7.06/9.37/11.00
Stage II skarn[2]	cpx, fl	Type I-L	p	4	23	-3.42/-2.27/-1.53	319/322/325	328/331/334	2.61/3.79/5.58
Stage II skarn[2]	cpx, fl	Type III-LVS	ps	4	19	-37.3/-32.8/-30.6	320/328/334	334/339/343	26.92/27.58/28.69
Veins with cst[2]	fl	Type I-L	p	1	9	- /-4.61/ -	- /339/ -	- /351/ -	- /7.27/ -
Veins with cst[2]	fl, cst	Type III-LVS	ps	11	67	-33.83/-21.87/-13.68	262/299/321	269/309/331	16.77/22.70/31.54
Veins without cst[2]	qz, fl	Type IV-LV	c, p	8	44	-5.93/-1.84/-0.55	255/288/310	272/300/318	0.96/3.02/9.12

Salinities were calculated according to Steele-MacInnis et al. (2012) for the H_2O-NaCl system and Steele-MacInnis et al. (2011) for the H_2O-NaCl-$CaCl_2$ system without taking potential CO_2 content into account. Min/avg/max values are given for fluid inclusion assemblages of one type in one alteration stage. Homogenization temperature was recalculated to a trapping pressure of [1]200 MPa and [2]15 MPa. *Cpx*, clinopyroxene; *fl*, fluorite; *cst*, cassiterite; *qz*, quartz; *p*, primary; *ps*, pseudosecondary; *c*, cluster and fluorite-quartz veins do not show distinct alteration halos and share many similarities. The only obvious difference is that the former includes cassiterite, whereas the latter does not. The occurrence of these veins is not restricted to skarn horizons; they cross-cut skarn as well as metasedimentary units and granitic rocks. Minor mineral phases in these veins are scheelite and arsenopyrite. Due to their similar mineralogy, we assume that these two vein types are coeval and reflect local mineralogical varieties of the same stage. Fluorite±quartz±cassiterite veins postdate the main skarn stages (including chlorite-cassiterite veins), which indicates that they reflect the latest stage of tin mineralization.

Fluid inclusions

Fluid inclusion microthermometric results related to skarns, greisen, and veins are described within their petrographic context in the following section.

Petrography of fluid inclusions

Fluid inclusions (FI) suitable for microthermometry were detected in pyroxene, fluorite, quartz, and cassiterite of the various textural stages described above. In total, 187 fluid inclusions (excluding vapor-rich fluid inclusions) in 33 fluid inclusion assemblages (FIA) were analyzed. These included primary, pseudosecondary, and clustered inclusions (Goldstein and Reynolds 1994; Roedder 1984). Based on observations at room temperature (20 °C; and in cooling experiments in the case of hydrohalite), four types of fluid inclusions were distinguished (Fig. 7).

Type I-L FIs (fluid-rich two-phase FIs) contain a liquid (70–80 vol%) and a vapor phase (20–30 vol%). They are ellipsoid or irregular in shape and commonly occur in pseudosecondary trails. The diameter of the inclusions is highly variable, ranging from <10–55 µm.

Type II-V FIs (vapor-rich two-phase FIs) are characterized by a high proportion of vapor (>90 vol%). They are usually irregular or show the shape of a negative crystal, ranging between 10 and 25 µm in diameter, with a few exceptions of larger inclusions. This type is intimately associated with some FIAs of type III and occurs in the same primary or pseudosecondary trails.

Type III-LVS FIAs (liquid-rich multiphase FIs) contain an aqueous liquid phase (60–80 vol%), a vapor phase (20–40 vol%), and one or more daughter crystals. The diameter of the inclusions does not exceed 25 µm and the shape is ellipsoid, irregular, or angular. Solid phases in the FIs are halite or hydrohalite, and less commonly fluorite.

Type IV-LV FIAs (two-phase FIs) contain a liquid phase (40–60 vol%) and a vapor phase (40–60 vol.%). Primary inclusions appear as clusters in fluorite or in quartz. Also, pseudosecondary trails with roundish and elongated inclusions that cross-cut one or two growth zones in fluorite are present. The diameter of these inclusions varies from <5–45 µm.

Microthermometry of fluid inclusions

The microthermometric data of the different fluid inclusion types are summarized in Table 2. The data are presented and grouped according to the textural position of the host minerals within the different alteration assemblages. A detailed background data set including individual fluid inclusion analyses is provided in ESM Table 1.

Stage I skarn Fluid inclusion assemblages in cogenetic hedenbergite (Fig. 7a) and fluorite of stage I skarn show homogeneous entrapment and are invariably type I-L inclusions. The average eutectic temperature is 21 °C, so these fluid inclusions are best described in the NaCl-H_2O system. The homogenization temperature T_h (LV➔ L) ranges from 279–293 °C (uncorrected; 447 to 468 °C for estimated pressures, see discussion for more details). The melting temperature of ice $T_{m(ice)}$ is between −4.4 °C and −7.4 °C, corresponding to a salinity of 7.1–11.0 % eq. w(NaCl).

Skarn, greisen, and vein stage II In the stage II skarn, FIAs of type I-L, II-V, and III-LVS of the NaCl-H_2O system and of the NaCl-$CaCl_2$-H_2O system were identified in fluorite and clinopyroxene (Fig. 7). Type I-L FIAs show T_h (LV-L) of 320–325 °C, $T_{m(ice)}$ of −1.5 to −3.4 °C, which corresponds to a salinity range of 2.6 and 5.6% eq. w(NaCl). Fluid inclusions of type III-LVS in clinopyroxene and fluorite have T_h of 325 to 335 °C. $T_{m(ice)}$ ranges from −37.2 to −31.0 °C, and the melting temperature of hydrohalite ($T_{m(hh)}$) is between −32.0 and −16.5°C, which corresponds to a salinity of 26.9–28.7% eq. w(NaCl+$CaCl_2$). Type III-LVS can locally be found in the same trail as type II-V fluid inclusions.

In chlorite-cassiterite and fluorite-cassiterite veins, fluid inclusions of type I-L, II-V, and III-LVS of the NaCl-H_2O system and the NaCl-$CaCl_2$-H_2O system were observed in fluorite and cassiterite. In trails with type III-LVS inclusions, FIs of type II-V can occur, which indicates heterogeneous entrapment. Neither the T_h nor the Tm could be determined in these inclusions since the phase transitions were not visible due to the high content of the vapor phase (Fig. 7b). Halite-bearing type III-LVS inclusions (Fig. 7c) have T_h of 305–310 °C, melting temperatures of halite $T_{m(h)}$ between 120 and 140 °C, which results in an average salinity of 31.5% eq. w(NaCl+CaCl2). Halite-free type III-LVS inclusions have a T_h between 275 and 320 °C, a $T_{m(hh)}$ of −44.1 to −22.7 °C, and a corresponding salinity of 20.0–32.2% eq. w(NaCl+$CaCl_2$). Fluid inclusions of type III-LVS hosted by fluorite, which are best described in the H_2O-NaCl system, have an average T_h of 340 °C, $T_{m(ice)}$ of −4.6°C, and a salinity of 7.3% eq. w(NaCl). In veins without cassiterite, fluid inclusions of type IV-LV, also best described in the H_2O-NaCl-system, were analyzed in fluorite (Fig. 7d) and quartz. The latter contains inclusions with a T_h of 285–295 °C, $T_{m(ice)}$ between −1.8 and 1.3 °C, corresponding to a salinity of 2.3–3.1% eq. w(NaCl). Fluorite contains fluid inclusions with T_h of 255 to 310 °C, $T_{m(ice)}$ between 0.6 and 5.9°C, and a resulting salinity of 1.0–5.9% eq. w(NaCl).

Geochronology

Five garnet samples with 144 and three cassiterite samples with 95 individual spot analyses were successfully dated by U-Pb LA-ICP-MS. The concentration of U and Pb and the calculated ages, sample location, and number of spot analyses are compiled in Table 1.

Samples GR4 (drill core Z626, 85 m) and GR5 (drill core Z606A, 79.5 m) are related to stage I skarn. The analyzed reddish to brown garnet is of grossular-rich grandite composition, accompanied by green to white, diopsidic clinopyroxene (Fig. 2a). Samples GR4 and GR5 contain only prograde calc-silicate minerals and there is no evidence of chloritization. The U content of garnet in sample GR4 ranges from 0.04–0.65 µg/g and in GR5 from 0.01–1.75 µg/g, and Pb concentrations in garnets range from 0.01–0.14 µg/g in GR4 and 0.06–0.39 µg/g in GR5. Results from these two samples yield overlapping lower intercept ages of 322.4 ± 5.1 Ma and 322.1 ± 11.8 Ma, respectively (Fig. 2a).

The garnet samples GR1 (96.5 m), GR2 (59 m), and GR6 (45.6 m) from drill core Z626 (Fig. 2b) are related to stage II skarn. Garnets in these samples are pale to dark green, andradite-rich and are intergrown with clinopyroxene. Samples GR2 and GR6 contain prograde minerals only, whereas GR1 is cross-cut by some thin chlorite veins (<1 mm). The U contents of the garnets in these samples vary between 0.01 µg/g and 1.4 µg/g, and Pb concentrations vary between 0.01 µg/g and 0.9 µg/g. The U-Pb data yield lower intercept ages of 307.3 ± 4.8, 305.1 ± 3.9, and 301.6 ± 5.0 Ma for samples GR6, GR2, and GR1, respectively. Cassiterite from sample GR657-02a (core Z657, 83.8 m) occurs in a vein accompanied by fluorite and quartz cross-cutting a skarn (Fig. 2c). The cassiterite is euhedral and exhibits distinct growth zones with dark brown to translucent domains. The U and Pb content of the cassiterite ranges between 1.4–16.5 µg/g and 0.08–1.2 µg/g, respectively. The U-Pb data result in a lower intercept age of 308.2 ± 3.7 Ma. Samples 60973 and 60974 ("Binge," Geyer) contain granite-hosted greisen with cassiterite closely associated with quartz, mica, and topaz (Fig. 2d). The U content of these cassiterite crystals ranges from 0.09–33.1 µg/g, with a Pb content between 0.06 and 14.1 µg/g, yielding a lower intercept age of 305.7 ± 3.7 and 306.6 ± 3.5 Ma, i.e., within the error of the ages obtained for cassiterite from veins and from garnets of skarn II assemblages.

Discussion

In the following, the geochronological data of garnet and cassiterite as well as cross-cutting relationships are discussed to constrain the temporal evolution of the Geyer magmatic-hydrothermal system. Furthermore, the geochronological data is used to evaluate potential causative intrusions in the area and to integrate the timing of hydrothermal activity at Geyer into the existing geochronological framework of the Erzgebirge region. Fluid inclusion data is used to constrain the fluid evolution of the magmatic-hydrothermal system, providing important clues to better understand hydrothermal tin enrichment in Variscan skarn systems.

Temporal evolution of the Geyer magmatic-hydrothermal system

In situ U-Pb geochronology on garnet yields an age of 322.4 ± 5.5 (GR4) and of 322.5 ± 11.4 Ma (GR5) for the stage I skarns, coinciding with the emplacement of the nearby Greifenstein intrusion, which was dated to 324 ± 4 to 320 ± 3 (Romer et al. 2007) and the early stage of emplacement of the large-volume Eibenstock granite intrusion, with an age range between 323 and 314 Ma (Förster et al. 2009; Kempe et al. 2004; Tichomirowa et al. 2019; Warkus 1997). This relates the formation of stage I skarns to the emplacement of the major batholiths in the area.

Stage II skarn garnet ages of 307 ± 5, 305 ± 4, and 301.6 ± 6 Ma are invariably younger than skarnoid garnet of stage I skarn, consistent with textural observations. Cassiterite ages of 305.7 ± 2.8, 306.6 ± 2.5 Ma (both greisen), and 308.2 ± 2.9 Ma (late-stage vein) relate stage II skarn, greisen alteration, and late-stage veins to the same magmatic-hydrothermal event which clearly postdates the emplacement of the known granitic intrusions in the area (Romer et al. 2007). This suggests that tin mineralization is related to a younger, yet previously unrecognized magmatic event (Fig. 8). The fine-grained quartz-topaz-rich intrusion and the rhyolitic dykes (Bolduan 1963a) that postdate the main intrusive stage at Geyer support this assumption, as these rocks are most likely related to the causative intrusions for tin mineralization. However, direct geochronological data that constrain the timing of these younger intrusions are unfortunately not available at Geyer.

The observation that hydrothermal mineralization postdates the emplacement of the large-volume intrusions (e.g., Eibenstock) in the Geyer district is consistent with the timing of skarn formation and magmatic-hydrothermal activity recently constrained in a regional reconnaissance study

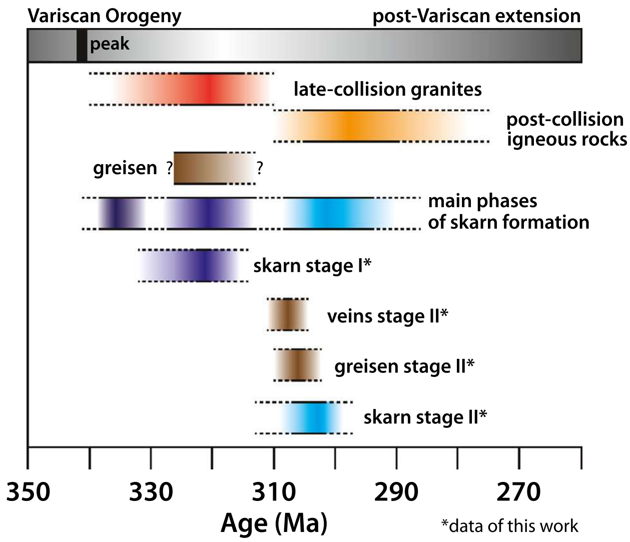

Fig. 8 Geodynamic overview and compilation of geochronological data of igneous rocks of the Erzgebirge and hydrothermal mineralization (after Reinhardt et al. 2022 and references therein). Data of this study is shown separately and marked with an asterisk

of skarns in the Erzgebirge metallogenic province (Burisch et al. 2019) as well as a geochronological study of skarns in the Schwarzenberg district further to the west (Reinhardt et al. 2022). Both studies recognized three distinct episodes: (A) 338–331 Ma, (B) 327–310 Ma, and (C) ~310–295 Ma.

Whereas stages A and B may be related to the emplacement of late-collisional granites, stage C coincides with post-collisional magmatic activity in the region (Förster et al. 1999; Hoffmann et al. 2013; Kröner and Willner 1998; Löcse et al. 2023; Luthardt et al. 2018).

The statistically robust age difference between stage I and stage II skarn, greisen, and veins suggests a distinct hiatus in the magmatic and magmatic-hydrothermal activity in the Geyer district of at least 12 Ma. Skarn deposits of the Schwarzenberg district show similar characteristics with an early-stage coinciding with the emplacement of large granitic batholiths in the area — and a distinctively younger skarn stage that is associated with extensive retrograde alteration and magmatic-hydrothermal mineralization. This bimodal age distribution seems thus to be a common feature in Erzgebirge skarn deposits (Burisch et al. 2019; Reinhardt et al. 2022), but rather atypical for skarn deposits in general (e.g., Burisch et al. 2023; Meinert et al. 2005).

Finally, it is important to point out that ages obtained for greisen- and skarn-hosted cassiterite in this study provide the first direct evidence that greisen- and skarn-type mineralization in the Erzgebirge are of similar age — and, hence, most likely related to the same magmatic-hydrothermal event (Figs. 8 and 9). Furthermore, the new ages document that formation of greisen-hosted tin mineralization in the Erzgebirge does not (only) coincide with late-collisional (Zhang et al. 2017) but (also) with post-collisional magmatic activity.

Genesis of the Geyer magmatic-hydrothermal system

Stage I

Geochronological data relate stage I skarn to the emplacement of the large late-collisional granitic batholith at ~324–315 Ma. Characteristically red garnet and pale green pyroxene of skarn I are typical of skarns that form relatively proximal to their causative intrusion (Fig. 9). The fine-crystalline nature and skarnoid texture indicate formation under almost contact-metamorphic conditions, with only limited hydrothermal fluid involved, related to the thermal anomaly associated with the emplacement of the batholith (Meinert et al. 2005; Papeschi et al. 2017). The low amount of fluid involved in stage I skarn formation is furthermore supported by the distinct absence of a stage associated with hydrous skarn minerals. Based on these considerations, the emplacement depth of the genetically associated intrusion should provide a good estimate for the depth of formation of stage I skarn. The nearby Greifensteine intrusion was emplaced at a depth between 2.5 and 4.0 km at a minimum pressure of 200 MPa (Breiter et al. 1999; Romer et al. 2007), which is assumed to also correspond to the Geyer intrusion. Since contact metamorphic and ductile conditions probably prevailed during this stage, we assume lithostatic conditions during the formation of stage I skarn. Consequently, fluid inclusion homogenization temperatures were corrected for pressures of 200 MPa (Fig. 7). This results in a formation temperature for stage I skarn of 450–470 °C, involving fluids with intermediate salinities, which is consistent with early-stage magmatic fluids that exsolve from granitic magmas (Driesner and Heinrich 2007; Korges et al. 2020). The absence of cassiterite and tin silicates associated with stage I skarn is likely related to one or more of the following factors: (a) formation of skarn stage I predates the main fluid exsolution event and (b) magmatic fractionation during the formation of skarn I stage was not sufficient to efficiently enrich tin in the associated fluids, which has been proposed to be a key factor for the formation of tin deposits (Simons et al. 2017; Taylor 1979).

Stage II skarn, greisen, and late-stage vein formation

In contrast to skarn I, skarn II shows distinct features that imply relatively distal and shallow formation conditions (Fig. 9) under hydrostatic pressure (mainly following the arguments of Meinert et al. 2005). These features include the abundance of green garnet as well as vein and cavity textures of skarn II. Using boiling assemblages, minimum

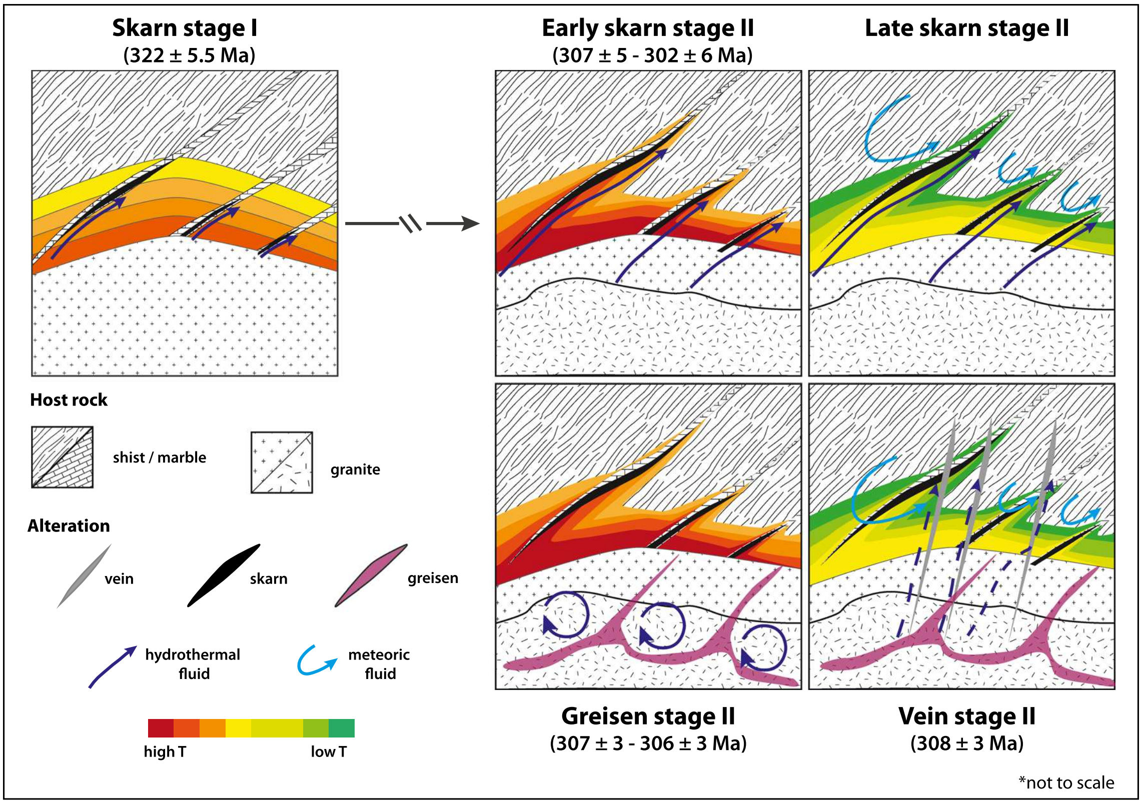

Fig. 9 Schematic genetic model illustrating the spatial and temporal evolution of the Geyer magmatic-hydrothermal system (not to scale)

pressures for the entrapment of fluid inclusions related to skarn stage II yield 10–15 MPa. Assuming hydrostatic conditions, these pressures correspond to formation depths of 1.5–2 km below the paleo water table (Driesner and Heinrich 2007). The differences between the depth of formation between stage I skarn (4.0–2.5 km) and stage II skarn are consistent with the fast tectonic uplift of the Erzgebirge that followed the collisional stage of the Variscides (Burisch et al. 2019; Schmädicke et al. 1995). A similar present-day position, but different formation conditions of skarn stage II and I suggest that the unknown causative granitic intrusion (fluid source) of skarn II can be expected to be a small (?), subvolcanic granite stock, similar to those exposed in the Eastern Erzgebirge (e. g. Zinnwald-Cinovec, Altenberg).

Fluid inclusion data suggest that the onset of skarn II formation occurred at >330 °C. Fluid inclusions related to the early stage of skarn II show a bimodal salinity distribution (Fig. 7). FIAs with low salinity do not show any indication for heterogeneous entrapment or phase separation. Therefore, these inclusions are interpreted to display the unmodified skarn-forming fluid. The occurrence of high-salinity fluid inclusion assemblages with indications of heterogeneous entrapment indicates that boiling occurred, whereas ingress of larger amounts of meteoric fluids during the early stage is unlikely (Fekete et al. 2016). Fluid salinities above ~20 wt% seem to be characteristic of the early stages of greisen- and skarn-hosted tin deposits in general (Korges et al. 2018, 2020; Peng and Bromley 1992). This is consistent with numerical hydraulic models (Fekete et al. 2016) that suggest that overpressure during the early stage inhibits entrainment of significant amounts of meteoric fluids into the magmatic-hydrothermal system.

Fluid inclusion homogenization temperatures could not be measured in minerals related to late-stage skarn II alteration, but a continuous cooling trend (340 to 240 °C) is recognized between skarn stage II and late-stage veins (Fig. 7). This cooling trend coincides with the transition from early- to late-phase skarn II formation and late-stage veining. Cooling has to be considered as a main controlling factor for base metal sulfide and cassiterite precipitation according to thermodynamic modeling and the relationship between ore and gangue minerals, as described in other skarn systems (Bertelli et al. 2009; Einaudi et al. 1981; Reed 2006). External input of sulfide from the metasedimentary host rock cannot be excluded.

The large range in salinities in fluid inclusions related to late veins suggests a continuous mixing trend of the highly saline magmatic-hydrothermal fluid with a diluted (probably meteoric) fluid during this late-stage evolution of the Geyer system. Since a clear correlation between salinity and temperature is lacking, it is likely that the meteoric fluids were heated up in the magmatic-hydrothermal system prior to entrainment (Audétat et al. 2000). The salinity and homogenization temperature of fluid inclusions from veins are consistent with fluid inclusions analyzed in greisen-hosted fluorite, which furthermore supports that greisen, skarn, and vein mineralization at Geyer are all different expressions of the same magmatic-hydrothermal event. Hence, the host rocks (igneous, marble, or mica schist) and cooling related to the temporal evolution of magmatic-hydrothermal tin systems are key factors that control the style of alteration and mineralization. At Geyer, younger hydrothermal fluorite quartz veins occur. The lack of cassiterite, epidote, and chlorite and significantly lower fluid inclusion homogenization temperatures (~110–170 °C) indicates that those veins are unrelated to tin mineralization.

Tin mineralization

The presence of malayaite in early skarn stage II marks the first enrichment of tin in the Geyer SW deposit. Backed by the cassiterite and garnet ages (308–302 Ma), this clearly indicates that tin mineralization is not associated with the emplacement of the large-volume batholith of the area, but is instead related to a probably more fractionated, smaller intrusion emplaced relatively more distal/deeper below the Geyer skarn system. The lack of tin silicates and the scarcity of distinct tin-bearing minerals in stage I skarn support a magmatic-hydrothermal source of tin and argue against local remobilization of tin from adjacent meta-sedimentary host rock units, as was recently proposed by (Lefebvre et al. 2019). The appearance of tin-rich silicates in early-stage skarn II assemblages rather indicates that tin was scavenged from an early-stage magmatic-hydrothermal fluid. This early-stage fixation in stage II skarn inhibited dispersion and promoted local concentration of tin in skarn layers.

A distinctly higher salinity of fluids related to cassiterite-bearing veins and greisen-altered domains compared to veins and greisen that are cassiterite-free indicates that chlorinity may have played a key role for cassiterite precipitation (Heinrich 1990) as tin is effectively transported as Sn-chloro-complexes (Schmidt 2018). The significant increase in salinity from about 4 to about 27 % eq. w($NaCl+CaCl_2$) appears to have been related to boiling of the early magmatic-hydrothermal fluid. Subsequent dilution and potentially concomitant cooling of chlorine-rich ore fluids are proposed as the controlling factor for cassiterite precipitation, which has been previously proposed as an efficient mechanism for tin enrichment in magmatic-hydrothermal systems (Audétat et al. 2000). The mineralogy and microthermometric data of cassiterite-free fluorite-quartz veins provide robust evidence that these veins do not belong to later Mesozoic mineralization styles, but instead imply that they are genetically related to the magmatic-hydrothermal stage. Therefore, we propose that such cassiterite-free fluorite-quartz veins likely formed from fluids which were along the fluid flow path already depleted in tin. Replacement of tin-bearing silicates by late-stage chlorite, actinolite, and calcite provided an additional source of tin, which promoted local enrichment of cassiterite and/or wood tin during the latest stages of the system.

Conclusions

The magmatic-hydrothermal tin deposit of Geyer, Erzgebirge, eastern Germany, shows various mineralization styles hosting tin ore minerals: greisen alteration restricted to the magmatic host rocks and skarns formed from former marbles and late-stage veins. The skarns occur as laterally extensive units comprised of several individual discontinuous skarn lenses replacing the marble of the metamorphic successions of the district. Mineral textures and cross-cutting relationships indicate two separate skarn-forming events — very similar to the observations made recently for skarn deposits of the Schwarzenberg district in the Erzgebirge (Reinhardt et al. 2021).

LA-ICP-MS U-Pb age dating of cassiterite and garnet was employed to constrain the temporal evolution of the magmatic-hydrothermal system at Geyer. The data provide the first direct evidence that greisen, skarn, and vein-type tin mineralization within one district/deposit in the Erzgebirge are different mineralogical expressions of the same magmatic-hydrothermal system.

The first skarn stage is not associated with any tin mineralization, shows characteristics of a proximal contact metamorphic skarn that formed under lithostatic conditions at probably 4 to 2.5 km depth, and coincides with the emplacement of large-volume batholiths in the area at around 320 Ma. Tin mineralization (malayaite and cassiterite) is, however, associated with the second, distinctly younger skarn-forming event at around 305 Ma. The formation depth of this skarn stage II is estimated to 2 to 1.5 km This shallower depth compared to skarn stage I is consistent with extensive uplift that occurred in the Erzgebirge between 320 and 305 Ma (Schmädicke et al. 1995). Although granitic intrusions coeval to skarn stage II are not documented in the area, there are abundant volcanic rocks of that age documented across the Erzgebirge. Hence, formation of skarn stage II is tentatively related to a younger and deeper intrusion. Based on fluid inclusion and petrographic observations, cooling and dilution of late-stage fluids by meteoric water is proposed as the key mechanism for cassiterite precipitation, that is mainly associated with late-stage chlorite-actinolite alteration and veining. The garnet/clinopyroxene ratio and colors of calc-silicates, the late occurrence of cassiterite in the paragenetic sequence, and the geometry of the skarn stage II at Geyer (and other skarns in the Erzgebirge) are different from classic, very proximal tin skarns (Kwak 1987). Instead, their mineralogy and fluid inclusion systematics suggest a more distal environment relative to the causative source intrusion. In contrast to classical skarn occurrences worldwide (Meinert et al. 2005), a systematic zoning of garnet/clinopyroxene ratios or a color change in the calc-silicates cannot be observed within the Geyer skarns. The lack of zoning is likely related to the large size of the system, and therefore, the recognition of zoning on a larger scale would require an even more extensive lateral grid of sampling (cf. Reinhardt et al. 2021).

Supplementary Information The online version contains supplementary material available at https://doi.org/10.1007/s00126-023-01194-8.

Acknowledgements We would like to thank Rongqing Zhang and two anonymous reviewers for their constructive comments that improved an earlier version of this manuscript. Manuel Lapp (LfULG Sachsen) is thanked for providing access to drill cores, thin sections, and exploration reports. We are grateful to Roland Würkert (Helmholtz Institute for Resource Technology) for sample preparation. Richard Albert is thanked for scans and support with geochronological measurements. This is FIERCE contribution No. 137.

Funding Open Access funding enabled and organized by Projekt DEAL. This project is financially supported by the German Science Foundation DFG via grant 3134023001 and 441189074 in the framework of the SPP 2238 DOME.

Declarations

Competing interests The authors declare no competing interests.

References

Audétat A, Günther D, Heinrich CA (2000) Causes for large-scale metal zonation around mineralized plutons: fluid inclusion LA-ICP-MS evidence from the Mole Granite, Australia. Econ Geol 95:1563–1581. https://doi.org/10.2113/gsecongeo.95.8.1563

Bauer ME, Seifert T, Burisch M, Krause J, Richter N, Gutzmer J (2019) Indium-bearing sulfides from the Hämmerlein skarn deposit, Erzgebirge, Germany: evidence for late-stage diffusion of indium into sphalerite. Miner Deposita 54:175–192

Bertelli M, Baker T, Cleverley JS, Ulrich T (2009) Geochemical modelling of a Zn–Pb skarn: constraints from LA–ICP–MS analysis of fluid inclusions. J Geochem Expl 102:13–26. https://doi.org/10.1016/j.gexplo.2008.11.015

Bolduan H (1963a) Geologie und Genese der Zinn-Wolframlagerstätte Geyer (Erzgeb.). Freiberger Forsch-Hefte C 167:7–34

Bolduan H (1963b) Geologische Ergebnisse von Bohrungen auf verdeckte Granitaufwölbungen im Raum Geyer-Ehrenfriedersdorf. Freiberger Forsch-Hefte C 167:95–105

Breiter K, Förster H-J, Seltmann R (1999) Variscan silicic magmatism and related tin-tungsten mineralization in the Erzgebirge-Slavkovský les metallogenic province. Miner Deposita 34:505–521. https://doi.org/10.1007/s001260050217

Breiter K, Ďurišová J, Hrstka T, Korbelová Z, Hložková Vaňková M, Vašinová Galiová M, Kanický V, Rambousek P, Knésl I, Dobeš P, Dosbaba M (2017) Assessment of magmatic vs. metasomatic processes in rare-metal granites: a case study of the Cínovec/Zinnwald Sn–W–Li deposit. Central Europe Lithos 292-293:198–217. https://doi.org/10.1016/j.lithos.2017.08.015

Burisch M, Gerdes A, Meinert LD, Albert R, Seifert T, Gutzmer J (2019) The essence of time – fertile skarn formation in the Variscan orogenic belt. Earth Planet Sci Lett 519:165–170. https://doi.org/10.1016/j.epsl.2019.05.015

Burisch M, Frenzel M, Seibel H, Gruber A, Oelze M, Pfänder JA, Sanchez-Garrido C, Gutzmer J (2021) Li-Co–Ni-Mn-(REE) veins of the Western Erzgebirge, Germany—a potential source of battery raw materials. Miner Deposita 56:1223–1238. https://doi.org/10.1007/s00126-021-01061-4

Burisch M, Markl G, Gutzmer J (2022) Breakup with benefits - hydrothermal mineral systems related to the disintegration of a supercontinent. Earth Planet Sci Lett 580:117373. https://doi.org/10.1016/j.epsl.2022.117373

Burisch M, Bussey SD, Landon N, Nasi C, Kakarieka A, Gerdes A, Albert R, Stein HJ, Gabites JA, Friedman RM, Meinert LD (2023) Timing of magmatism and skarn formation at the Limon, Guajes, and Media Luna gold ± copper skarn deposits at Morelos, Guerrero State, Mexico. Econ Geol 118:695–718. https://doi.org/10.5382/econgeo.4985

Černý P (1991) Fertile granites of Precambrian rare-element pegmatite fields: is geochemistry controlled by tectonic setting or source lithologies? Precamb Res 51:429–468. https://doi.org/10.1016/0301-9268(91)90111-M

Chen J, Halls C, Stanley CJ (1992) Tin-bearing skarns of South China: geological setting and mineralogy. Ore Geol Rev 7:225–248. https://doi.org/10.1016/0169-1368(92)90006-7

Driesner T, Heinrich CA (2007) The system H_2O–NaCl. Part I: correlation formulae for phase relations in temperature–pressure–composition space from 0 to 1000°C, 0 to 5000 bar, and 0 to 1 XNaCl. Geochim Cosmochim Acta 71:4880–4901. https://doi.org/10.1016/j.gca.2006.01.033

Einaudi MT, Meinert LD, Newberry RJ (1981) Skarn deposits. Econ Geol. https://doi.org/10.5382/AV75.11

Elsner H (2014) Zinn - Angebot und Nachfrage bis 2020, 2014th edn. DERA Rohstoffinformationen, 20. DERA, Berlin

Fekete S, Weis P, Driesner T, Bouvier A-S, Baumgartner L, Heinrich CA (2016) Contrasting hydrological processes of meteoric water incursion during magmatic–hydrothermal ore deposition: an oxygen isotope study by ion microprobe. Earth Planet Sci Lett 451:263–271. https://doi.org/10.1016/j.epsl.2016.07.009

Förster H-J, Tischendorf G, Trumbull RB, Gottesmann B (1999) Late-collisional granites in the Variscan Erzgebirge, Germany. J Petrol 40:1613–1645. https://doi.org/10.1093/petroj/40.11.1613

Förster HJ, Romer RL, Gottesmann B, Tischendorf G, Rhede D (2009) Are the granites of the Aue-Schwarzenberg Zone (Erzgebirge, Germany) a major source for metalliferous ore deposits? A geochemical, Sr-Nd-Pb isotopic, and geochronological study. N Jb Mineral Abh 186:163–184

Gerdes A, Zeh A (2006) Combined U–Pb and Hf isotope LA-(MC-) ICP-MS analyses of detrital zircons: comparison with SHRIMP and new constraints for the provenance and age of an Armorican metasediment in Central Germany. Earth Planet Sci Lett 249:47–61. https://doi.org/10.1016/j.epsl.2006.06.039

Gerdes A, Zeh A (2009) Zircon formation versus zircon alteration — new insights from combined U–Pb and Lu–Hf in-situ LA-ICP-MS analyses, and consequences for the interpretation of Archean zircon from the Central Zone of the Limpopo Belt. Chem Geol 261:230–243. https://doi.org/10.1016/j.chemgeo.2008.03.005

Goldstein RH, Reynolds TJ (1994) Systematics of fluid inclusions in diagenetic materials. SEPM Society for Sedimentary Geology, Tulsa, Okla

Guilcher M, Albert R, Gerdes A, Gutzmer J, Burisch M (2021) Timing of native metal-arsenide (Ag-Bi-Co-Ni-As±U) veins in continental rift zones – in situ U-Pb geochronology of carbonates from the Erzgebirge/Krušné Hory province. Chem Geol 584:120476. https://doi.org/10.1016/j.chemgeo.2021.120476

Haschke S, Gutzmer J, Wohlgemuth-Ueberwasser CC, Kraemer D, Burisch M (2021) The Niederschlag fluorite-(barite) deposit, Erzgebirge/Germany—a fluid inclusion and trace element study. Miner Deposita 56:1071–1086. https://doi.org/10.1007/s00126-020-01035-y

Heinrich CA (1990) The chemistry of hydrothermal tin(-tungsten) ore deposition. Econ Geol 85:457–481. https://doi.org/10.2113/gsecongeo.85.3.457

Hermann G (1967) Die Granite des Westerzgebirges und des Vogtlandes und ihre Beziehungen zu granitischen Gesteinen benachbarter Räume (Unpubl PhD thesis). Bergakademie Freiberg, Freiberg, p 205p

Hoffmann U, Breitkreuz C, Breiter K, Sergeev S, Stanek K, Tichomirowa M (2013) Carboniferous–Permian volcanic evolution in Central Europe—U/Pb ages of volcanic rocks in Saxony (Germany) and northern Bohemia (Czech Republic). Int J Earth Sci (Geol Rundsch) 102:73–99. https://doi.org/10.1007/s00531-012-0791-2

Hösel G, Fritsch E, Josiger U, Wolf P (1996) Das Lagerstättengebiet Geyer. Bergbau in Sachsen, 4. Sächsisches Druck- und Verlagshaus GmbH, Dresden

Hösel G (1994) Das Zinnerz-Lagerstättengebiet Ehrenfriedersdorf/Erzgebirge. Bergbau in Sachsen, 1. Sächsisches Druck- und Verlagshaus GmbH, Dresden

Hösel G (2002) Die polymetallische Skarnlagerstätte Pöhla-Globenstein. Bergbau in Sachsen, 8. Sächsisches Druck- und Verlagshaus GmbH, Dresden

Hoth K, Wolf P (1986) Pinge Geyer, Geologische Situation übertage, M 1 : 1000. Internal report, VEB GFE Freiberg,

Jackson NJ (1979) Geology of the Cornubian tin field 'a review'. Bull Geol Surv Malaysia 11:209–237. https://doi.org/10.7186/bgsm11197909

Kempe U, Bombach K, Matukov D, Schlothauer T, Hutschenreuter J, Wolf D, Sergeev S (2004) Pb/Pb and U/Pb zircon dating of subvolcanic rhyolite as a time marker for Hercynian granite magmatism and Sn mineralisation in the Eibenstock granite, Erzgebirge, Germany: considering effects of zircon alteration. Miner Deposita 39:646–669

Kern M, Kästner J, Tolosana-Delgado R, Jeske T, Gutzmer J (2019) The inherent link between ore formation and geometallurgy as documented by complex tin mineralization at the Hämmerlein deposit (Erzgebirge, Germany). Miner Deposita 54:683–698. https://doi.org/10.1007/s00126-018-0832-2

Korges M, Weis P, Lüders V, Laurent O (2018) Depressurization and boiling of a single magmatic fluid as a mechanism for tin-tungsten deposit formation. Geology 46:75–78. https://doi.org/10.1130/G39601.1

Korges M, Weis P, Lüders V, Laurent O (2020) Sequential evolution of Sn–Zn–In mineralization at the skarn-hosted Hämmerlein deposit, Erzgebirge, Germany, from fluid inclusions in ore and gangue minerals. Miner Deposita 55:937–952. https://doi.org/10.1007/s00126-019-00905-4

Kröner A, Willner AP (1998) Time of formation and peak of Variscan HP-HT metamorphism of quartz-feldspar rocks in the central Erzgebirge, Saxony, Germany. Contrib Mineral Petrol 132:1–20. https://doi.org/10.1007/s004100050401

Kuschka E (1994) Zur Mineralisation und Minerogenie der hydrothermalen Mineralgänge des Vogtlandes, Erzgebirges und Granulitgebirges. PhD thesis. TU Bergakademie Freiberg

Kwak TAP (1987) W-Sn skarn deposits, and related metamorphic skarns and granitoids. Elsevier, p 451

Lefebvre MG, Romer RL, Glodny J, Kroner U, Roscher M (2019) The Hämmerlein skarn-hosted polymetallic deposit and the Eibenstock granite associated greisen, western Erzgebirge, Germany: two phases of mineralization—two Sn sources. Miner Deposita 54:193–216. https://doi.org/10.1007/s00126-018-0830-4

Legler C (1985) Die schichtgebundenen Mineralisationen des Erzgebirges. Freib Forsch-Hefte C401 (Top. Report of IAGOD). Vol. XIV:93

Lehmann B (1990) Metallogeny of tin. Springer, p 211

Lehmann B (2021) Formation of tin ore deposits: a reassessment. Lithos 402-403:105756. https://doi.org/10.1016/j.lithos.2020.105756

Löcse F, Schneider G, Linnemann U, Rößler R (2023) Carboniferous–Permian volcanic evolution in the mid-European Variscides: U-Pb LA-ICP-MS zircon ages, geochemical and petrographical constraints from the NW Saxonian Volcanic Basin (Germany). Z Dt Ges Geowiss 174:7–30. https://doi.org/10.1127/zdgg/2023/0359

Lorenz W, Hoth K (1967) Räumliche Gesetzmäßigkeiten der Skarnverbreitung im Erzgebirge (Geologische Fragen der Skarnprognose im Erzgebirge - Teil 2). Geologie 16:1007–1030

Luthardt L, Hofmann M, Linnemann U, Gerdes A, Marko L, Rößler R (2018) A new U–Pb zircon age and a volcanogenic model for the early Permian Chemnitz Fossil Forest. Int J Earth Sci (Geol Rundsch) 107:2465–2489. https://doi.org/10.1007/s00531-018-1608-8

Makarevic̑ W, Fritsch E, Velickin W, Kargatev W, Ivanov I, Serov B, Nasarov WG, Lohrmann H (1976) Über die Ergebnisse der geologischen Erkundungsarbeiten im Bereich der Lagerstätte Geyer einschließlich der Vorratsberechnung auf Zinn mit Stand vom 1. Juli 1976. Internal report, SDAG Wismut Chemnitz

Meinert LD, Dipple GM, Nicolescu S (2005) World skarn deposits. In: Hedenquist JW, Thompson JFH, Goldfarb RJ, Richards JP (eds) One Hundredth Anniversary Volume. Society of Economic Geologists, pp 299–336

Millonig LJ, Albert R, Gerdes A, Avigad D, Dietsch C (2020) Exploring laser ablation U–Pb dating of regional metamorphic garnet–the Straits Schist, Connecticut, USA. Earth Planet Sci Lett 552:116589

Neymark LA, Holm-Denoma CS, Moscati RJ (2018) In situ LA-ICPMS U–Pb dating of cassiterite without a known-age matrix-matched reference material: examples from worldwide tin deposits spanning the Proterozoic to the tertiary. Chem Geol 483:410–425

Ondrus P, Veselovsky F, Gabasova A, Hlousek J, Srein V (2003) Geology and hydrothermal vein system of the Jachymov (Joachimsthal) ore district. J Geosci 48:3–18

Papeschi S, Musumeci G, Mazzarini F (2017) Heterogeneous brittle-ductile deformation at shallow crustal levels under high thermal conditions: the case of a synkinematic contact aureole in the inner northern Apennines, southeastern Elba Island, Italy. Tectonophysics 717:547–564. https://doi.org/10.1016/j.tecto.2017.08.020

Peng Q, Bromley AV (1992) Fluid inclusion studies of the skarn-type tin mineralization at Red-A-ven, Northwest Dartmoor, England. Chin J Geochem 11:362–369. https://doi.org/10.1007/BF02869067

Raimbault L, Cuney M, Azencott C, Duthou J-L, Joron JL (1995) Geochemical evidence for a multistage magmatic genesis of Ta-Sn-Li mineralization in the granite at Beauvoir, French Massif Central. Econ Geol 90:548–576. https://doi.org/10.2113/gsecongeo.90.3.548

Reed MH (2006) Sulfide mineral precipitation from hydrothermal fluids. Rev Mineral Geochem 61:609–631

Reinhardt N, Frenzel M, Meinert LD, Gutzmer J, Kürschner T, Burisch M (2021) Mineralogy and fluid characteristics of the Waschleithe Zn skarn – a distal part of the Schwarzenberg mineral system, Erzgebirge Germany. Ore Geol Rev 131:104007. https://doi.org/10.1016/j.oregeorev.2021.104007

Reinhardt N, Gerdes A, Beranoaguirre A, Frenzel M, Meinert LD, Gutzmer J, Burisch M (2022) Timing of magmatic-hydrothermal activity in the Variscan orogenic belt: LA-ICP-MS U–Pb geochronology of skarn-related garnet from the Schwarzenberg District, Erzgebirge. Miner Deposita 57:1071–1087. https://doi.org/10.1007/s00126-021-01084-x

Roedder E (1984) Fluid inclusion. Rev Mineral 12:1–644

Romer RL, Kroner U (2015) Sediment and weathering control on the distribution of Paleozoic magmatic tin–tungsten mineralization. Miner Deposita 50:327–338. https://doi.org/10.1007/s00126-014-0540-5

Romer RL, Kroner U (2016) Phanerozoic tin and tungsten mineralization—tectonic controls on the distribution of enriched protoliths and heat sources for crustal melting. Gondwana Res 31:60–95. https://doi.org/10.1016/j.gr.2015.11.002

Romer RL, Thomas R, Stein HJ, Rhede D (2007) Dating multiply overprinted Sn-mineralized granites—examples from the Erzgebirge, Germany. Miner Deposita 42:337–359. https://doi.org/10.1007/s00126-006-0114-2

Rötzler K (1995) Die PT-Entwicklung der Metamorphite des Mittel- und Westerzgebirges. Scientific Technical Report 95/14. Geoforschungszentrum Potsdam

Schmädicke E, Mezger K, Cosca MA, Okrusch M (1995) Variscan Sm-Nd and Ar-Ar ages of eclogite facies rocks from the Erzgebirge, Bohemian Massif. J Metamorph Geol 13:537–552. https://doi.org/10.1111/j.1525-1314.1995.tb00241.x

Schmidt C (2018) Formation of hydrothermal tin deposits: Raman spectroscopic evidence for an important role of aqueous Sn(IV) species. Geochim Cosmochim Acta 220:499–511. https://doi.org/10.1016/j.gca.2017.10.011

Schuppan W, Hiller A (2012) Die Komplexlagerstätten Tellerhäuser und Hämmerlein: Uranbergbau und Zinnerkundung in der Grube Pöhla der SDAG Wismut. Bergbau in Sachsen, 17. Sächsisches Landesamt für Umwelt, Landwirtschaft und Geologie, Dresden

Seman S, Stockli DF, McLean NM (2017) U-Pb geochronology of grossular-andradite garnet. Chem Geol 460:106–116. https://doi.org/10.1016/j.chemgeo.2017.04.020

Simons B, Andersen JC, Shail RK, Jenner FE (2017) Fractionation of Li, Be, Ga, Nb, Ta, In, Sn, Sb, W and Bi in the peraluminous Early Permian Variscan granites of the Cornubian Batholith: Precursor processes to magmatic-hydrothermal mineralisation. Lithos 278-281:491–512. https://doi.org/10.1016/j.lithos.2017.02.007

Steele-MacInnis M, Bodnar RJ, Naden J (2011) Numerical model to determine the composition of H2O–NaCl–$CaCl_2$ fluid inclusions based on microthermometric and microanalytical data. Geochim Cosmochim Acta 75:21–40. https://doi.org/10.1016/j.gca.2010.10.002

Steele-MacInnis M, Lecumberri-Sanchez P, Bodnar RJ (2012) HokieFlincs_H_2O-NaCl: a Microsoft Excel spreadsheet for interpreting microthermometric data from fluid inclusions based on the PVTX properties of H_2O–NaCl. Comp Geosci 49:334–337. https://doi.org/10.1016/j.cageo.2012.01.022

Štemprok M (1967) Genetische Probleme der Zinn-Wolfram-Vererzung im Erzgebirge. Miner Deposita 2:102–118

Swinkels LJ, Schulz-Isenbeck J, Frenzel M, Gutzmer J, Burisch M (2021) Spatial and temporal evolution of the Freiberg epithermal Ag-Pb-Zn district, Germany. Econ Geol 116:1649–1667. https://doi.org/10.5382/econgeo.4833

Tapster J, Bright JWG (2020) High-precision ID-TIMS cassiterite U–Pb systematics using a low-contamination hydrothermal decomposition: implications for LA-ICP-MS and ore deposit geochronology. GChron 2:425–441

Taylor RG (1979) Geology of tin deposits. Elsevier, p 543

Tera F, Wasserburg GJ (1972) U-Th-Pb systematics in three Apollo 14 basalts and the problem of initial Pb in lunar rocks. Earth Planet Sci Lett 14:281–304. https://doi.org/10.1016/0012-821x(72)90128-8

Thomas R, Klemm W (1997) Microthermometric study of silicate melt inclusions in Variscan granites from SE Germany: volatile contents and entrapment conditions. J Petrol 38:1753–1765. https://doi.org/10.1093/petroj/38.12.1753

Tichomirowa M, Sergeev S, Berger H-J, Leonhardt D (2012) Inferring protoliths of high-grade metamorphic gneisses of the Erzgebirge using zirconology, geochemistry and comparison with lower-grade rocks from Lusatia (Saxothuringia, Germany). Contrib Mineral Petrol 164:375–396. https://doi.org/10.1007/s00410-012-0742-8

Tichomirowa M, Käßner A, Sperner B, Lapp M, Leonhardt D, Linnemann U, Münker C, Ovtcharova M, Pfänder JA, Schaltegger U, Sergeev S, von Quadt A, Whitehouse M (2019) Dating multiply overprinted granites: the effect of protracted magmatism and fluid flow on dating systems (zircon U-Pb: SHRIMP/SIMS, LA-ICP-MS, CA-ID-TIMS; and Rb–Sr, Ar–Ar) – granites from the Western Erzgebirge (Bohemian Massif, Germany). Chem Geol 519:11–38. https://doi.org/10.1016/j.chemgeo.2019.04.024

Tischendorf G, Förster H-J (1990) Acid magmatism and related metallogenesis in the Erzgebirge. Geol J 25:443–454. https://doi.org/10.1002/gj.3350250326

Tischendorf G, Wasternack J, Bolduan H, Bein E, Tischendorf G (1965) Zur Lage der Granitoberfläche im Erzgebirge und Vogtland mit Bemerkungen über ihre Bedeutung für die Verteilung der endogenen Lagerstätten. Z angew Geol 11(1965):410–423

von Seckendorff V, Timmerman MJ, Kramer W, Wrobel P (2004) New 40 Ar/39 Ar ages and geochemistry of late Carboniferous-early Permian lamprophyres and related volcanic rocks in the Saxothuringian Zone of the Variscan orogen (Germany). Geol Soc London Spec Publ 223:335–359. https://doi.org/10.1144/GSL.SP.2004.223.01.15

Warkus F (1997) U-Pb Altersdatierungen an Graniten des Erzgebirges und deren geochemische Einordnung (Unpubl Dipl thesis). University Göttingen, p 68

Willner AP, Rötzler K, Maresch WV (1997) Pressure-temperature and fluid evolution of quartzo-feldspathic metamorphic rocks with a relic high-pressure, granulite-facies history from the Central Erzgebirge (Saxony, Germany). J Petrol 1997:307–336

Zhang R, Lehmann B, Seltmann R, Sun W, Li C (2017) Cassiterite U-Pb geochronology constrains magmatic-hydrothermal evolution in complex evolved granite systems: the classic Erzgebirge tin province (Saxony and Bohemia). Geology 45:1095–1098. https://doi.org/10.1130/G39634.1

Anlage II

Arbeit 2

Akzeptierte Publikation

Mineralium Deposita (2025) 60:85–111
https://doi.org/10.1007/s00126-024-01297-w

ARTICLE

Mineral chemistry of the Geyer SW tin skarn deposit: understanding variable fluid/rock ratios and metal fluxes

Nicolas Meyer[1] · Mathias Burisch[2] · Jens Gutzmer[3] · Joachim Krause[3] · Henning Scheibert[4] · Gregor Markl[1]

Received: 12 February 2024 / Accepted: 2 July 2024 / Published online: 14 August 2024

Abstract

The Geyer tin skarn in the Erzgebirge, Germany, comprises an early skarnoid stage (stage I, ~320 Ma) and a younger metasomatic stage (stage II, ~305 Ma), but yet, the source and distribution of Sn and the physicochemical conditions of skarn alteration were not constrained. Our results illustrate that contact metamorphic skarnoids of stage I contain only little Sn. REE patterns and elevated concentrations of HFSE indicate that garnet, titanite and vesuvianite of stage I formed under rock-buffered conditions (low fluid/rock ratios). Prograde assemblages of stage II, in contrast, contain two generations of stanniferous garnet, titanite-malayaite and vesuvianite. Oscillation between rock-buffered and fluid-buffered conditions are marked by variable concentrations of HFSE, W, In, and Sn in metasomatic garnet. Trace and REE element signatures of minerals formed under high fluid/rock ratios appear to mimic the signature of the magmatic-hydrothermal fluid which gave rise to metasomatic skarn alteration. Concomitantly with lower fluid-rock ratio, tin was remobilized from Sn-rich silicates and re-precipitated as malayaite. Ingress of meteoric water and decreasing temperatures towards the end of stage II led to the formation of cassiterite, low-Sn amphibole, chlorite, and sulfide minerals. Minor and trace element compositions of cassiterite do not show much variation, even if host rock and gangue minerals vary significantly, suggesting a predominance of a magmatic-hydrothermal fluid and high fluid/rock ratios. The mineral chemistry of major skarn-forming minerals, hence, records the change in the fluid/rock ratio, and the arrival, distribution, and remobilization of tin by magmatic fluids in polyphase tin skarn systems.

Keywords Erzgebirge · Tin skarn · Garnet · Cassiterite · Mineral chemistry

Introduction

The skarns of the Erzgebirge are host to a significant share of Sn resources in Europe with a known endowment exceeding 360 kt of Sn (Elsner 2014). The regions with the most prolific Sn skarns are the Schwarzenberg District in the western part of the Erzgebirge (Korges et al. 2020; Lefebvre et al. 2019; Reinhardt et al. 2021), and the Geyer SW Sn-skarn deposit in the central part of the Erzgebirge. Indicated resources of the Geyer SW skarn bodies have been estimated to 8.3 Mt of ore at 0.53 wt% Sn and up to 1.12 wt% Zn (Elsner 2014; Hösel et al. 1996). However, some of the Sn is hosted by calc-silicates and thus cannot be economically extracted. The skarns of the Schwarzenberg District and Geyer SW are exceptionally well exposed by existing underground mine workings (Schwarzenberg District) and exploration drilling (Geyer SW). Yet, published data on the petrography and mineral chemistry of the skarns are very limited (Hösel et al. 1996; Schuppan and Hiller 2012).

Editorial handling: N. F. Jansson

✉ Nicolas Meyer
nicolas.meyer@uni-tuebingen.de

✉ Mathias Burisch
burisch@mines.edu

1 Fachbereich Geowissenschaften, Petrologie und mineralische Rohstoffe, Eberhard Karls Universität Tübingen, Tübingen, Germany

2 Mineral Systems Analysis Group, Department of Geology and Geological Engineering, Colorado School of Mines, 1516 Illinois StreetGolden CO 80401, USA

3 Helmholtz-Zentrum Dresden-Rossendorf, Institute Freiberg for Ressource Technology Germany, Chemnitzer Straße 40 09599 Freiberg, Germany

4 Cemex Deutschland AG, Rüdersdorf, Germany

A resurgence of Sn exploration has spurred scientific interest with recent studies providing a robust geological, geochronological, and mineralogical context (e.g., Bauer et al. 2019; Burisch et al. 2019; Kern et al. 2019; Korges et al. 2020; Lefebvre et al. 2019; Meyer et al. 2024; Reinhardt et al. 2021). Some of these studies have documented that most Sn in the skarn deposits of the Schwarzenberg District and at Geyer SW is hosted by cassiterite accompanied by actinolite, chlorite and quartz related to late-stage skarn alteration (Kern et al. 2019; Meyer et al. 2024). However, Kern et al. (2019) illustrated for the Hämmerlein skarn in the Tellerhäuser deposit that up to 0.1 wt% of total Sn may be hosted by calc-silicate minerals, including stanniferous garnet, malayaite ($CaSnSiO_5$), amphibole and epidote. As a result of detailed petrographic descriptions of the Geyer SW skarns (Meyer et al. 2024), a similarly complex distribution of Sn between various silicates and cassiterite has been rather tentatively proposed. Hence, the present follow-up study was conducted to provide a comprehensive set of mineral chemical data for the Geyer SW skarns. Results allow an assessment of the partitioning of Sn amongst various skarn minerals, and thus provides valuable information on the distribution of Sn across different paragenetic stages which is important for possible metal recovery. The results can also be used to provide important constraints on the origin of Sn in the skarns of the Erzgebirge. The recognition of a pre-metamorphic background enrichment of Sn in the metasediments that also host skarn mineralization (Romer and Kroner 2015; Romer et al. 2022; Weber et al. 2023) has led to a resurgence of the hypothesis that a significant share of the Sn in the Erzgebirge skarns is related to proximal redistribution of Sn of sedimentary origin (Lefebvre et al. 2019). This contrasts with the hypothesis that Sn was introduced from magmatic sources (Lehmann 2021).

Despite the recent advances in understanding skarn-hosted Sn mineralization of the Erzgebirge, systematic investigations of trace elements are scarce up to date. Here, we employ LA-ICP-MS and EPMA to determine the major, minor and trace element mineral chemistry of calc-silicates and cassiterite from a suite of drill core samples from the Geyer SW skarn bodies. We integrate the mineral chemical data with detailed petrographic observations and available petrogenetic constraints (Meyer et al. 2024) in order to better understand the mode of skarn formation in different environments (rock-buffered vs. fluid-buffered) and related fluctuations in fluid/rock ratios. Furthermore, we aim to constrain Sn fluxes (magmatic-hydrothermal vs. sedimentary) and the redistribution of Sn amongst various silicates and oxides during the evolution of a polyphase skarn mineral system. We include previously unpublished EPMA data from Hämmerlein (Erzgebirge) and Crown Mine (Cornwall) into our discussion to illustrate that our findings are relevant to other Sn skarn systems as well.

Skarn formation and genetic implications of calc-silicate compositions

Skarn assemblages form during regional or contact metamorphism, due to metasomatic replacement reactions of any kind of lithology, but especially carbonate-bearing rocks, with most economic skarns being related to magmatic-hydrothermal fluids (Meinert et al. 2005). Commonly, skarns are divided into endo- and exoskarn indicating an igneous or sedimentary protolith, respectively. Exoskarns can further be subdivided into skarns *sensu stricto* replacing calcite marble (calcic) or dolomite marble (magnesian) and skarn *sensu lato*, which relates to skarn alteration of marly schists with higher content of silica and aluminum (Meinert 1992). Most skarns show a transition from small scale diffusion-controlled reactions to infiltration metasomatism within their spatiotemporal evolution (Einaudi et al. 1981; Harlov and Austrheim 2013; Jamtveit and Hervig 1994; Kwak 1987; Meinert 1992; Park et al. 2017a). The interaction between fluid and host rock is mainly controlled by diffusion rates, composition of the fluid and the protolith, dictating textural characteristics and chemical compositions of skarn minerals (Einaudi et al. 1981; Pertsev 1974; Watanabe 1960; Zharikov 1970). Within reaction skarns, diffusion relies on chemical gradients in pore solutions with low fluid/rock ratio and is inefficient in transporting components over a larger distance, which typically results in the formation of skarnoid textures (Einaudi et al. 1981; Jamtveit and Hervig 1994). In contrast, advective metasomatic skarn formation is characterized by fluid flow driven by pressure gradients along percolation pathways, forming anhydrous (early) and hydrous (late) skarn assemblages (Harlov and Austrheim 2013; Meinert et al. 2005; Norton 1987). In these skarns, textures and compositions of minerals are a direct result of interaction with a (magmatic-) hydrothermal fluid that can efficiently transport chemical constituents. The mineral chemistry, zoning textures and cross-cutting relationships of skarn minerals, hence, record physicochemical changes during the spatiotemporal evolution of a skarn system.

An increasing number of trace element studies on skarn-related garnet have recently become available (Chen et al. 2022; Gaspar et al. 2008; Hong et al. 2022; Huang et al. 2022; Jamtveit et al. 1993; Jamtveit and Hervig 1994; Park et al. 2017b). The vast majority of these studies are dedicated to W, Cu-Au or polymetallic skarns; no trace element data have yet been published for calc-silicate minerals in tin-dominated skarn systems. These studies illustrate that the composition of skarn minerals formed under low fluid/

rock ratios is primarily controlled by the bulk composition of the host rock. In such an environment, HFSE (high field strength elements) and Al can be transported over short distances to then be incorporated in newly formed skarn minerals (Jamtveit and Hervig 1994). In contrast, the chemical composition of skarn minerals formed under high fluid/rock ratios will more likely reflect the characteristics of the magmatic-hydrothermal fluids involved. Typically, these fluids transport an abundance of Fe and Si, and can introduce elements such as B, F, Li, W, Sn (and many more) into the skarn mineral assemblage (Einaudi and Burt 1982).

The rare earth elements (REE) are typical examples of HFSE – and the study of their distribution may provide interesting insight into the origin of skarn minerals. The overall concentration of REE in magmatic-hydrothermal fluids is typically low and marked by relative enrichment in LREEs and relative depletion in HREEs (Ayers and Eggler 1995; Bai and Koster van Groos 1999; Bauer et al. 2019; Reed et al. 2000). The extent to which the signature of the fluid is incorporated or whether the incorporation of the REE into minerals follows crystallographic restrictions depends largely on the kinetics of the growing minerals (Gaspar et al. 2008; Jamtveit and Hervig 1994). The more the growth rate of the minerals exceeds the diffusion rate of the fluid, the more the signature of the fluid is incorporated. Additionally, high (but variable) fluid flow will lead to strong oscillatory chemical zonation, euhedral mineral shapes, and complex twinning, which is best described as an isometric texture (Gaspar et al. 2008; Jamtveit and Hervig 1994; Meinert 1992).

Regional geology

The Erzgebirge (in German) or Krušné Hory (in Czech) region straddles the border between the Free State of Saxony in Germany and the Czech Republic (Fig. 1A). It comprises a sequence of metamorphic nappes (Fig. 1B) that formed during the Variscan orogeny in central Europe (Kroner et al. 2007). Protolith to these nappes was a variable volcano-sedimentary succession comprising greywackes, conglomerates, sandstones, clay stones, marls, and carbonate rocks as well as minor volcanic rocks of mafic to felsic composition (Ondrus et al. 2003; Tichomirowa et al. 2012), ranging from early Paleozoic to Neoproterozoic in age. These were deposited along the northern edge of the Gondwana Supercontinent (Mingram 1998); they underwent variable degrees of deformation and metamorphism during the Variscan Orogeny, owing to the collision of Gondwana with Laurussia during the Carboniferous. Peak metamorphism occurred at approximately 340 Ma, followed by rapid exhumation of the nappes to middle to upper crustal level (Kröner and Willner 1998) and the intrusion of voluminous granitic intrusions (Fig. 1B), facilitated by extensional tectonics (Wenzel et al. 1997). This late-Variscan phase (Breiter et al. 1999) was characterized by post-kinematic peraluminous magmatism and took place between 327 and 310 million years (Romer and Meixner 2014; Tichomirowa et al. 2019, 2022). Intrusions of this period comprise of crustal and minor mantle-derived melts, and their geochemical heterogeneity is attributed to the lithological variability of the stacked continental crust (Förster et al. 1999). Granitic batholiths of A-, I- and S-type composition (such as syeno- and monzogranites), evolved porphyries, lamprophyres, and extensive rhyolitic and dacitic volcanic rocks were emplaced after the main collisional stage (Breiter 2012; Förster et al. 1999; Tischendorf and Förster 1990). Later on, during the post-orogenic extensional tectonic phase from 305 to 286 million years, mainly (sub-)volcanic felsic magmatism occurred (Hoffmann et al. 2013; Luthardt et al. 2018; Zieger et al. 2019).

Following the collapse of the Variscan Orogen, subsidence and basin formation led to the deposition of a substantial (2–3 km, Wolff et al. 2015) sedimentary sequence that covered the Variscan basement (Pälchen and Walter 2011). During the Cretaceous Period, reactivation of the Elbe rift led to marine transgression and subsequent sedimentation. Rifting of the Eger Graben caused the Erzgebirge block to tilt towards the north in the Cenozoic. Rapid uplift and erosion were locally accompanied by local mafic (sub)volcanic magmatism – processes that resulted in the current exposure level as a Variscan basement window in Central Europe (Pälchen and Walter 2011).

Skarns in the Erzgebirge

The Variscan basement of the Erzgebirge is well known to host various types of magmatic-hydrothermal mineral systems, including greisen (Baumann et al. 2000; Korges et al. 2018), skarn (Burisch et al. 2019; Reinhardt et al. 2021), and epithermal vein-type mineralization (Swinkels et al. 2021). Recent geochronological studies have documented that the bulk of magmatic-hydrothermal mineralization in the Erzgebirge is associated with post-kinematic, late-orogenic (330–310 Ma) and post-orogenic granitic magmatism (305–285 Burisch et al. 2019; Meyer et al. 2024; Reinhardt et al. 2022; Romer et al. 2007; Tichomirowa et al. 2019). This includes the known skarn deposits (Reinhardt et al. 2022; Meyer et al. 2024).

Skarns across the Erzgebirge are mostly associated with carbonate-bearing metasediments of the Cambro-Ordovician succession of the Schwarzenberg Anticlinorium, which forms a SW-NE trending belt across the Erzgebirge. The metasediments consist of alternating sequences of metapelites, mica schists, marbles, and mafic metavolcanic

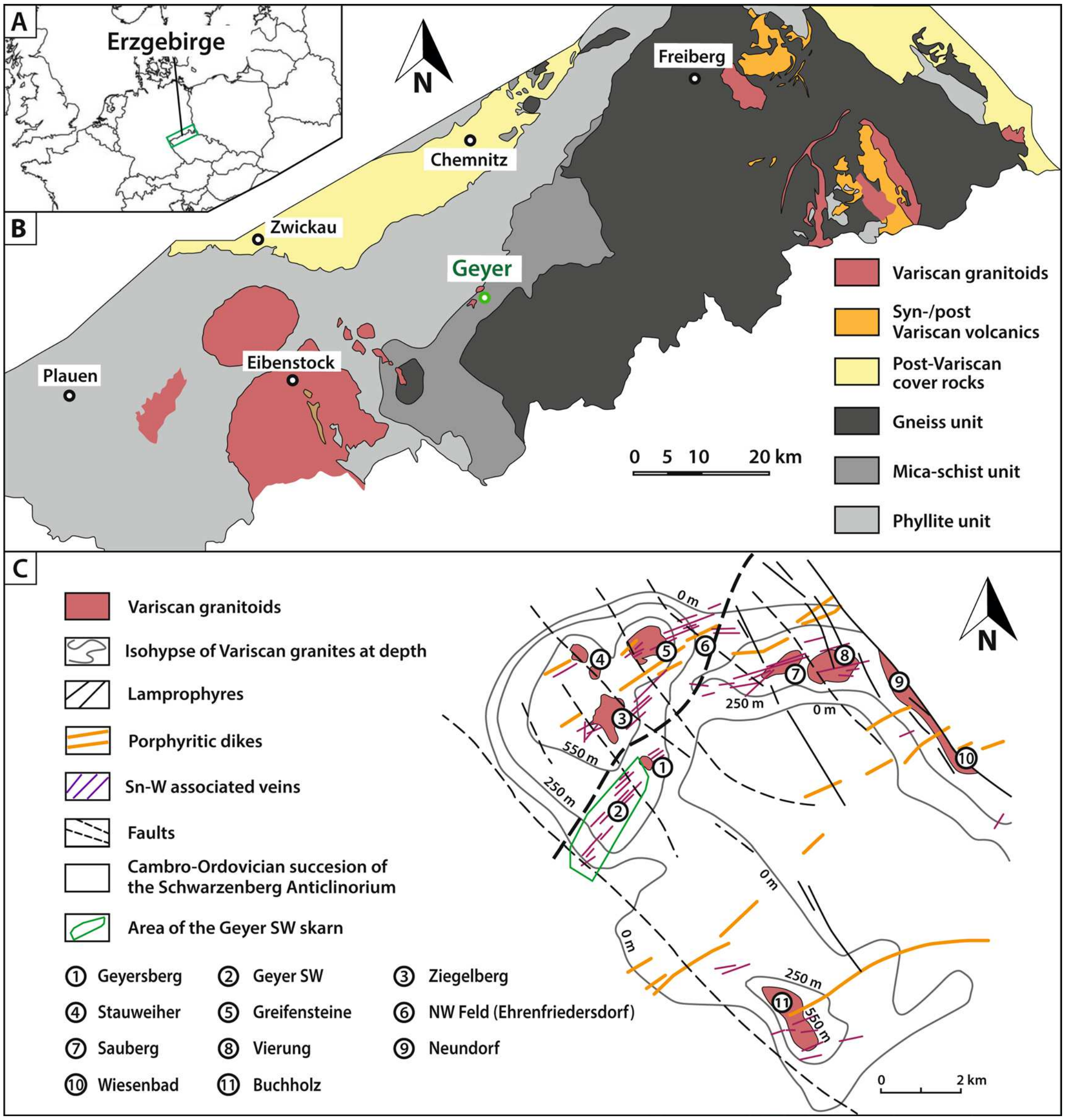

Fig. 1 (**A**) Geographical position of the Erzgebirge region in Central Europe. (**B**) Geological overview of the Erzgebirge with the location of the Geyer system (modified after Meyer et al. 2024). (**C**) Some relevant geological features in the Geyer-Ehrenfriedersdorf district, focusing on important localities where magmatic-hydrothermal mineralization styles (greisen, skarn) are known to occur (after Hösel 1994)

rocks. The skarn bodies vary significantly in size, mineralogy, and the metal tenor: They may host subeconomic to economic grades of Sn, W, Fe, Zn, and/or In (Burisch et al. 2019; Hösel 2002; Reinhardt et al. 2021; Schuppan and Hiller 2012).

The most common skarn lithotypes in the Erzgebirge comprise garnet-pyroxene ± magnetite ± amphibole ± chlorite skarns marked by a polyphase origin (Burisch et al. 2019; Reinhardt et al. 2021). Oldest skarn occurrences are typically small and linked to the peak of regional metamorphism around 340 Ma (Burisch et al. 2019; Reinhardt et al. 2022) without significant metal endowment. Skarns of considerable size and, in some cases, well-endowed in tin formed later in two distinct stages that have been distinguished by garnet U-Pb dating (Burisch et al. 2019; Reinhardt et al. 2022; Meyer et al. 2024). Garnets of the first stage have ages of 325 to 313 Ma, coinciding with the age of many greisen deposits that are associated with the emplacement of late-collisional granites (Burisch et al. 2019; Romer et al. 2007). Garnets of the second stage of skarn formation range between and 308 to 295 Ma in age. These garnets are associated with abundant cassiterite mineralization in greisen and veins, and they are contemporaneous with post-collisional magmatism and the earliest onset of Permian rifting (Burisch et al. 2019; Hoffmann et al. 2013; Meyer et al. 2024).

Geyer SW skarn

The skarns at Geyer SW (Fig. 1C) are bound to three units of interbedded calcite marble, dolomitic marble, and muscovite-biotite schist (Fig. 2A). The regional metamorphic, amphibolite-facies metasedimentary host rocks strike northeast, dip 30–40° NW, and are underlain at 200–400 m depth by granite of the Ehrenfriedersdorf batholith (Fig. 2B; Hösel et al. 1996). The skarns are 1–10 m thick and can be followed along strike for up to 300 m; their Sn content decreases gradually with distance to the granite contact – from 0.67% Sn at 100 m to 0.30% Sn at 400 m from the granite contact (Bolduan 1963; Hösel et al. 1996; Meyer et al. 2024).

Based on careful petrographic studies, Meyer et al. (2024) distinguished in all three skarn units two temporally distinct events of skarn formation at Geyer SW. The older *stage I* assemblage is devoid of any Sn mineralization and exhibits characteristics typical of a proximal contact metamorphic skarnoid (Meinert et al. 2005), e.g., the texture of the host rock is still recognizable, fractures are absent, and anhydrous skarn minerals show small, anhedral crystal sizes with intense intergrowths. U–Pb ages of ~322 Ma for garnets of *stage I* relate the origin of these skarnoids to the emplacement of the large Ehrenfriedersdorf batholith at 324 to 315 Ma (Meyer et al. 2024; Romer et al. 2007). These skarnoid assemblages formed under lithostatic conditions, experiencing a minimum pressure of 200 MPa at depths between 2.5 and 4 km, with limited fluid flow at a temperature of 450 °C and 470 °C (Breiter et al. 1999; Meyer et al. 2024; Romer et al. 2007). Extensive retrograde alteration as well as cassiterite mineralization are conspicuously absent from *stage I* assemblages (Meyer et al. 2024).

Tin mineralization, specifically the formation of malayaite and cassiterite, is linked to a second, distinctly younger event of skarn formation (*stage II;* ~ 305 Ma from overlapping garnet and cassiterite U–Pb ages; Meyer et al. 2024). While no granitic intrusions of this age are known to occur in the Geyer district, abundant rhyolitic volcanic rocks of this age occur across the Erzgebirge, providing ample evidence for province-scale felsic magmatism (Förster et al. 1999; Hoffmann et al. 2013; Löcse et al. 2023; Luthardt et al. 2018).

According to fluid inclusion analyses, the onset of *stage II* skarn formation occurred at > 330 °C under hydrostatic conditions (10–15 MPa). The presence of high salinity fluid inclusion assemblages with heterogeneous entrapment hosted by prograde pyroxene grains of *stage II* has been used to suggest boiling (Meyer et al. 2024). Low fluid inclusion salinities hosted by amphibole, chlorite, sphalerite

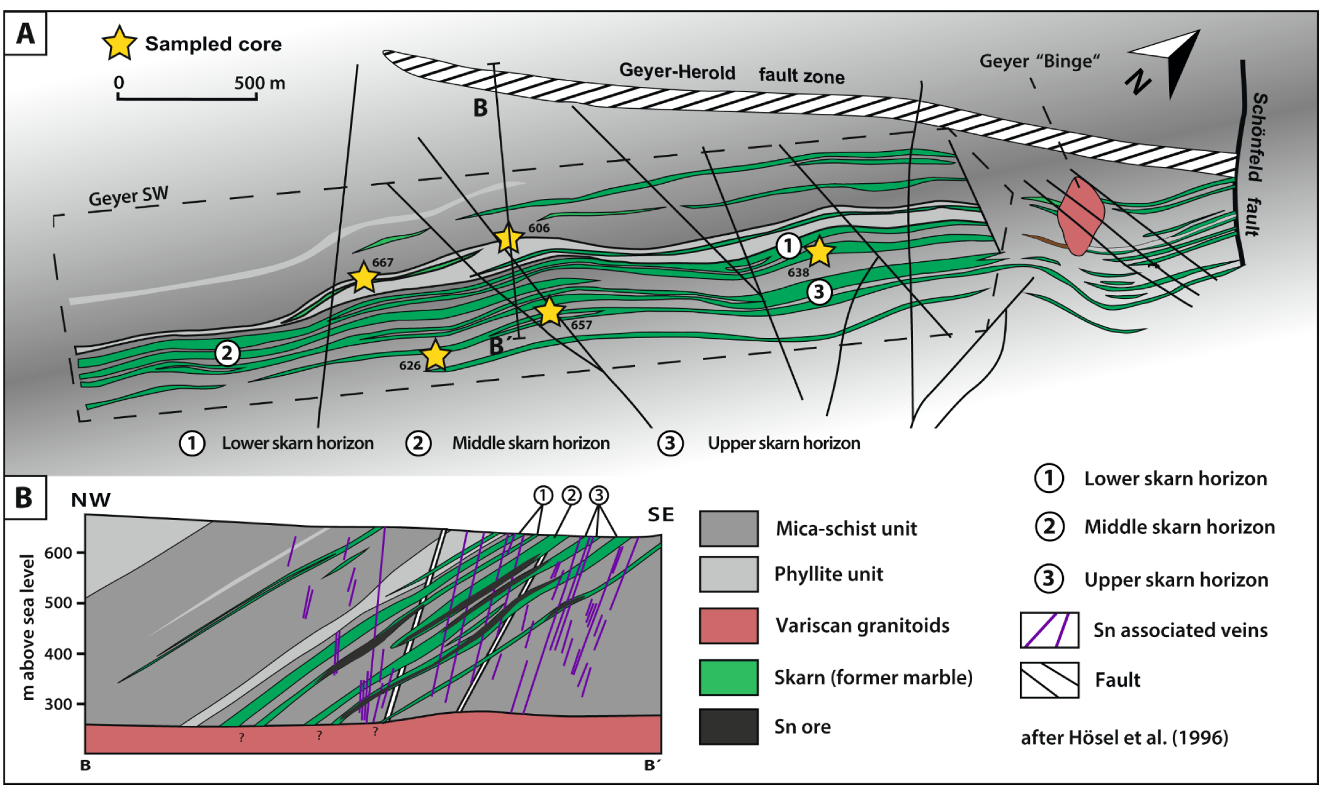

Fig. 2 (**A**) Geological map of the Geyer system with the exposed Geyersberg stock and profile line of B-B’. Collar positions of sampled drill cores are indicated with yellow stars (after Hösel et al. 1996). (**B**) Cross-section of the Geyer SW area including skarn- and vein-hosted Sn mineralization underlain by the Ehrenfriedersdorf composite batholith (after Hösel et al. 1996)

and cassiterite suggest dilution of the ore-fluid by meteoric fluids during the retrograde phase of *stage II* (Meyer et al. 2024). The bulk of cassiterite mineralization in the Geyer magmatic-hydrothermal system is related to late retrograde veinlets of *stage II* comprising fluorite or topaz, chlorite, white mica and/or quartz (Bolduan 1963; Hösel et al. 1996; Meyer et al. 2024).

Yet unpublished mineral chemical data from two other tin skarn localities are used in this study for comparison with the data from Geyer SW. These additional data are from the Hämmerlein skarn in the Schwarzenberg District (Kern et al. 2019) and from the Crown Mine of the Cornwall District, UK (van Marcke de Lummen 1986). More detailed information on the geological setting of these two Sn skarns is provided in electronic supplementary ESM 1.

Samples and methods

Access to six drill cores from the Wismut SDAG and Tin International exploration campaigns of the Geyer SW prospect was provided by the Geological Survey of the Free State of Saxony. These were sampled, resulting in a total of 60 individual samples of half drill cores, ranging in length from 5 to 20 cm. The main target of sampling was the selection of a wide range of macroscopically different unmineralized and mineralized portions of the three skarn units. 84 polished thin sections for petrographic investigations were produced of the 60 samples, 48 of which were analyzed by electron microprobe and LA-ICP-MS. Sample location, analytical condition, and representative analyses as well as the mineral calculation procedures are provided in ESM-1.

All sections were first examined by transmitted and reflected light microscopy on a Leica DM750P microscope equipped with an Olympus single-lens reflex camera. In addition, a Phenom XL scanning electron microscope (SEM) with an energy dispersive (EDS) X-ray spectrometer at the University of Tübingen was used for mineral identification and texture documentation in thin sections. Backscattered electron (BSE) images were acquired at an acceleration voltage of 15 kV and a beam current of 15 nA. Element distribution maps of polished hand specimens and thin sections were generated by microbeam X-ray fluorescence element mapping using a Bruker Tornado M4 instrument at the University of Tübingen. This instrument is equipped with a rhodium target X-ray tube operating at 50 kV and 500 nA and two EDS X-ray detectors, which produce unquantified false-color maps corresponding to the height of the Kα peaks of the respective elements.

This study includes three electron microprobe datasets that were obtained under slightly different measurement conditions and corrections. The data sets are collated in ESM-2 (Geyer SW), ESM-3 (Hämmerlein) and ESM-4 (Crown Mine). Analytical conditions used to obtain this data are summarized below and reported in detail in ESM 1.

Major and minor element chemistry of skarn minerals of Geyer SW was determined using a JEOL JXA-8230 electron microprobe at the Department of Geosciences, University of Tübingen. The analyses were conducted in wavelength-dispersive (WD) mode, employing an acceleration voltage ranging from 15 to 20 kV, a probe current of 20 nA, and a focused beam for all minerals except for amphibole and chlorite, for which a spot size of 5 µm was used. Counting times of 16/8 sec (peak/background) were applied for major elements, while minor elements were counted for 30/15 sec. To process the data, the PRZ correction was applied to all minerals (garnet, clinopyroxene, vesuvianite, epidote, amphibole, chlorite, titanite, malayaite and cassiterite).

Quantitative analyses of silicates and oxides were performed on samples from the Hämmerlein Deposit, Erzgebirge, and Crown Mine, Cornwall, with a JEOL JXA 8530 F Hyperprobe at the Helmholtz Institute Freiberg for Resource Technology, Germany, using WDS. An acceleration voltage of 20 kV, a probe current of 40 nA and spot sizes between 0.1 and 4 µm were chosen. Analyses were recalculated by the JEOL software with reference materials used for calibration matching the measured phases as closely as possible. Analyzed concentrations were corrected offline for instrument drift using natural mineral reference materials (ASTIMEX MIN25 and MAC Cassiterite). Mutual interferences were corrected following the procedure described in Osbahr et al. (2015).

Forty trace elements, including rare earth elements (REE), of gangue and ore minerals were analyzed by LA-ICP-MS at the Laboratory of Environment and Raw Materials Analysis (LERA), Karlsruhe Institute of Technology (KIT, Germany), using a Teledyne 193 nm Excimer Laser coupled to a sector-field ICP-MS (Element XR ThermoFisher). Ablation was done under a helium atmosphere and mixed with argon and nitrogen before the plasma torch. The ICP-MS was tuned for maximum sensitivity while keeping the oxide formation ($UO/U < 0.1\%$) and element fractionation low (i.e., $Th/U = \sim 1$). Static ablation used a spot size of 35 µm in diameter and an energy flux of ca. 5 J/cm^2 at 10 Hz for 30 s. Before the analysis, each spot was pre-ablated (ca. 1 µm) to remove surface contamination. Calibration and data quality checking was done using the National Institute of Standards (NIST) 612 glass, BIR, BHVO-1 and BCR-2G. Silicon concentrations, previously determined by electron microprobe, served as an internal standard for garnet, clinopyroxene, epidote, amphibole, chlorite, titanite and malayaite. For cassiterite, the concentration of Sn was used as an internal standard. Data were reduced and evaluated using the iolite software package v4. The complete dataset of LA-ICP-MS analyses of Geyer SW may be found in ESM-5. All REE data were normalized to C1 chondrite after McDonough and Sun (1995), an approach adopted from recent studies dealing with the distribution of trace elements in skarn systems (e.g. Chen et al. 2022; Gaspar et al. 2008; Huang et al. 2022; Liu et al. 2022; Ordosch et al. 2019; Park et al. 2017a, b; Smith et al. 2004) in order to improve comparability. Eu anomalies were calculated based on the formula $Eu/Eu^* = (Eu)_{cn}/[(Sm)_{cn} \times (Gd)_{cn}]^{0.5}$ of McLennan (1989), where values below 1 show a negative Eu anomaly and vice versa.

Results

In the following, a brief summary of the macroscopic and microscopic characteristics of skarns from Geyer SW is provided. Please refer to Meyer et al. (2024) for a more detailed description. Following that, mineral chemistry data are presented for the localities Geyer SW, Hämmerlein and Crown Mine.

Petrography Geyer SW

Based on observations from drill cores (Fig. 3) and detailed petrography (Figs. 4 and 5), three characteristic mineral assemblages are recognized in samples from the Geyer SW skarn. All three of these assemblages may occur in close spatial proximity to one another, often rendering the recognition of paragenetic relations difficult on hand specimen scale. However, the identification of discrete generations of, e.g., garnet can be based on cross-cutting relationships, textures, crystal shape and color. Different garnet generations also include core to rim associations, which are regarded as generations because of strikingly different appearances. Similar features apply to other skarn minerals, which have been assigned to distinct assemblages following Meyer et al. (2024).

Stage I

Macroscopically, *stage I* skarn shows remnants of host rock and metamorphic banding is preserved to variable degrees (Fig. 3A and B). Predominantly calcite marble and marly mica schist are replaced by skarn. Lenses of skarn exhibiting *stage I* alteration do not commonly exceed 1 m in thickness; the transition to surrounding altered mica schist is gradational. *Skarn I* mineral associations are characterized by variable ratios of garnet to clinopyroxene with a significant proportion of wollastonite, vesuvianite, quartz, feldspar, and epidote (Fig. 3C and D).

Garnet-rich areas display a fine crystalline texture, albeit with multiple larger garnet crystals reaching sizes of up to 1 cm (Fig. 3D). Two garnet generations (Grt Ia and Grt Ib) were identified. Garnet Ia is usually some millimeters up to 1.5 cm large, has an orange to beige color and irregular rims. These garnets are strongly anisotropic, very weakly zoned and commonly show sector or dodecahedral twins (Fig. 4A). They are intergrown with green clinopyroxene (Fig. 5A), euhedral, red vesuvianite (Ves I; Fig. 5B) and epidote (Ep I; Fig. 5C). Titanite (Ttn I) is commonly enclosed in garnet (Fig. 5D). In contact between former marble and mica schist, titanite occurs as aggregates with inclusions of relict ilmenite and rutile (Fig. 5C). The outer zones of garnet Ia are overgrown by garnet Ib. This alteration generally does not exceed 100 µm and is best visible with the SEM (Fig. 4B and C). Garnet Ib is accompanied by increasing amounts of wollastonite, fluorite, and quartz.

Stage II

Early skarn stage IIA Drill cores illustrating *substage IIA* show a highly variable clinopyroxene to garnet ratio, where minerals are generally coarse-grained and show isometric textures Fig. 3e, F, G). This association is most widespread in the studied sample set, and the thickness of skarn lenses differ, ranging from 30 cm up to 3 m. Yellow to brown garnet crystals reach sizes of up to 6 cm (Fig. 3E, F) and, more rarely, a mineral association which is dominated by green garnet can be encountered (Fig. 3F and G), occurring in lenses and small veins with sizes up to 50 cm. Fluorite and malayaite constitute additional phases that mark the IIa mineral assemblage (Fig. 3H).

Microscopically, the first garnets of the *stage II* skarn (Grt IIa) are of anhedral, porous appearance with numerous inclusions of other minerals, primarily clinopyroxene (Cpx II), remnants of earlier formed garnet, and fluorite. This garnet generation has cream to light brown colors, is slightly anisotropic without recognizable twins, but notably shows distinct dodecahedral crystal shapes (Fig. 4E). Vesuvianite (Ves II) has deep red to pale green colors and forms lath-shaped to acicular crystals (Fig. 5F). Occasionally, Ves II is zoned, with a darker core passing to a brighter rim. Clinopyroxene is only euhedral and of considerable size when it is intergrown with magnetite, forming up to 1.5 cm large crystals. (Fig. 5G). Malayaite replaces titanite to variable degrees, forming titanite-malayaite solid solutions ($Ttn\text{-}Mly_{ss}$), resulting in patchy zonation with malayaite-rich and -poor domains. In some samples, titanite and the surrounding host minerals are crosscut by fractures, with only the portion no longer shielded by the host mineral being more Sn-rich (Fig. 5D). Garnet IIa is subsequently overgrown by garnet IIb (Fig. 4D and E). The most distinctive feature of these garnets is the scarcity of inclusions, their strongly

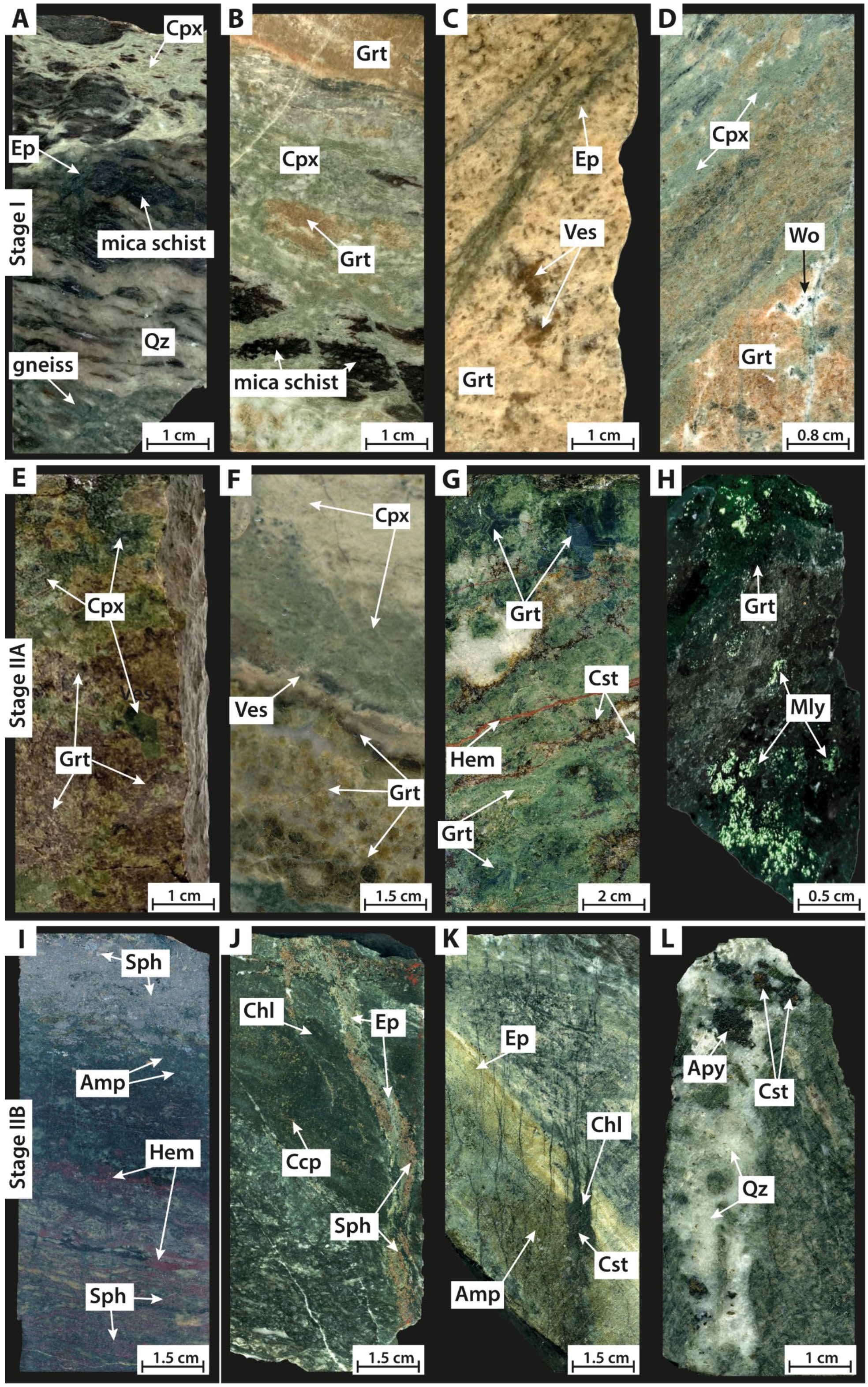

Fig. 3 Representative samples from drill cores (core and depth in brackets). (**A**) Mica schist replaced by pyroxene skarn (667-7-01; 391.1–391.2 m). (**B**) Fine-crystalline pyroxene (Cpx) skarn with remnants of mica shist and areas with higher proportion of red garnet (Grt; 667-5-01; 382.5–382.6 m). (**C**) Garnet-rich sample with cream-colored garnet and red vesuvianite (Ves; 667-11-01; 409.3–409.4 m). (**D**) Large pocket of red garnet with wollastonite (Wol) in a pyroxene-dominated area of *stage I* skarn (626-07; 85.0–85.2 m). (**E**) Densely intergrown large crystals of dark brown garnet and dark green pyroxene (667-15-01; 429.6–429.7 m). (**F**) Green clinopyroxene skarn cut by a vein containing vesuvianite at the rim and green garnet in the central part (626-02; 45.6–45.7 m). (**G**) Garnet-rich skarn with dark green, euhedral garnet crystals which are crosscut by veinlets containing hematite (Hem) and cassiterite (Cst; GM-08-1; 22.0–22.1 m). (**H**) Malayaite (Mly)-dominated parts in a garnet skarn under short-wave ultraviolet light (GM-08-2; 22.3–22.4 m). (**I**) Skarn mainly composed of amphibole with abundant sphalerite (Sph) (617-02; 167.2–167.4 m). (**J**) Vein with epidote (Ep) and euhedral, red sphalerite crosscutting skarn containing disseminated chalcopyrite mineralization (606-02; 81.4–81.5 m). (**K**) Chlorite- and cassiterite-filled veins intersecting epidote- and amphibole-rich skarn (657-03; 114.9-115.1). (**L**) Gneiss crosscut by a cassiterite (Cst)-quartz (Qz)-arsenopyrite (Apy)-bearing vein. (606-5; 242.6–242.7 m)

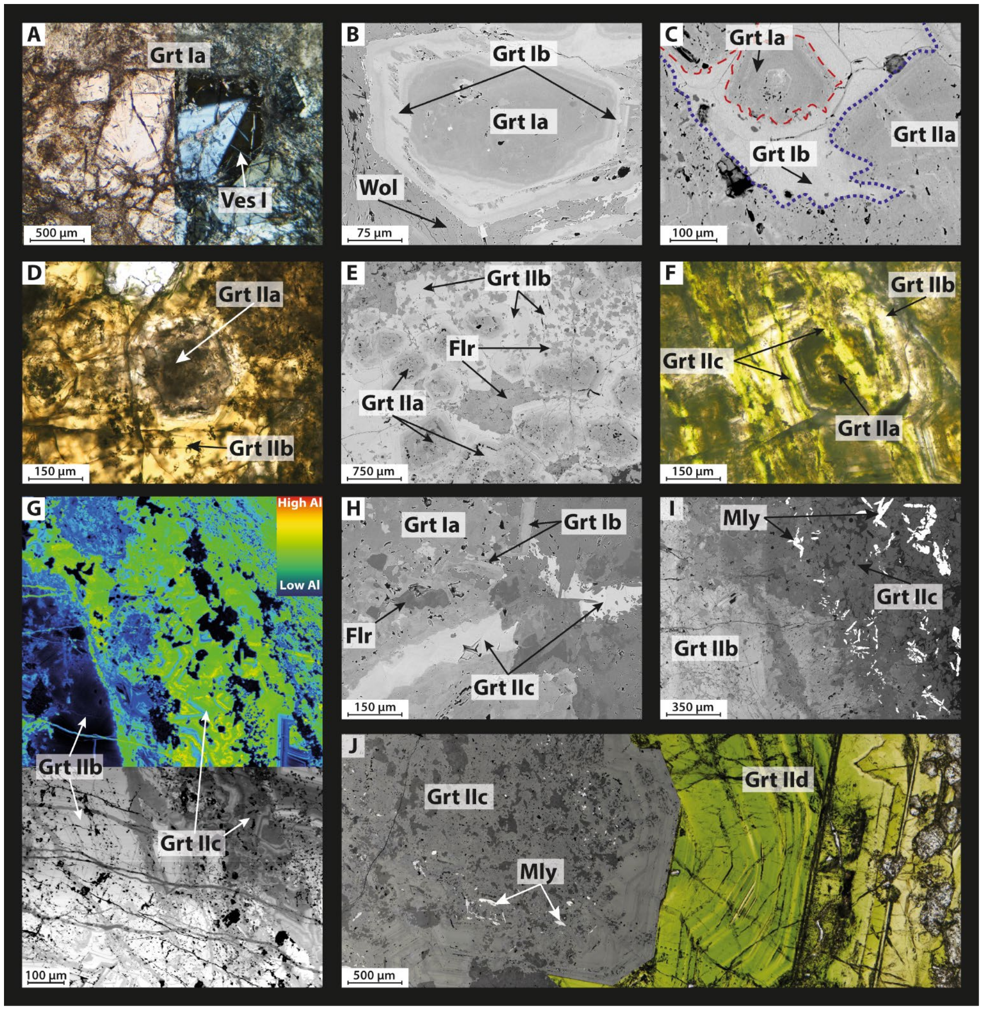

Fig. 4 Typical textures and intergrowths of garnet illustrated in SEM-BSE (**B, C, E, H, I, J**) and transmitted light microscopic images (**A, D, F, J**). (**A**) Euhedral, sector twinned garnet Grt I (plane and cross polarized image; 667-1-01a). (**B**) SEM-BSE image of Grt Ia overgrown by Grt Ib with wollastonite (Wol; 657-01). (**C**) Replacement of Grt Ia and Ib by Grt IIa (SEM-BSE; 667-4-05). (**D**) Poikilitic cores of Grt IIa overgrown by Grt IIb (plane polarized image; 626-08). (**E**) Grt IIa intergrown with fluorite and pyroxene, overgrown by Grt IIb (SEM-BSE; 667-10-02). (**F**) Brown Grt IIb crosscut by green Grt IIIa in veins (626-05; plane polarized image). (**G**) Stanniferous Fe-rich Grt IIb replaced by Al-rich Grt IIc, starting from veins. Al-mapping done with microprobe; black and blue represent low Al (and high Fe) areas while green to yellow represents Al-rich areas (667-10-04). (**H**) Anhedral Grt Ia and Ib intersected by Grt IIIa (SEM-BSE; 626-03). (**I**) Euhedral, lath shaped malayaite (Mly) in the vicinity of a replaced stanniferous garnet (SEM-BSE; 626-04). (**J**) Poikilitic Grt IIc intergrown with malayaite, fluorite and clinopyroxene overgrown by Grt IId with strong oscillatory zonation (SEM-BSE combined with plane polarized image; GM-8-02)

oscillatory zoning, and their euhedral shape (Fig. 4F). Their coloration ranges from yellow to dark brown and they are nearly isotropic. Towards the edge of single grains, the color intensity gradually diminishes, and the spacing between individual bands increase. Very locally, garnet IIb and vesuvianite II are intergrown with green, euhedral amphibole (Amp IIa; Fig. 5H).

As skarn alteration progresses, mineral formation starts from veins and replaces previously formed minerals. The first generation of garnet in these veins (Grt IIc) is of bright green color with weak oscillatory zoning (Fig. 4F). This generation of garnet crosscuts garnet I and garnet IIa and b, but also clinopyroxene (Fig. 5G, H, I). Malayaite (Mly) is the most common inclusion in garnet IIc and is usually present as euhedral, lath-shaped crystals or acicular aggregates up to 1 mm (Fig. 4I). Garnet IId, which overgrows garnet IIc, forms euhedral, dodecahedral, mostly isotropic crystals up to 2 cm in diameter (Fig. 4J). Compared to other garnet generations, growth zones are of considerable size, up to 400 µm wide, and they may be bent or tilted (Fig. 4J). Inclusions are scarce; fluorite is observed as a minor mineral only.

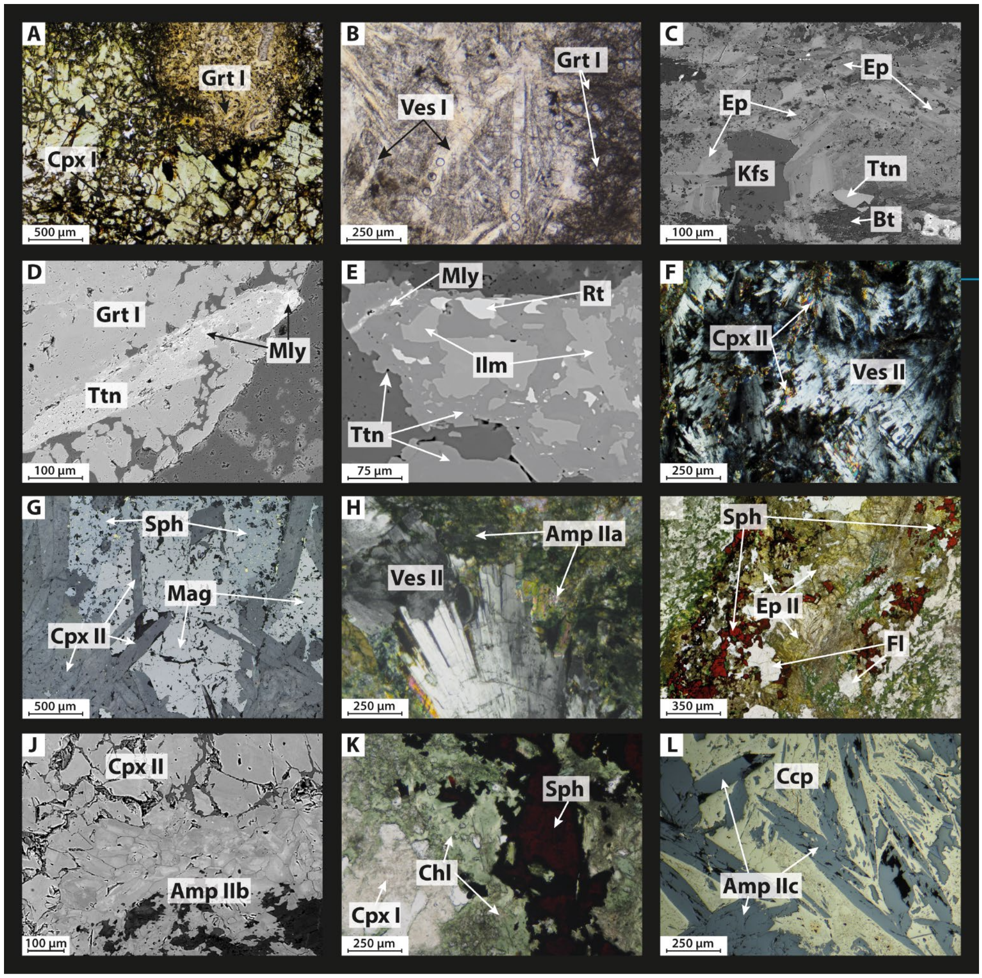

Fig. 5 Other minerals. (**A**) Green clinopyroxene intergrown with anhedral, poikilitic Grt Ia in transmitted light (667-8-04). (**B**) Lath-shaped, euhedral vesuvianite (Ves I) with anhedral Grt Ia (667-11-01). Circles in Vesuvianite are laser ablation marks (transmitted light). (**C**) Small euhedral epidote I (Ep I) replacing biotite (Bt) and feldspar (Kfs; SEM image; 667-14-02). (**D**) Titanite enclosed by Grt I. Where titanite is no longer shielded by the garnet, it is replaced by malayaite (SEM image; 667-1-01)). (**E**) Titanite containing remnants of rutile (Rt) and ilmenite (Ilm) is replaced in the upper left corner by malayaite (Mly) (SEM image; 606-01). (**F**) Fibrous, densely intergrown vesuvianite (Ves II) with clinopyroxene (transmitted light, crossed polarized; 606-01). (**G**) Large, lath shaped clinopyroxene (Cpx II) intergrown with magnetite (Mag). Both are subsequently replaced by sphalerite (Sph; reflected light; 626-06). (**H**) Euhedral vesuvianite intergrown with early euhedral amphibole without replacement (667-16-04). **I**) Green epidote (Ep II) in a vein together with deep red sphalerite and subhedral fluorite (Fl; 606-02). **J**) Clinopyroxene replaced by euhedral, internally zoned amphibole (Amp IIb; 606-04)). **K**) Chlorite and sphalerite replace clinopyroxene and amphibole (638-04). **L**) Partly replaced amphibole (Amp IIc) enclosed by chalcopyrite (reflected light; 657-06)

Late-stage skarn IIB The late-stage alteration of *stage II* skarn (*substage IIB*) comprises epidote, amphibole, chlorite, and other hydrous minerals in varying proportions (Fig. 3I, J and K). These minerals occur as massive aggregates, but also in veins and their alteration aureoles (Fig. 3J and K). The late-stage skarn alteration is in some samples associated with base metal sulfides (Fig. 3J and K) or with cassiterite mineralization (Fig. 3L).

Green epidote (Ep II) and dark green to black amphibole (Amp IIb and c) occur in veins (Fig. 5I) as dense aggregates or as replacement products (Fig. 5J), but they are rarely intergrown with each other. Epidote and amphibole crystals can reach sizes of up to 1 cm, featuring well-defined growth zones and only few inclusions. In certain areas, amphibole may undergo local replacement by chlorite (Fig. 5K) or become enclosed by chalcopyrite, sphalerite, and other sulfides (Fig. 5L). The formation of cassiterite is consistently associated with veins, veinlets, and their alteration aureoles, typically affecting the host rock (skarn as well as metasedimentary units) within a limited zone, rarely extending more than a few tens of centimeters. Cassiterite crystals are predominantly euhedral and exhibit well-defined growth zones. In veins, they can attain sizes of up to 1.5 cm, although they are generally smaller in impregnated areas. The highest quantities of cassiterite are typically

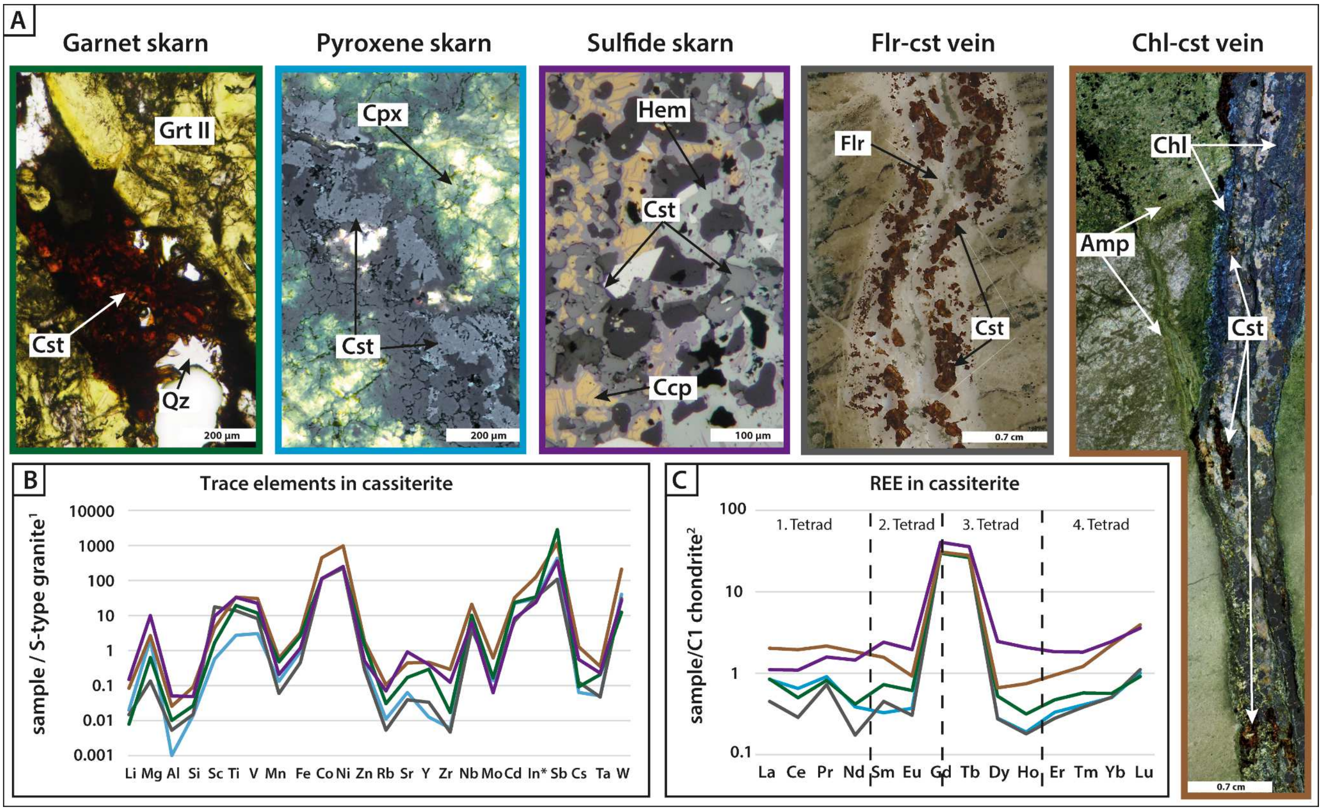

Fig. 6 (**A**) Occurrences of cassiterite (Cst), commonly in veins with fluorite (Flr) or chlorite (Chl) crosscutting garnet (Grt) or pyroxene (Px) skarn or in impregnated areas with hematite (Hem) or chalcopyrite (Ccp; transmitted light; only sulfide skarn image in reflected light). (**B**) Trace elements of cassiterite normalized to the high- fluorine S-type Eibenstock granite. The elements of cassiterite are remarkably consistent irrespective of different host rocks and different gangue minerals.[1]Förster et al. 2021; *divided by 1000. (**C**) REE pattern of cassiterite from veins with different gangue minerals and host rocks. Please note that colors of frames around pictures in (**A**) correspond to line colors in graphs B and C

encountered in fluorite- and chlorite-filled veinlets. These veinlets often exhibit the most substantial alteration halos. However, cassiterite was also found overgrowing magnetite and sphalerite in clinopyroxene-dominated skarn, replacing garnet and malayaite in garnet-dominated skarn and appearing as interstitial phase between amphibole, hematite, and chlorite (Fig. 6A). Manganiferous calcite, prehnite, feldspar and fluorite together with "wood tin" and stokesite ($CaSn(Si_3O_9)*2H_2O$) occur in different proportions and are the latest observed minerals associated with the Sn system; they replace most of the previously formed skarn minerals.

Mineral chemistry

In the following, the results obtained for the major, minor and trace element chemistry of all major groups of silicate minerals present in the Geyer SW skarn units will be reported, following their position in the different stages (Fig. 7). Results are presented for each mineral group – and within these groups compositional differences between the three different stages (I, IIA, IIB) will be highlighted. In addition, we will report the mineral chemistry of cassiterite. The procedures for mineral formula calculation and representative chemical analyses of the mineral groups may be found in the ESM-1.

Garnet Group The first garnet generation in *stage I* (Grt Ia) occupies a large compositional range of $And_{4–55}Grs_{43–95}$ with up to 0.16 apfu F. Sn remains invariably below or near the detection limit of the electron microprobe (EPMA, LOD is 0.05 wt%), but LA-ICP-MS data show concentrations between 11 and 600 µg/g. Grt Ia is overgrown and replaced by garnet Ib, which still belongs to *stage I*. It is identified only by its Fe concentration that is always higher than that of the immediately adjacent Grt Ia. Grt Ib also covers a wide range of compositions from $And_{19–82}Grs_{15–77}$ with F concentrations up to 0.11 wt%. Sn contents in Grt Ib only rarely exceed the LOD of the EPMA (Fig. 8A), but Sn is well detectable with LA-ICP-MS (12–980 µg/g).

The oldest garnets of *stage II* (Grt IIa) cover a compositional range of $And_{2–39}Grs_{55–92}$ with F concentrations up to

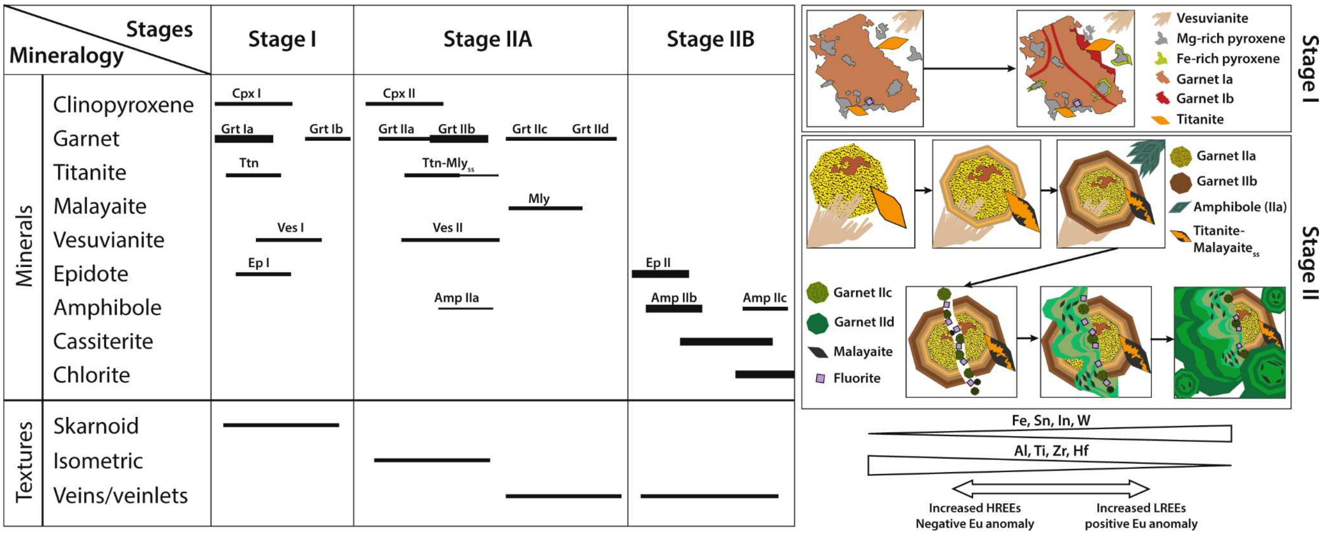

Fig. 7 Simplified paragenetic sequence of minerals. (modified from Meyer et al. 2024) analyzed by EPMA and LA-ICP-MS. The sketch on the right side schematically illustrates the different generations of garnet and their typical intergrowths

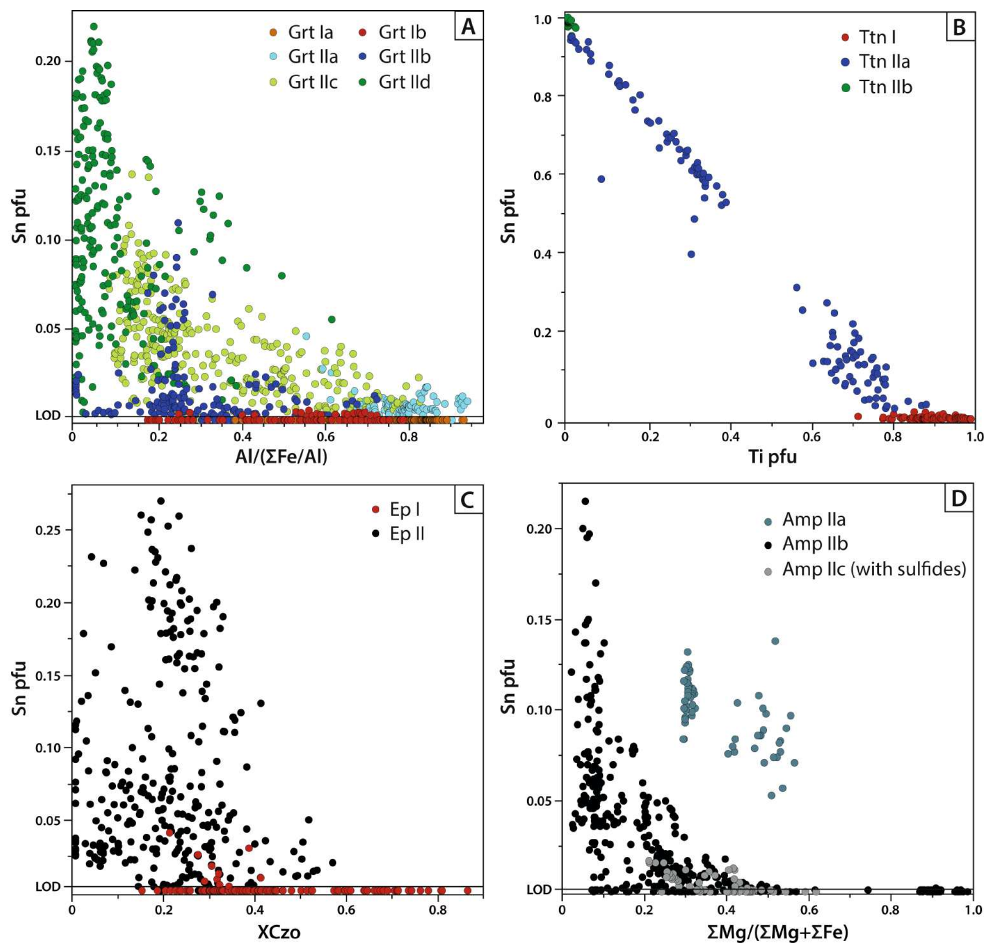

Fig. 8 Electron microprobe analyses of skarn minerals of the different skarn stages. (**A**) Garnet with Sn per formula unit against Al divided by the sum of total Fe and Al, reflecting the compositional range between grossular and andradite. (**B**) Sn versus Ti in atoms per formular unit of titanite group minerals showing the solid solution between titanite and malayaite with a prominent miscibility gap. (**C**) Sn per formula unit against the clinozoisite component of epidote-group minerals. Sn is more enriched in Fe-rich epidote. (**D**) Analyses of amphibole with Sn per formula unit plotted against the Mg number. Analyses with intermediate Mg number but high Sn are amphiboles of the substage IIA.

0.51 apfu. Sn is still low (0.02 apfu), but consistently above the LOD of the EPMA. The concentration of Fe increases in garnet IIb ($And_{29–99}Grs_{0–65}$), accompanied by low F and high Sn concentrations (up to 0.11 apfu; Fig. 8A). Garnet IIc has a wide range of compositions between $And_{13}Grs_{77}$ and $And_{90}Grs_{5}$, with highly variable F concentrations between LOD and 0.55 apfu, and Sn concentrations ranging between 0.01 and 0.12 apfu (Fig. 8A). The final garnet generation of *stage II* (Grt IId) has again a large range of compositions ($And_{36–100}Grs_{0–55}$), with low F contents but (on average) highest Sn concentrations (up to 0.22 apfu; Fig. 8A), which corresponds to ~7 wt% of Sn. In all these metasomatic garnet generations, F concentrations increase with increasing grossular component, while Sn concentrations increase with increasing andradite component.

Among the trace elements, REE provide the most remarkable results. Different garnet generations have rather distinct REE compositions – and these differ strikingly between the different paragenetic associations. REE patterns of different garnet generations from Geyer SW are shown in Fig. 9A. The corresponding LA-ICP-MS data is collated in ESM 5. Grt Ia of *stage I* exhibits a distinctive left-sloping REE distribution, which is characterized by depletion of light REEs (La–Nd; LREE), relative to elevated middle (Sm–Ho; MREE) and heavy REEs (Er–Lu; HREE), and an insignificant to negative Eu anomaly (δEu = 0.2–1.8). In contrast, the REE patterns of Grt Ib are relatively flat, with a slight deficit in LREE, a more variable distribution of HREEs and small negative Eu anomalies (δEu = 0.4–1.3).

Grt IIa, the first garnet generation of *stage II*, exhibits a LREE-depleted pattern broadly similar to Grt Ia but it is less depleted in LREEs, a minor decrease in HREEs and moderate negative Eu anomaly (δEu = 0.2–2.1). More andradite-rich Grt IIb displays a relatively flat REE pattern. It features low La and HREE, but high Sm and Nd concentrations, and a strong positive Eu anomaly (δEu = 1.3–29.7). The REE_N pattern of Grt IIc shows a significant decrease in La and an increase in Ce–Gd, along with no or an only slight negative Eu anomaly (δEu = 0.3–1.75). HREE concentrations are variable, but generally lower than LREEs, except for La. Grt IId, the final garnet generation, has the highest La concentrations of all garnets. LREEs are high, but decrease rapidly towards HREEs, except for a strongly positive Eu anomaly (δEu = 0.9–25.4).

High field strength elements (HFSE), such as Ti, Zr (Fig. 9B), Y, Nb, and Ta, are typically higher in garnets with a higher grossular component (e.g., Grt Ia, Grt IIa, Grt IIc). Sn, W and In, on the other hand (Fig. 9B), Fig. 10, 11, 12are highest in garnets with an elevated andradite component. The content of Li is generally low in *stage I* garnet but increase in Grt IIc and IId of *substage IIA*. Within the garnet generations, a trend from low W concentrations with high HREEs to high W with high LREEs can be observed (Fig. 13A). This coincides with deviations towards higher ΣREEs against Y (Fig. 13B), while the Y/Ho ratio stays rather constant (Fig. 13C).

Pyroxene Group Clinopyroxene of *stage I* (Cpx I) is variable in composition ($Di_{21–88}Hd_{11–73}Jhn_{1–6}$) with a distinct positive correlation between the hedenbergite and johannsenite components. *Stage II* clinopyroxene (Cpx II) has a similarly variable composition of $Di_{14–99}Hd_{1–79}Jhn_{0–7}$. The most diopside-rich (i.e. iron-poor) clinopyroxene of *stage II* are typically present in magnetite-bearing skarns. The major element compositions of Cpx I and Cpx II thus occupy a similar broad range and can only be subdivided

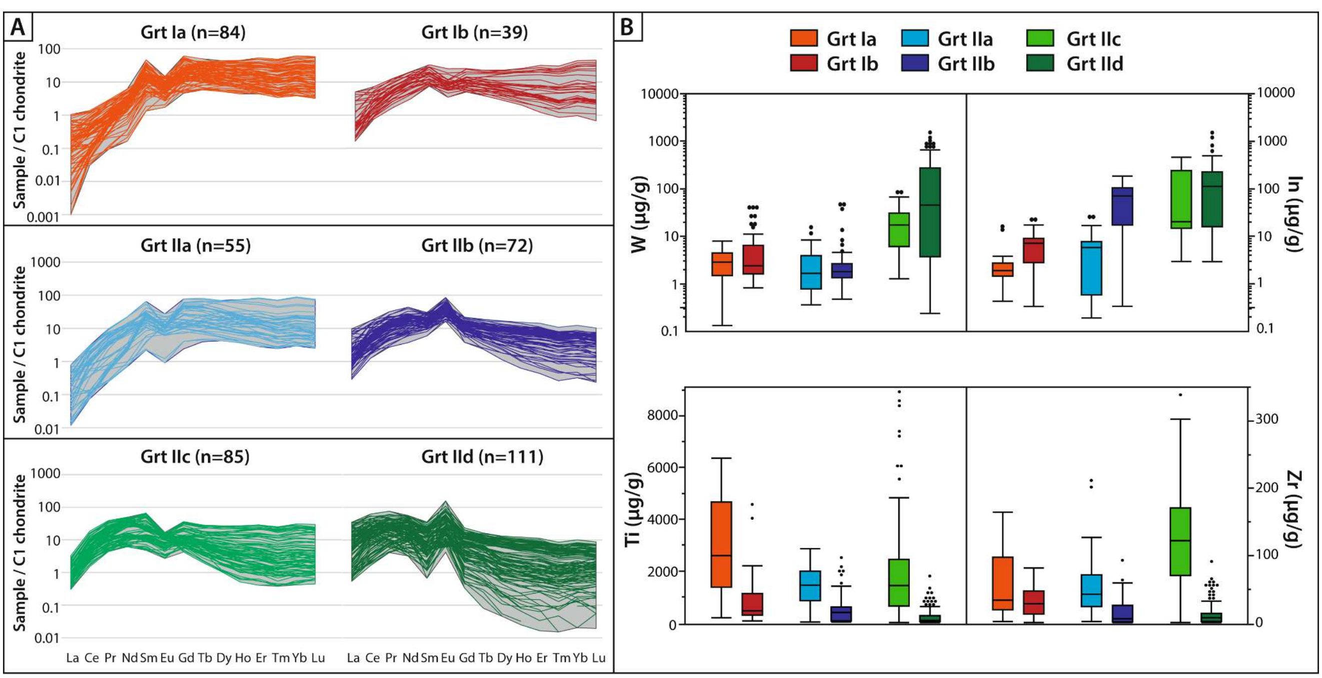

Fig. 9 (**A**) REE distribution normalized to C1 chondrite (McDonough and Sun 1989) in garnet from Geyer SW. See text for more details. (**B**) Trace element contents of W and In in µg/g and HFSE content represented by Ti and Zr of different garnet generations. Note the differences in scale

petrographically. Trace element contents and “typical” clinopyroxene minor elements Na (up to 200 µg/g), Li (up to 40 µg/g) or Ti (up to 480 µg/g) are low and do not differ significantly between the two skarn stages. The only exception is Zn, which shows elevated concentrations in both *stage I* (30–2150 µg/g) and *II* (50–1600 µg/g). In contrast, Cpx II intergrown with magnetite, yields significantly lower Zn concentrations with a range between 20 µg/g and 85 µg/g. These clinopyroxenes are also the only ones to show somewhat elevated concentrations of REEs with a significant negative Eu anomaly, while all the other pyroxenes have remarkably low REE concentrations.

Vesuvianite $(Ca_{19}(Al, Mg, Fe)_{13}(SiO_4)_{10}(Si_2O_7)_4(OH, F,O)_{10})$. Vesuvianite of *stage I* (Ves I) displays the highest concentrations of Mg (4.00 apfu) and Ti (1.14 apfu; 3 wt%), while Sn is generally below the detection limit of the EPMA. The REE pattern of vesuvianite I is marked by depletion of HREEs with enriched LREEs and without a significant Eu anomaly. Concentrations of HFSE, B and Sb are high, other elements like In and W are present in low concentrations. *Stage II* vesuvianite (Ves II) contains somewhat higher Fe and Mn contents and Sn concentrations of up to 0.21 apfu, corresponding to 1 wt% Sn. The REE concentrations in vesuvianite define a consistent chondrite-normalized fractionation trend with depleted LREE and a positive Eu anomaly. HFSE, Y, Ho and B contents in Ves II are lower compared to Ves I, whereas Li, In, and W contents are higher.

Titanite - Malayaite solid solution series $Ca(Ti, Sn)(SiO_4)O$. Titanite with Sn concentrations below the detection limit (Ttn I) of the electron microprobe is found exclusively in association with *stage I* garnet (Fig. 8B). This titanite has a composition of $Ttn_{100}Mly_0$ to $Ttn_{94}Mly_0$ where Ti is substituted by Al. The resulting imbalance in charge is likely accommodated by the following coupled substitution: $(Al, Fe)^{3+} + (OH, F)^{-} \Longleftrightarrow Ti^{4+} + O^{2-}$ (Ribbe 1982). The REE patterns of Ttn I are generally flat, with a minor negative Eu anomaly (δEu = 0.4–0.9). and exhibit high ΣREE concentrations ranging from 51 to 1168 µg/g (Fig. 10A). Concentrations of elements such as W (1–28 µg/g), In (below LOD–26 µg/g), and Sn (17–324 µg/g) are relatively low, while Y (43–1026 µg/g) and Zr (5–1114 µg/g) concentrations are rather high.

In *stage II*, increasing amounts of Sn are incorporated into the crystal lattice of the solid solution series titanite – malayaite - until the malayaite component becomes predominant (Ttn IIa). A distinct miscibility gap is observed within the compositional range between $Ttn_{63}Mly_{37}$ and $Ttn_{42}Mly_{58}$, corresponding to 0.55 to 0.35 apfu Ti in malayaite and vice versa (Fig. 8B). This has also been described in previous studies (Aleksandrov and Trenova 2007). With a higher malayaite component, REE patterns remain flat, but exhibit more pronounced HREE depletion, a stronger negative Eu anomaly, and an overall decrease in ΣREE (Fig. 10A). Higher Sn concentrations in the solid solution correlate with increased contents of In (0.4–1751 µg/g) and W (2–760 µg/g). In contrast, higher titanite contents are associated with elevated concentrations of Y and Zr, along with higher ΣHREE.

Malayaite that contains only an insignificant titanite component (ranging from Ttn_2Mly_{98} to Ttn_0Mly_{100}) is primarily found in assemblages relating to late *stage II* (Ttn IIb). Ttn IIb is mainly enclosed by garnet IIc. No coupled substitution involving Al, Fe, or other elements is observed. In this group, In (667–2589 µg/g) and W (0.5–140 µg/g) exhibit the highest concentrations in members of the titanite-malayaite solid solution series, while Zr (0.8–221 µg/g) and Y (0.5–58 µg/g) are comparatively low in concentration. Malayaite has the lowest ΣREE concentrations (up to 103 µg/g) and displays a REE pattern characterized by depleted HREE, a clear negative Eu anomaly (δEu = 0.04–0.72), and in some cases, a clear positive anomaly of Gd and Tb (Fig. 10B), often referred to as the third tetrad anomaly (Masuda et al. 1987).

Epidote Group Epidotes in *stage I* (Ep I) occur together with calcite and quartz, preferentially at the transition between skarn and altered mica schist. Compositionally, Ep I occupy a wide range between $Czo_{84}Ep_{14}Pmt_2$ and $Czo_{16}Ep_{83}Pmt_2$ with generally low Sn concentrations (Fig. 8C). Because of the crystal size and the tight intergrowth with garnet, only a few LA-ICP-MS measurements could be conducted on Ep I. The REE_N pattern of Ep I is relatively flat with an insignificant positive Eu anomaly (δEu = 1.9–2.3) and a gradual decrease of the HREEs. Most trace element abundances in Ep I are also low (see ESM 2 for details).

The bulk of the epidote at Geyer SW is associated with *substage IIB* (Ep II). The compositional range is similar to Ep I, spanning a range between $Czo_{59}Ep_{39}Pmt_2$ and $Czo_0Ep_{94}Pmt_6$, but with Sn concentrations (Fig. 8C) reaching up to 0.27 apfu (equivalent to 7.8 wt% Sn). Concentrations of Ti or REEs, on the other hand, are only minor. The REE pattern of Ep II is strongly depleted in HREEs and shows a distinct positive Eu anomaly (δEu = 0.9–18.6). High In concentrations are associated with elevated Sn contents, while other trace elements exhibit insignificant concentrations (see ESM 2 for more details).

Amphibole Supergroup Amphiboles were only recognized in *stage II*, and they belong to the Ca-amphibole subgroup (Hawthorne et al. 2012; Locock 2014). Amphiboles are scant in *mineral association IIA* (Amp IIa); they occur together with vesuvianite and clinopyroxene and are euhedral, with well-developed chemical zonation. Most commonly, they belong to the pargasite-hastingsite series, with variable amounts of K, Mg, and Fe^{2+}, as well as intermediate to high concentrations of Sn (0.05–0.14 apfu; Fig. 8D). Amphibole IIa also has the highest concentrations of F (0.46–0.64 apfu) among the analyzed amphiboles. The REE_N patterns of Amp IIa (Fig. 10B) are characterized by low La and relatively high Ce–Nd concentrations, and a decrease in HREEs with a discernable negative Eu anomaly (δEu = 0.55–0.97).

Most amphibole occurs in *mineral association IIB* (Amp IIb and Amp IIc). These amphiboles are of heterogeneous composition, but mainly belong to the root groups of tremolite, actinolite, hornblende, pargasite, and hastingsite. Amphibole IIb occurs in veins or as replacement product of clinopyroxene and garnet; it is commonly enriched in ΣFe and can contain up to 0.21 apfu Sn (2.7 wt%). Tremolite-rich Amp IIb is restricted to clinopyroxene skarn with a substantial proportion of diopside (Fig. 8D) and contains only low concentrations of Sn. The REE signature of Amp IIb is characterized by depletion of La, high Ce–Nd concentrations, and only a minor positive Eu anomaly (δEu = 0.79–2.37). Further, Amp IIb is marked by an enrichment of the heaviest REEs whilst maintaining a consistent Y/Ho ratio. Amp IIc, in contrast, is intergrown with or replaced by base metal sulfides. It belongs to the (ferro)-actinolite group and commonly contains only low Sn concentrations (Fig. 8D). Amp IIc is, however, enriched in HREEs, depleted in LREEs, and may display a negative Eu anomaly (δEu = 0,36–1,05). The Y/Ho ratio in Amp IIc deviates strongly from that of the other amphibole generations – which is due to lower Ho concentrations (Fig. 13F). Details about the endmember calculations, major and trace element data for amphiboles can be found in ESM 1, 2 and 5, respectively.

Chlorite Group Minerals of the chlorite group are an important constituent of the *late* part of the *substage IIB* assemblage; they belong to the chamosite (Fe-rich) and clinochlore (Mg-rich) solid solution series, with only a minor presence of the pennantite (Mn) component (ESM 1, 2). Where chlorite replaces clinopyroxene, amphibole or epidote, its composition largely depends on the precursor mineral. In cases where chlorite coexists with newly grown cassiterite as infill of veinlets, it tends to be Fe-rich (chamosite-rich). In all cases, Sn contents in chlorite were found to be below the detection limit of both EPMA and LA-ICP-MS. Other minor and trace elements (including the REEs) also showed low to very low concentrations (ESM 5).

Cassiterite Well-developed euhedral cassiterite is only common in veinlets of *substage IIB*, where it commonly displays optical and chemical zonation. Cassiterite occurring in aureoles around these veinlets is of smaller, anhedral appearance and typically shows less pronounced zoning. Fe is the most common substituent in cassiterite with up to 0.12 apfu (ESM 1, 2). Elements such as Al and Si are

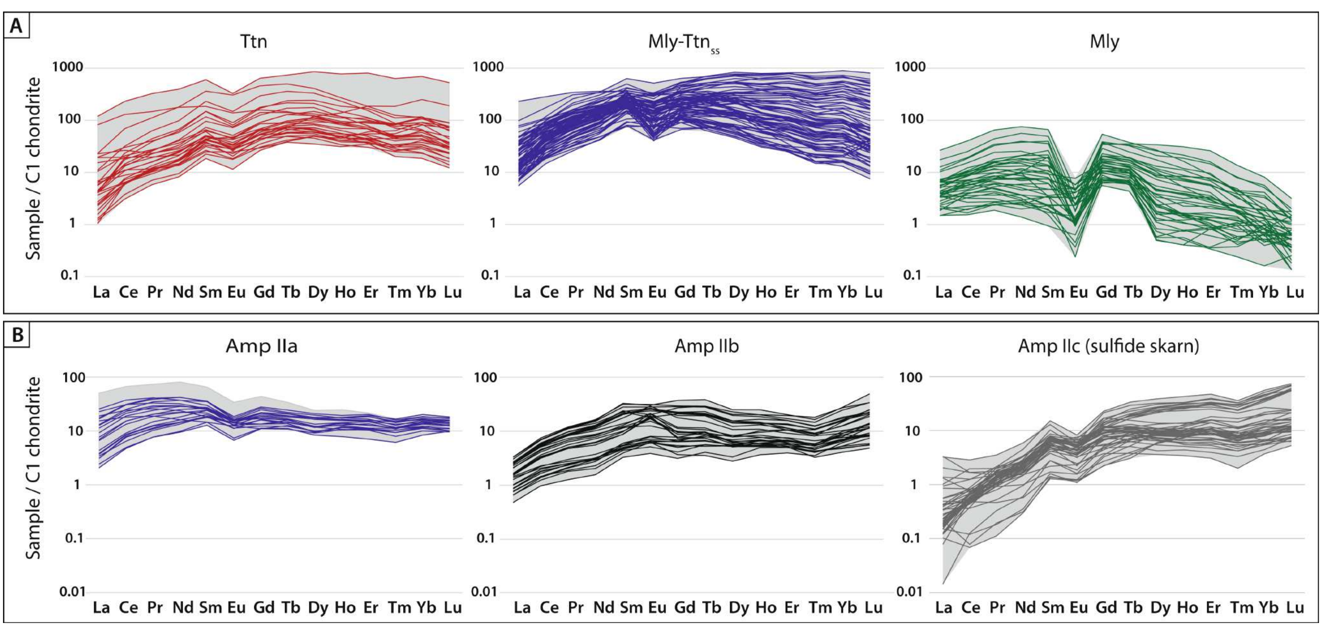

Fig. 10 REE distribution normalized to C1 chondrite (McDonough and Sun 1989) of (**A**) titanite-malayaite$_{ss}$ and (**B**) amphibole

present in smaller quantities (0.02 and 0.07 apfu, respectively). Despite the variable textural context in which cassiterite is found, its trace element composition is remarkably uniform. Compared to whole rock data of the Geyer granite (Förster et al. 2021), cassiterite is depleted in Li, Rb, Y, Zr, Pb, enriched to a certain degree in V, Co, Ni, Zn, Nb, Mo, and notably enriched in Sb, W, and In (Fig. 6B). Indium may be enriched in cassiterite by up to four orders of magnitude (note that In in Fig. 6B is divided by 1000). Furthermore, the normalized REE patterns are strikingly consistent, all marked by low ΣREE (6.6 to 57.7 µg/g), low LREE and HREE concentrations, an insignificant Eu anomaly, but a significant third tetrad anomaly (Fig. 6C).

Garnet and clinopyroxene from the crown mine skarn

An introduction of the regional and local geology is summarized in the ESM 1. The mineral chemistry of clinopyroxene and garnet from the Crown Mine skarns are presented below; the complete dataset of all important skarn phases can be found in the ESM 3.

Garnet occurs in two different generations (stage I and II). The first garnet stage is accompanied by titanite, chlorite or magnetite. Garnet stage I shows complex extinction features, but only a very weak chemical zonation and has a composition of $And_{15–45}Grs_{51–85}$ with Sn invariably below the detection limit of the EPMA. Associated with the first garnet generation is clinopyroxene, which commonly shows a bright core and a greenish rim. This is further reflected in the chemical composition, where the core is more diopside-rich compared to the hedenbergite-rich and johannsenite-bearing rim. The composition of clinopyroxene ranges from $Hd_{23}Di_{74}Jhn_{1,6}$ to $Hd_{63}Di_{33}Jhn_4$. Sn concentrations are always below the detection limit of the EPMA.

The second garnet generation (stage II) occurs in monomineralic, vein-like structures cross-cutting older garnet generations and other skarn minerals. Garnet II is mainly associated with stanniferous titanite, malayaite, and axinite; clinopyroxene is distinctly lacking. The composition of garnet II ranges from $And_{0–60}Grs_{39–73}$ with, in parts, a pronounced spessartine and almandine component and elevated Sn concentrations up to 0.03 apfu, corresponding to 1.58 wt%.

Garnet and clinopyroxene from the hämmerlein skarn

Information about the local geological setting of the Hämmerlein skarn is summarized in the ESM 1. Mineral chemical analyses were performed by EPMA on major skarn-forming minerals of the Hämmerlein skarn (details results are provided in ESM 4). Here, only data of garnet and clinopyroxene are presented, as these are the main constitutes of the skarns. A subdivision between different generations of these skarn-forming minerals was not possible because analyses were carried out on grain mounts rather than polished thin sections. However, a general petrographic description of calc-silicates from this skarn can be found in Kern et al. (2019), Korges et al. (2018), Lefebvre et al. (2019) and Schuppan and Hiller (2012).

Garnet from the Hämmerlein skarn has a composition between $And_{14}Grs_{86}$ to $And_{95}Grs_5$ with only minor spessartine and pyrope component. The Sn concentration ranges from below the detection limit of the EPMA up to 0.04 apfu, corresponding to 2.25wt.% Sn. Although the Sn content increases with increasing andradite component, andradite-rich garnets with very low tin concentrations are also present. Clinopyroxene, commonly associated with garnet, has a composition between almost endmember diopside ($Hd_{0.25}Di_{99.75}Jhn_0$) and $Hd_{34}Di_{62}Jhn_4$. In none of the analyses did Sn contents exceed the detection limit of the EPMA.

Discussion

We will start the discussion by a general overview of mineral data from tin skarns by comparing the detailed and petrographically well-based major element composition of garnet and clinopyroxene from Geyer SW to the data from the Hämmerlein and Waschleithe skarns (Erzgebirge, Germany), the Crown Mine (Cornwall, England) and further Sn skarns (worldwide) compiled by Meinert (1992). We will then present a mineral system model of tin skarns based on which, as a last step, our major, minor and trace elements will be interpreted within the context of the multi-stage origin of the skarn mineral system at Geyer SW. A particular emphasis will be placed on the abundance and distribution of Sn in the skarn-forming minerals at Geyer SW.

Classification and comparison of skarns in the Erzgebirge and worldwide

Skarn stage I

Early stage skarnoid skarn alteration is documented for most of the skarn deposits in the Erzgebirge (Burisch 2019; Meyer 2024). Furthermore, they are also often reported from skarn systems elsewhere (Cornwall; Alderton and Jackson (1978), Burisch et al. (2023), Canada; Layne and Spooner (1991), China; Huang et al. (2022). Commonly, such early skarn stages are barren or only host significant mineralization if overprinted by subsequent skarn stages, as they are

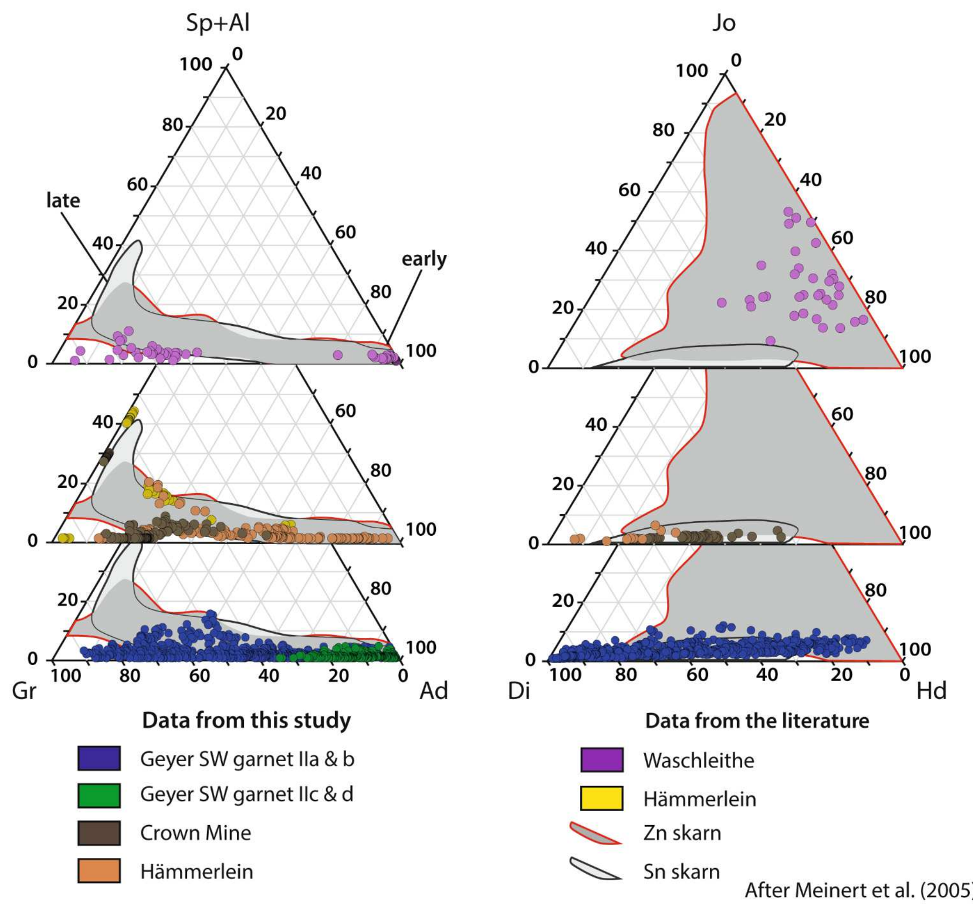

Fig. 11 Ternary plots of garnet (left) and clinopyroxene (right) composition from individual deposits of this study (Geyer SW (blue and green), Hämmerlein (orange) and Crown mine (brown)) compared with literature data from Hämmerlein skarn, Erzgebirge (yellow; Lefebvre et al. 2019) and the Waschleithe skarn, Erzgebirge (purple; Reinhardt et al. 2021). Grey areas are garnet and clinopyroxene compositions observed in association with skarn deposits with distinct metal tenor (Meinert 1992)

mainly related to the contact metamorphic overprint, which pre-dates the main magmatic-hydrothermal event. For this reason, we exclude the mineral data of skarn stage I from the following comparison.

Skarn stage II

In the following, the second skarn stage at Geyer, which is genetically related to tin mineralization, is compared to other Variscan tin skarns. The data comprise major and minor element concentrations of garnet and clinopyroxene of the Hämmerlein skarn, Erzgebirge (Lefebvre et al. 2019; this study), the Waschleithe skarn, Erzgebirge (Reinhardt et al. 2021), and the Crown Mine skarn, Cornwall (this study).

Meinert (1992) suggested that major element compositional trends of both garnets and clinopyroxenes can be linked to metal endowment in skarn systems (see Fig. 11A). Differences between the various skarn types, however, are actually only recorded in the variable proportions of spessartine + almandine (in garnet), and johannsenite (in clinopyroxene) endmembers. The data presented here for Variscan Sn skarn deposits can be evaluated in the context of Meinert (1992).

As shown in Fig. 11, each of the Variscan Sn skarn deposits shows two different groups of garnet compositions: one very (Sps + Alm)-poor spanning most of the range between Grs and And, and another group with significantly higher (Sps + Alm) content. In the case of Hämmerlein and Crown mine, the (Sps + Alm) enrichment closely follows the trend shown by Meinert (1992), while in Geyer SW and Waschleithe (a distal Zn-skarn in the Schwarzenberg District, Reinhardt et al. 2021), this enrichment is indistinct.

Accordingly, the major element composition of garnet and clinopyroxene from Variscan Sn skarns does not correspond well to the trends proposed by Meinert (1992). However, high Sn concentrations in most skarn-forming minerals in combination with an abundance of sphalerite suggests that Geyer SW may be classified as an intermediate Sn-Zn skarn with Sn dominance (note, that Sn concentrations in garnet from Geyer SW are higher than elsewhere in the Erzgebirge and in Cornwall; Lefebvre et al. 2019; Reinhardt et al. 2021; this study). Similarly, the Waschleithe skarn with its much higher amounts of sphalerite and only negligible known Sn mineralization can be regarded as an intermediate Sn-Zn skarn with Zn dominance (as also suggested by Reinhardt et al. 2021), while the Crown Mine skarn is a more or less "pure" endmember Sn skarn. The Hämmerlein skarn deposit, however, does not really fit into this classification scheme. There, the skarn shows extensive sphalerite mineralization together with abundant cassiterite and other Sn-bearing minerals (Korges et al. 2020). Despite its enrichment in Zn and Sn, the Hämmerlein skarn shows similar patterns of garnet and clinopyroxene compositions as the Crown Mine Sn-skarn (Fig. 11B). This leads to the conclusion that – in contrast to Meinert (1992) – garnet and clinopyroxene major element compositions do not allow to unequivocally constrain the metal endowment of skarns in the Variscan orogen. Obviously, a multitude of complex variables control skarn mineral composition and a direct inference of mineralization type based on mineral chemistry alone is often not possible. These variables include the composition of the precursor rocks, formation temperature, and fluid- or rock-buffering of the system. As these factors can vary significantly, not just within one skarn category, but even within one single deposit, the resulting compositional trends are very wide and any overlap with the fields defined by Meinert (1992) is thus of limited significance, especially if only small datasets are considered.

A concise mineral system model

Detailed petrographically work, microthermometric data, precise in-situ geochronology (Meyer et al. 2024), together with major, minor and trace element mineral chemistry of important skarn forming minerals allow the establishment of a coherent mineral system model for the Geyer SW skarn system which is depicted in Fig. 12.

The first stage of skarn formation at Geyer is characterized by the development of fine-grained calc-silicate assemblages dominated by garnet, clinopyroxene and vesuvianite with a skarnoid texture (Meinert et al. 1992; Meyer et al. 2024), i.e., the skarn preserves the metamorphic fabric of the protolith, and calc-silicate minerals are not chemically zoned. U–Pb ages for garnet of *stage I* coincide in time with the emplacement of the Ehrenfriedersdorf batholith, which is known to immediately underlie the skarn units (Bolduan 1963; Hösel et al. 1996). Fluid inclusions in pyroxene constrain the formation temperature of skarn I to about 450–470 °C under lithostatic conditions (Meyer et al. 2024), which is consistent with p-T-X(CO_2) conditions predicted by component reaction calculation in Einaudi et al. (1981) and Hochella et al. (1982). Such skarnoids are widely believed to form under rock-buffered conditions (Gaspar et al. 2008; Jamtveit et al. 1993; Meinert 1992), which is proved by the composition (including REE pattern) of stage I skarn minerals, which provide evidence for a mainly rock-buffered system without tin mineralization. Only in the latest stage, a minor influence of a magmatic-hydrothermal fluid is discernible.

U–Pb ages of garnet and cassiterite unequivocally show a temporal gap of more than 10 million years between *stage I* (~320 Ma) and *stage II* (~305 Ma) of skarn formation at Geyer SW, indicating that they are temporally and genetically clearly distinct. *Stage II* skarn also shows characteristics indicative of formation at a relatively shallow depth (1.5–2 km) under hydrostatic conditions (Meyer et al. 2024), probably related to a small, highly evolved following intrusion at a shallower level. Mineral reactions (following Einaudi et al. 1981; Hochella et al. 1982) and microthermometric data for clinopyroxene (Meyer et al. 2024) additionally confirm a lower temperature of skarn formation for *stage II* (320–335 °C). Textures along with mineral compositions and REE signatures record an overall trend from a rock-buffered, nearly closed system towards a fluid-buffered, open skarn environment corresponding to increasing

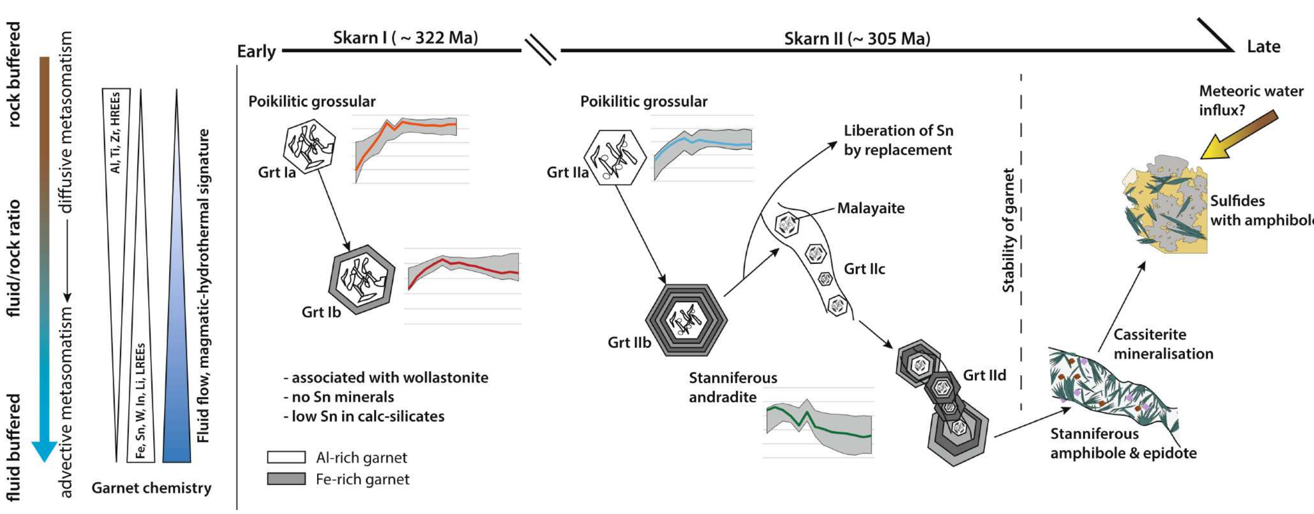

Fig. 12 Composite sketch showing the main characteristics of calc-silicate formation in the different steps of skarn formation with typical elements, REE patterns and textures

fluid/rock ratios in *stage II* at Geyer SW (Fig. 12). However, oscillations in the fluid/rock ratio are indicated by garnet IIc which records lower fluid/rock ratios than garnet IIb. Hence, we propose that at least two distinct fluid pulses occurred during the *prograde stage II* skarn alteration. High Sn concentrations in minerals are invariably related to magmatic-hydrothermal fluids in a fluid- buffered environment. Here, garnet is host to the bulk of Sn in the system.

The *late stage II* is characterized as the retrograde phase during skarn alteration in a purely fluid-buffered environment under hydrostatic conditions and brittle deformation (veining). The onset of this stage is marked by a change of silicate assemblages from tin-bearing garnet (Grt IId) to tin-bearing epidote (Ep II) and tin-bearing amphibole (Amp IIb). Amphibole (Amp IIb and IIc) and chlorite replace existing Fe-Mg-silicates; their formation suggests lower temperatures and the presence of an aqueous fluid as compared to *the prograde stage II (substage IIA)*. Formation temperatures calculated from the mineral chemistry of chlorite after Cathelineau (1988) (210–350 °C; ESM 2) are in good agreement with fluid inclusion data associated with this stage (255–340 °C; Meyer et al. 2024) that also show a prolonged dilution of a more saline magmatic fluid with a low-salinity meteoric fluid. During retrograde alteration, the majority of cassiterite precipitates, leading to the formation of the important and extractable Sn mineralization.

The following chapter will in detail discuss the variable fluid/rock ratios, the impact of magmatic-hydrothermal and meteoric fluids and the (re-)distribution of Sn in the framework of the model presented above. Some of the trace element characteristics, especially during stage I skarn alteration, are inherited from the replaced host rock. Nevertheless, systematic changes can be observed during the development of the skarn system, as elaborated below.

Rock vs. fluid buffered: the evolution of the skarn system reflected by mineral chemistry

Stage I: A rock-buffered start

Garnet Ia has a grossular-rich composition with elevated concentrations of HFSE. Similar is true for clinopyroxene and vesuvianite associated with Garnet Ia – both have a distinct Mg-component. The enrichment in Al, Mg and HFSE in early-stage calc-silicates is indicative for a rock-buffered environment as those elements are abundant in the metamorphic host rocks but are typically depleted in most hydrothermal fluids (Corfu and Davis 1991; Jamtveit and Hervig 1994). Under such rock-buffered conditions, pore fluid may enhance local element mobility, promoting diffusion of e.g., Al, Mg and HFSE like Zr or Ti during skarn formation (Burt 1981; Capitani and Mellini 2000; Chu et al. 2023; Jamtveit and Hervig 1994). The absence of a significant hydrothermal input from a fertile (e.g. Sn, W, Li or In-rich) magmatic source is furthermore supported by invariably low concentrations of such metals in the calc-silicates of *stage I* – in combination with the absence of cassiterite, malayaite or other distinct ore minerals.

The REE pattern of Garnet Ia is strongly depleted in LREEs and enriched in HREEs, which is typical for slow growth rates that promote trace element incorporation controlled by the crystal structure (Røhr et al. 2007; Yang et al. 2013). Divalent Eu is considered to be the stable and predominant species at temperatures higher than 250 °C (Bau 1996; Sverjensky 1984), which is the case in *stage I* at Geyer. The negative Eu values may also be inherited from the host rock. Both might explain the deviation of Eu from the normal distribution pattern of REEs in minerals. Major and trace element systematics of garnet Ib mark a slight but distinct change towards less depleted LREE and less enriched HREE compositions as well as a less pronounced negative Eu anomaly. This is tentatively interpreted to reflect the influence of at least some magmatic-hydrothermal fluid and thus a higher fluid/rock ratio during the waning of *stage I*.

Substage IIA: oscillations between rock and fluid buffering

Skarn *stage II* comprises four garnet generations which range in textures from paragenetically early fine-grained poikilitic (Grt IIa and c) garnet to late coarse-grained euhedral garnet with prominent oscillatory zoning (Grt IIb and d). Consistent with its poikilitic texture, the first generation of garnet (**Grt IIa**) is grossular-rich, high in HFSE, depleted in LREE, and enriched in HREE suggesting growth under low fluid/rock ratios analogous to garnet related to *stage I*. However, Grt IIa is marked by elevated concentrations of Sn, Li, and W, which may indicate some involvement of a magmatic-hydrothermal fluid endowed in these elements.

The textures of **Grt IIb** and associated vesuvianite (Ves II) and amphibole (Amp IIa) mark a distinct change in mineral and skarn textures as they form coarser grained euhedral crystals with well-developed oscillatory zoning. Such textures generally indicate a progressive increase in fluid flow and permeability from fluid migration along interconnected pore space to fractures and veins (Gaspar et al. 2008; Huang et al. 2022; Jamtveit et al. 1993; Jamtveit and Hervig 1994; Meinert 1992; Park et al. 2017a). Concomitant to the textural change, Grt IIb is andradite-rich, enriched in LREE relative to HREEs and has elevated concentrations of Li, W, and In. All of this suggests fluid-buffered conditions with the involvement of a magmatic-hydrothermal fluid (Ayers and Eggler 1995; Bai and Koster van Groos 1999; Douville et al. 1999; Jamtveit et al. 1993; Wood 1990). This notion is

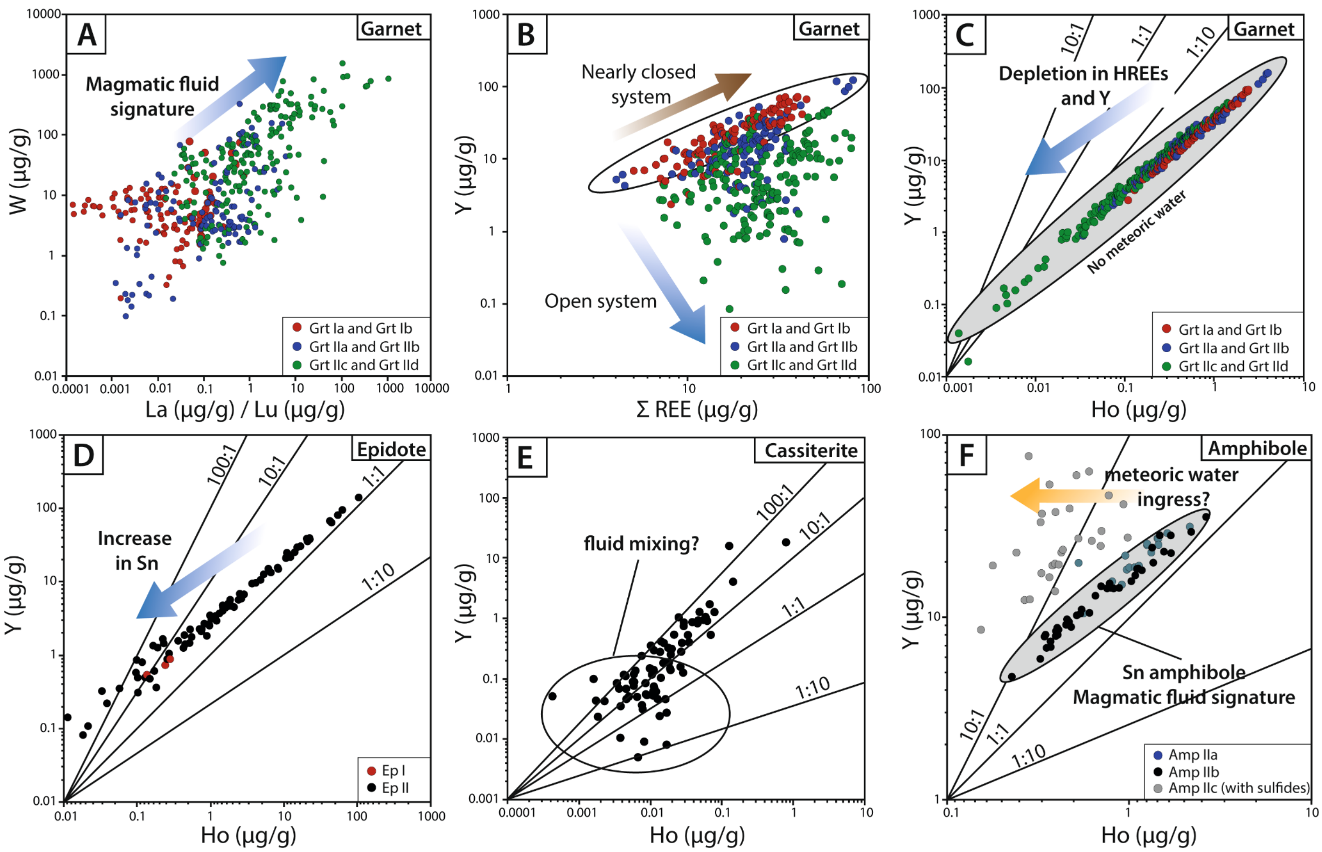

Fig. 13 (**A**) W (µg/g) against the ratio of La (µg/g) vs. Lu (µg/g) of garnet showing the development from rock-buffered (stage I and substage IIA) to fluid-buffered (substage IIB) signatures. (**B**) Y (µg/g) vs. total REEs (µg/g). Lower Y values with relatively constant total REE suggests an open system while constant ratios are evident for a closed system. (**C**) A constant ratio of Ho (µg/g) vs. Y (µg/g) in garnet over a wide range of concentrations indicates that the influx of meteoric fluid in the prograde skarn stages I and II is very limited. (**D**) Similarly, the Y vs. Ho ratio of epidote remains constant, suggesting an absence of fractionation which would indicate an influx of meteoric water. Note also that decreasing Y and Ho concentrations in epidote are accompanied by increasing Sn contents, (**E**). Influx of meteoric water is evident in Y/Ho ratios of cassiterite by the variations of Y vs. Ho. (**F**) The deviation of the Y to Ho ratio of amphibole intergrown with sulfides indicates an enhanced influx of meteoric water while stanniferous amphibole grows under hydrothermal conditions with limited meteoric water influx

further supported by the first occurrence of magnetite in the skarn assemblage, typically requiring externally derived Fe from a magmatic-hydrothermal fluid source (Meinert 1992). Further evidence for an influx of a magmatic-hydrothermal fluid is the high F concentrations of amphibole IIa (intergrown with Grt IIb), as fertile Sn granites in the Erzgebirge have invariably high concentrations of F (Förster et al. 1999; Lehmann 2021). High F activities may also promote precipitation of amphibole IIa early in the prograde skarn stage, whereas it is usually related to the retrograde alteration stage (Dobson 1982; Meinert et al. 2005).

The positive Eu-anomaly in Grt IIb marks a sharp contrast to previous garnet generations that are all marked by negative Eu-anomalies. This anomaly is most likely related to a new batch of magmatic-hydrothermal fluid without buffering by the host rock (Smith et al. 2004). The observation that prograde garnet formed in a fluid-buffered environment shows a positive Eu-anomaly, is widespread in literature (e.g.Chen et al. 2022; Gaspar et al. 2008; Jamtveit and Hervig 1994; Park et al. 2017a, b; Smith et al. 2004) but has not been explained so far. As crystal chemical effects can be ruled out (else, Grt Ib should have a positive Eu anomaly), we suggest that the magmatic-hydrothermal fluid probably itself had a positive Eu anomaly at this stage. This could be due to its residual character after extensive crystallization of minerals with negative Eu anomalies (Breiter et al. 1999; Terekhov and Shcherbakova 2006) or the positive Eu-signature was obtained by dissolution of plagioclase in the rock units it percolated through (Möller et al. 2021). However, positive Eu anomalies were identified in whole-rock data of apical parts of the Ehrenfriedersdorf deposit adjacent to Geyer SW (Lehmann and Seltmann 1995) and in highly evolved, peraluminous granites in France (Raimbault and Azencott 1987). This supports the interpretation that the origin of these garnets displaying a distinct positive Eu anomaly is genetically associated with a magmatic fluid from a highly evolved source.

Following the fluid-dominated formation of garnet IIb, the system evolved towards an intermediate stage, which shows ingress of magmatic fluid but also rock buffering. Under these conditions, **Grt IIc** formed again with poikilitic texture. Grt IIc is intergrown with fluorite, malayaite and remnant clinopyroxene. The following mineral chemical arguments support an increased importance of rock-buffering during the formation of Grt IIc: higher contents of fluid-immobile elements (Al, Ti and Zr) in garnet, and a REE pattern that is less depleted in HREE. The REE pattern is governed by garnet crystal chemistry (Marks et al. 2008), which indicates the amount of fluid was low enough to allow rock buffering, similar to the observations of Jamtveit and Hervig (1994) and similar to the conditions of Grt IIa growth, which is exemplified by the similar, slightly negative Eu anomaly (Fig. 9A). The fact that the garnets have elevated contents of W and In indicates, however, shows that a magmatic fluid was still present at this stage.

This intermediate stage was followed by the most fluid-dominated stage, in which **Grt IId** grew with an andradite-rich composition, the highest concentrations of Sn, Li, W and In, high LREE and low HREE. This type of REE pattern and the again strongly positive Eu anomaly (even stronger that Grt IIb; see Fig. 9A) support the fluid-dominated nature of the system at this stage (Gaspar et al. 2008; Jamtveit and Hervig 1994).

Lanthanum concentrations in Grt IId are ten time higher than in Grt IIc and five times higher than in Grt IIb, with overall similar REE patterns in all three garnet generations. This increase in La may be related to higher fluid salinities, as high chlorinity increases La solubility (Allen and Seyfried 2005). This is supported by fluid inclusion observations (Meyer et al. 2024). Thus, we propose that the high La concentrations and the tetrad effect visible in measurements of garnet and malayaite (Fig. 10A) are related to phase separation, salinity increase and REE fractionation of the magmatic-hydrothermal fluid (Flynn and Burnham 1978; Bai and Koster van Groos 1999; Gaspar et al. 2008; Lehmann 2021; Monecke et al. 2011).

Substage IIB: a fluid-buffered finish

Both epidote II and amphibole IIb of substage IIB precipitated from a cooling magmatic-hydrothermal fluid, indicated by the still strong magmatic-hydrothermal REE signature (slightly positive Eu anomaly and a small tetrad effect; see Fig. 10B). Similar epidote textures have been described in the skarn system of in Petrovitsa, Bulgaria, by Hantsche et al. (2021).

Chlorite commonly replaces both clinopyroxene and amphibole during the waning phase of *substage IIB*, suggesting further cooling of the system (Meinert 1992). Chlorite shows partly elevated concentrations of Li, B and Zn, indicating that it also likely precipitated in the presence of a magmatic-hydrothermal fluid, albeit parts of these traces may originate from the precursor minerals. The most common mineral accompanying chlorite is cassiterite, both in veins and alteration halos. The concentration of trace elements in cassiterite is strongly dependent on crystallographic properties (Schneider et al. 1978). The strong enrichment of In and W suggests a strong influence of a magmatic-hydrothermal fluid. This is supported by the obvious third tetrad anomaly, which is considered to be a primary feature of a magmatic-hydrothermal fluid from a highly evolved granite (Bau 1996; Irber 1999; Förster and Tischendorf 1994; Gemmrich et al. 2021; Monecke et al. 2011).

Magmatic vs. meteoric fluids

Apart from isotopic signatures (which are beyond the scope of this study), the Y/Ho ratio is arguably the best parameter to constrain the source of a hydrothermal fluid from whole rock compositions (Bau and Dulski 1995; Bau 1996) or mineral chemistry (Chu et al. 2023) in a fluid-dominated hydrothermal system. Neither fractional crystallization of a granitic system nor modifications of the fluid like boiling or cooling lead to fractionation between Y and Ho (Bau and Dulski 1995). Variations of the Y/Ho ratio have thus been attributed to the dilution of a magmatic-hydrothermal by a meteoric fluid (Bau 1996).

Figure 12 shows that all garnet generations, both epidote generations and the first two amphibole generations (Amp IIa and IIb) show constant Y/Ho ratios over a wide range of concentrations. This suggests that all these minerals formed from a magmatic fluid of constant Y/Ho composition (Ayers and Eggler 1995; Bai and Koster van Groos 1999; Bau 1996; Park et al. 2017b). However, amphiboles that coexist with sulfides (Amp IIc) show a deviation in the Y/Ho ratio (Fig. 13F) and a different REE distribution (Fig. 10B), suggesting the influx of meteoric water (Bau and Dulski 1995). This is consistent with the abundance of sulfides in this assemblage, which is a typical response to enhanced influx of meteoric water into a retrograde skarn system (Gao et al. 2020; Meinert et al. 2003; Öztürk et al. 2008). Later phases (chlorite and cassiterite) probably formed from a mixture of magmatic and meteoric fluids as prominently shown in the Y/Ho systematics of cassiterite (Fig. 11E).

The fate of tin

Skarn *stage I* at Geyer SW lacks discrete tin minerals and maximum concentrations of Sn in calc-silicates do not exceed 900 µg/g (Table 1). This leads to two important conjectures, namely (a) that the precursor rock of the skarnoid did not contain significant concentrations of Sn and (b) that the skarnoid formed under rock-buffered conditions as stipulated above.

Conversely, the major skarn minerals malayaite-titanite, garnet, vesuvianite, and amphibole related to *stage II* contain considerable amounts of Sn (Table 1), of which garnet can be considered as the main host of the bulk Sn due to its high abundance and high Sn contents (Table 1).

Mineral chemistry data (Table 1) document clearly that during stage II, the influx of Sn-bearing magmatic-hydrothermal fluids progressively increased, which resulted in an overall trend of increasing Sn concentrations in skarn minerals and also the occurrence of malayaite. The observed increase in Sn concentration in calc-silicates obviously coincides with high fluid/rock ratios and a fluid-dominated system of skarn mineral formation (Table 1).

During the waning of stage II (*substage IIB*), cassiterite, epidote and amphibole are the main hosts of Sn (Table 1). Cooling of the system displayed by the stabilization of amphibole and chlorite (Meinert 1992), and the dilution of the magmatic fluid with meteoric water, indicated by the diverging Y/Ho ratio in cassiterite, are most likely reason for cassiterite and sulfide precipitation.

The mineral chemical data of all analyzed silicates in Geyer suggests an incorporation of Sn^{4+} via isovalent substitution (titanite-malayaite; Deer et al. 2013) or coupled substitution with Fe^{2+} Mg, and Mn^{2+}, as it was shown for garnet (Amthauer et al. 1976; Chen et al. 1992; Plimer 1984; Yu et al. 2020) and epidote (Armbruster et al. 2006; Van Marcke de Lummen 1986). This indicates, in contrast to common belief and in accordance with recent experiments (Chou et al. 2021; Schmidt 2018; Wang et al. 2021) as well as with thermodynamic modelling (Liu et al. 2023), that a considerable amount of tin can be transported as Sn^{4+}-complexes. An oxidized environment during the formation of stanniferous calc-silicates is also supported by the high concentration of Fe^{3+} compared to reduced Fe^{2+} in minerals such as andradite and epidote of *stage II*. Following this argumentation, an external oxidizing agent is not necessary to either incorporate tin into silicates or to precipitate cassiterite – oxidizing of the system by temperature decrease and fluid mixing are sufficient (see also Schmidt 2018).

During the evolution of the skarn system, two different stages of tin remobilization can be distinguished. The first one is associated with substage IIA, in which Al-rich garnet (garnet IIc), replaces stanniferous calc-silicates. Due to the lower ability of grossular-rich garnet to incorporate Sn (Sonnet and Verkaeren 1989; Park et al. 2017b; Plimer 1984), malayaite forms as a Sn-rich mineral. Relatively high temperatures and a high silica activity, which is assumed at this stage (Meyer et al. 2024), stabilized malayaite rather than cassiterite (Aleksandrov and Troneva 2007). The second remobilization of Sn occurred during the waning of *substage IIB*, when most skarn minerals were replaced by hydrothermal calcite, quartz and prehnite, implying a further cooling of the system. During this process, cassiterite is replaced by stokesite. A similar late-stage occurrence of stokesite has been described by Kern et al. (2019) for the Hämmerlein skarn.

Table 1 Average and maximum concentrations of Sn and F and the ratio between the LREEs (La–Nd) and HREEs (Er–Lu)

Mineral / Nr of analyses	Av. Sn (wt%)	Max Sn (wt%)	SD (1σ)	Av F. (wt%)	Max. F (wt%)	SD (1σ)	Av. LREE / HREE
Stage I (~322–315 Ma)							
Garnet Ia /179	0.03	0.09	0.02	0.20	1.33	0.21	0.1
Garnet Ib /102	0.04	0.1	0.03	0.22	1.44	0.16	1.1
Titanite / 80	0.33	1.34	0.32	0.79	3.06	0.62	0.4
Vesuvianite / 138	0.09	0.16	0.03	1.24	3.07	0.72.	7.98
Epidote / 112	0.39	1.22	0.36	-	-	-	0.65
Stage II (~307–302 Ma)							
Garnet IIa /197	0.25	0.90	0.14	0.55	2.32	0.47	0.4
Garnet IIb /184	0.54	3.35	0.62	0.18	1.22	0.17	4.6
Garnet IIc /316	1.23	4.15	0.86	0.41	2.26	0.46	7.2
Garnet IId /198	3.16	6.54	1.60	0.15	1.26	0.14	36.1
Titanite IIa[1] / 115	27.4	58.6	19.1	0.70	2.23	0.42	0.66
Titanite IIb[1] / 29	58.1	59.5	2.93	-	-	-	1.16
Vesuvianite / 242	0.26	0.99	0.23	1.67	3.45	0.60	46.82
Amphibole IIa / 60	1.30	1.88	0.22	1.08	1.34	0.13	1.09
Amphibole IIb / 340	0.59	2.71	0.51	0.40	1.09	0.21	0.63
Amphibole IIc / 119	0.17	0.53	0.12	0.17	0.80	0.17	0.17
Epidote / 293	2.46	7.81	2.08	-	-		4.06

[1] Some of these measurements are the Sn-endmember malayaite

Conclusions

Detailed petrography, microthermometry, and precise geochronology are sufficient to characterize the general structure of a Sn skarn system. However, the integration of major, minor and trace elements (especially REEs) of relevant calc-silicate minerals is necessary to understand the details of the physicochemical evolution of skarn systems. Only a combination of these observations allows the establishment of a concise mineral system model.

The present contribution has combined careful petrography with major, minor and trace element compositions of important rock-forming and ore minerals of the Geyer SW skarn to show the importance of such studies in a textbook example. Importantly, the oscillation between fluid-buffered and rock-buffered conditions during skarn mineralization and alteration governs the texture of minerals and determines their chemical composition. Changes in the fluid/rock ratio directly respond to discontinuous fluid pulses exiting the intrusion at depth. The invariably high concentrations of Sn, In, and W in minerals which formed under high fluid-rock ratios strongly supports that these elements were introduced by the magmatic-hydrothermal fluid rather than being remobilized from the surrounding metasediments.

This investigation and comparison with other Variscan tin skarn data showed that the metal classification of Variscan Sn-Zn skarns solely based on the major mineral chemistry of garnet and clinopyroxene is inadequate and does not help to constrain the dominant metal tenor of a skarn system; therefore, it is of limited use as an exploration vector.

Supplementary Information The online version contains supplementary material available at https://doi.org/10.1007/s00126-024-01297-w.

Acknowledgements Manuel Lapp (LfULG Sachsen) is thanked for providing access to drill cores, thin sections, and exploration reports. We are grateful to Roland Würkert and Michael Stoll (HIF) for sample preparation. We are also grateful to Dr. Aratz Beranoaguirre (KIT) for operating the LA-ICP-MS and Dr. Sebastian Staude and Dr. Thomas Wenzel (University of Tübingen) for microprobe analyses. Additionally, we would like to thank N. F. Jansson as well as the two reviewers, Andrew Martin and Andreas Müller, for their very constructive comments that profoundly improved this paper.

Funding Open Access funding enabled and organized by Projekt DEAL. This project is funded as part of the German Research Foundation DFG priority program Dynamics of Ore Enrichment (DOME; SPP2238) via grant 3134023001. Electron microprobe analyses have partly funded by the German Research Foundation (DFG; grant INST 37/1026-1 FUGG).
Open Access funding enabled and organized by Projekt DEAL.

Declarations

Competing interests The authors declare no competing interests.

References

Alderton DHM, Jackson NJ (1978) Discordant calc-silicate bodies from the St. Just aureole, Cornwall. Mineral Mag 42:427–434. https://doi.org/10.1180/minmag.1978.042.324.03

Aleksandrov SM, Troneva MA (2007) Composition, mineral assemblages, and genesis of titanite and malayaite in skarns. Geochem Int 45:1012–1024. https://doi.org/10.1134/S0016702907100059

Allen DE, Seyfried WE (2005) REE controls in ultramafic hosted MOR hydrothermal systems: an experimental study at elevated temperature and pressure. Geochim Cosmochim Acta 69:675–683. https://doi.org/10.1016/j.gca.2004.07.016

Amthauer G, Annersten H, Hafner SS (1976) The Mössbauer spectrum of ^{57}Fe in silicate garnets. Z Krist 143:14–55

Ayers JC, Eggler DH (1995) Partitioning of elements between silicate melt and H2O-NaCl fluids at 1.5 and 2.0 GPa pressure: implications for mantle metasomatism. Geochim Cosmochim Acta 59:4237–4246. https://doi.org/10.1016/0016-7037(95)00244-T

Bai TB, Van Koster AF (1999) The distribution of na, K, Rb, Sr, Al, Ge, Cu, W, Mo, La, and ce between granitic melts and coexisting aqueous fluids. Geochim Cosmochim Acta 63:1117–1131. https://doi.org/10.1016/S0016-7037(98)00284-1

Bau M (1996) Controls on the fractionation of isovalent trace elements in magmatic and aqueous systems: evidence from Y/Ho, Zr/Hf, and lanthanide tetrad effect. Contrib Mineral Petrol 123:323–333. https://doi.org/10.1007/s004100050159

Bau M, Dulski P (1995) Comparative study of yttrium and rare-earth element behaviour in fluorine-rich hydrothermal fluids. Contrib Mineral Petrol 119:213–223. https://doi.org/10.1007/BF00307282

Bauer ME, Burisch M, Ostendorf J, Krause J, Frenzel M, Seifert T, Gutzmer J (2019) Trace element geochemistry of sphalerite in contrasting hydrothermal fluid systems of the Freiberg district, Germany: insights from LA-ICP-MS analysis, near-infrared light microthermometry of sphalerite-hosted fluid inclusions, and sulfur isotope geochemistry. Min Deposita 54:237–262. https://doi.org/10.1007/s00126-018-0850-0

Baumann L, Kuschka E, Seifert T (2000) Lagerstätten Des Erzgebirges. Enke in Thieme-, Stuttgart

Bolduan H (1963) Geologie Und Genese Der Zinn-Wolframlagerstätte Geyer (Erzgeb). Freib Forsch-Hefte C 167:7–34

Breiter K (2012) Nearly contemporaneous evolution of the A- and S-type fractionated granites in the Krušné hory/Erzgebirge Mts., Central Europe. Lithos 151:105–121. https://doi.org/10.1016/j.lithos.2011.09.022

Breiter K, Förster H-J, Seltmann R (1999) Variscan silicic magmatism and related tin-tungsten mineralization in the Erzgebirge-Slavkovský les metallogenic province. Min Deposita 34:505–521. https://doi.org/10.1007/s001260050217

Burisch M, Gerdes A, Meinert LD, Albert R, Seifert T, Gutzmer J (2019) The essence of time – fertile skarn formation in the Variscan Orogenic Belt. Earth Planet Sci Lett 519:165–170. https://doi.org/10.1016/j.epsl.2019.05.015

Burisch M, Bussey SD, Landon N, Nasi C, Kakarieka A, Gerdes A, Albert R, Stein HJ, Gabites JA, Friedman RM, Meinert LD (2023) Timing of magmatism and skarn formation at the Limon, Guajes, and Media Luna gold ± copper skarn deposits at Morelos, Guerrero State, Mexico. Econ Geol 118(4):695–718

Burt DM (1981) Acidity-salinity diagrams; application to greisen and porphyry deposits. Econ Geol 76:832–843. https://doi.org/10.2113/gsecongeo.76.4.832

Capitani GC, Mellini M (2000) The johannsenite-hedenbergite complete solid solution: clinopyroxenes from the Campiglia Marittima Skarn. Eur J Mineral 12:1215–1227. https://doi.org/10.1127/0935-1221/2000/0012-1215

Cathelineau M (1988) Cation site occupancy in chlorites and illites as a function of temperature. Clay Miner 23(4):471–485

Chen J, Halls C, Stanley CJ (1992) Tin-bearing skarns of South China: geological setting and mineralogy. Ore Geol Rev 7:225–248. https://doi.org/10.1016/0169-1368(92)90006-7

Chen K, Shao Y, Zhang J, Zhang Y, Tan H, Zhang Y, Liu Z (2022) Garnet U-Pb geochronology and geochemistry reveal deposit types and fluid evolution: an example from the Dongguashan Cu-Au deposit, eastern China. Ore Geol Rev 145:104883. https://doi.org/10.1016/j.oregeorev.2022.104883

Chou I-M, Wang R, Fang J (2021) In situ redox control and Raman spectroscopic characterisation of solutions below 300°C. Geochem Persp Lett 1–5. https://doi.org/10.7185/geochemlet.2135

Chu G, Chen H, Zhang S, Zhang Y, Cheng J (2023) Geochemistry and geochronology of multi-generation garnet: new insights on the genesis and fluid evolution of prograde skarn formation. Geosci Front 14:101495. https://doi.org/10.1016/j.gsf.2022.101495

Corfu F, Davis DW Comment on Archean hydrothermal zircon in the Abitibi greenstone belt: constraints on the timing of gold mineralization by, Claoué-Long JC, King RW, Kerrich R (1991) Earth Planet Sci Lett 104:545–552. https://doi.org/10.1016/0012-821X(91)90229-B

Deer WA, Howie RA, Zussman J (2013) An introduction to the rock-forming minerals. The Mineralogical Society, London

Dobson DC (1982) Geology and alteration of the Lost River tin-tungsten-fluorine deposit, Alaska. Econ Geol 77:1033–1052. https://doi.org/10.2113/gsecongeo.77.4.1033

Douville E, Bienvenu P, Charlou JL, Donval JP, Fouquet Y, Appriou P, Gamo T (1999) Yttrium and rare earth elements in fluids from various deep-sea hydrothermal systems. Geochim Cosmochim Acta 63:627–643. https://doi.org/10.1016/S0016-7037(99)00024-1

Einaudi MT, Burt DM (1982) Introduction; terminology, classification, and composition of skarn deposits. Econ Geol 77(4):745–754

Einaudi MT, Meinert LD, Newberry RJ (1981) Skarn deposits. In: Skinner BJ (ed) Economic geology, seventy-fifth anniversary volume 1905–1980. Society of Economic Geologists, Littleton, CO, pp 317–391

Elsner H (2014) Zinn - Angebot und nachfrage bis 2020, vol 20, 2014th edn. DERA Rohstoffinformationen, DERA, Berlin

Flynn RT, Burnham WC (1978) An experimental determination of rare earth partition coefficients between a chloride containing vapor phase and silicate melts. Geochim Cosmochim Acta 42:685–701. https://doi.org/10.1016/0016-7037(78)90087-X

Förster H-J (2021) Geochemistry of late-Variscan felsic igneous rocks of the Erzgebirge – Vogtland metallogenic province. – part 1: P- und F-rich Li-mica granites. https://doi.org/10.5880/GFZ.4.8.2021.005. GFZ Data Services

Förster H-J, Tischendorf G (1994) The western Erzgebirge-Vogtland granites: implications to the Hercynian magmatism in the Erzgebirge-Fichtelgebirge anticlinorium. Czech Geol Surv Prague :35–48

Förster H-J, Tischendorf G, Trumbull RB, Gottesmann B (1999) Late-Collisional granites in the Variscan Erzgebirge, Germany. J Petrol 40:1613–1645. https://doi.org/10.1093/petroj/40.11.1613

Gao X, Yang L-Q, Yan H, Meng J-Y (2020) Ore-forming processes and mechanisms of the Hongshan Skarn Cu–Mo deposit, Southwest China: insights from mineral chemistry, fluid inclusions, and stable isotopes. Ore Energy Resource Geol 4–5:100007. https://doi.org/10.1016/j.oreoa.2020.100007

Gaspar M, Knaack C, Meinert LD, Moretti R (2008) REE in skarn systems: a LA-ICP-MS study of garnets from the Crown Jewel gold deposit. Geochim Cosmochim Acta 72:185–205. https://doi.org/10.1016/j.gca.2007.09.033

Gemmrich L, Torró L, Melgarejo JC, Laurent O, Vallance J, Chelle-Michou C, Sempere TPA (2021) Trace element composition and U-Pb ages of cassiterite from the Bolivian tin belt. Min Deposita 56:1491–1520. https://doi.org/10.1007/s00126-020-01030-3

Hantsche AL, Kouzmanov K, Milenkov G, Vezzoni S, Vassileva R, Dini A, Sheldrake T, Laurent O, Guillong M (2021) Metasomatism and cyclic skarn growth along lithological contacts: physical and geochemical evidence from a distal pb zn skarn. Lithos 400–401. https://doi.org/10.1016/j.lithos.2021.106408

Harlov DE, Austrheim H (2013) Metasomatism and the chemical transformation of rock: the role of fluids in terrestrial and extraterrestrial processes. Lecture notes in earth system sciences. Springer, Berlin, New York

Hawthorne FC, Oberti R, Harlow GE, Maresch WV, Martin RF, Schumacher JC, Welch MD (2012) Nomenclature of the amphibole supergroup. Amer Min 97:2031–2048. https://doi.org/10.2138/am.2012.4276

Hochella MF, Liou JG, Keskinen MJ, Kim HS (1982) Synthesis and stability relations of magnesium idocrase. Econ Geol 77(4):798–808

Hoffmann U, Breitkreuz C, Breiter K, Sergeev S, Stanek K, Tichomirowa M (2013) Carboniferous–Permian volcanic evolution in Central Europe—U/Pb ages of volcanic rocks in Saxony (Germany) and northern Bohemia (Czech Republic). Int J Earth Sci (Geol Rundsch) 102:73–99. https://doi.org/10.1007/s00531-012-0791-2

Hong J, Zhang H, Li D, Ouyang Y, Zhai D, Liu F, Liu J (2022) In situ LA-ICP-MS U-Pb geochronology and geochemical characteristics of garnet from the Zhuxi Skarn W-Cu deposit, South China. Ore Geol Rev 140:104577. https://doi.org/10.1016/j.oregeorev.2021.104577

Hösel G (1994) Das Zinnerz-Lagerstättengebiet Ehrenfriedersdorf/Erzgebirge. Bergbau in Sachsen, 1. Sächsisches Druck- und Verlagshaus GmbH, Dresden

Hösel G (2002) Die polymetallische Skarnlagerstätte Pöhla-Globenstein. Bergbau in Sachsen, 8 edn. Sächsisches Druck- und Verlagshaus GmbH, Dresden

Hösel G, Fritsch E, Josiger U, Wolf P (1996) Das Lagerstättengebiet Geyer. Bergbau in Sachsen, 4 edn. Sächsisches Druck- und Verlagshaus GmbH, Dresden

Huang XD, Lu JJ, Zhang RQ, Sizaret S, Ma DS, Wang RC, Zhu X, He ZY (2022) Garnet and Scheelite chemistry of the Weijia tungsten deposit, South China: implications for fluid evolution and W skarn mineralization in F-rich ore system. Ore Geol Rev 142:104729. https://doi.org/10.1016/j.oregeorev.2022.104729

Irber W (1999) The lanthanide tetrad effect and its correlation with K/Rb, Eu/Eu*, Sr/Eu, Y/Ho, and Zr/Hf of evolving peraluminous granite suites. Geochim Cosmochim Acta 63:489–508. https://doi.org/10.1016/S0016-7037(99)00027-7

Jamtveit B, Hervig RL (1994) Constraints on transport and kinetics in hydrothermal systems from zoned garnet crystals. Science 263:505–508. https://doi.org/10.1126/science.263.5146.505

Jamtveit B, Wogelius RA, Fraser DG (1993) Zonation patterns of skarn garnets: records of hydrothermal system evolution. Geology 21:113. https://doi.org/10.1130/0091-7613(1993)021%3C0113:ZPOSGR%3E2.3.CO;2

Kern M, Kästner J, Tolosana-Delgado R, Jeske T, Gutzmer J (2019) The inherent link between ore formation and geometallurgy as documented by complex tin mineralization at the Hämmerlein deposit (Erzgebirge, Germany). Min Deposita 54:683–698. https://doi.org/10.1007/s00126-018-0832-2

Korges M, Weis P, Lüders V, Laurent O (2018) Depressurization and boiling of a single magmatic fluid as a mechanism for tin-tungsten deposit formation. Geology 46:75–78. https://doi.org/10.1130/G39601.1

Korges M, Weis P, Lüders V, Laurent O (2020) Sequential evolution of Sn–Zn–In mineralization at the skarn-hosted Hämmerlein deposit, Erzgebirge, Germany, from fluid inclusions in ore and gangue minerals. Min Deposita 55:937–952. https://doi.org/10.1007/s00126-019-00905-4

Kroner U, Hahn T, Romer RL, Linnemann U (2007) The Variscan orogeny in the Saxo-Thuringian zone—heterogenous overprint of Cadomian/Paleozoic Peri-gondwana crust. In: Linnemann U, Nance RD, Kraft P, Zulauf G (eds) The evolution of the Rheic Ocean: from avalonian-cadomian active margin to Alleghenian-Variscan collision. Geological Society of America

Kröner A, Willner AP (1998) Time of formation and peak of Variscan HP-HT metamorphism of quartz-feldspar rocks in the central Erzgebirge, Saxony, Germany. Contrib Mineral Petrol 132:1–20. https://doi.org/10.1007/s004100050401

Kwak TAP (1987) W-Sn skarn deposits and related metamorphic skarns and granitoids. Developments in economic geology. Elsevier; Distributors for the United States and Canada, vol 24. Elsevier Science Pub. Co, Amsterdam, New York

Layne GD, Spooner ETC (1991) The JC tin skarn deposit, southern Yukon Territory; I, Geology, paragenesis, and fluid inclusion microthermometry. Econ Geol 86(1):29–47

Lefebvre MG, Romer RL, Glodny J, Kroner U, Roscher M (2019) The Hämmerlein skarn-hosted polymetallic deposit and the Eibenstock granite associated greisen, western Erzgebirge, Germany: two phases of mineralization—two Sn sources. Min Deposita 54:193–216. https://doi.org/10.1007/s00126-018-0830-4

Lehmann B (2021) Formation of tin ore deposits: a reassessment. Lithos 402–403:105756 https://doi.org/10.1016/j.lithos.2020.105756

Lehmann B, Seltmann R (1995) : Der Übergangsbereich Pegmatit-/Aplit- in Hydrothermal-Systeme am Beispiel Ehrenfriedersdorf/Erzgebirge: Abschlußbericht zum DFG-Projekt Le 578/7 – 1 und Se 594/3 – 1, (Scientific Technical Report; 95/20)

Liu B, Wu QH, Kong H, Chen SF, Li H, Zhang DX, Xi XS, Wu JH, Jiang H (2022) Tungsten mineralization process and oxygen fugacity evolution in the Weijia W deposit, South China: constraints from the microstructures, geochemistry, and oxygen isotopes of scheelite, garnet, and calcite. Ore Geol Rev 146:104952. https://doi.org/10.1016/j.oregeorev.2022.104952

Liu X, Yu P, Xiao C (2023) Tin transport and cassiterite precipitation from hydrothermal fluids. Geosci Front 14:101624. https://doi.org/10.1016/j.gsf.2023.101624

Locock AJ (2014) An Excel spreadsheet to classify chemical analyses of amphiboles following the IMA 2012 recommendations. Comput Geosci 62:1–11. https://doi.org/10.1016/j.cageo.2013.09.011

Löcse F, Schneider G, Linnemann U, Rößler R (2023) Carboniferous–Permian volcanic evolution in the Mid-european Variscides: U-Pb LA-ICP-MS zircon ages, geochemical and petrographical constraints from the NW Saxonian Volcanic Basin (Germany). T Dtsch Geol Gesell 174:7–30. https://doi.org/10.1127/zdgg/2023/0359

Luthardt L, Hofmann M, Linnemann U, Gerdes A, Marko L, Rößler R (2018) A new U–Pb zircon age and a volcanogenic model for the early Permian Chemnitz Fossil Forest. Int J Earth Sci (Geol Rundsch) 107:2465–2489. https://doi.org/10.1007/s00531-018-1608-8

Marks MA, Coulson IM, Schilling J, Jacob DE, Schmitt AK, Markl G (2008) The effect of titanite and other HFSE-rich mineral (Ti-bearing andradite, zircon, eudialyte) fractionation on the geochemical evolution of silicate melts. Chem Geol 257:153–172. https://doi.org/10.1016/j.chemgeo.2008.09.002

Masuda A, Kawakami O, Dohmoto Y, Takenaka T (1987) Lanthanide tetrad effects in nature: two mutually opposite types, W and M. Geochem J 21:119–124. https://doi.org/10.2343/geochemj.21.119

McDonough WF, Sun SS (1995) The composition of the Earth. Chem Geol 120(3–4):223–253

McLennan SM (1989) Chap. 7. Rare Earth elements in sedimentary rocks. Influence of provenance and sedimentary processes. In: Lipin BR, McKay GA (Eds.) Geochemistry and Mineralogy of Rare Earth Elements. De Gruyter, pp 169–200

Meinert LD (1992) Skarns and Skarn deposits. Geosci Can 19:145–162

Meinert LD, Hedenquist JW, Satoh H, Matsuhisa Y (2003) Formation of anhydrous and hydrous skarn in Cu-Au Ore deposits by magmatic fluids. Econ Geol 98:147–156. https://doi.org/10.2113/gsecongeo.98.1.147

Meinert LD, Dipple GM, Nicolescu S (2005) World Skarn deposits. In: Hedenquist JW, Thompson JFH, Goldfarb RJ, Richards JP (eds) One hundredth anniversary volume. Society of Economic Geologists

Meyer N, Markl G, Gerdes A, Gutzmer J, Burisch M (2024) Timing and origin of skarn-, greisen-, and vein-hosted tin mineralization at Geyer, Erzgebirge (Germany). Min Deposita. https://doi.org/10.1007/s00126-023-01194-8

Mingram B (1998) The Erzgebirge, Germany, a subducted part of northern Gondwana: geochemical evidence for repetition of early palaeozoic metasedimentary sequences in metamorphic thrust units. Geol Mag 135:785–801. https://doi.org/10.1017/S0016756898001769

Möller P, Dulski P, de Lucia M (2021) REY patterns and their natural anomalies in Waters and Brines: the correlation of Gd and Y anomalies. Hydrology 8:116. https://doi.org/10.3390/hydrology8030116

Monecke T, Kempe U, Trinkler M, Thomas R, Dulski P, Wagner T (2011) Unusual rare earth element fractionation in a tin-bearing magmatic-hydrothermal system. Geology 39:295–298. https://doi.org/10.1130/G31659.1

Norton DL (1987) Advective Metasomatism. In: Helgeson HC (ed) Chemical Transport in Metasomatic processes. Springer Netherlands, Dordrecht, pp 123–132

Ondrus P, Veselovsky F, Gabasova A, Hlousek J, Srein V (2003) Geology and hydrothermal vein system of the Jachymov (Joachimsthal) ore district. J Geosci 48:3–18

Ordosch A, Raith JG, Schmidt S, Aupers K (2019) Polyphase scheelite and stanniferous silicates in a W-(Sn) skarn close to Felbertal tungsten mine, Eastern Alps. Min Petrol 113:703–725. https://doi.org/10.1007/s00710-019-00675-x

Osbahr I, Krause J, Bachmann K, Gutzmer J (2015) Efficient and Accurate Identification of Platinum-Group Minerals by a combination of Mineral Liberation and Electron Probe Microanalysis with a New Approach to the Offline Overlap correction of platinum-group element concentrations. Microsc Microanal 21:1080–1095. https://doi.org/10.1017/S1431927615000719

Öztürk YY, Helvacı C, Satır M (2008) The influence of meteoric water on skarn formation and late-stage hydrothermal alteration at the Evciler skarn occurrences, Kazdağ, NW Turkey. Ore Geol Rev 34:271–284. https://doi.org/10.1016/j.oregeorev.2008.01.001

Pälchen W, Walter H (eds) (2011) Geologie Von Sachsen, 2nd edn. Schweizerbart, Stuttgart

Park C, Song Y, Kang IM, Shim J, Chung D, Park C-S (2017a) Metasomatic changes during periodic fluid flux recorded in grandite garnet from the Weondong W-skarn deposit, South Korea. Chem Geol 451:135–153. https://doi.org/10.1016/j.chemgeo.2017.01.011

Park C, Choi W, Kim H, Park MH, Kang I-M, Lee H-S, Song Y (2017b) Oscillatory zoning in Skarn Garnet: implications for tungsten ore exploration. Ore Geol Rev 89:1006–1018. https://doi.org/10.1016/j.oregeorev.2017.08.003

Pertsev NN (1974) Skarns as magmatic and postmagmatic formations. Int Geol Rev 16:572–582. https://doi.org/10.1080/00206817409471840

Plimer IR (1984) Malayaite and tin-bearing silicates from a skarn at Doradilla via Bourke, New South Wales. Aust J Earth Sci 31:147–153. https://doi.org/10.1080/08120098408729286

Raimbault L, Azencott C (1987) Géochimie Des éléments majeurs et traces du granite a métaux rares de beauvoir (Sondage GPF, échassieres). GÃ©ologie de la France 2–3:189–198

Reed MJ, Candela PA, Piccoli PM (2000) The distribution of rare earth elements between monzogranitic melt and the aqueous volatile phase in experimental investigations at 800°C and 200 MPa. Contrib Mineral Petrol 140:251–262. https://doi.org/10.1007/s004100000182

Reinhardt N, Frenzel M, Meinert LD, Gutzmer J, Kürschner T, Burisch M (2021) Mineralogy and fluid characteristics of the Waschleithe Zn skarn – a distal part of the Schwarzenberg mineral system, Erzgebirge, Germany. Ore Geol Rev 131:104007. https://doi.org/10.1016/j.oregeorev.2021.104007

Reinhardt N, Gerdes A, Beranoaguirre A, Frenzel M, Meinert LD, Gutzmer J, Burisch M (2022) Timing of magmatic-hydrothermal activity in the Variscan Orogenic Belt: LA-ICP-MS U–Pb geochronology of skarn-related garnet from the Schwarzenberg District, Erzgebirge. Min Deposita 57:1071–1087. https://doi.org/10.1007/s00126-021-01084-x

Ribbe PH (1982) CHAPTER 5. TITANITE (SPHENE). In: Burns RG (ed) Orthosilicates. De Gruyter, Berlin, Boston, pp 137–154

Røhr TS, Austrheim H, Erambert M (2007) Stress-induced redistribution of yttrium and heavy rare-earth elements (HREE) in garnet during high-grade polymetamorphism. Amer Min 92:1276–1287. https://doi.org/10.2138/am.2007.2479

Romer RL, Kroner U (2015) Sediment and weathering control on the distribution of paleozoic magmatic tin–tungsten mineralization. Min Deposita 50:327–338. https://doi.org/10.1007/s00126-014-0540-5

Romer RL, Meixner A (2014) Lithium and boron isotopic fractionation in sedimentary rocks during metamorphism – the role of rock composition and protolith mineralogy. Geochim Cosmochim Acta 128:158–177. https://doi.org/10.1016/j.gca.2013.11.032

Romer RL, Thomas R, Stein HJ, Rhede D (2007) Dating multiply overprinted Sn-mineralized granites—examples from the Erzgebirge, Germany. Min Deposita 42:337–359. https://doi.org/10.1007/s00126-006-0114-2

Romer RL, Kroner U, Schmidt C, Legler C (2022) Mobilization of tin during continental subduction-accretion processes. Geology 50:1361–1365. https://doi.org/10.1130/G50466.1

Schmidt C (2018) Formation of hydrothermal tin deposits: Raman spectroscopic evidence for an important role of aqueous sn(IV) species. Geochim Cosmochim Acta 220:499–511. https://doi.org/10.1016/j.gca.2017.10.011

Schneider HJ, Dulski P, Luck J, Moeller P, Villalpando A (1978) Correlation of trace element distribution in cassiterites and geotectonic position of their deposits in Bolivia. Min Deposita 13:119–122

Schuppan W, Hiller A (2012) Die Komplexlagerstätten Tellerhäuser Und Hämmerlein. Bergbau in Sachsen, 17. Sächsisches Druck- und Verlagshaus GmbH, Dresden

Smith MP, Henderson P, Jeffries TE, Long J, Williams CT (2004) The Rare Earth elements and uranium in garnets from the Beinn an Dubhaich Aureole, Skye, Scotland, UK: constraints on processes in a dynamic Hydrothermal System. J Petrol 45:457–484. https://doi.org/10.1093/petrology/egg087

Sonnet PM, Verkaeren J (1989) Scheelite-, malayaite-, and axinite-bearing skarns from El Hammam, central Morocco. Econ Geol 84:575–590. https://doi.org/10.2113/gsecongeo.84.3.575

Sverjensky DA (1984) Europium redox equilibria in aqueous solution. Earth Planet Sci Lett 67:70–78. https://doi.org/10.1016/0012-821X(84)90039-6

Swinkels LJ, Schulz-Isenbeck J, Frenzel M, Gutzmer J, Burisch M (2021) Spatial and temporal evolution of the Freiberg Epithermal Ag-Pb-Zn District, Germany. Econ Geol 116:1649–1667. https://doi.org/10.5382/econgeo.4833

Terekhov EN, Shcherbakova TF (2006) Genesis of positive Eu anomalies in acid rocks from the Eastern Baltic Shield. Geochem Int 44:439–455. https://doi.org/10.1134/S0016702906050028

Tichomirowa M, Sergeev S, Berger H-J, Leonhardt D (2012) Inferring protoliths of high-grade metamorphic gneisses of the Erzgebirge using zirconology, geochemistry and comparison with lower-grade rocks from Lusatia (Saxothuringia, Germany). Contrib Mineral Petrol 164:375–396. https://doi.org/10.1007/s00410-012-0742-8

Tichomirowa M, Käßner A, Sperner B, Lapp M, Leonhardt D, Linnemann U, Münker C, Ovtcharova M, Pfänder JA, Schaltegger U, Sergeev S, von Quadt A, Whitehouse M (2019) Dating multiply overprinted granites: The effect of protracted magmatism and fluid flow on dating systems (zircon U-Pb: SHRIMP/SIMS, LA-ICP-MS, CA-ID-TIMS; and Rb–Sr, Ar–Ar) – Granites from the Western Erzgebirge (Bohemian Massif, Germany). Chem Geol 519:11–38. https://doi.org/10.1016/j.chemgeo.2019.04.024

Tichomirowa M, Käßner A, Repstock A, Weber S, Gerdes A, Whitehouse M (2022) New CA-ID-TIMS U–Pb zircon ages for the Altenberg–Teplice Volcanic Complex (ATVC) document discrete and coeval pulses of Variscan magmatic activity in the Eastern Erzgebirge (Eastern Variscan Belt). Int J Earth Sci (Geol Rundsch) 111:1885–1908. https://doi.org/10.1007/s00531-022-02204-2

Tischendorf G, Förster H-J (1990) Acid magmatism and related metallogenesis in the Erzgebirge. Geol J 25:443–454. https://doi.org/10.1002/gj.3350250326

van Marcke G (1986) Tin-bearing epidote from skarn in the Land's End aureole, Cornwall, England. Canad Mineral 411–415

Wang T, She JX, Yin K, Wang K, Zhang Y, Lu X, Liu X, Li W (2021) Sn(II) chloride speciation and equilibrium sn isotope fractionation under hydrothermal conditions: a first principles study. Geochim Cosmochim Acta 300:25–43. https://doi.org/10.1016/j.gca.2021.02.023

Watanabe T (1960) Characteristic features of ore deposits found in contact-meatamorphic aureoles in Japan. Int Geol Rev 2:946–966. https://doi.org/10.1080/00206816009473516

Weber S, Legler C, Kallmeier E, Schulz B, Burisch M (2023) Metamorphic origin of stratiform cassiterite mineralization in the Schwarzenberg -Aue district – clues to the metamorphic history and pre-orogenic sn enrichment of the Erzgebirge (Germany). Lithos 454–455. https://doi.org/10.1016/j.lithos.2023.107273

Wenzel T, Mertz DF, Oberhänsli R, Becker T, Renne PR (1997) Age, geodynamic setting, and mantle enrichment processes of a K-rich intrusion from the Meissen massif (northern Bohemian massif) and implications for related occurrences from the Mid-european Hercynian. Geol Rundsch 86:556–570. https://doi.org/10.1007/s005310050163

Wolff R, Dunkl I, Kempe U, von Eynatten H (2015) The age of the latest thermal overprint of Tin and Polymetallic deposits in the Erzgebirge, Germany: constraints from Fluorite (U-Th-Sm)/He Thermochronology. Econ Geol 110:2025–2040. https://doi.org/10.2113/econgeo.110.8.2025

Wood SA (1990) The aqueous geochemistry of the rare-earth elements and yttrium. Chem Geol 88:99–125. https://doi.org/10.1016/0009-2541(90)90106-H

Yang J, Peng J, Hu R, Bi X, Zhao J, Fu Y, Shen NP (2013) Garnet geochemistry of tungsten-mineralized Xihuashan granites in South China. Lithos 177:79–90. https://doi.org/10.1016/j.lithos.2013.06.008

Yu F, Shu Q, Niu X, Xing K, Li L, Lentz DR, Zeng Q, Yang W (2020) Composition of Garnet from the Xianghualing Skarn Sn Deposit, South China: its Petrogenetic significance and exploration potential. Minerals 10:456. https://doi.org/10.3390/min10050456

Zharikov VA (1970) Skarns (Part I). Int Geol Rev 12:541–559. https://doi.org/10.1080/00206817009475262

Zieger J, Bittner L, Gärtner A, Hofmann M, Gerdes A, Marko L, Linnemann U (2019) U–Pb ages of magmatic and detrital zircon of the Döhlen Basin: geological history of a Permian strike-slip basin in the Elbe Zone (Germany). Int J Earth Sci (Geol Rundsch) 108:887–910. https://doi.org/10.1007/s00531-019-01683-0

Anlage III

Arbeit 3

Eingereichtes Manuskript

Sn-Zn±W±In skarn deposits in the Erzgebirge/Krušné hory metallogenic province (Germany and Czech Republic)

Nicolas Meyer[1*], Mathias Burisch[2], Jens Gutzmer[3], Jens Geier[4], Axel Gerdes[5,6], Gregor Markl[1]

1 Fachbereich Geowissenschaften, Petrologie und mineralische Rohstoffe, Eberhard Karls Universität Tübingen, Tübingen, Germany

2 Mineral Systems Analysis Group, Department of Geology and Geological Engineering, Colorado School of Mines, 1516 Illinois Street Golden CO 80401, USA

3 Helmholtz-Zentrum Dresden-Rossendorf, Institute Freiberg for Ressource Technology Germany, Chemnitzer Straße 40 09599 Freiberg, Germany

4 Orchideenstraße 2, 72534 Hayingen, Germany

5 Institut für Geowissenschaften, Goethe-Universität Frankfurt, Frankfurt, Germany

6 Frankfurt Isotope and Element Research Center (FIERCE), Goethe-Universität Frankfurt, Frankfurt, Germany

* Corresponding author: Nicolas.Meyer@uni-tuebingen.de

Abstract

This paper provides a review of skarns in the Erzgebirge/Krušné hory region (Germany/Czech Republic) with a particular emphasis on the Aue-Schwarzenberg and Geyer-Ehrenfriedersdorf districts that host the most prolific skarn systems. Most skarns replace thin carbonate units that occur intercalated with metamorphosed volcano-sedimentary host rock successions of pre-Variscan age. Their compositions range from calcic to magnesian, depending on the protolith carbonate rocks, and they occur in environments ranging from proximal to distal relative to their source intrusions. The timing of formation of the skarns is constrained by U-Pb ages of garnet and cassiterite to ~340 to ~295 Ma, broadly coinciding with different episodes of late- to post-Variscan magmatism. Geochronological evidence illustrates that many of the skarns have a multistage origin, with individual skarn stages 5-10 Ma apart, indicating that these stages are related to distinct magmatic events. Commonly, an initial skarnoid stage is followed by at least one metasomatic prograde and a subsequent retrograde skarn stage. Early skarns formed in deep-seated systems under rock-buffered conditions, whereas younger skarns developed in shallower, fluid-buffered environments, suggesting a telescoping effect driven by uplift and exhumation of the Erzgebirge following the collisional phase of the Variscan orogeny. Most Sn mineralization is hosted in cassiterite, commonly associated with retrograde actinolite and chlorite. However, a significant portion of Sn remains locked within prograde calc-silicate phases (e.g., malayaite, Sn-bearing garnet), rendering it inaccessible for economic extraction. Base metal sulfides, partly elevated in In concentration, occur during retrograde skarn alteration, commonly in distal settings. Mineralization with W is ambiguous and can be developed during prograde alteration or during subsequent processes in the waning stage of skarn alteration.

Keywords

Variscan Orogen, Erzgebirge, Skarn, Metasomatism, Tin

Author contributions

All authors contributed to the study conception and design. Material preparation, data collection and analysis were performed by Nicolas Meyer, Jens Geier, Mathias Burisch. The first draft of the manuscript was written by Nicolas Meyer and all authors commented on previous versions of the manuscript. All authors read and approved the final manuscript. The idea for the review was from Mathias Burisch, Nicolas Meyer and Jens Gutzmer. Nicolas Meyer did literature research, data evaluation. Jens Geier and Axel Gerdes did data analyses. First draft was done by Nicolas Meyer, which was critically reviewed by Gregor Markl, Marhias Burisch and Jens Gutzmer.

Nicolas Meyer

Data production, data interpretation, writing – original draft

Mathias Burisch

Conceptualization, data interpretation, funding acquisition, supervision, writing – review & editing

Jens Gutzmer

Conceptualization, data interpretation, Writing – review & editing

Jens Geier

Data production, data interpretation

Axel Gerdes

Data production, data interpretation

Gregor Markl

Conceptualization, data interpretation, supervision, funding acquisition, writing – review & editing

Autor	**Conceptualization**	*Data generation*	*Analysis and interpretation*	**writing**
Meyer, N.	60	80	60	60
Burisch, M.	15	5	20	20

Gutzmer, J.	15	0	10	10
Geier, J.	0	10	0	0
Gerdes, A.	0	5	0	0
Markl, G.	10	0	10	10

Introduction

The Erzgebirge (Krušné hory in Czech language), spans across the Czech Republic and Germany and has been a source of raw materials at least since the Bronze Age (Tolksdorf et al. 2020). Historically, mining focused on Fe, Sn, and Ag. During the last period of active mining (1945-1990) the focus shifted to Sn, W, U, barite and fluorite, whilst currently many skarn and greisen-hosted deposits are explored for Li, Sn, W, Zn, and In. Skarns were mined only for their Fe content from medieval times until the 20th century, where magnetite extraction ended with the closure of the Měděnec-Přísečnice deposit in 1992 (Baumann et al. 2000). Tin and tungsten resources hosted by skarns, on the other hand, were never subject to commercial exploitation. This has been so despite extensive exploration and even trial mining of the Hämmerlein deposit. Arguably the most important reason for the lack of commercial production has been the difficulty to achieve reasonable recoveries from the skarn ores, given their fine grain size and polymineralic character (Kern et al. 2019). Another important reason was the availability of Sn (as well as minor amounts of W) from greisen-type deposits in the Erzgebirge, in particular Altenberg and Zinnwald/Cínovec (Štemprok 2016; Seltmann et al. 1995; Weinhold et al. 2002) with a total production of at least 96,500 t of Sn until 1990, and stockwork-hosted Sn mineralization of the Ehrenfriedersdorf deposit, which was in operation until 1990 and produced 10,650 t of Sn (Baumann et al. 2000; Breiter et al. 2017; Hösel et al. 1994). This renders the skarn deposits of the Erzgebirge an important resource for future exploitation. Historic and recent mineral resource estimates for skarn deposits across the region amount to 80 Mt of ore at an average grade of 0.49 % Sn, ~ 62 Mt ore at 0,85 % Zn, and ~ 15 Mt ore at 0.32 % W (Elsner 2014; Saxore Bergbau GmbH; Starý et al. 2024). Compared to global Sn skarns, the Erzgebirge skarns have relatively low grades and intermediate tonnages (Fig. 1). Nevertheless, they present the largest tin resource in Europe and are, thus, of economic and strategic significance

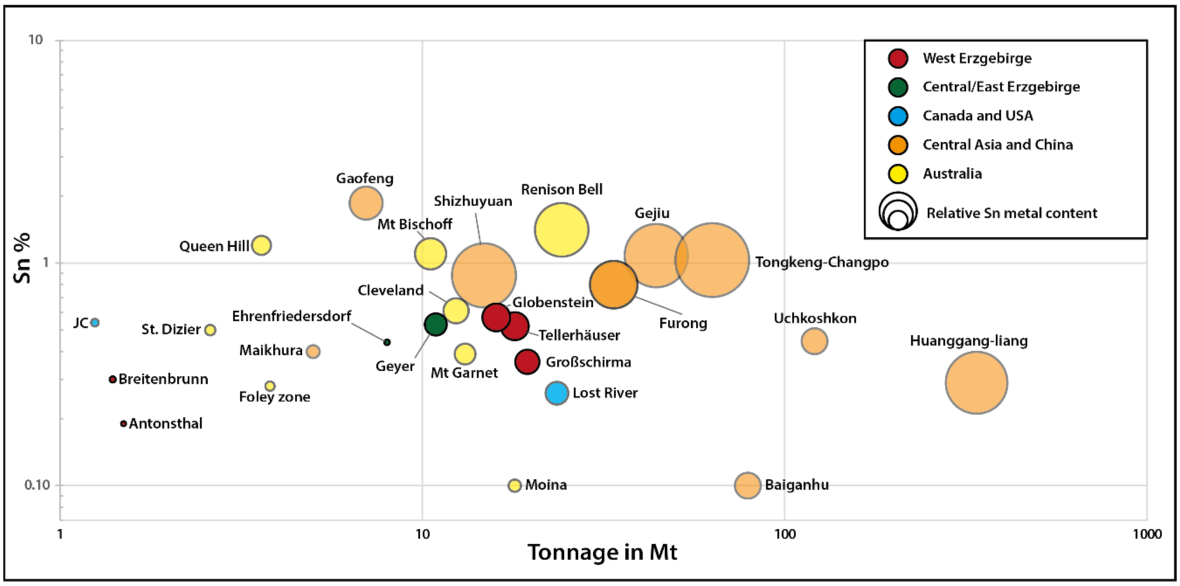

Fig. 1 Plot of Sn grade vs. tonnage of skarn hosted deposits of China (Chang et al. 2019; Chen et al. 2022; 2023; Cheng et al. 2012; 2013; Huang et al. 2019; Li et al. 2022; Lu et al. 2003; Zhao and Jiang 2007; Zhou et al. 2017), Kyrgyzstan (Solomovich et al. 2012), Tajikistan (Soloviev et al. 2019), North America (Aleksandrov 2010; Ray 2013;), Australia (Seymore et al. 2006) and Germany (Hösel 1994; Hösel et al. 1996; 2003; Sächsisches Oberbergamt 2008; Schuppan and Hiller 2012)

Earliest scientific descriptions of skarn mineralization in the Erzgebirge date back to Breithaupt (1849), followed by other studies at the beginning of the 20th century (Beck 1902; Groth 1926; von Hoerner 1910). Research in conjunction with extensive exploration programs of the 1950s, 1960s and 1970s in the former German Democratic Republic (GDR) and Czechoslovakia resulted in comprehensive data sets on the mineralogy and geometry of skarn-hosted mineralization (Bolduan 1963; Hoth and Lorenz 1966; Kühne et al. 1972; Legler 1985; Legler and Baumann 1983; Makareviĉ et al. 1976; Pfeiffer and Schützel 1969; Štemprok 1967). Yet, most of these studies are descriptive and provide limited information on skarn genesis. The wealth of research data from this era is summarized in several monographs (available in German language only) that provide an overview for some of the relevant skarn prospects and occurrences in the German part of the Erzgebirge (Hiller and Schuppan 2008; 2016; Hösel 1994; Hösel et al. 1996; Schuppan and Hiller 2012).

Interest in skarns resurged in the last 15 years, spurred by renewed exploration for Sn, W, Zn and In. More recent studies on these systems include petrology and mineral chemistry (Bauer et al. 2019; Brosig et al. 2020; Kern et al. 2019; Lefebvre et al. 2019; Reinhardt et al. 2021; Meyer et al. 2024; 2025), geochronology of garnet and cassiterite (Burisch et al. 2019, Meyer et al. 2024; Reinhardt et al. 2022) and fluid inclusion microthermometry (Korges et al. 2020; Meyer et al. 2024; Reinhardt et al. 2021). Most of these recent studies provide insight into the origin, formation conditions, and metal tenor of single case studies. In this contribution we, therefore, compile and critically review data on the skarn deposits across the Erzgebirge and discuss their implication for ore-formation in the context of a province-scale metallogenetic model.

Skarn characteristics

Following Einaudi et al. (1981) and Meinert et al. (2005), the term skarn is used in this study as a descriptive term. Petrogenetically, three types of skarns are distinguished, which have distinct textural features. Hence, these textures may also be used in a strictly descriptive context. 1) Reaction skarns occur as a result of contact or regional metamorphism along contacts of compositionally contrasting lithologies with minimal influence of external fluids. 2) Metasomatic skarns are the opposite endmember and form in fluid-buffered environments, which produce commonly coarse-grained textures that may completely overprint the textural features of the protolith (Burisch et al. 2023; Meinert et al. 2005; Mrozek et al. 2020). 3) Skarnoids (Kwak 1987; Meinert et al. 2005) are typically fine- to medium grained with commonly alternating banding of garnet- and pyroxene-dominated domains. Genetically, they are transitional between the reaction and purely metasomatic skarn endmembers and are typically related to the early, primarily contact metamorphic stage of an intrusive event (Burisch et al. 2023; Einaudi et al. 1981; Meinert et al. 2005).

Conceptually and in practical field observations, individual skarn deposits may show a continuum between purely metamorphic and entirely metasomatic processes. Metasomatic skarns typically display a prograde stage characterized by nominally anhydrous minerals such as garnet and pyroxene, followed by a retrograde stage that typically comprises minerals such as epidote, actinolite, and chlorite (Einaudi et al. 1981; Meinert et al. 2005). The retrograde stage is commonly absent during the formation of skarnoids. Skarns can be grouped according to their host rock (endo- and exoskarn), calc-silicate mineralogy (magnesian and calcic) or metal tenor. The metal tenor is the most accepted way to classify skarn deposits, which is relatively well suited for economic, but may not be useful for sub-economic skarn deposits (Meinert et al. 2005). A main challenge in classifying skarn deposits arises from the fact that they are typically strongly zoned and hence their characteristics may widely vary across one individual skarn body. Therefore, the distance of a skarn zone relative to its causative source intrusion, i.e., proximal, intermediate, and distal, is commonly also used to describe an occurrence. Additional information on characteristics and genesis of skarn deposits is provided in numerous review papers on global skarn deposits such as Einaudi et al. (1981), Kwak (1981; 1987), Meinert (1992), and Meinert et al. (2005).

Regional Geology

The Erzgebirge presents the northern part of the Bohemian Massif and belongs to the Saxothuringian Zone of the Variscan orogeny (Kossmat 1927). During the Middle to Late Paleozoic, the Variscan Orogenic Belt formed by the closure of the Rheic ocean and subsequent continent-continent collision of Gondwana and Laurussia, resulting in the formation of the Supercontinent Pangea (Kroner et al. 2008). The Erzgebirge forms an ~ 140 x 80 km erosional basement window striking NE-SW (Fig. 2). It is delineated by the Eger/Ohře Graben in the southeast, the Elbe lineament in the northeast, the Central Saxonian Lineament in the northwest; it gradually transitions into the Fichtelgebirge in the southwest. The central zone of the Erzgebirge is composed of Neoproterozoic greywackes with intercalated limestones and pelites (Přísečnice group), a succession that was already metamorphosed during the Cadomian orogeny and subsequently intruded by magmatic rocks related to the Cadomian orogeny (Tichomirowa 2003; Tichomirowa et al. 2012). In the north and west of the Erzgebirge, Cambro-Ordovician metamorphosed volcano-sedimentary successions of the Klínovec, Jáchymov, Thum, and Frauenbach groups occur, which mainly comprise pelites intercalated with carbonate rocks (Lorenz 1974; 1979; Pälchen and Walter 2008).

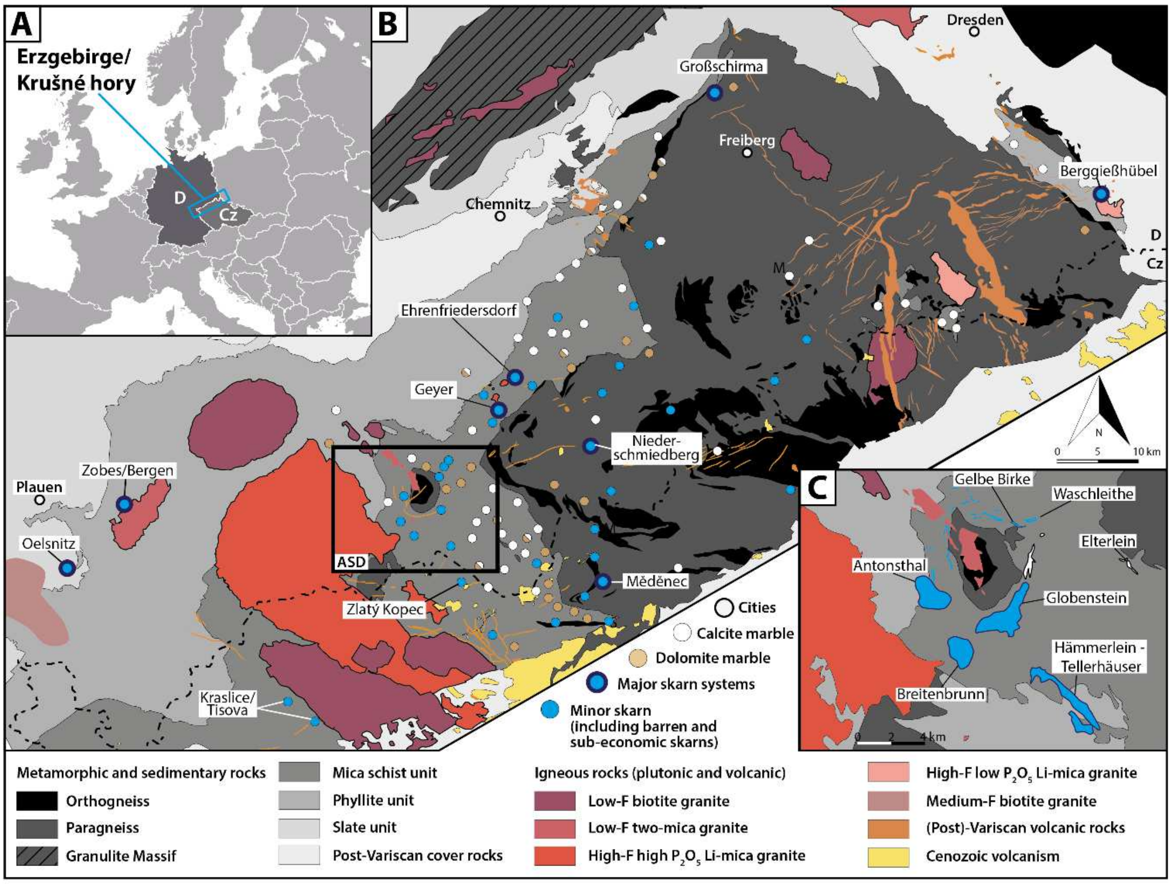

Fig. 2 A) Geographical position of the Erzgebirge/Krušné hory at the border between Germany and Czech Republic. B) Geological overview of the Erzgebirge/Krušné hory showing marble and skarn occurrences. C) Inlet in B showing a detailed map of the Aue-Schwarzenberg cluster of skarn deposits

During the Variscan orogeny, these successions underwent various grades of metamorphic overprint, ranging from lower amphibolite to eclogite facies conditions (Schmädicke et al. 1995) and were stacked as nappes. The peak of the Variscan metamorphic overprint in the Erzgebirge occurred at ~ 340 Ma (Kröner and Willner 1998). This regional metamorphism was followed by a rapid exhumation to middle or upper crustal levels (Collett et al. 2020), a process that was associated with syn- and postkinematic magmatism.

Emplacement of late-Variscan granitoid plutons and stocks occurred discontinuously within ~330-310 Ma (Romer et al. 2007; Tichomirowa et al. 2019b; 2022). These granitic rocks are related to three individual batholiths (Štemprok and Blecha 2015): the eastern batholith with the associated Teplice-Altenberg caldera, the central (middle) batholith with only few smaller stocks exposed, and the western batholith with the prominent Eibenstock-Nejdek granite massif. This suite of magmatic rocks was followed by post-Variscan magmatism of which volcanic, sub-volcanic and only a few plutonic rocks are exposed today, yielding ages between 306–303 Ma and 301–296 Ma for the western and eastern Erzgebirge, respectively (Gottesmann et al. 2017; Tichomirowa et al. 2025). The emplacement of the various granite bodies was accompanied by lamprophyre dikes, which also have a very variable age distribution like the other igneous rocks (Förster et al. 1999; Štemprok and Seifert 2011).

Förster et al. (1999) introduced a classification that distinguishes five geochemical groups of granitoids in the Erzgebirge/Krušné hory: 1) low-F biotite granites (e.g., Aue suite), 2) low-F two-mica granites (e.g., Schwarzenberg suite), 3) high-F high-P_2O_5 Li-mica granites (e.g., Ehrenfriedersdorf-Geyer suite), 4) high-F low-P_2O_5 Li-mica granites (e.g., Markersbach granite), 5) medium-F biotite granites (Schönbrunn granite). The batholiths are composite intrusions that include igneous rocks of various composition (Fig. 2). Late- and post-Variscan magmatism is associated with various types of magmatic-hydrothermal mineralization including greisen, stockwork, and vein-hosted Sn±Li±W±Mo deposits (Burisch et al. 2025, Leopardi et al. 2024a, Štemprok 1967), skarn-hosted Sn-Zn±W±In deposits (Meyer et al. 2024; Reinhardt et al. 2022) and epithermal Ag-Pb-Zn vein systems (Swinkels et al. 2021). The metallogenetic link between specific types of intrusion and their metal tenor is insufficiently understood. However, there seems to be a link between high-F and low or high-P_2O_5 magmas and Li-rich greisen systems (Burisch et al. 2025), whereas there are few constraints on the causative source intrusions to most skarns.

The late and post-orogenic phase was followed by extensional tectonics that prevailed across Central Europe until the Upper Cretaceous. Subsidence resulted in the formation of extensive basins filled with thick successions of sedimentary rocks that buried the Erzgebirge crystalline basement (Ziegler 1990). The Permian to Mesozoic period was associated with hydrothermal U, native-metal arsenide (U-Bi-Co-Ni-Ag = five element) as well as fluorite-barite±sulfide mineralization (Burisch et al 2022; Romer and Cuney 2018).

Eventually, Alpine tectonics resulted in the formation of local rift systems and graben structures across Europe. One of them, the Eger/Ohře Graben initiated uplift and exhumation of the Erzgebirge (Ziegler and Dèzes 2007). This exhumation was accompanied by basaltic and nephelinitic magmatism, especially within the graben and along the southern border of the Erzgebirge (Ulrych et al. 2011). Quartz-Fe-Mn veins enriched in Co, Ni, and Li are linked to Cenozoic tectonics (Burisch et al. 2021), presenting the youngest stage of hydrothermal ore formation in the Erzgebirge.

Skarns of the Erzgebirge

Numerous skarn occurrences have been described across the Erzgebirge (Tab. 1). They are associated with variable host rocks, ranging from marble to metapelites and metavolcanic rocks. A particular abundance of skarns, however, is hosted by the meta-sedimentary successions of the Přísečnice, Klínovec, Jáchymov, and Thum groups (Hösel et al. 1996; 2010; Hoth et al. 2010; Schuppan and Hiller 2012). Less common and volumetrically much less significant are skarns hosted by metavolcanic rocks that occur, for example, in the regions around Berggießhübel, Zobes and Schlema-Aue (Baumann et al. 2000; Hiller and Schuppan 2008; 2016). A specific sub-group of skarns is related to marble lenses within high-grade metamorphic gneiss units. These skarns seem to be unrelated to any known magmatic intrusions (Burisch et al 2019) and were only historically of economic interest for Fe production. Examples of such skarns are known around Měděnec and Niederschmiedeberg; they lack in any Sn, W, In and Zn mineralization (Tab. 2). Those skarns are not well studied and are of subordinate economic significance.

The main focus of this contribution is on late- to post-Variscan magmatic-hydrothermal skarns with their economically significant metal endowment. Late- to post-Variscan skarns are invariably exoskarns that encompass proximal, intermediate and distal skarn zones, relative to the causative source intrusion. Whilst causative source intrusions may be overprinted by greisen alteration, there is no occurrence of endoskarn documented in the Erzgebirge (see Tab. 1; Burisch et al. 2024; Hösel 1994; Meyer et al. 2024; Schuppan and Hiller 2012; Reinhardt et al. 2022; Weinhold 2002).

The overall geometry of Late- to post-Variscan magmatic-hydrothermal skarns in the Erzgebirge is usually controlled by the thickness and orientation of marble layers within the meta-sedimentary host rocks (Pälchen and Walter 2008; Schuppan and Hiller 2012). Individual marble layers and associated skarns vary in thickness from a few centimeters to several tens of meters and usually occur in groups of several parallel layers separated by mica schist, phyllite and/or paragneiss. Individual skarns form horizontally discontinuous horizons, which may reach a thickness of up to 40 m and may be traced several hundreds of meters to several kilometers along strike. Available data on skarn systems of the Erzgebirge are summarized in Table 1, ordered by the major commodity. The most relevant skarns are presented in more detail below, ordered by their geographic position.

Table 1. Compilation of data available for skarn occurrences of the Erzgebirge/ Krušné hory.

Localities	Major Metal	Historic production	Tonnage/grade	Stratigraphy / host rock sequence
Niederschmiede-berg, Boden	Fe	unknown quantities of Fe ore	Not reported	Muscovite paragneiss / Měděnec group
Horní Halže, Měděnec, Přísečnice, Kovářská	Fe-Cu	0.95 Mt Fe, 323 t Cu, 0.8 t Ag	12-15 Mt at 33-38 % Fe (Kovářská deposit)	Mica-schist and paragneiss, associated with orthogneiss;Měděnec group Přísečnice succession (Kovářská-Halže fold)
Berggießhübel	Fe-Cu-Sn-In	300 kt Fe ore of unknown grade; Fe mined out	Not reported	Intercalations of slate, marl, carbonates and tuff; Devonian rocks of the Elbtal slate massif
Zobes	W-Fe-Cu±Mo±Bi±Be	Unknown quantities of Fe, Cu, 260 t W	1.6 Mt of ore at 0.24 % W	intercalation of marble, organic-rich phyllites and metavolcanis rocks (Zobes-Horizont); Ordovician age
Pöhla-Globenstein	W-Sn-Fe-In-Cd±Ag±B	34.1 kt Fe, 8 kt W, 4.1 kt Sn,	16 Mt kt of ore at 0.57 % Sn, 0.36 % W and 0.81 % Zn	intercalation of marble, amphibolites and mica-schist; Klínovec group (Raschau succession)
Antonsthal	Sn-W-Zn	Mainly mined for marble	14.7 Mt ore at 0.19 % Sn and 0.37 % W with minor Pb, Cd, Cu, Bi, Ag	Marble intercalated in mica-schist; Klínovec group (Obermittweida and Fichtelberg succession)

Hämmerlein-Tellerhäuser	Sn-Fe-Zn±Ag±In	31.3 kt of Fe; unknown quantities of Sn	Indicated: 9.97 Mt ore at 0.45 % Sn, 10.24 % Fe, 0.42 % Zn, 2.49 g/t Ag, 22.49 g/t In; Inferred: 17.97 Mt ore at 0.52 % Sn, 8.63 % Fe, 0.62 % Zn, 2.59 g/t Ag, 26.94 g/t In	Intercalations of marble, mica-schist and paragneiss; mainly Jáchymov group (Breitenbrunn succession)
Breitenbrunn	Sn-Fe-Zn	Mainly Fe of unknown quantities	without St. Christoph and St. Margarete: 1.45 Mt ore at 0.3 % Sn, 2.0 % Zn, 30 % Fe	Intercalations of marble, mica-schist and Muscovite gneiss; Jáchymov group (Breitenbrunn succession)
Zlatý Kopec / Boží Dar	Sn-Fe-Zn-(Cu-W-Mo-In)	Sn and Cu mining of unknown quantities	1 Mt of ore at 0.95 % Sn and 0.5 % Zn	Intercalations of carbonaceous phyllites, quartzites, marbles, and metabasites; Jáchymov Group (Breitenbrunn succession)
Geyer	Sn-Zn-In-Fe	Minor Fe mining of unknown quantity	Geyer SW: 8 Mt of ore at 0.56 % Sn and 1.1 % Zn; Geyer E: 2.7 Mt ore at 0.52 % Sn and 0.4 % Zn	Intercalations of mica-schist and phyllites; Jáchymov group (Grießbach and Breitenbrunn succession)
Ehrenfrieders-dorf	Sn-Zn	No mining on skarn ore	0.8 Mt of ore at 0.44 % of Sn	Jáchymov group (Grießbach and Breitenbrunn succession)
Großschirma	Sn-Zn	-	19.4 Mt of ore at 0.36 % Sn, 0.14 % Zn	Mylonite of the „Felsit horizont“; Přísečnice and Niederschlag succession

Oelsnitz	Fe-Zn-Cu-Sn	Historic Fe mining; about 6 kt Sn between 1922 and 1938	Not reported	Ordovician to Silurian successions of the Vogtland synclinorium
Waschleithe/ Gelbe Birke	Zn-Cu-Sn-W	600 t Zn	Not reported	Intercalations of biotite-beairng mica-schist, quartz-mica-schist and marble; Klínovec group (Obermittwaida succession)

Continuation of Tab. 1

Localities	Protolith of skarn	Skarn architecture	Skarn alteration	Skarn age (Ma)
Nieder-schmiede-berg, Boden	Calcite marble, pure	Single skarn lenses; max. 70 m x 30 x 11 m (known)	Prograde: Alm-Grt, Cpx, Mag, Retrograde: Akt	342.9±5.1, 333.5±4.3, 330.7±10
Horní Halže, Měděnec, Přísečnice, Kovářská	dolomite>calcite marble,	Three parallel skarn horizon of 6.5 km strike length; skarn bodies up to 450 x 250 x 20 m	Prograde: Alm-Sps-Grt, Hd-Cpx, Mag; retrograde: Ccp, Py, Act, Qz	-
Berggießhübel	Calcite>dolomite marble, pure	Four skarn units, with two to nine skarn layers each; skarn layer max. length 1000 m, thickness 0.5-10 m	Prograde: Grt, Cpx, Mag; retrograde: Mica, Fl, Cst, Sph, Ccp, Apy	304.9±3.2 301.5±5.7
Zobes	Calcite marble and mafic volcanic rocks	1 Skarn unit; 800 x > 4 km; Discontinuous lenticular bodies of max. 350 x 30 x 4 m	Prograde: Grs-Grt, Wol, Ves, Di-Cpx, Plg; Retrograde: Ep ± qz, cal	325.5±2.3, 323.6±2.7, 321.5±3.5

Pöhla-Globenstein	Dolomite>calcite marble	3 parallel skarn unit; lower skarn unit: 2 skarn layer (~ 12 m thickness); middle unit: 1 skarn layer (12-80 m thickness), upper skarn unit: 1 skarn (20-50 m thickness)	1. stage: prograde: Ol, Di-Cpx, Spl; retrograde: Phl 2. Stage: Prograde: Grs-And-Grt, Mag; retrograde: Fl,Fe-Amp, Ep, Ldw, Cst; Breccia hosted ore: Sch, Fl, Qt, Chl	338.2±2.5, 331.2±3.0, 336.4±3.7, 337.8±3.2, 337.1±3.6
Antonsthal	Calcite>dolomite marble	One skarn unit, one major and four minor skarn layers; striking length several km, dipping length 600 m, thickness 6 m	Prograde: Di-Cpx, Grt, Ves; retrograde: Ep, Chl, Sph, Sch, Cst,	320.3±3.2, 319.6±5.2, 318.2±2.5, 312.6±3.9, 300±11, 302±2.7
Hämmerlein-Tellerhäuser	Calcite>dolomite marble, impure	Three skarn units (Dreiberg, Zweibach, Hämmerlein, combines strike length 9km, 500m width and 3 m thickness on average, additional mineralization in mica-schist (Schiefererz)	1.Stage: Erlane, Plag, Cpx, Ep, Tre; 2. stage: prograde: And-grt, Cpx, Ves, Wol, Ep?, Ax; retrograde: Grt, Mag, Tre, Act; late stage: Qz, Fl, Mica, Cst	327.3±8.4 324±7.4 312.8±3.4 304±5.7 302.7±4.3 299.2±4.3 294±8.3
Breitenbrunn	Calcite>>dolomite marble, impure; marl	One skarn unit, Five skarn layers, striking length 1.2 km, dipping length 700-800 m; thickness ~ 5 m; continuation of Dreiberg skarn horizon	1. Stage: Prograde: Ves, Cpx, Grt; 2. Stage: Prograde: Hd-Cpx, Grt, Retrograde: Act, Ep, Chl, Qz, Cst, Sph	337.5±3.3 317.3±6.3 313.5±4.7 302±2.7
Zlatý Kopec / Boží Dar	Dolomite>Calcite marble	One skarn unit; two skarn layers measuring 600 x 300 m x 1.5-3 m	Prograde: Di-Cpx, Grt, Retrograde: Mag, borates, Chl, Cst, Sulfides	-

Geyer	Calcite>>dolomite marble, impure; marl	Three skarn units with a multitude of skarn layers; 6 km x 650 m x 4-20 m	Stage 1: Cpx, Grs-Grt, Ves, Wol; Stage 2: Prograde: Grt, Hd-Cpx, Mly; Retrograde: Ep, Amp, Fl, Chl, Cst, Sph	322.4±5.5, 322.5±11.4, 308.2±3.7*, 307.3±4.8, 305.1±3.9, 301.6±5.0
Ehrenfrieders-dorf	Calcite marble, marl	One skarn unit with up to 3 skarn layers	Stage 1: Cpx, Grs-Grt, Ves, Wol; Stage 2: Prograde: Hd-Cpx, And-Grt; Retrograde: Ep, Amp, Fl, Chl, Cst, Sph	322.3 ± 4.5, 305.3 ± 2.7
Großschirma	-	Tectonic structure 18 x 8 km; unreported ore bodies	Mylonititc rock; Grt, Chl, Amp, Py, Mag, Cst, Ccp, Sch	-
Oelsnitz	Calcite>Dolomite marble	Three skarn units and two discontinuous lens shaped bodies, max. thickness of skarn and ore bodies 6 m; striking length unknown	1. Stage: Grt, Ep, Sph, Gn, Hem; 2. Stage: Prograde: And-Grt, Cpx, Wol, Mag; Retrograde: Ep, Sph, Chl, Gn, Cst	297.9 ± 4.0, 295.5 ± 4.4
Waschleithe/ Gelbe Birke	Dolomite-calcite marble	One skarn unit with two skarn layers not exceeding 10 m and irregular in shape	Prograde: Cpx, Ves, Grs-Grt; Retrograde: Bst, Rdn, Amp, Sph, Ccp, Gn	313.1±2.3

Continuation of Tab. 1

Localities	Fluid characteristics	Nearby intrusion, alteration and distance to granite surface	Related faults	References
Nieder-schmiede-berg, Boden	-	not present	-	Burisch et al. 2019; Hoth et al. 2010*; Legler et al. 1985*

Horní Halže, Měděnec, Přísečnice, Kovářská	-	not present	Měděnec fault (NW-SE)	Baumann et al. 2000*; Hoth et al. 2010*; Pauliš and Haake 1991; Pokorný and Zemánek 1960*; Starý et al. 2024
Berggießhübel	-	Markersbach granite (high-F low P2O5 Li-mica granite); greisen alteration; ~200 - 800? m	Elbe-lineament (NW-SE)	Baumann et al. 2000*; Hösel 1967*; Jobst and Grundig 1961*; Vossen 2018;
Zobes	-	Bergen granite (low-F two mica granite); no alteration; 0 – 500 m	Zobes-Tirpersdorf fault (NE-SW)	Burisch et al. 2019; Schuppan and Hiller 2012*
Pöhla-Globenstein	Cst-vein: 440 – 400 °C / 30.0 wt. % eq. NaCl; Retrograde: 320 – 150 °C / 1.5 wt. % eq. NaCl	Eibenstock granite (high F high P2O5 Li-mica granite), microgranitic and rhyolitic dykes; 0 - > 800 m	Arnoldshammer fault (80 °NE-SW), Globenstein fault (60 ° NE-SW), Luchsbach fault I and II (60° NW-SE)	Burisch et al. 2019; Hösel et al. 2003*; Reinhardt et al. 2022
Antonsthal	-	Eibenstock granite; >300 m?	Weißer Hirsch (NW-SE), minor faults, partly mineralized (NE-SE and NE-SW)	Hösel et al. 1997*; Hoth et al. 2010*; Reinhardt et al. 2022
Hämmerlein-Tellerhäuser	Cassiterite: 400 – 500 °C / 30 – 40 Prograde: 270 – 300 °C; / 2.0 to 3.8 Retrograde: 335 °C - 185 °C / 2 - 6.7	Aue-Schwarzenberg granite suite (low F biotite granite + low-F two mica granite) + Eibenstock granite (high F high P2O5 Li-mica granite); Eibenstock: rare greisen in endocontact; 0 - >1000 m	Gera-Jáchimov fault zone; Rittersgrün fault (NW-SE); Hirtenberg, Dreiberg, Zweibach, Wilder Mann fault (NE-SW)	Bauer et al. 2019; Kern et al. 2019; Korges et al. 2020; Lefebvre et al. 2019; Saxore Bergbau GmbH; Schuppan and Hiller 2012*

Breitenbrunn	-	Eibenstock granite; Greisen alteration and lamprophyres; 100 - 800 m	Schildbach, Luchsbach, Ehrenzipfel fault (NW-SE), Dreiberg, Zweibach, Wilder Mann fault (NE-SW)	Hösel et al. 1997*; 2003*; Hoth et al. 2010*; Saxore Bergbau GmbH
Zlatý Kopec / Boží Dar	-	Eibenstock granite; Alteration in granite not reported/drilled; 350 - 950 m	-	Baumann et al. 2000*; Pauliš et al. 2015; Starý et al., 2024; Tichomirowa et al. 2019
Geyer	1. Stage: 450 – 470 °C / 7.1 – 11.0; 2, Stage: Prograde: 330 – 340 °C / 26.9 – 28.7 and 2.6 – 5.6; Retrograde: 270 – 320 °C / 16.8 – 31.5 and 0.9 – 3.2	Ehrenfriedersdorf Batholith (high F high P2O5 Li-mica granite); Rhyolites and microgranitic dykes; Greisen alteration within Geyersberg and underlying pluton; 0 - 750 m	Geyer-Herold (NE-SW) and Geyer-Schönfeld (NW-SE) fault	Bolduan 1963*; Brosig et al. 2020*; Hösel et al. 1996*; Meyer et al. 2024; Romer et al. 2007
Ehrenfrieders-dorf	-	Ehrenfriedersdorf Batholith (high F high P2O5 Li-mica granite); Rhyolites and microgranitic dykes; Endo- and exo-greisen formation in granite and metasediments; 0 – 450 m?	Wiesenbaden (NW-SE) Geyer-Schönfeld, Greifenbach fault (NE-SW)	Lehmann and Seltmann 1995; Hösel 1994*; Romer et al. 2007; this study
Großschirma	-	not present	Mylonitic zone; Central Saxonian Lineament (NE-SW)	Baumann and Weinhold 1963*; Baumann 1965*; Jaroka 2013; Kormilicyn 1987*; Lorenz and Schirn 1987*
Oelsnitz	-	Schönbrunn-Eichigt granite massif (concealed; A-type granite); albitisation within endocontact?	Not reported	Baumann et al. 2000*; Gottesmann et al. 2017; Kuschka and Hahn 1996*

Waschleithe/ Gelbe Birke	Prograde: 365 - 385 °C / 0.3 – 2.3; Retrograde: 285 – 318 °C / 0.6 – 1.4	Eibenstock granite; > 1000 m from granite surface	Minor faults (NE-SW and NW-SE)	Hoth and Lorenz 1966*; Hoth et al. 2010*; Reinhardt et al. 2021

*References in German

Zobes (Western Erzgebirge)

The Zobes skarn is located about 10 km E of Plauen (see Fig. 3B). Some historic mining of Fe and Cu is documented, but production numbers are not available. Between the beginning of the 20th century 1918, at least 260 t of W were produced mainly from skarn-hosted ore. Several mineralized skarn bodies were intersected during U exploration and mining. Skarn-hosted resources were estimated to 1.6 Mt of ore at 0.24 % W (Sächsisches Oberbergamt 2008).

Skarns at Zobes occur in immediate contact with the 320 – 325 Ma Bergen pluton (low-F two-mica granite; Förster et al. 1998; Fig. 3) that intruded into a series of Ordovician-Silurian-Devonian meta-volcano-sedimentary host rock succession. Dating of skarn-related garnet by LA-ICP-MS U-Pb yielded an age range between 325.5 ± 2.3 Ma and 321.5 ± 3.5 Ma (Burisch et al. 2019), thus coinciding well with the intrusion age of the Bergen pluton.

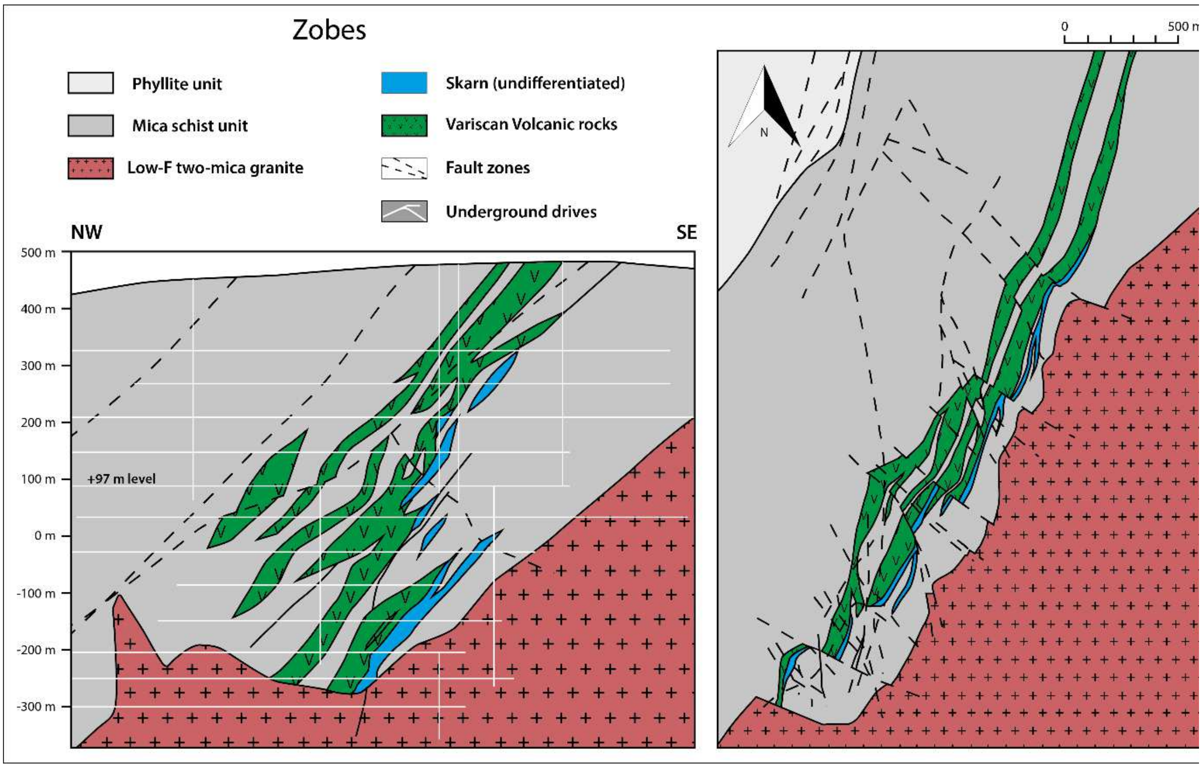

Fig. 3 Cross-section of the Zobes skarn and the corresponding geological map on the +97 m level. Note the proximity of the skarns to the granitic intrusion and the prevalence of mafic meta-volcanic rocks that are besides marble affected by skarn alteration

Skarns in the Zobes area are hosted by one marble layer, intercalated with organic-rich phyllites in the footwall of metavolcanic rocks of Ordovician age (Hiller and Schuppan 2016). Skarn bodies are discontinuous, lenticular bodies with typical thicknesses of 25 by 1 – 4 m that extend over 800 m down dip and several km along strike (Fig. 6). Their extent is limited by the Neusalzer fault in the SW but remains unexplored towards the NE (Hiller and Schuppan 2016). Prograde skarn exhibits a skarnoid texture including garnet, vesuvianite, clinopyroxene, and wollastonite accompanied by scheelite. Retrograde overprint is subordinate with only local epidote, actinolite and chlorite developed along veinlets (Hiller and Schuppan 2016).

Aue-Schwarzenberg district (Western Erzgebirge

The Aue-Schwarzenberg district is well-known as the most prolific area of skarn-type mineralization in the Erzgebirge (Hoth et al. 2010). It spans across an area of ~ 12 x 15 km in the western part of the Erzgebirge (Fig. 1C). The central portion of the district comprises Ordovician orthogneiss and paragneiss of the Přísečnice group overlain by a succession of metasediments including the highest abundance of calcitic and dolomitic marbles within the Erzgebirge region (Hoth and Lorenz 1966; Hoth et al. 2010; Fig. 1). These metasedimentary units are cut by the major Gera-Jáchymov fault zone, which was active since pre-Variscan until at least Cretaceous times (Guilcher et al. 2024; Hösel et al. 2003; Romer et al. 2010). Late-Variscan granites of the low-F biotite and two mica series (Aue-Schwarzenberg granite suite) occur mainly in the central part of the district. In the western section of the Aue-Schwarzenberg district, the large volume high-F, high-P_2O_5 Li-mica Eibenstock composite batholith is exposed. The flanks of this pluton dip towards the northeast below the metamorphic rock units. The slopes of the intrusive contact flatten out to a sub-horizontal orientation toward the NE (Förster et al. 1999). The Aue-Schwarzenberg district is host to a considerable number of skarns of different ages and different metal endowment (see Fig. 1C for reference). These will be described in the following from North to South.

Waschleithe-Gelbe Birke cluster

The Waschleithe-Gelbe Birke skarn cluster is located in the NE part of the Aue-Schwarzenberg district (Fig. 1C). Around 600 t of Zn metal, 9000 t of marble and 30 t of Cu ore with an unknown grade were produced from historic underground mines of Herkules Frisch-Glück, Himmlisch Heer am Fürstenberg, and Fundgrube am Sauerwiesenbächle (Hoth and Lorenz 1966; Hoth et al. 2010; Fig. 3). The Waschleithe and Gelbe Birke skarns are hosted by two marble units that occur within a sequence of mica schist and paragneiss dipping towards the N. The vertical distance of the skarn to the contact of the underlying Eibenstock granite exceeds 1000 m (Reinhardt et al. 2021 and references therein).

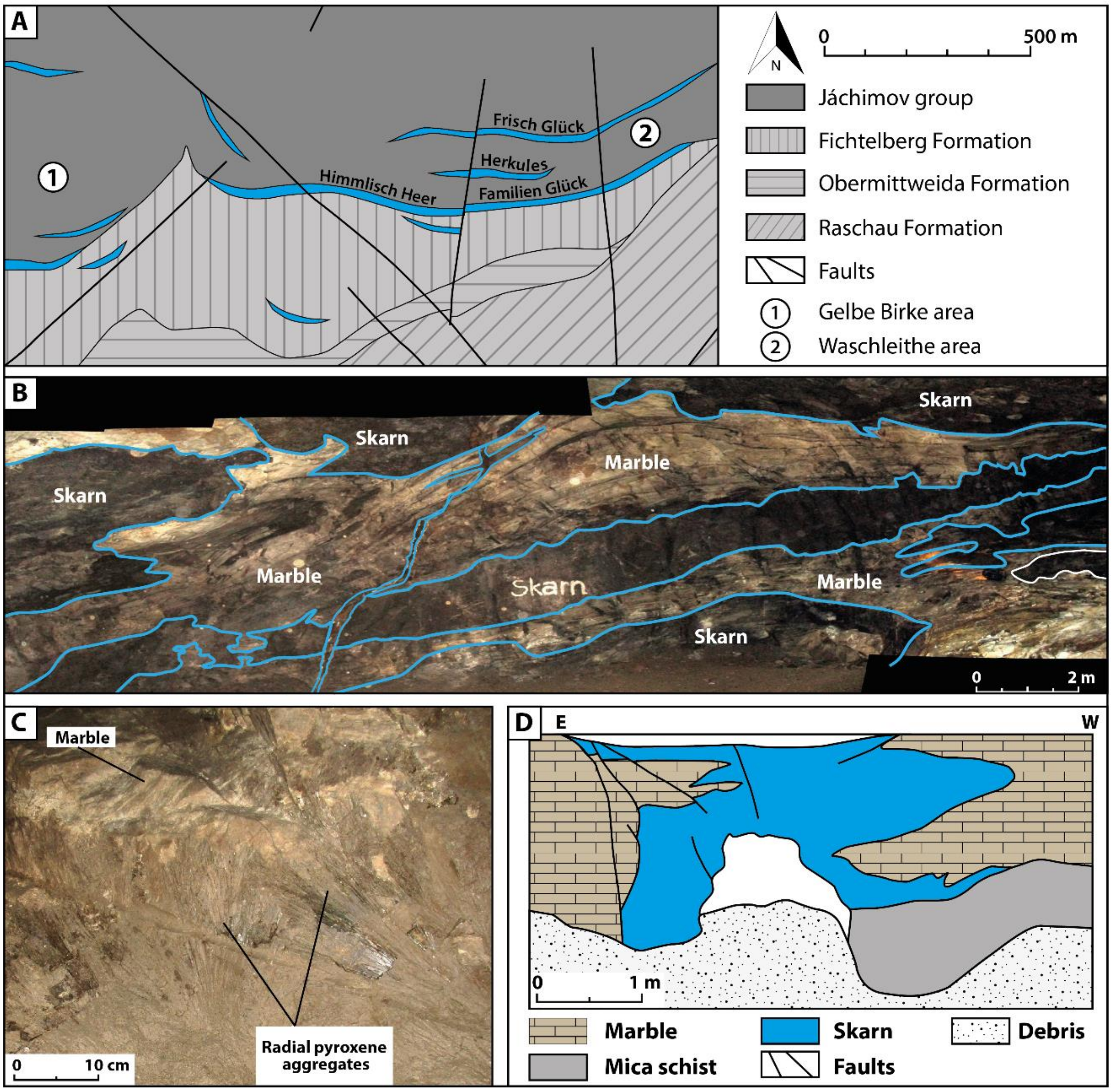

Fig. 4 A) Simplified map of the Waschleithe and Gelbe Birke cluster of skarns. Several marble and

skarn bodies are present, some of which were mined for Fe. B) Underground picture of a stratabound skarn situated in the middle of a marble unit (Waschleithe). C) Large radial aggregates of clinopyroxene replacing marble. D) Sketch of skarn cutting across a marble unit (Herkules Frisch-Glück mine; after Hoth et al. 2010)

The marble layers, which are up to 10 m thick, are only partly replaced by skarn. Skarn forms several irregular- to lenticular-shaped zones (Reinhardt et al. 2021). Generally, the skarns can be traced over distances of 250 m with a thickness reaching 3 m (Hoth et al. 2010). Prograde skarn comprises a coarse metasomatic texture and consist predominantly of a prograde mineral assemblage of dark brown clinopyroxene with only subordinate amounts of garnet. The retrograde mineral assemblage comprises manganoan ilvaite, rhodonite and Mn-bearing calcite. Ore minerals associated with this retrograde assemblage include sphalerite along with chalcopyrite, galena and magnetite as well as accessory cassiterite, acanthite and scheelite (Hoth et al. 2010; Reinhardt et al. 2021). The overall high pyroxene/garnet ratio and the significant Mn content in clinopyroxene are indicative of a distal position of skarn formation (Meinert et al. 2005; Reinhardt et al. 2021). LA-ICP-MS U-Pb dating of garnet from Gelbe Birke yields an age of 313.1 ± 2.3 (Burisch et al. 2019).

Pöhla-Globenstein

The laterally extensive skarn bodies of Pöhla-Globenstein are located in the central part of the Aue-Schwarzenberg district and were mined for Fe from the 17th century until 1941, with an estimated production of ~ 27 kt of magnetite. From 1950 until 1988, a total of 34.1 kt Fe (9.5 – 11%), 4,136 t Sn (0.41 – 0.55 %) and 8,079 t W (0.29 – 0.44 %) were produced from underground trial mining operations. Between 1956 and 1988, a total of 438 exploration boreholes with a combined length of 112,500 m were drilled from the underground adits (Hösel 2003). Geological resources were estimated to 16 Mt of ore at 0.57 % Sn, 0.36 % W and 0.81 % Zn (Hösel 2003). In 2015, three exploration holes were drilled by Saxony Minerals & Exploration AG with a total length of 502 m in order to twin historic drill cores. In 2019, the company constructed an exploration shaft to recover a bulk sample of scheelite-bearing ore for metallurgical test work. The results of this test work were not published, nor was a revised resource statement released by SME.

Skarns of the Pöhla-Globenstein deposit occur in close to moderate distance to the contact of the large Eibenstock batholith (Fig. 4A and B). However, geochronological data (U-Pb ages of prograde garnet, 338.2 ± 2.5 to 331.2 ± 3.0 Ma, Reinhardt et al. 2022) suggest that at least some of the skarns formed prior to the main emplacement of the Eibenstock granite (314 – 315 Ma; Tichomirowa et al. 2025). Stratabound skarns bodies are laterally extensive; they are developed along three major dolomitic and, to a lesser extent, calcitic marble horizons intercalated with mica schists and amphibolites. The skarns are cross-cut by swarms of microgranitic and rhyolitic dikes of unknown age (Hösel 2003) and displaced by several faults, which dip either towards the SW or to the SE (Hösel 2003). The stratigraphically lowermost skarn body reaches a thickness of up to 12 m and can be traced over 2.4 km eastwards. The distance to the underlying granite intrusion ranges between 10 to 350 m (Fig. 4A and B). The second skarn horizon strongly varies in thickness, reaching up to 12 m northwest of the Globenstein Fault and up to 80 m to the southeast, before decreasing again to 30 m (Hösel 2003). The distance to the underlying granite intrusion ranges between 50 and 500 m (Fig. 4A and B). A third, predominantly calcic skarn is exposed at surface along its western limit but is found approximately 50 to 100 m below the surface elsewhere. This third skarn body has a thickness of 20 to 50 m and can be traced over 500 m eastward from the surface, though its eastward continuation remains unconstrained.

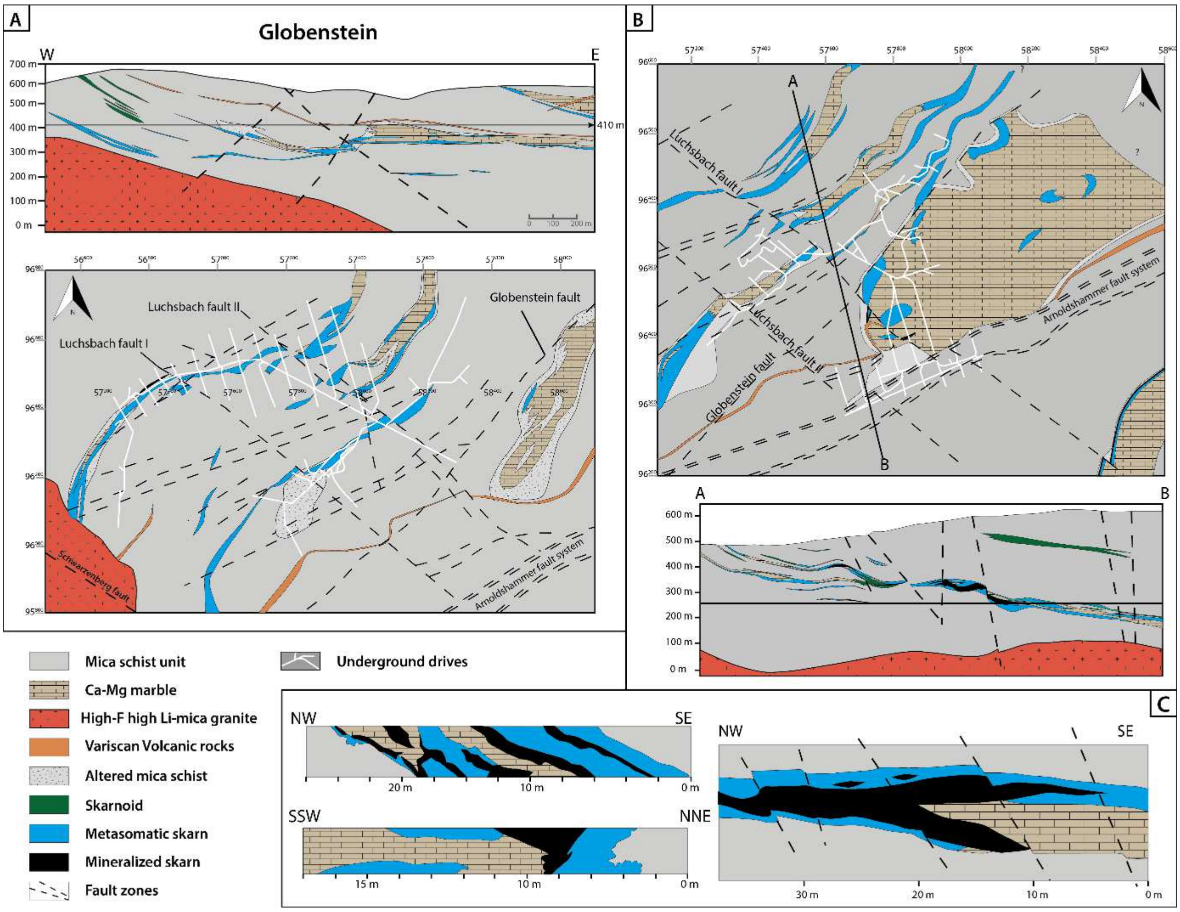

Fig. 5 A) Cross-section and corresponding geological map on the 410 m level of the Globenstein system after Hösel et al. (2003). B) Geological map on the 260 m level at Globenstein with the respective cross-section that shows mineralized skarn proportions (after Hösel et al. 2003). C) Typical structure of skarn alteration and mineralization at Globenstein (after Hösel et al. 2003)

The stratigraphically lowest skarn horizon is characterized by abundant cassiterite, cadmium-bearing sphalerite, and minor magnetite. The middle skarn unit is exceptionally rich in magnetite, with the largest magnetite ore body measuring 6 x 300 x 300 meters, northwest of the Globenstein fault (Hösel 2003). Only minor Sn and W mineralization is recognized in this skarn unit. To the SE of the Globenstein fault, the bulk of Sn-W mineralization is associated with the central and shallowest skarn units. Typically, the Sn mineralization is spatially separated from the W mineralization. Tungsten-rich ores predominantly comprise scheelite that occurs in poorly consolidated breccia zones referred to as “Zersatzerz”. Scheelite is accompanied by fluorite, siderite, kaolinite, sulfides, and cassiterite. Scheelite mineralization has been described as postdating skarn formation and is mostly associated with faults and alteration halos of veins, resulting in irregularly shaped ore bodies of variable grades (Hösel et al. 2003).

Tin (cassiterite) mineralization, in contrast, appears to form part of retrograde skarn alteration assemblages (Fig. 4C), with relatively constant distribution and abundance along skarn-altered units. The distance from the granite contact does not seem to have a significant control on the skarn mineralogy, at least on the scale of the known extent of the skarns (Hösel 2003).

Unfortunately, modern investigations of the mineralogy and petrography of the skarns at Pöhla-Globenstein are sorely lacking. Previous petrographic studies have suggested two main stages of prograde skarn formation at Pöhla-Globenstein (Hösel 2003): The first stage is described as skarnoid comprising clinopyroxene, minor forsterite and Mg-spinel. This is followed and often strongly replaced by a second prograde alteration stage with green grandite garnet (containing up to 0.23 wt. % Sn), clinopyroxene and vesuvianite, with interstitial scheelite, magnetite and ludwigite (Hösel 2003). Retrograde alteration follows this second, metasomatic skarn stage, associated with the formation of epidote, amphibole, chlorite, and fluorite, and cassiterite (Hösel 2003).

Breitenbrunn

The Breitenbrunn deposit, located in the south-western part of the Aue-Schwarzenberg District, was mined for Fe, Sn, Zn, and marble between 1567 and 1924 (Hoth et al. 2010). Since 2012 Saxore Bergbau GmbH holds the exploration license for this deposit. Systematic exploration was conducted between 1938 and 1943, yielding 26 boreholes with a total length of 2570 m. Between 1946 until 1967 another 506 diamond core boreholes (>11,000 m) were drilled. Mineral resources were estimated at 2.2 Mt of ore at grades between 0.25 % Sn, 2.0 % Zn, 2.0 % Cu and 30 % of Fe (Hösel et al. 1997; Hoth et al. 2010).

Skarns at Breitenbrunn are hosted by five southwest-dipping marble horizons that are intercalated with mica schists and phyllites of the Jáchymov Group. The Eibenstock granite is exposed about 100 – 500 m to the W and SW of the deposit and dips below the skarns. Detailed petrographic descriptions are still unavailable for the Breitenbrunn skarns, but some preliminary observations have been published (Hoth et al. 2010; Reinhardt et al. 2022). According to these observations, three phases of skarn formation can be distinguished. The prograde stage of the first phase comprises green andradite garnet with abundant magnetite. U-Pb dating of garnet (Reinhardt et al. 2022; Burisch et al. 2019) suggests this stage to have formed at 337.5 ± 3.3 Ma. The second phase is marked by the formation of a skarnoid comprising pyroxene, minor fine-grained red garnet and vesuvianite. Geochronological evidence suggests this assemblage to have formed between 317.3 ± 6.3 Ma and 313.5 ± 4.7 Ma. The skarnoid was later replaced by an even younger metasomatic skarn, comprising green garnet and clinopyroxene, representing a third phase of skarn formation at 302 ± 2.7 Ma. Retrograde alteration includes actinolite, epidote, chlorite, and prehnite, as well as cassiterite and sphalerite (Hoth et al. 2010; Reinhardt et al. 2022). The exact age of cassiterite mineralization remains unknown at present.

Hämmerlein-Tellerhäuser cluster

The prolific Hämmerlein-Tellerhäuser skarn cluster forms a concealed 7 x 3 km laterally continuous ore body in the SE sector of the Aue-Schwarzenberg district. The cluster includes the Dreiberg and Zweibach (Tellerhäuser sector) and the Hämmerlein (sector) skarn deposits (Fig. 5). Mining in the area began in 1750 and continued until 1852, focusing on Sn, Ag, Fe, and Cu (Baumann et al. 2000). In 1965, the exploration focus shifted to U, which included several drilling and mapping campaigns, resulting in the construction of the Pöhla adit that was built primarily for exploration. It was not until 1972 that exploration of skarn-hosted Sn mineralization began. In total, 138,900 m of diamond core drilling was carried out from 32,000 m of underground drifts. Moreover, during pilot mining large volume samples for test work were collected which were also included in the resource estimates (Schuppan and Hiller 2012). Additionally, 186 drill cores were drilled from surface on a grid of 100 m to 200 m. Until 1991, extensive test work for the extraction of tin was conducted, but remained unsuccessful – hence, commercial production of Sn never commenced. Successful beneficiation was accomplished in 2019 by a pilot experiment coordinated by the Helmholtz Institute Freiberg for Resource Technology in cooperation with Saxore Bergbau GmbH (a subsidiary of First Tin PLC) and other research partners. Since acquiring the license in 2013, Saxore Bergbau/First Tin has confirmed historical drill results with thirteen new diamond core drillings spread across the Hämmerlein-Tellerhäuser skarn cluster. Recent resource estimates include indicated resources of 9.9 Mt at 0.45 % Sn, 10.24 % Fe_2O_3, 0.42 % Zn, 2.49 g/t Ag, and 22.49 g/t In with and additional inferred resources of 17.97 Mt of ore at 0.52 % Sn, 8.63 % Fe_2O_3, 0.62 % Zn, 2.59 g/t Ag, and 26.94 g/t In (First Tin PLC 22.04.2024).

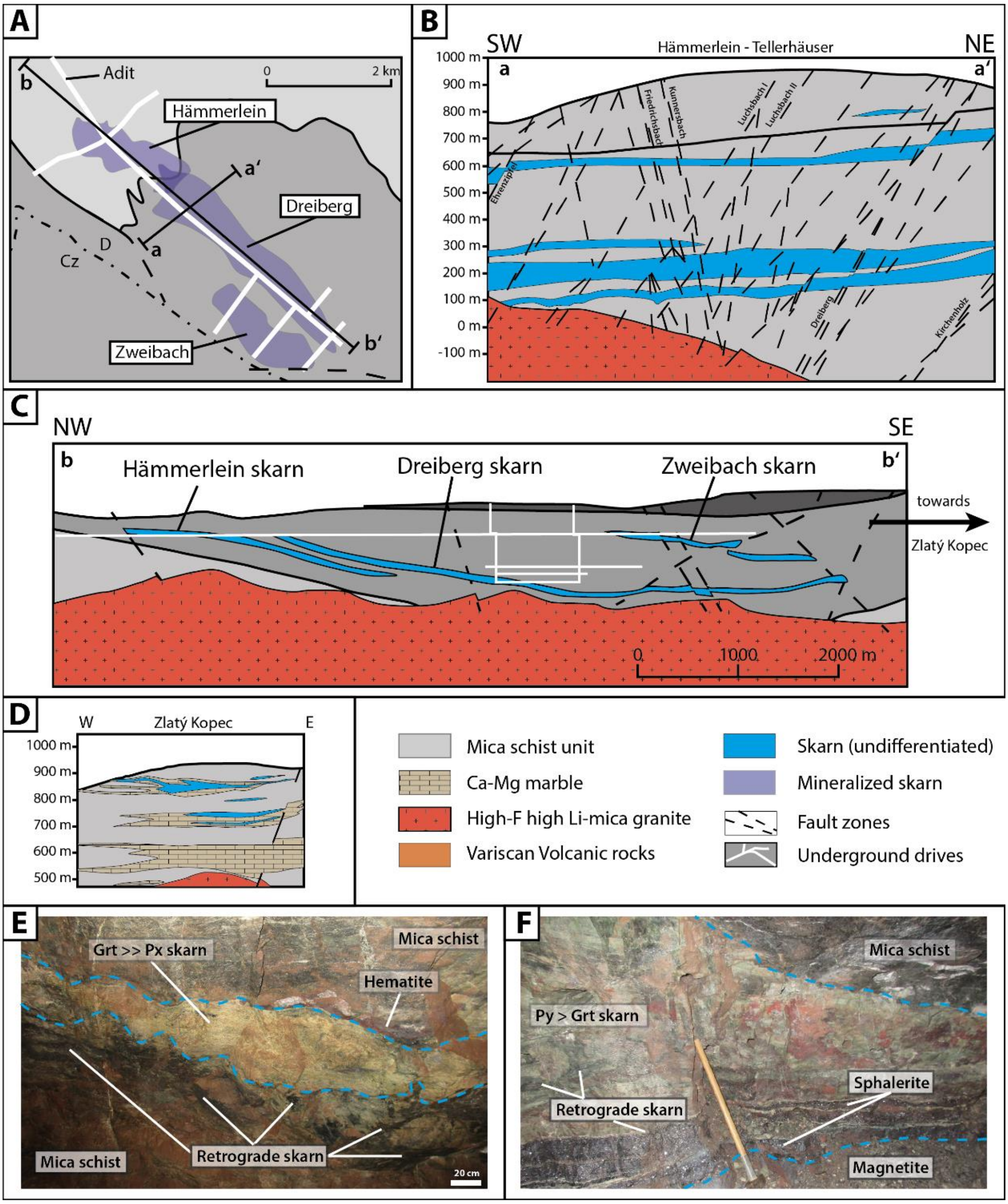

Fig. 6 A) Mineralized skarns and underground drifts within the Hämmerlein-Tellerhäuser system (after Saxore GmbH). B) Simplified section through the Hämmerlein skarn with numerous faults intersecting the skarn units (after Schuppan and Hiller 2016). C) Overview section of the Hämmerlein-Tellerhäuser cluster with the Hämmerlein, Dreiberg and Zweibach skarn deposits. Zlatý Kopec presents the SE extension of the skarn cluster into the Czech Republic (after Baumann et al. 2000). D) Cross-section of Zlatý Kopec at same scale as B for comparison. Note the abundance of dolomitic marble not affected by skarn alteration (after Pauliš et al. 2015). E) Garnet-rich skarn in

mica schist with minor retrograde alteration near the footwall contact. F) Pyroxene-rich skarn with notably retrograde overprint and massive sphalerite and magnetite mineralization in the footwall

Laterally extensive stratabound skarn bodies are related to three distinct marble units of the Jáchymov group that dip shallowly to the SE (Fig. 5A-C): the Hämmerlein skarn in the northwest and the Dreiberg and Zweibach skarn in the southeast. Locally, stockwork-hosted cassiterite-quartz-fluorite mineralization (“Schiefererz”; Schuppan and Hiller 2012) occurs in mica-schist in the immediate footwall of the skarn zones. The general dip of the skarn units is 10 to 15° to the SE; they partly overlap at different depths (Fig. 5B and C). The entire area is underlain by the western flank of the Eibenstock-Nejdek batholith that dips shallowly to the NE (Förster et al. 1999; Schuppan and Hiller 2012). The contact metamorphic halo around this batholith extends up to 1000 m into the metasedimentary host rocks – with the skarn units located within this halo (Schuppan and Hiller 2021).

Petrographic observations summarized by Schuppan and Hiller (2012) suggest the presence of at least two distinct skarn stages. The first stage is expressed as a prograde skarnoid comprising clinopyroxene, Sn-poor garnet, wollastonite, and vesuvianite. Pale red and green garnet from this skarnoid stage were dated at 327.3±8.4 Ma to 324±7.4 Ma (Reinhardt et al. 2022). This prograde skarnoid assemblage was only overprinted by a retrograde assemblage of epidote and axinite. The second stage comprises a coarse crystalline prograde metasomatic skarn assemblage with clinopyroxene and stanniferous, green garnet and abundant magnetite (Fig. 5E; Schuppan and Hiller 2012). Dark brown to greenish garnet of this prograde metasomatic stage yield ages of 304 ± 5.7 to 294 ± 8.3 Ma (Burisch et al. 2019; Reinhardt et al. 2022). This younger prograde skarn assemblage was extensively overprinted by a retrograde assemblage of (Fig. 5F) tremolite-actinolite, chlorite, fluorite, quartz, cassiterite, In-rich sphalerite, and chalcopyrite (Bauer et al. 2019; Kern et al. 2019).

Zlatý Kopec

Several skarns in the area northwest of Boží Dar in the Czech Republic are considered to represent the SE continuation of the Hämmerlein-Tellerhäuser cluster, of which Zlatý Kopec is the most important one (Fig. 5D). Mining of this skarn deposit took place between the 16th and the late 18th century (Pauliš et al. 2015). Between the 1950s and the 1980s, several exploration campaigns proved around 1 Mt of ore at 0.95 % Sn, 0.5 % Zn, and relatively high concentrations of Cd, In, Sc, and Tl (Pauliš et al. 2015; Starý et al., 2024). The opportunity for renewed exploration ceased, when the area became a landscape heritage zone in 2016.

The skarns at Zlatý Kopec form lenticular bodies within marble and mica schist of the Jáchymov Group within a succession of carbonaceous phyllites, quartzites, and metabasites (Baumann et al. 2000). The deposit consists of one main skarn-bearing marble horizon, and one smaller skarn-bearing horizon about 70 m below the main horizon. Skarn bodies predominantly strike NW-SE with a gentle dip of 5-20° to the NE. The thickness of the skarn units varies from typically 1.5 to 3 meters which may locally increase up to 9.5 meters. The lateral extent of the skarn is constrained by drilling to about 600 x 300 meters. About 350 meters below the skarn zone, a high-F high-P_2O_5 Li-mica granitic intrusion was intersected in drill core (Pauliš et al. 2015) that likely belongs to the Eibenstock batholith. Radiometric ages at Zlatý Kopec are not available.

The skarns comprise a prograde assemblage of clinopyroxene (diopside) and garnet in variable ratios. Magnetite is abundant, together with borates, chlorite, cassiterite and sulfides it forms the retrograde assemblage. Fe-rich sphalerite (containing up to 0.15 wt.% In; Pauliš et al. 2015) occurs in skarn as well as metapelites (possibly similar to the "Schiefererz" at Hämmerlein-Tellerhäuser). Locally, the skarn-bearing units are replaced by a mineral association comprising hulsite, schoenfliesite and ludwigite (Pauliš et al. 2015), which are common for skarns with Mg-rich protoliths (Burisch et al. 2023). The skarn texture is not described in detail in the available literature.

Geyer - Ehrenfriedersdorf District (Central Erzgebirge)

The Geyer-Ehrenfriedersdorf District is located in the central part of the Erzgebirge, covering an area of about 11 km^2. It includes the historic mines and mine camps of Geyersberg, Geyer SW and NE, Sauberg, Vierung, Greifensteine, and several other smaller Sn occurrences (Fig. 2A). Historic Sn production occurred discontinuously between 1395 and 1990 and mainly focused on greisen-, stockwork-, and vein-hosted cassiterite mineralization at Geyersberg and Ehrenfriedersdorf (Hösel

1994; Hösel et al. 1996). Tin ore was extracted from stockwork zones crosscutting the metasedimentary host rock (exocontact) and the intrusion (endocontact; Fig. 2B; Hösel 1994). Additionally, some skarn-hosted Sn was mined at Geyer between 1667 and 1853. Skarn-hosted mineralization at Geyer SW was extensively drilled in1968/69 and 1975/76 by the SDAG Wismut, resulting in 123 boreholes with more than 37,000 m of core recovered (Hösel et al. 1996). Skarn-hosted resources were inferred to 8.2 Mt of ore at grades of 0.56 % Sn and 1.1 % Zn (Elsner 2014). In addition, resources of 353 t of Ga and 441 t of In were reported without detailed information (Hösel et al. 1996). In 2011 and 2012, twin holes drilled by Tin International confirmed previous results, but renewed exploration did not yield a new resource assessment.

The Ehrenfriedersdorf tin mine was closed in 1990. It exploited stockwork-type Sn mineralization in biotite-rich schist of the Klínovec and Jáchymov group (Hösel 1994). Several thin skarn units (< 1 m thickness) that occur intercalated with the biotite schist are exposed in drifts of the historic underground mine (Fig. 2B). Previously, those were not studied in detail, but the associated geological resource was estimated to about 0.8 Mt of ore at 0.44 % of Sn (Hösel 1994). Skarns form irregular, lens-shaped bodies that range between several tens of meters up to 500 m in lateral extent and between 0.2 and 5 m in thickness (ESM 1; Hösel 1994). At Geyer SW, three skarn horizons strike NE-SW and dip to the NW at 30–40° (Fig. 2C; Hösel et al. 1996). The skarn units can be traced over a strike length of up to 4 km and extend down to the sub-horizontal igneous contact (5D). The thickness of skarn horizons varies between 5 and 40 m (Hösel et al. 1996). The skarn packages are truncated in the north by the Herold-Schönfeld fault; their continuation to the south-west is unconstrained.

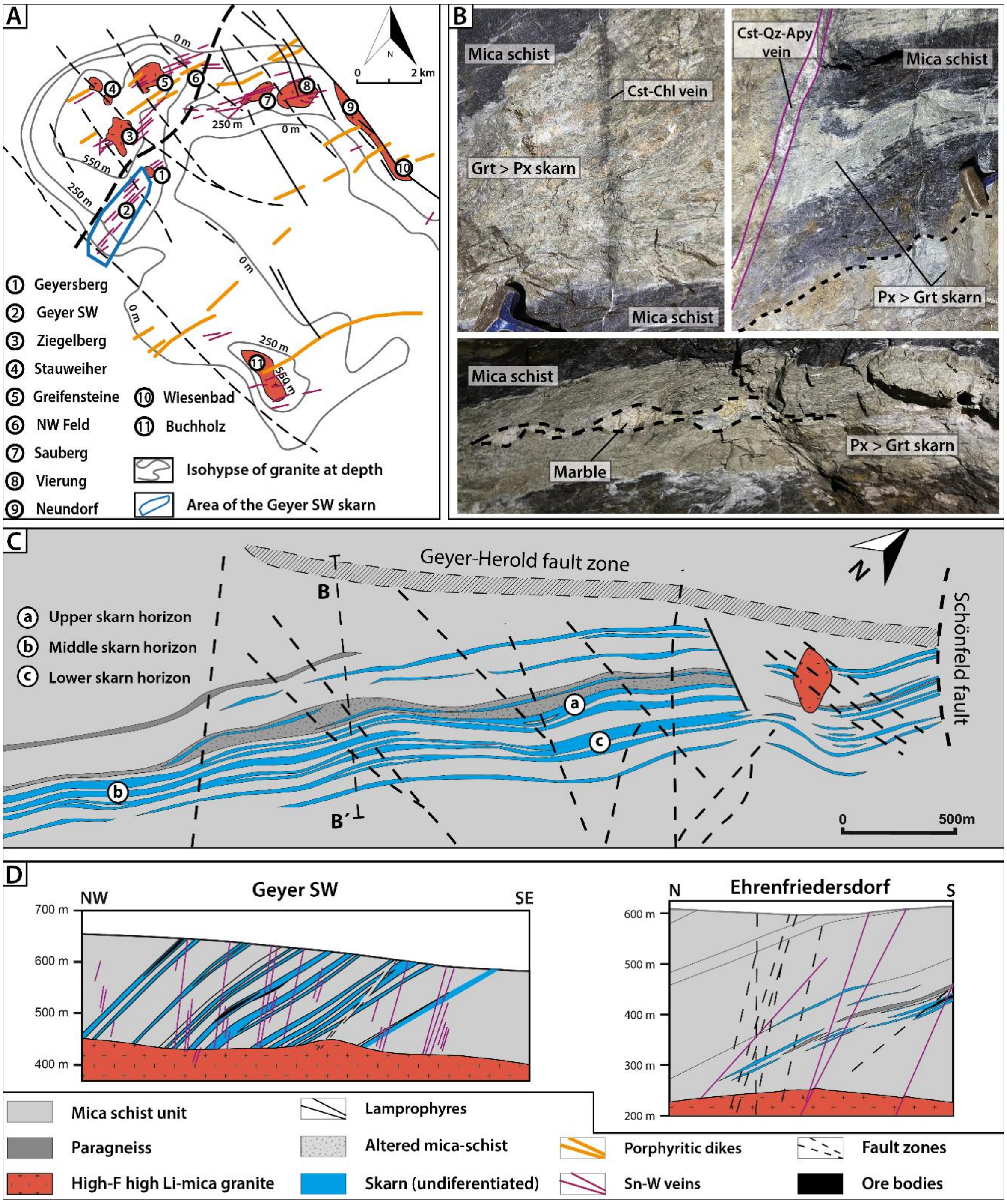

Fig. 7 A) Overview of the Geyer-Ehrenfriedersdorf district with historically important mine camps (after Hösel 1994). B) Underground skarn exposure in the historic Ehrenfriedersdorf mine showing typical textural and structural features. C) Simplified geological map of the Geyer SW skarn project (after Hösel et al. 1996). D) Cross-section through the Geyer SW skarns (left) and Ehrenfriedersdorf-Sauberg (right; after Hösel 1994 and Hösel et al. 1996)

Skarns of the Geyer-Ehrenfriedersdorf district are hosted by a succession of low- to medium metamorphic metasediments of the Jáchymov Group. The metasedimentary succession is underlain by the Ehrenfriedersdorf composite pluton. The contact between the granite and metasediments was intersected in drill core at depths between 150 and 450 m below the surface; the intrusive contact forms a subtle dome-structure with steeper slopes to the N and a gently dipping slope to the S forming a horse-shoe-shaped topography of the concealed intrusion (Fig. 2A; Brosig et al. 2020). Exposure of the mostly concealed granite massif is limited to several smaller stocks and cupolas such as the Greifensteine, Geyersberg and Ziegelberg (Hösel et al. 1996). Geochronological Th-U-Pb ages of uraninite in granites from the Greifensteine and Sauberg and U-Pb ages of apatite from the Sauberg granite indicate intrusion ages ranging from 324 ± 4 to 319.7 ± 3 Ma and from 323.9 ± 3 to 317.3 ± 2 Ma, respectively (Romer et al. 2007). Cassiterite from Ehrenfriedersdorf show a wide age range from ~ 320 to 311.7 ± 2.1 (Meyer et al. 2024; Zhang et al. 2017). Note, however, that the published ages of Zhang et al. (2017) are about 8 Ma too old because they used an inaccurate reference material (Zhang and Lehmann pers. comm.). More recent ages of similar sample material from Ehrenfriedersdorf are in the range of 313 to 311 Ma (Leopardi et al. 2024a; Meyer et al. 2024). Cassiterite from Geyersberg are of distinctly younger age than these intrusions, with U-Pb ages between 305.7 ± 3.7 and 308.2 ± 3.7 Ma (Meyer et al. 2024). Skarn-hosted cassiterite yields ages of 308.2 ± 3.7 Ma (Geyer) and 311.5 ± 3.6 Ma (Ehrenfriedersdorf; Meyer et al. 2024; this study).

Based on textural observations and radiometric dating, two distinct stages of skarn formation in the Geyer - Ehrenfriedersdorf district are distinguished (Meyer et al. 2024; 2025). The paragenetically older skarn stage comprises calcsilicate rocks with commonly fine-grained prograde skarn minerals that form a skarnoid texture. Those skarnoids are barren and are not enriched in Sn. Moreover, they are not associated with retrograde alteration, unless they are overprinted by the second, paragenetically younger skarn event (Meyer et al. 2024: ESM 1). LA-ICP-MS U-Pb geochronology on garnet constrains the older skarn stage to ~322 Ma at Geyer (Meyer et al. 2024) and 322.3 ± 4.5 Ma at Ehrenfriedersdorf (ESM 2). The second stage is best described as a typical metasomatic skarn with a coarse crystalline prograde assemblage of garnet, pyroxene and vesuvianite, followed by intense retrograde skarn alteration with a mineral assemblage comprising variable amounts of actinolite, chlorite, cassiterite, fluorite and base metal sulfides. Uranium-Pb LA-ICP-MS ages of prograde garnet of this second stage range between 307.3 ± 4.8 and 301.6 ± 5.0 Ma at Geyer (Meyer et al. 2024), whereas one garnet sample from Ehrenfriedersdorf yielded 305.3 ± 2.7 Ma (Burisch et al. 2019). More information on the Ehrenfriedersdorf and Geyer skarns is available in Meyer et al. (2024) and ESM 1. Geochronological data are listed in ESM 2, mineral chemical data may be found in ESM 3.

Common characteristics

Despite their diversity, most skarns in the Erzgebirge show some common paragenetic and textural features. Although mineralogy varies considerably as a function of protolith composition and distance to the fluid source, at least two distinct prograde stages and one retrograde stage can be recognized in most skarns (Fig. 7). The general similarities of these different types of alteration are presented below.

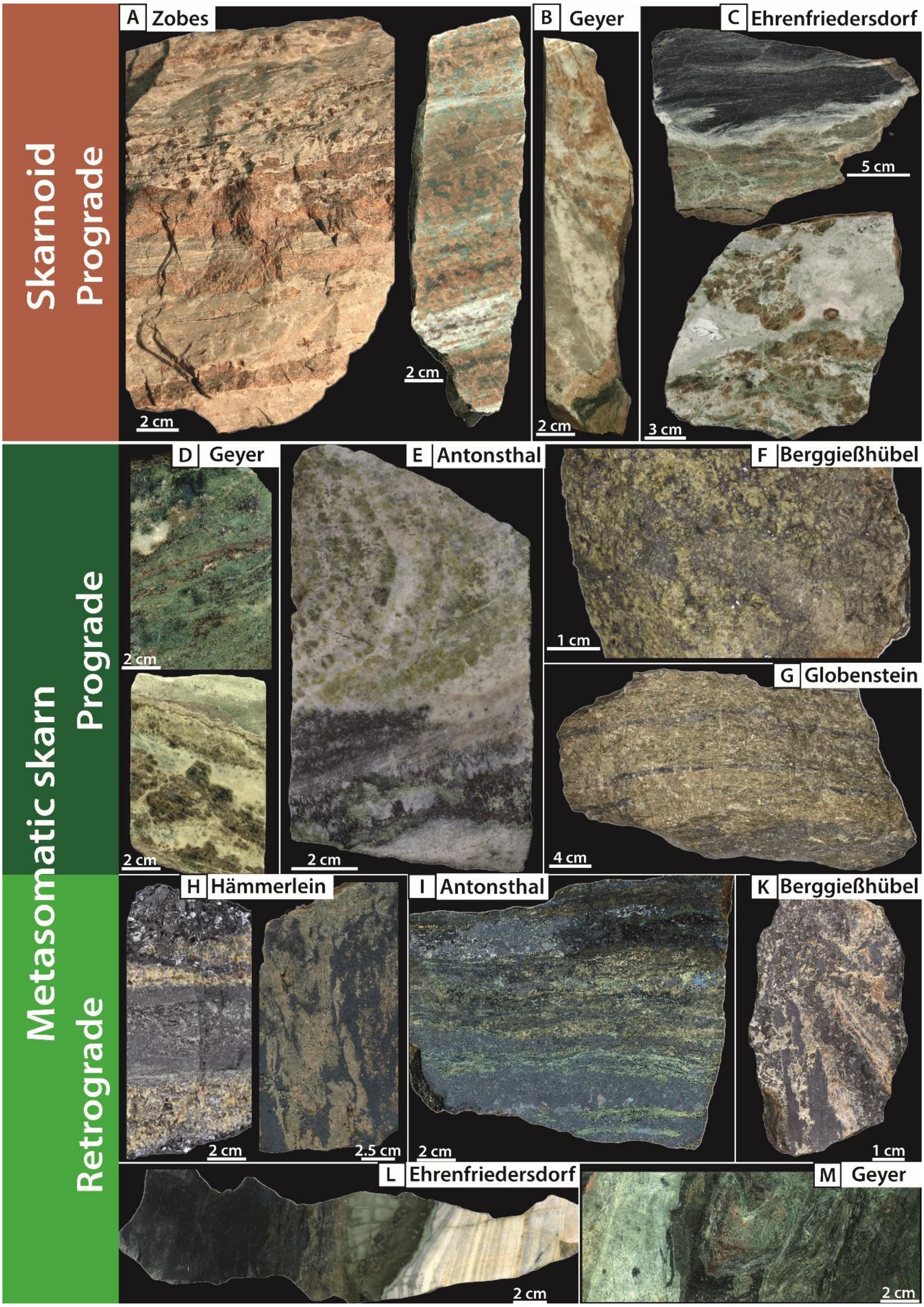

Fig. 8 Characteristic rock types of skarn systems. A) Skarnoid with red garnet intercalated by green clinopyroxene, Zobes. B) Red garnet and grey wollastonite in a skarnoid, Geyer. C) Contact and

center of a skarn lenses with partly preserved fabric of the protolith and higher abundance of K-feldspar and plagioclase, Ehrenfriedersdorf. D) Metasomatic skarn with a variable ratio between green garnet and beige clinopyroxene, Geyer. E) Green metasomatic garnet replacing calcic marble. The lower part comprises dark grey sphalerite, Antonsthal. F) Green metasomatic skarn replaced by sphalerite and hematite, Berggießhübel. G) Pale green garnet skarn with layers comprising mainly clinopyroxene, Globenstein. H) Retrograde skarn with predominantly sphalerite (left) and magnetite (right), Hämmerlein. I) Clinopyroxene-rich skarn replaced by epidote as well as base metal sulfides and magnetite, Antonsthal. K) Sphalerite in a clinopyroxene-rich skarn, Berggießhübel. L) Contact between mica schist (dark), retrograde skarn with mainly amphibole and chlorite (green) and dolomitic marble, Ehrenfriedersdorf). M) Retrograde chlorite and amphibole replacing clinopyroxene-rich prograde skarn, Geyer

Skarnoid (prograde association)

Entire skarn bodies (e.g., Zobes) or only local domains within skarns (e.g. Geyer) exhibit a skarnoid texture, i.e., they comprise of a prograde calc-silicate assemblage that is fine-grained and preserves some of the macroscopic textures of the protolith, most notably compositional banding. Pale green clinopyroxene with a hedenbergite-rich composition is the prevalent mineral in skarnoids. It is intergrown with pale red garnet of variable composition (Hiller and Schuppan 2012; Meyer et al. 2025). Wollastonite is a typical mineral in skarnoids, with highest abundances typically found close to the marble front (Hiller and Schuppan 2016). Vesuvianite commonly has an Al- and Mg-rich composition. Magnesian skarns comprise forsterite-rich olivine instead of garnet, intergrown with pyroxene and spinel (sensu stricto; Hösel et al. 2003; Pfeiffer and Schützel 1969). In marly protoliths, K-feldspar and plagioclase constitute large parts of a skarnoid (Hösel et al. 1994). Minor clinozoisite and phlogopite can occur in a paragenetically late position (Fig. 8). A retrograde stage is commonly absent. The mineral chemistry of calcsilicates in skarnoids is dictated by the composition of the protolith and indicates low fluid/rock ratios (Jamtveit and Hervig 1994; Meyer et al. 2025). Skarnoids are typically not associated with ore minerals; the only exception is the scheelite-bearing skarnoid at Zobes, where scheelite is invariably hosted by calcic skarn zones (Hiller and Schuppan 2012).

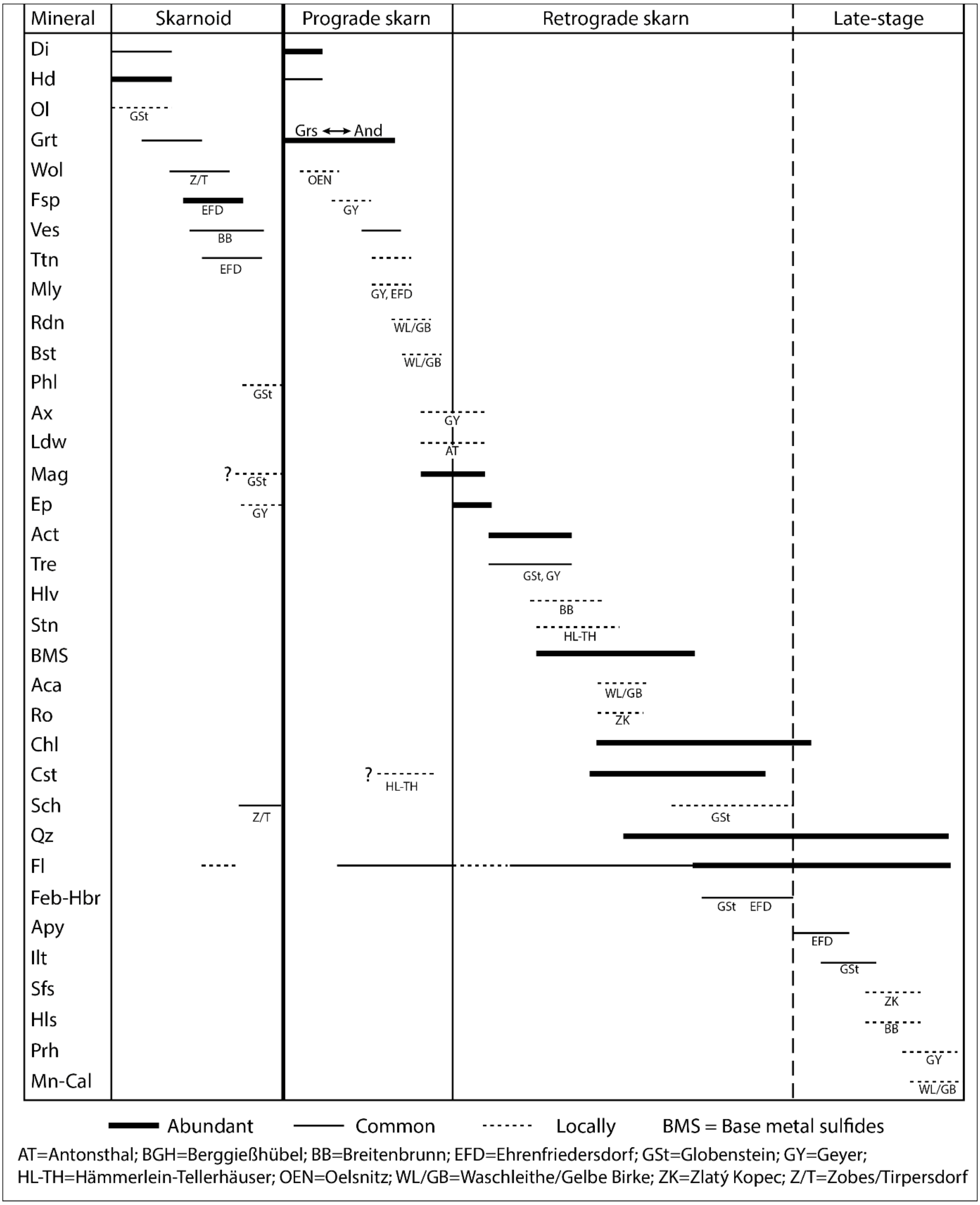

Fig. 9 Generalized paragenetic sequence of skarns of the Erzgebirge/Krušné hory. Minerals that were described or occur in abundance in single systems are indicated below the bar (after Hiller and Schuppan 2012; Hösel et al. 1996; 1997; 2003; Hoth et al. 2010; Korges et al. 2020; Kuschka and Hahn 1996; Meyer et al. 2024; 2025; Pauliš et al. 2015; Schuppan and Hiller 2012; Reinhardt et al. 2021. Mineral abbreviation after Warr (2021)

Metasomatic skarn (prograde assiciation)

Metasomatic textures are recognized in most skarns except Zobes and are characterized by medium- to coarse-grained euhedral garnet and pyroxene having an isometric fabric. Clinopyroxene and garnet occur in variable proportions ranging from pyroxene to pyroxene-garnet skarn. Garnet skarn is common but usually forms only smaller lenses within the overall pyroxene-rich skarn units (Hoth et al. 2010; Korges et al. 2020; Meinert et al. 2005; Reinhardt et al. 2021). Pyroxene color varies from cream white to pale green to dark brown in most distal zones (e.g. Waschleithe). Garnet color ranges from brown to green to pale green. Clinopyroxene (Fig. 9A) composition varies as a function of host rock with higher diopside-component in (calcic-)magnesian skarns (Meyer et al. 2025; Pfeiffer and Schützel 1969) and becomes progressively Mn-richer with increasing distance to the source intrusion. In most metasomatic skarns, garnet composition lies within the grossular-andradite solid solution with insignificant spessartine, almandine, pyrope components (Fig. 9A). Garnet is commonly intergrown or replaced by vesuvianite, which shows high concentrations of B, Be, Sb, and Sn (Meyer et al. 2025). Malayaite occurs regularly together with garnet (Hösel 1994; Meyer et al. 2024; Reinhardt et al. 2021). Bustamite and/or rhodonite are recognized in distal prograde skarn environments (Reinhardt et al. 2022). Andradite-rich garnet and malayaite may contain significant Sn concentrations in the wt.%-range (Fig. 10; Hösel 2003; Lefebvre et al. 2019; Meyer et al. 2025; Reinhard et al. 2021; this study). Additionally, paragenetically early cassiterite occurs rarely in prograde skarn (Korges et al. 2020). Garnet typically shows elevated W concentrations even in skarn not associated with significant Sn or W mineralization (Meyer et al. 2025).

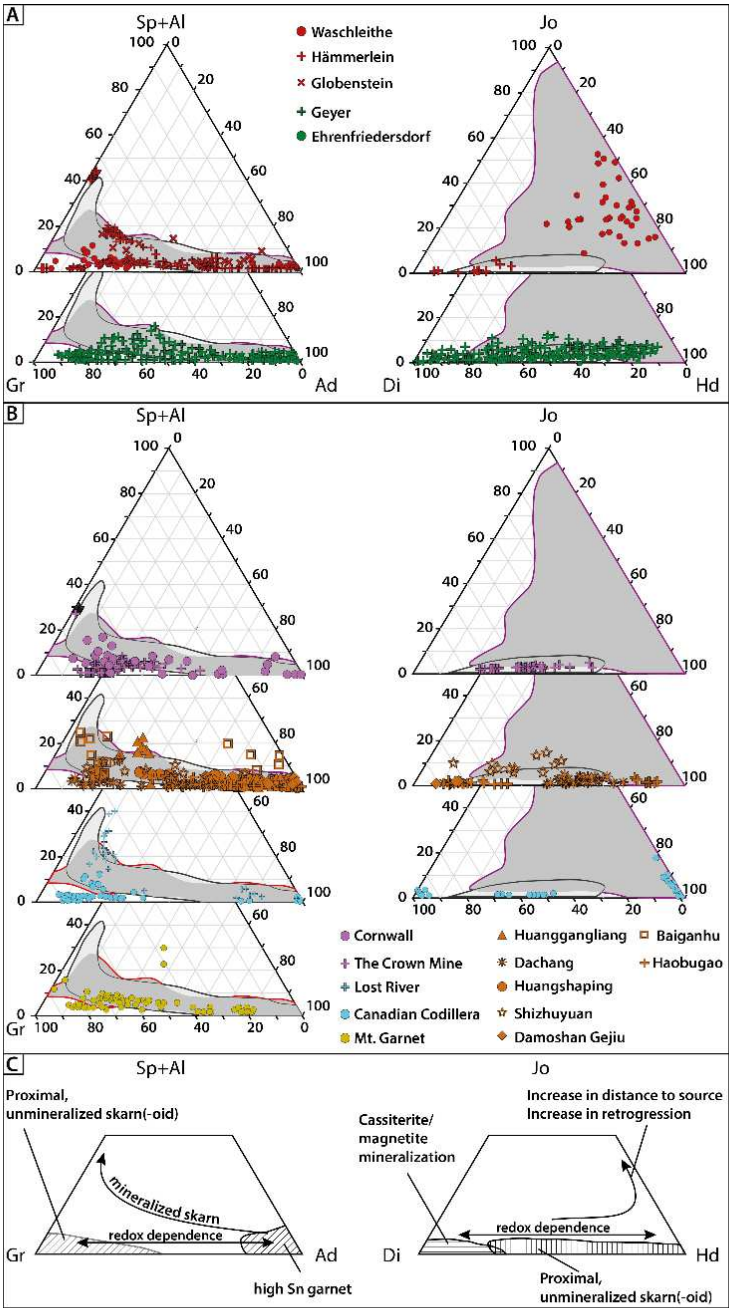

Fig. 10 Ternary diagrams of garnet (left) and clinopyroxene (right). Grey areas are compositions observed in association with skarns with distinct metal tenor (after Meinert 1992). A) Data from the Erzgebirge/Krušné hory (Lefebvre et al. 2019; Meyer et al. 2025; Reinhardt et al. 2021; this study). B) Mineral composition of garnet and clinopyroxene worldwide (Alderton 2018; Chen et al. 1992; Dobson 1982; He et al. 2024; Li et al. 2024; Liu et al. 2021; Meyer et al. 2025; Ray 2013; Wang et al. 2024; Yuan et al. 2018; Zhao et al. 2021; Zhou et al. 2017). C) Sketch to illustrate the dependence between mineral composition and spatial and temporal position within a skarn system

Magnetite is an abundant mineral in most skarns of the Erzgebirge. It invariably occupies a transitional paragenetic position between the prograde and retrograde stage (Fig. 8). Particularly in pyroxene-rich magnesian skarn, it may form extensive almost monomineralic lenses (Hösel et al. 2003; Meyer et al. 2024; Pauliš and Haake 1991). Magnetite is commonly accompanied by axinite and/or ludwigite, which are common minor minerals in magnesian skarn in B-rich systems (Burisch et al. 2023; Hösel et al. 2003; Reinhardt et al. 2021; Schuppan and Hiller 2012).

Metasomatic skarn (retrograde association)

Particularly Sn-endowed skarns are characterized by an intense retrograde stage that pervasively overprints prograde skarns along stockwork zones and veins. The retrograde mineralogy varies locally, strongly depending on protolith composition. Retrograde associations replacing calcic(-magnesian) skarns are characterized by a high abundance of epidote and actinolite, whereas retrograde associations in magnesian(-calcic) skarns are characterized by chlorite, actinolite, tremolite, as well as minor serpentine and ludwigite. In addition to these major mineral phases, retrograde skarn may contain various accessory minerals, as summarized in Figure 8. The retrograde association typically contains abundant cassiterite and sulfide minerals that are commonly intergrown with mainly chlorite, actinolite and other retrograde phases. Sulfide minerals include sphalerite, chalcopyrite, galena, stannite and acanthite (Korges et al. 2021; Reinhardt et al. 2021; Schuppan and Hiller 2012). Paragenetically early retrograde minerals, such as epidote, may have significant Sn concentrations (Fig. 10), whereas chlorite and amphiboles intergrown with cassiterite contain distinctly lower Sn concentrations (Meyer et al. 2025; Reinhardt et al. 2021). Retrograde tungsten mineralization is typically minor and economically relevant only at Pöhla-Globenstein. Scheelite-hosted by retrograde skarn is typically accompanied by chlorite and fluorite. However, scheelite mainly occurs on veins or in breccia zones that appear to postdate the retrograde skarn formation. Here, scheelite is accompanied by fluorite and quartz.

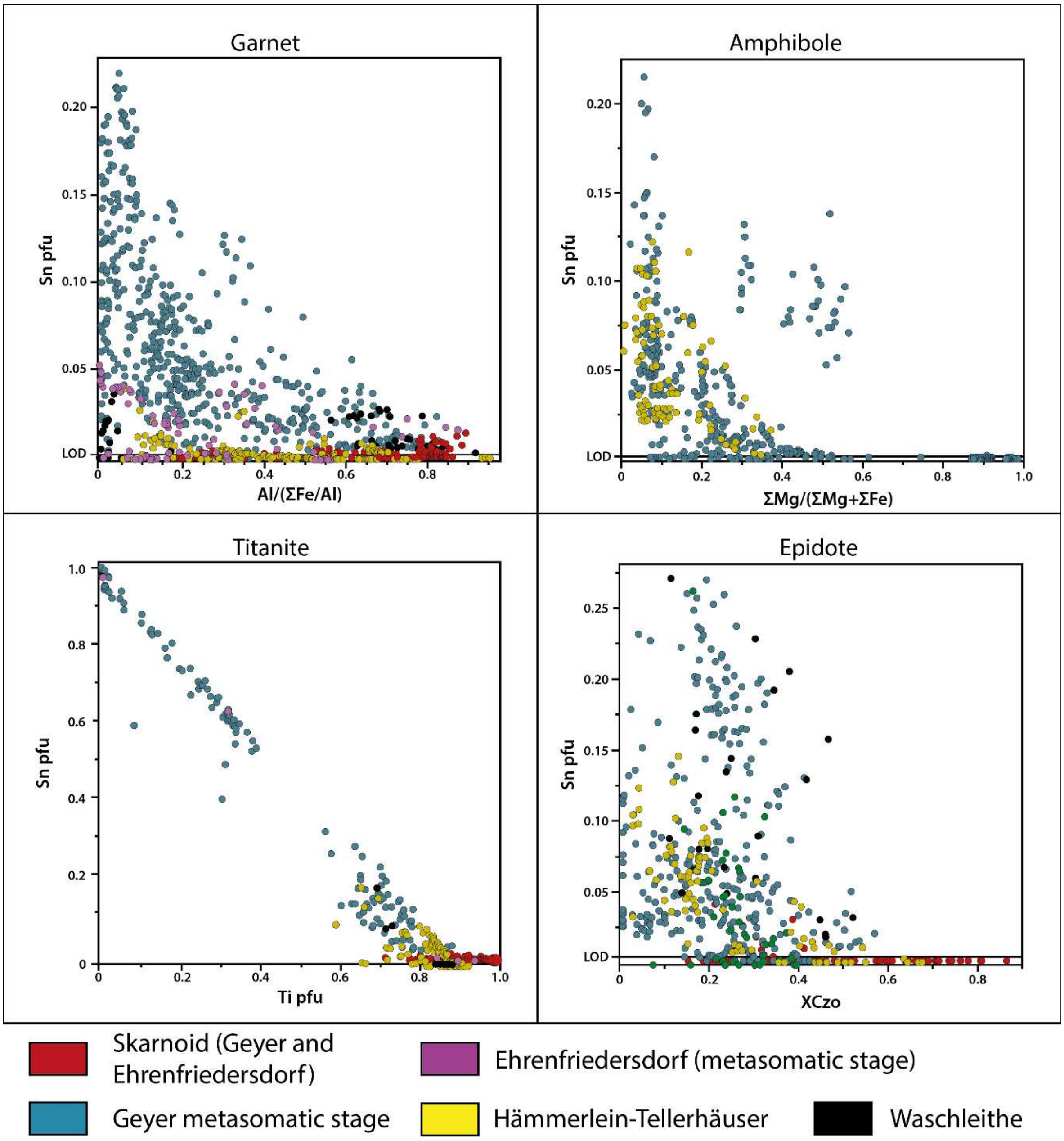

Fig. 11 Sn concentrations of garnet, amphibole, titanite, and epidote from the Geyer, Hämmerlein-Tellerhäuser (Meyer et al. 2025; Lefebvre et al. 2019), Waschleithe (Reinhard et al. 2021) and Ehrenfriedersdorf (this study)

Some retrograde skarn zones in the Erzgebirge are distinctly enriched in In (Bauer et al. 2019; Kern et al. 2019; Schwarz-Schampera and Herzig 2000; Seifert and Sandmann 2006). Sphalerite, chalcopyrite, and stannite with elevated In concentration as well as minor roquesite have been reported from Hämmerlein, Zlatý Kopec, and Oelsnitz (Bauer et al. 2019; Seifert and Sandmann 2006; Starý et al. 2024). Exceptionally sulfide-rich zones are often spatially (but not paragenetically) associated with magnetite zones (Hämmerlein, Globenstein, Geyer; Korges et al. 2020; Hösel 2003; Meyer et al. 2024), which preferentially occur in pyroxene-rich magnesian skarns (Waschleithe, Breitenbrunn, Antonsthal; Reinhardt et al. 2021; Schuppan and Hiller 2012).

The retrograde stage is followed by late-stage vein and cavity infill that mainly includes quartz, fluorite, manganiferous calcite, prehnite, illite, and arsenopyrite. Minor Sn-silicates such as stokesite ($CaSn(Si_3O_9)\cdot 2H_2O$), wickmanite ($Mn[Sn(OH)_6]$), and schoenfliesite ($Mg[Sn(OH)_6]$) occur, most likely related to late-stage replacement of prograde Sn-silicates and cassiterite (Kern et al. 2019; Meyer et al. 2024; Pauliš et al. 2015).

Fluid inclusion characteristics

Fluid inclusion assemblages in pyroxene with skarnoid texture were measured only in samples from Geyer and have estimated formation temperatures of 450 – 470 °C and salinities of 7 – 11 % NaCl eq (Meyer et al. 2024). Fluid inclusions in garnet and clinopyroxene in metasomatic skarns show a wide temperature and salinity range between 270 and 385 °C (Fig. 11; Korges et al. 2020; Meyer et al. 2024; Reinhardt et al. 2021). Some of these fluid inclusion assemblages show a bimodal distribution of salinities clustering around 0.3 – 3.8 and 28.7 – 30 wt. % NaCl eq., observed in heterogeneous fluid inclusion assemblages at Geyer (see Fig. 11; Meyer et al. 2024). A few cassiterite-hosted fluid inclusions from Hämmerlein were reported to have anomalously high homogenization temperature of 470-500 °C and high salinities (Korges et al. 2020).

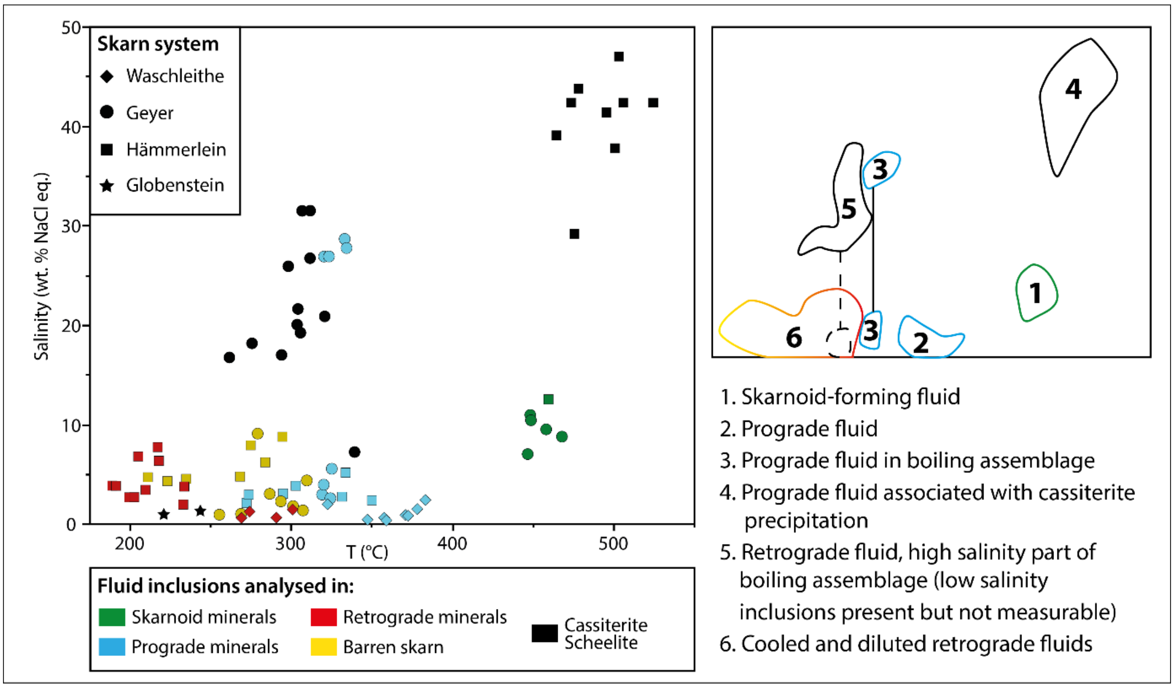

Fig. 12 Salinity (wt. % NaCl eq.) versus homogenization temperature in °C of fluid inclusion assemblages of the Hämmerlein (Korges et al. 2020), Geyer (Meyer et al. 2024), Waschleithe (Reinhardt et al. 2021) and Globenstein (Hösel et al. 2003) skarn system. Note that vapor-rich fluid inclusions are not depicted. Skarnoid assemblages are pressure corrected (200 MPa; Thomas et al 1997), other fluid inclusions are corrected assuming hydrostatic conditions according to Korges et al. (2020), Meyer et al. (2024) and Reinhardt et al. 2021)

Most of the reported fluid inclusion data of retrograde skarns are found in cassiterite, fluorite and sphalerite, having a salinity between 0.6 to 6.7 wt. % NaCl eq. (Korges et al. 2020; Kuschka and Hahn 1996; Meyer et al. 2024; Reinhardt et al. 2021). In addition, some fluid inclusions in cassiterite have high salinities between 16.8 and 31.5 wt. % NaCl eq. and occur together with vapor-rich inclusions for which no estimations for temperature or salinity are possible. The homogenization temperature of fluid inclusions ranges from 330 to 185 °C (Korges et al. 2020; Kuschka and Hahn 1996; Meyer et al. 2024; Reinhardt et al. 2021). These temperatures are consistent with temperature estimated using compositions of coeval chlorite (Korges et al. 2019; Meyer et al. 2025; this study). Fluid inclusion assemblages hosted in fluorite and quartz of late-stage veins without cassiterite have homogenization temperatures of 295 °C to 310 °C with salinities between 0.96 and 5.9 wt. % NaCl eq. (Korges et al. 2020; Meyer et al. 2024; Reinhardt et al. 2021).

Discussion

Timing of skarn formation and associated Sn-mineralization

Recent geochronological studies on garnet (LA-ICP-MS U-Pb) from prograde skarnoid and metasomatic skarn assemblages have revealed that hydrothermal skarns formed in three phases across the Erzgebirge: I) an early late-Variscan phase (341 – 330 Ma), II) a late Variscan phase (330 – 313 Ma) and a III) post-Variscan phase (313 – 295 Ma). Garnet ages of the early late-Variscan phase I (~338 – 331 Ma) are almost all from the Pöhla-Globenstein and Breitenbrunn deposit in the Aue-Schwarzenberg District and skarns hosted within gneiss units. Skarns of this age overlap with the collisional phase of the Erzgebirge (Kröner and Willner 1998) Although some of these skarns show characteristics of metasomatic alteration, no known magmatic intrusions coincide temporally with this group (Reinhardt et al. 2022; Tichomirowa et al. 2019b; 2022), suggesting an unconstrained hydrothermal event at this time. Garnets from all other Sn and/or W endowed skarns yield mostly ages belonging to phase II and III. These phases of prograde skarn formation coincide with late and post Variscan felsic magmatism (Fig. 12; Burisch et al. 2019; Meyer et al. 2024; Reinhardt et al. 2022).

Although the timing of prograde skarn formation across the Erzgebirge is well constrained by garnet U-Pb dating, the timing of associated Sn and W mineralization remains insufficiently constrained for most occurrences. Cassiterite and scheelite typically occupy a late paragenetic position (with the notable exception of the Zobes locality), overprinting prograde skarnoid and metasomatic calcsilicate minerals (Korges et al. 2020; Hösel et al. 2003; Meyer et al. 2024; Reinhardt et al. 2021; Schuppan and Hiller 2012). Recently published cassiterite and garnet U-Pb ages of the Geyer skarn have confirmed this relationship (Meyer et al. 2024). Skarnoid-hosted garnet at Geyer was dated at 322 Ma, whilst garnet associated with prograde metasomatic skarn yielded ages ranging between 307 – 302 Ma. Cassiterite as part of the retrograde skarn assemblage yielded ages of 308 – 306 Ma – a range also obtained for cassiterite present in greisen-type mineralization in the Geyer-Ehrenfriedersdorf District (Meyer et al. 2024). This provides the first direct evidence that skarn- and greisen-related Sn mineralization in the Erzgebirge is related to the same magmatic-hydrothermal mineral system.

Moreover, the garnet ages of Geyer are consistent with the observation that garnet with skarnoid textures is generally older than garnet with metasomatic textures across the Erzgebirge (Burisch et al. 2019; Reinhardt et al. 2022). Skarnoid and metasomatic stages within one skarn occurrence have statistically significant age differences of > 5 Ma (taking the analytical uncertainty into account) and are, hence, not related to the same intrusive event. This observation is atypical for skarn systems elsewhere, where both skarnoid and metasomatic skarn stages are typically related to the same magmatic-hydrothermal event (Burisch et al 2023, Meinert et al. 2023). Ages of skarnoids mostly overlap with ages of nearby large volume intrusions (e.g. Eibenstock batholite and garnet ages obtained for the Hämmerlein and Breitenbrunn skarns), whereas the metasomatic stage typically postdates voluminous intrusions in the immediate vicinity of the skarns and were therefore related to hypothesized younger intrusions (the plutonic equivalents to subvolcanic and volcanic rocks outcropping at surface or underground; Tichomirowa et al. 2025) that occur deeper relative to the present-day surface (Burisch et al. 2019; Meyer et al. 2024).

Considering all available cassiterite ages across the Erzgebirge (greisen and skarn-hosted), Sn mineralization is related to the terminal stage of the late Variscan phase (~313-310 Ma) as well as to the post Variscan phase (~30x Ma; Leopardi et al. 2024a; Meyer et al. 2024).

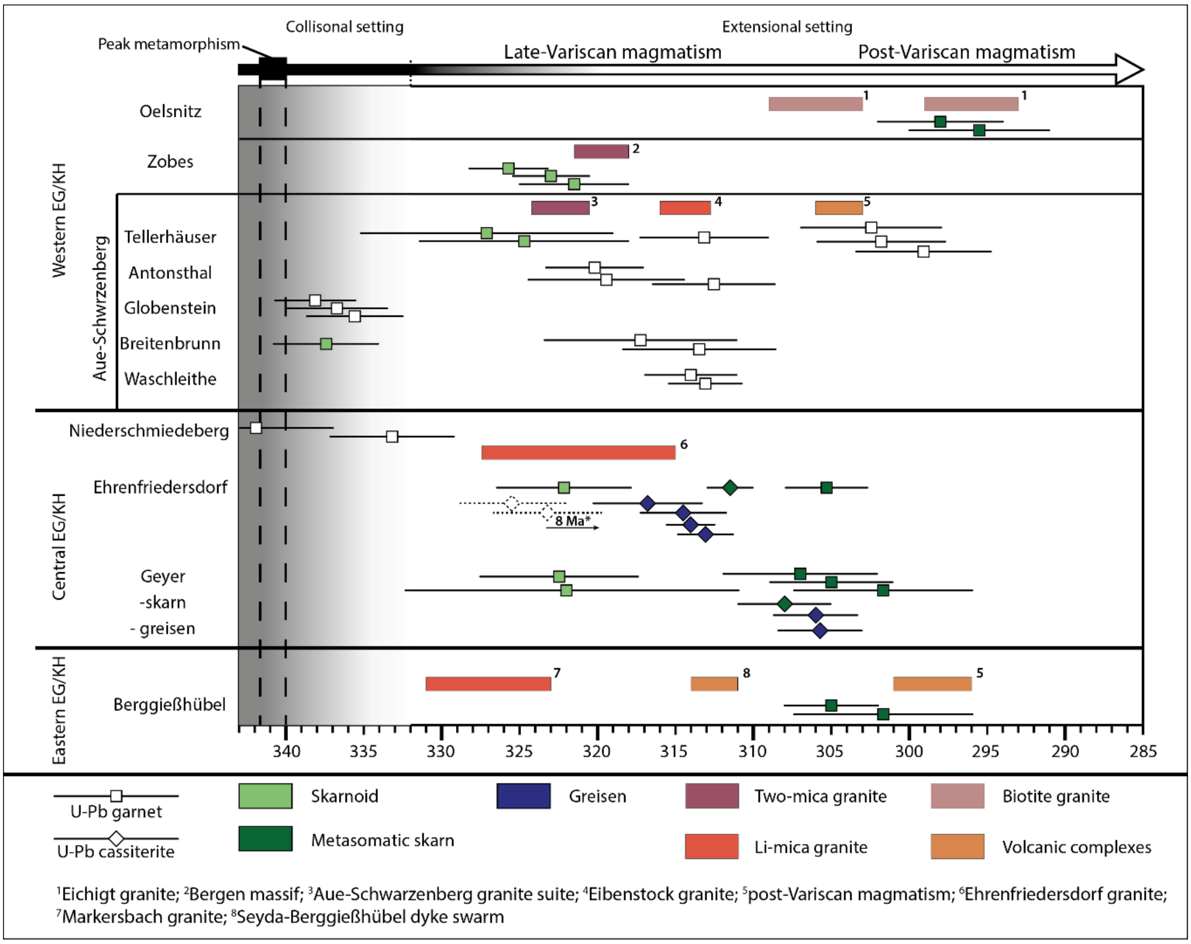

Fig. 13 Geochronological data of igneous rocks (Leonhardt et al. 2018; Tichomirowa and Leonhardt 2010; Tichomirowa et al. 2019; 2022), prograde skarn a formation (Burisch et al. 2019; Meyer et al. 2024; Reinhardt et al. 2022; this study) and cassiterite mineralization (Meyer et al. 2024; Zhang et al. 2017; this study) in the Erzgebirge. Three major sequences of skarn formation are recognized on the scale of the province. Most skarns show a twofold age distribution while skarns of multistage origin only occur within the Aue-Schwarzenberg District

Genetic model

Skarn deposits of the Erzgebirge may be the result of up to three separate hydrothermal events that can be discriminated on cross-cutting relationships and geochronological data. The oldest skarns (343 – 331 Ma) are evidence for hydrothermal activity shortly after the peak metamorphic stage of the Variscan orogeny, yet their metallogenetic relevance and the origin of fluids remains poorly constrained. There seems to be a spatial relationship between those early late-Variscan skarns and the Gera-Jáchymov

Fault zone, a pre-Variscan deep-reaching fault zone that runs NW-SW across the Aue-Schwarzenberg district (Guilcher et al. 2024; Hösel et al. 2003; Romer et al. 2010).

The second event of skarn formation occurred between 325 and 310 Ma and is related to the intrusion of voluminous granite batholiths that are widespread across the Erzgebirge. Most skarns of this stage have characteristics of skarnoids and occur in proximal and intermediate positions relative to their causative source intrusions in a rock-buffered environments. Textural arguments indicate a relatively deep formation environment of these, which is consistent with estimated emplacement depths of 3 – 6 km of the related granites (Thomas 1997). This is also supported by the fluid inclusion data, which show higher homogenization temperatures compared to other systems. These fluids were exsolved from an igneous body without undergoing phase separation (Driesner and Heinrich 2007; Leopardi et al. 2024b). The formation of skarnoids or metasomatic skarns, however, depends on the spatial position to the causative fluid source. The Waschleithe pyroxene Zn-skarn is one example, which falls in this age group. Here, metasomatic skarn features prevail, especially the strong retrograde overprint, which is probably due to its distal formation position. The Eibenstock pluton is relatively deeply eroded (Burisch et al 2025) which further supports a deep formation environment of related skarns.

The third event of skarn formation is related to post-Variscan magmatism (Tichomirowa et al 2025). By this stage, the Erzgebirge block already occupied a shallower crustal position, which is supported by the high abundance of subvolcanic and volcanic rocks of this age (Tichomirowa et al. 2025). Textural characteristics, mineral trace element compositions, and fluid inclusion data suggest hydrostatic and fluid-buffered conditions consistent with a relatively shallow skarn formation (1 – 1.5 km; Meyer et al. 2024; 2025), which is consistent with greisen system emplaced at this time at same depth ranges (. Homogenization temperatures in prograde skarn minerals are relatively low, indicating intermediate to distal positions relative to the causative intrusions (Korges et al. 2020; Meyer et al. 2024). Additionally, fluid inclusion assemblages of some skarns provide evidence for boiling (Korges et al. 2020; Meyer et al. 2024), a phenomenon more commonly observed in shallow systems (Driesner and Heinrich 2007; Leopardi et al. 2024b). These fluids are able to transport elements such as Sn, W, and In, which are subsequently incorporated into prograde calcsilicates (Meyer et al. 2025).

This final phase of skarn formation is typically associated with a stronger retrograde overprint than earlier events, which furthermore supports a relatively shallow depth of formation. Retrograde skarn alteration is associated with the main phase of ore mineral precipitation, partly due to the replacement of stanniferous prograde skarn minerals. Fluid inclusions of retrograde skarns show indications of boiling within the causative intrusion and subsequent cooling and admixture of meteoric fluids, leading to cassiterite precipitation (Heinrich 1990). A few cassiterite-hosted fluid inclusions from Hämmerlein were reported to have anomalously high homogenization temperature of 470-500 °C and high salinities. As such high temperatures conflict with a retrograde origin of the cassiterite, we speculate that some of the cassiterite at Hämmerlein may have formed during the prograde stage.

This apparent age-depth relationship suggests a prominent superimposition (telescoping), which is consistent with rapid uplift and exhumation of the Erzgebirge during the post-collisional stage (Fig. 13; Collett et al. 2020). This hypothesis is furthermore supported by a high abundance of volcanic rocks that have similar ages as the metasomatic skarns and support a relatively shallow crustal position of the Erzgebirge during the post Variscan phase (313 – 295 Ma Burisch et al. 2019; Tichomirowa et al. 2025). However, scheelite and minor cassiterite associated with the prograde stage at Zobes and greisen-hosted cassiterite from the eastern Erzgebirge indicates that tin mineralization occurred prolonged during the late- and post-Variscan stage. Thus, both stages seem to have significantly contributed to the Sn endowment of the Erzgebirge.

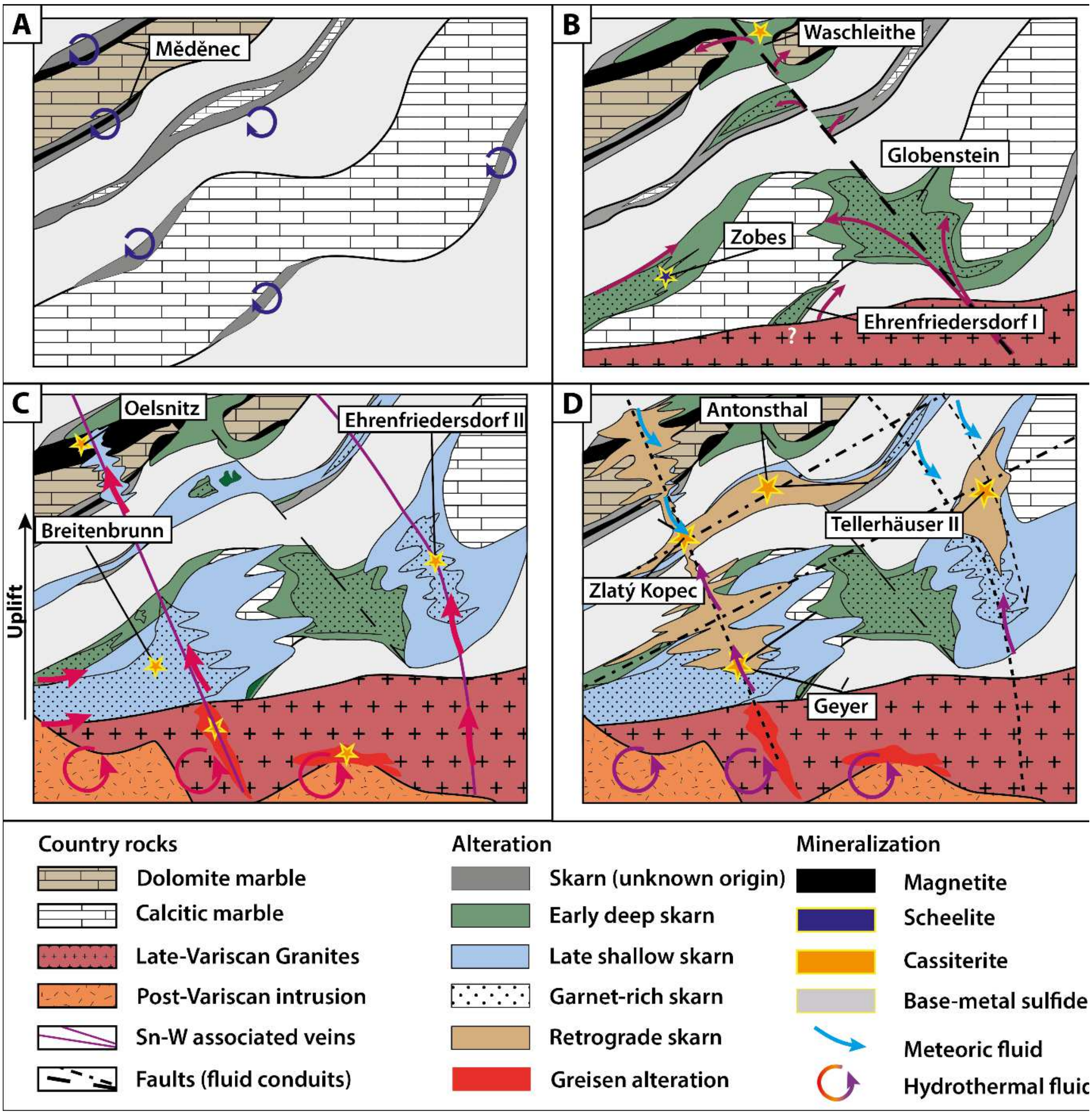

Fig. 14 Schematic model illustrating the spatial and temporal evolution of different skarn systems of the Erzgebirge. A) First metasomatic skarn alteration unrelated to igneous processes (e.g., Mědĕnec, Niederschmiedeberg, first stage of Antonsthal?). B) Deep situated formation of skarnoids that formed under rock-buffered conditions. C) Main phase of prograde, metasomatic skarn formation. Shallow skarn formation after uplift of the Erzgebirge to higher crustal level. Alteration occurs in intermediate to distal position in relative to the fluid source. D) The retrograde stage, which occurs mainly along faults or other fluid conduits, is host to the major proportion of mineralization. Cooled magmatic fluids, in case mixed with meteoric fluids, led to the replacement of stanniferous minerals and the precipitation of cassiterite along base metal sulfides

Comparison to other Sn skarn systems

The skarns of Erzgebirge/Krušné hory show striking similarities to the skarns of the Cornubian ore field. As both provinces occur within the Variscan orogenic belt, the two regions have fairly similar tectonic histories (Anderson et al. 2016; Jackson et al. 1989; Moscati and Neymark 2020; Shail and Leveridge 2009). The Cornubian skarns are also multi-stage and comprise intermediate to distal Sn-Zn-In skarns (Andersen et al. 2016; Alderton and Jackson 1978). Similar to the Erzgebirge, the Cornubian skarns exhibit a pronounced early barren skarnoid stage (locally known as "calc-flintas"; Alderton and Jackson 1978; van Marcke de Lummen 1986) that is superimposed/overprinted by metasomatic skarn stages. However, geochronological data is lacking for the skarns in the Cornubian ore field; thus, it is unclear if a similar temporal hiatus between skarnoid and metasomatic skarn exists. Significant In (as well as Cd and Ga) is hosted by skarn-related sphalerite and chalcopyrite (Andersen et al. 2016) in both provinces, but more prominent in the Erzgebirge region.

Compared to W skarn provinces such as the Canadian Cordillera (Elongo et al. 2020) or Shizhuyuan and the Nanling range in South China (Ni et al. 2023), W skarns in the Erzgebirge are minor. The only typical W skarn in the Erzgebirge is Zobes, which shows characteristic features such as a calcic composition with skarnoid textures in a proximal position similar to W skarns elsewhere (Chang et al. 2019; Štemprok and Blecha 2015; Ray 2013). The Globenstein skarn differs from this category and shows features of a more distal formation that is overprinted by late-stage W mineralization.

Skarns with Sn mineralization are associated with S- and A-type granites in post-collisional settings such as the UK, Malaysia, Australia, Canada, or China (Aleksandrov 2010; Brown et al. 1984; Chang et al. 2019; Chen et al. 1992; Einaudi et al. 1981; Jackson et al. 1989; Kwak 1983; 1987; Layne and Spooner 1991; Ray 2013). In such settings, skarn alteration primarily occurs as exoskarn, whereas greisen alteration is predominant in the endocontact (Einaudi et al. 1981; Aleksandrov 2010; Kwak and Askin 1981; Meinert 2005; Burisch et al 2025). In some skarn deposits such as Mt. Garnet, Lost River or JC Tin skarns, cassiterite is recognized to occur early during prograde alteration (Aleksandrov 2010; Brown et al. 1984; Layne and Spooner 1991). Conversely, in the Erzgebirge/Krušné hory cassiterite occurs invariably paragenetically late, typically intergrown with actinolite and chlorite. Only locally at the Hämmerlein deposit, some cassiterite appear to have formed during the prograde stage (Korges et al. 2020). A strong affiliation of cassiterite with the retrograde minerals seems to be typical of intermediate to distal Sn skarns globally (Einaudi et al. 1981; Kern et al. 2019; Kwak 1987; Meinert et al. 2005; Ray et al. 2000). The relatively pronounced Zn tenor in the Erzgebirge skarns is also documented for other intermediate to distal Sn skarns (Chang et al. 2019). In addition to Zn, some intermediate to distal skarns may be associated with significant Ag, Pb and/or Cu concentrations. The Erzgebirge skarns do not contain significant amounts of Ag and Pb, whereas some are associated with subeconomic Cu (e.g. Berggießhübel).

Conclusions

The Erzgebirge skarns range in composition from calcic to magnesian and form vertically discontinuous, yet laterally extensive alteration zones. Most skarns consist of skarnoid and metasomatic domains that are not related to the same magmatic-hydrothermal event. Instead, different skarn domains record a multi-stage formation history linked to distinct magmatic-hydrothermal episodes. Three age groups of skarns occur across the Erzgebirge/Krušné hory:

1. **Early late Variscan skarns (339–334 Ma)** formed in the aftermath of peak metamorphism in the region. These skarns suggest an early, unconstrained magmatic-hydrothermal activity with no clear relationship to Sn and W mineralization.

2. **Late Variscan skarns (328–312 Ma)** are associated with late-Variscan granitic magmatism. Most skarns of this stage exhibit skarnoid textures and calc-silicate compositions, typical of deep, proximal to intermediate, and rock-buffered formation environments. If not overprinted by a younger skarn event, stage II skarnoid skarns generally lack significant retrograde alteration and mineralization, with the exception of the Zobes skarn. However, some of the youngest skarns in this stage, formed around 313 Ma, exhibit metasomatic textures, occur in intermediate to distal positions relative to their source intrusions, and may be associated with retrograde alteration. Some of these skarns, such as Hämmerlein and Waschleithe, are linked to Sn ± Zn

mineralization. Skarns of this stage have a distinct temporal and often spatial relationship to large-volume late-Variscan plutons.

3. **Post-Variscan skarns (306–299 Ma)** are invariably characterized by metasomatic textures and calc-silicate compositions, indicating a shallow, intermediate to distal, and strongly fluid-buffered formation environment. These skarns typically exhibit intense retrograde alteration, which also overprints earlier skarn stages I and II where present. This retrograde stage is closely associated with significant Sn mineralization. Unlike stage II skarns, stage III skarns lack a clear spatial relationship to nearby intrusions and instead coincide with widespread post-Variscan volcanism, while only a few plutonic rocks of this age have been documented.

Limited U-Pb ages of skarn-hosted cassiterite from Ehrenfriedersdorf and Geyer show a bimodal distribution at 314–313 Ma and 305–303 Ma, suggesting that Sn mineralization is related to the late phase of late-Variscan and post-Variscan magmatism. However, the timing of Sn mineralization in the Aue-Schwarzenberg district and its relationship to multi-stage skarn formation remains poorly constrained.

Skarn-hosted, low-grade, high-tonnage resources in the Erzgebirge represent an underexplored source of Sn, W, In, and other critical elements within the European Union. Although scientific understanding of these systems has advanced significantly over the past decade, fundamental aspects remain unresolved. This contribution aims to assist future skarn researchers in navigating the often difficult-to-access literature and, hopefully, to inspire new interest in studying the skarns of the Erzgebirge/Krušné hory region.

Acknowledgements

Dr. Sebastian Staude is thanked for microprobe analyses. We are grateful to Roland Stopp and Andy Tauber to provide access to the underground mine of Ehrenfriedersdorf for sampling.

Funding

This contribution is funded as part of the German Research Foundation DFG priority program Dynamics of Ore Enrichment (DOME; SPP2238) via grant 3134023001. Electron microprobe analyses have partly funded by the German Research Foundation (DFG; grant INST 37/1026-1 FUGG).

Declarations Competing interests

The authors declare no competing interests. The authors have no relevant financial or non-financial interests to disclose.

Data availability statement

The authors declare that the data supporting the findings of this study are available within the paper, its supplementary information files, and within the publications in the references. Additional data on monographs (in german language) may be found under: https://publikationen.sachsen.de/bdb/artikel.

Bibliography

Alderton DHM (2018) Skarn garnets from south-west England. Geoscience in South-West England 14:91-97

Alderton DHM, Jackson NJ (1978) Discordant calc-silicate bodies from the St. Just aureole, Cornwall. Mineral Mag 42:427–434. https://doi.org/10.1180/minmag.1978.042.324.03

Aleksandrov SM (2010) Skarn-greisen deposits of the lost river and mount ear ore field, Seward Peninsula, Alaska, United States. Geochem Int 48:1220-1236.

Andersen JC, Stickland RJ, Rollinson GK, Shail RK (2016). Indium mineralisation in SW England: host parageneses and mineralogical relations. Ore Geol Rev 78:213-238.

Bauer ME, Seifert T, Burisch M, Krause J, Richter N, Gutzmer J (2019) Indium-bearing sulfdes from the Hämmerlein skarn deposit, Erzgebirge, Germany: evidence for late-stage difusion of indium into sphalerite. Miner Deposita 54:175–192.

Baumann L (1965) Zur Erzführung und regionalen Verbreitung des „Felsithorizontes“ von Halsbrücke. Freiberger Forschungshefte C 186:63–81.

Baumann L, Weinhold G (1963) Zum Neuaufschluss des sogenannten „Felsithorizontes“ von Halsbrücke. Zeitschrift für angewandte Geologie 9(7):338–345.

Baumann L, Kuschka E, Seifert T (2000) Lagerstätten des Erzgebirges. Enke im Georg Thieme Verlag, Stuttgart, New York

Beck R (1902) Über die Erzlager der Umgebung von Schwarzenberg im Erzgebirge. Jb. Berg- und Hüttenwesen im Königreich Sachsen, 1902:51–87.

Bolduan H (1963) Geologie und Genese der Zinn-Wolframlagerstätte Geyer (Erzgeb.). Freiberger Forsch-Hefte C 167:7–34.

Breiter K (2012) Nearly contemporaneous evolution of the A- and S-type fractionated granites in the Krušné hory/Erzgebirge Mts., Central Europe. Lithos 151:105–121.

Breiter K, Förster H-J, Seltmann R (1999) Variscan silicic magmatism and related tin-tungsten mineralization in the Erzgebirge-Slavkovský les metallogenic province. Miner Deposita 34:505–521. https:// doi. org/ 10. 1007/ s0012 60050 217

Breithaupt, A. (1849) Die Paragenesis der Mineralien: mineralogisch, geognostisch und chemisch beleuchtet, mit besonderer Rücksicht auf Bergbau. Freiberg, JG Engelhardt, 276 S.

Brosig A, Barth A, Knobloch A, Dickmayer E (2020) Rohstoffprognosen für Zinn, Wolfram, Fluss-und Schwerspat im Mittelerzgebirge. Bergbau in Sachsen, 19. Sächsisches Druck- und Verlagshaus GmbH, Dresden

Brown WM, Kwak TAP, Askins PW (1984) Geology and geochemistry of a F-Sn-W skarn system—The Hole 16 deposit, Mt Garnet, North Queensland, Australia. Journal of the Geological Society of Australia, 31(3):317-340. https://doi.org/10.1080/14400958408527934

Bubal J, Dolejš D (2013) Magnetite chemistry in skarns of the Bohemian Massif: evaluating competing effects of protolith inheritance, crystal chemistry, fluid composition and pressure-temperature conditions. - Proceedings 12th SGA Biennial Meeting 1:264-267.

Burisch M, Gerdes A, Meinert LD, Albert R, Seifert T, Gutzmer J (2019) The essence of time – fertile skarn formation in the Variscan orogenic belt. Earth Planet Sci Lett 519:165–170. https://doi.org/10.1016/j.epsl.2019.05.015

Burisch M, Frenzel M, Seibel H, Gruber A, Oelze M, Pfänder JA, Sanchez-Garrido C, Gutzmer J (2021) Li-Co–Ni-Mn-(REE) veins of the Western Erzgebirge, Germany—a potential source of battery raw materials. Miner Deposita 56:1223-1238.

Burisch M, Markl G, and Gutzmer J (2022) Breakup with benefits-hydrothermal mineral systems related to the disintegration of a supercontinent: Earth and Planetary Science Letters 580:117373.

Burisch M, Leopardi D, Guilcher M, Šešulka V, Dittrich T, Lehmann B (2025) Greisen-Hosted Lithium Resources of the Erzgebirge/Krušné Hory Province (Germany and Czech Republic). Economic Geology 2025; doi: https://doi.org/10.5382/econgeo.5136

Burisch M, Bussey SD, Landon N, Nasi C, Kakarieka A, Gerdes A, Albert R, Stein HJ, Gabites JA, Friedman RM (2023) Timing of magmatism and skarn formation at the Limon, Guajes, and Media Luna gold±copper skarn deposits at Morelos, Guerrero State, Mexico. Econ Geol 118:695-718.

Casas-García R, Rapprich V, Repstock A, Magna T, Schulz B, Kochergina YVE, Breitkreuz C (2021) Crustal vs. mantle contributions in the Erzgebirge/Krušne hory Mts. magmatism: Implications for generation of zoned, A-type silicic rocks in the late-Variscan Altenberg-Teplice Caldera, Central Europe. Lithos. https://doi.org/10.1016/j.lithos.2021.106429

Chang Z, Shu Q, Meinert LD (2019) Skarn deposits in China. In: Mineral deposits of China. 6: 189-234.

Chen J, Halls C, Stanley, CJ (1992) Tin-bearing skarns of South China: Geological setting and mineralogy. Ore Geol Rev 7(3):225-248.

Chen SC, Yu JJ, Bi MF, Lehmann B (2022) Tin-bearing minerals at the Furong tin deposit, South China: Implications for tin mineralization. Geochemistry, *82*(1):125856.

Chen SC, Yu JJ, Zhao XF, Bi MF, Lehmann B (2023) Various chlorite alteration styles in the Furong Sn deposit, South China: chlorite chemistry and implication for tin mineralization. Ore Geol Rev 105680

Cheng YB, Mao, JW, Chang ZS, Pirajno F (2013) The origin of the world class tin-polymetallic deposits in the Gejiu district, SW China: Constraints from metal zoning characteristics and 40Ar-39Ar geochronology: Ore Geol Rev 53:50–62.

Consolidated Tin Mines (2013) Mount Garnet Tin Project.

Collett S, Schulmann K, Štípská P, Míková J (2020) Chronological and geochemical constraints on the pre-variscan tectonic history of the Erzgebirge, Saxothuringian Zone. Gondwana Res 79:27-48.

Dipple GM, Gerdes ML, Lentz D (1998) Reaction-infiltration feedback and hydrodynamics at the skarn front. Mineralized intrusion-related skarn systems. Mineralogical Association of Canada Short Course 26:71-97.

Dobson, D. C. (1982). Geology and alteration of the Lost River tin-tungsten-fluorine deposit, Alaska. Econ Geol 77:1033-1052

Driesner T, Heinrich CA (2007) The system H_2O–NaCl. Part I: correlation formulae for phase relations in temperature–pressure–composition space from 0 to 1000°C, 0 to 5000 bar, and 0 to 1 XNaCl. Geochim Cosmochim Acta 71:4880–4901. https://doi.org/10.1016/j.gca.2006.01.033

Eadington PJ, Kinealy K (1983) Some aspects of the hydrothermal reactions of tin during skarn formation. J Geol Soc Aust 30:461-471.

Einaudi MT, Meinert LD, Newberry RJ (1981) Skarn deposits: Economic Geology, 75. Anniversary Volume 317-391.

Elongo V, Lecumberri-Sanchez P, Legros H, Falck H, Adlakha E, Roy-Garand A (2020) Paragenetic constraints on the Cantung, Mactung and Lened tungsten skarn deposits, Canada: Implications for grade distribution. Ore Geol Rev 125:103677.

Elsner H (2014) Zinn - Angebot und Nachfrage bis 2020, 2014th edn. DERA Rohstofnformationen, 20. DERA, Berlin

Finger F, Gerdes A, René M, Riegler G (2009) The Saxo-Danubian Granite Belt: magmatic response to post-collisional delamination of mantle lithosphere below the southwestern sector of the Bohemain Massif (Variscan orogen). Geol. Carpath 60:205-212.

Franke W, Żelaźniewicz A (2023) Variscan Evolution of the Bohemian Massif (Central Europe): fiction, facts and problems. Gondwana Res 124:351-377.

Förster H-J, Tischendorf G, Trumbull RB, Gottesmann B (1999) Late-collisional granites in the Variscan Erzgebirge, Germany. J Petrol 40:1613–1645. https://doi.org/10.1093/petroj/40.11.1613

Förster HJ, Romer RL, Gottesmann B, Tischendorf G, Rhede D (2009) Are the granites of the Aue-Schwarzenberg Zone (Erzgebirge, Germany) a major source for metalliferous ore deposits? A geochemical, Sr-Nd-Pb isotopic, and geochronological study. N Jb Mineral Abh 186:163–184

Förster, H.-J., and Romer, R. L., 2010, Carboniferous magmatism, in Linnemann, U., and Romer, R. L., eds., Pre-Mesozoic geology of Saxo-Thuringia: From the Cadomian active margin to the Variscan orogen: Stuttgart, Schweizerbart, p. 287-308

Gottesmann B, Seltmann R, Förster HJ (1995) Felsic subvolcanic intrusions within the Eibenstock granite pluton (Saxony, Germany): The Gottesberg volcano-plutonic system. In 2nd Symp. on Permocarboniferous Igneous Rocks.

Gottesmann, B., Förster, H. J., Müller, A., & Kämpf, H. (2017). The concealed granite massif of Eichigt− Schönbrunn (Vogtland, Germany): petrography, mineralogy, geochemistry and age of the Eichigt apical intrusion. Freiberg Online Geoscience, 49:1-46.

Groth, P. (1926). Zusammenvorkommen (Paragenesis) der Mineralien und Entwicklung der Lagerstättenkunde. Entwicklungsgeschichte der Mineralogischen Wissenschaften, 194-211.

Guilcher M, Albert R, Gerdes A, Gutzmer J, Burisch M (2021) Timing of native metal-arsenide (Ag-Bi-Co-Ni-As±U) veins in continental rift zones – In situ U-Pb geochronology of carbonates from the Erzgebirge/Krušné Hory province. Chem Geol 584:120476

Guilcher M, Gutzmer J, Hiller A, Krause J, Blamey N, Härtel B, Burisch M (2024) The Origin of Native Metal-Arsenide Mineralization in the World-Class Schlema-Alberoda Uranium Deposit (Germany): Insights from Arsenide Compositions and Fluid Inclusion Characteristics. Econ Geol 119(6):1329-1354.

He L, Liang T, Wang D, Zhang J, Liu B (2024) Skarn Formation and Zn–Cu Mineralization in the Dachang Sn Polymetallic Ore Field, Guangxi: Insights from Skarn Rock Assemblage and Geochemistry. Minerals 14:193

Heinrich CA (1990) The chemistry of hydrothermal tin(-tungsten) ore deposition. Econ Geol 85:457–481. https://doi.org/10.2113/gseco ngeo.85.3.457

Hiller A, Schuppan W (2008) Geologie und Uranbergbau im Revier Schlema-Alberoda. Bergbau in Sachsen, 14. Sächsisches Landesamt für Umwelt, Landwirtschaft und Geologie, Dresden.

Hiller A, Schuppan W (2016) Das Lagerstättengebiet Zobes-Bergen im Vogtland und benachbarte Uranvorkommen im Bereich des Bergener Granitmassivs. Bergbau in Sachsen, 18. Sächsisches Landesamt für Umwelt, Landwirtschaft und Geologie, Dresden.

Hoffmann U, Breitkreuz C, Breiter K, Sergeev S, Stanek K, Tichomirowa M (2013) Carboniferous–Permian volcanic evolution in Central Europe—U/Pb ages of volcanic rocks in Saxony (Germany) and northern Bohemia (Czech Republic). Int J Earth Sci 102:73-99

Hösel G (1967) Zur Genese der Skarne von Berggießhübel (Osterzgebirge). Report der VEB Geologische Erkundung Süd, Freiberg.

Hösel G (1994) Das Zinnerz-Lagerstättengebiet Ehrenfriedersdorf/ Erzgebirge. Bergbau in Sachsen, 1. Sächsisches Druck- und Verlagshaus GmbH, Dresden.

Hösel G (2003) Die polymetallische Skarnlagerstätte Pöhla-Globenstein. Bergbau in Sachsen, 8. Sächsisches Druck- und Verlagshaus GmbH, Dresden.

Hösel G, Fritsch E, Josiger U, Wolf P (1996) Das Lagerstättengebiet Geyer. Bergbau in Sachsen, 4. Sächsisches Druck- und Verlagshaus GmbH, Dresden.

Hösel G, Tischendorf G, Wasternack J (1997) Erläuterungen zur Karte'Mineralische Rohstoffe Erzgebirge-Vogtland/Krushé hory 1: 100 000, Karte 2: Metalle, Fluorit/Baryt-Verbreitung und Auswirkungen auf die Umwelt. Bergbau in Sachsen, 3. Sächsisches Druck- und Verlagshaus GmbH, Dresden.

von Hoerner T (1910). Über die Axinitvorkommnisse von Thum in Sachsen und die bedingungen der Axinitbildung überhaupt. Universitäts-buchdr. von G. Schade (O. Francke).

Hoth K, Lorenz W (1966) Die skarnhöffigen Horizonte des westlichen Erzgebirges (Geologische Fragen der Skarnprognose im Erzgebirge - Teil 1). Geologie: Zeitschrift für das Gesamtgebiet der Geologischen Wissenschaften 15 (7):769–799.

Hoth K., Krutsky N, Schilka W, Schellenberg F (2010) Marmore im Erzgebirge. Bergbau in Sachsen, 16. Sächsisches Landesamt für Umwelt, Landwirtschaft und Geologie, Dresden

Huang W, Liang H, Zhang J, Wu J, Chen X, Ren L (2019) Genesis of the Dachang Sn-polymetallic and Baoshan Cu ore deposits, and formation of a Cretaceous Sn-Cu ore belt from southwest China to western Myanmar. Ore Geol Rev 112:103030

Jamtveit B, Hervig RL (1994) Constraints on transport and kinetics in hydrothermal systems from zoned garnet crystals. Science 263:505–508. https://doi.org/10.1126/science.263.5146.505

Jackson NJ, Willis-Richards J, Manning DA, Sams MS (1989) Evolution of the Cornubian ore field, Southwest England; Part II, Mineral deposits and ore-forming processes. Economic Geology, 84(5):1101-1133.

Járóka T (2013) Mineralogische und geochemische Charakterisierung von Kassiterit-führenden Mineralisationen in metamorphen Gesteinen der ‘Felsitzone’ im Raum Großschirma, Lagerstättendistrikt Freiberg. Unpub. M.Sc. Thesis, Freiberg.

Jobst W, Grundig H (1961) Um Gottleuba, Berggießhübel und Liebstadt. Ergebnisse der heimatkundlichen Bestandsaufnahme im Gebiet von Gottleuba – 4:140 S., Berlin (Akademie-Verlag; Werte der deutschen Heimat).

Jonsson E, Högdahl K, Majka J, Lindeberg T (2013) Roquesite and associated indium-bearing sulfides from a Paleoproterozoic carbonate-hosted mineralization: Lindbom’s prospect, Bergslagen, Sweden. Canad Mineral 51:629-641.

Kern M, Kästner J, Tolosana-Delgado R, Jeske T, Gutzmer J (2019) The inherent link between ore formation and geometallurgy as documented by complex tin mineralization at the Hämmerlein deposit (Erzgebirge, Germany). Miner Deposita 54:683–698. https://doi.org/10.1007/s00126-018-0832-2

Kim E-J, Shin D, Shin S, Nam H-T, Park S (2015) Skarn zonation and rock physical properties of the Wondong Fe-Pb-Zn polymetallic deposit, Korea. Geosciences Journal 19:587-598

Korges M, Weis P, Lüders V, Laurent O (2020) Sequential evolution of Sn–Zn–In mineralization at the skarn-hosted Hämmerlein deposit, Erzgebirge, Germany, from fluid inclusions in ore and gangue minerals. Miner Deposita 55:937–952. https://doi.org/10.1007/ s00126-019-00905-4

Kormilicyn VS (1987) Über die Genese und die metallogenetische Bedeutung der Sulfid-Kassiterit-Vererzung des „Felsit-horizontes“ im Erzgebirge (DDR). Zeitschrift für geologische Wissenschaften 15(5):599-618.

Kroner U, Mansy J-L, Mazur S, Aleksandrowski P, Hann HP, Huckriede H, Lacquement F, Lamarche J, Ledru P, Pharaoh TC, Zedler H, Zeh A, Zulauf G (2008) Variscan tectonics. In: McCann T (ed) The Geology of Central Europe Volume 1: Precambrian and Palaeozoic. The Geological Society of London, London, 1:599–6.

Kröner A, Willner AP (1998) Time of formation and peak of Variscan HP-HT metamorphism of quartz-feldspar rocks in the central Erzgebirge, Saxony, Germany. Contrib Mineral Petrol 132:1–20. https://doi.org/10.1007/s004100050401

Kossmat F (1927) Gliederung des varistischen Gebirgsbaues. Abh Sächs Geol L.-A. 1: 39

Kühne R, Wasternack J, and Schulze H (1972) Fortschritte der Metallogenie im Erzgebirge: Postmagmatische Metasomatose im Endo-Exokontakt der jüngeren postkinematischen Granite des Erzgebirges: Geologie 21:494-520.

Kuschka, E., & Hahn, W. (1996). Flußspatlagerstätten des SW-Vogtlandes: Schönbrunn, Bösenbrunn, Wiedersberg. Bergbau in Sachsen, 2. Sächsisches Druck- und Verlagshaus GmbH, Dresden

Kwak, T A P (1983). The geology and geochemistry of the zoned, Sn-W-F-Be skarns at Mt. Lindsay, Tasmania, Australia. Econ Geol 78(7):1440-1465.

Kwak, T A P (1987) W-Sn skarn deposits and related metamorphic skarns and granitoids. Developments in Economic Geology, 24. Elsevier, Amsterdam, 451 pp.

Kwak T A P, Askins PW (1981) Geology and genesis of the F-Sn-W (-Be-Zn) skarn (wrigglite) at Moina, Tasmania. Econ Geo 76(2):439-467.

Layne GD, Spooner ETC (1991) The JC tin skarn deposit, southern Yukon Territory; I, Geology, paragenesis, and fluid inclusion microthermometry. Econ Geol 86(1):29–47.

Lefebvre MG, Romer RL, Glodny J, Kroner U, Roscher M (2019) The Hämmerlein skarn-hosted polymetallic deposit and the Eibenstock granite associated greisen, western Erzgebirge, Germany: two phases of mineralization—two Sn sources. Miner Deposita 54:193–216. https://doi.org/10.1007/s00126-018-0830-4

Legler C (1985) Die schichtgebundenen Mineralisationen des Erzgebirges. – Freiberger Forsch.-H., C 401, 93 S. Leipzig.

Legler C, Baumann L (1983) Bildungsmöglichkeiten kalksilikatischer Erzlagerstätten – ein Beitrag zur Skarnproblematik. – Z. geol. Wiss., 11: 1417-1442, Berlin.

Lehmann B (1990) Metallogeny of tin. Springer, p 211

Lehmann B (2021) Formation of tin ore deposits: a reassessment. Lithos 402-403:105756. https://doi.org/10.1016/j.lithos.2020.105756

Lehmann B, Seltmann R (1995): Der Übergangsbereich Pegmatit-/Aplit- in Hydrothermal-Systeme am Beispiel Ehrenfriedersdorf/Erzgebirge: Abschlußbericht zum DFG-Projekt Le 578/7-1 und Se 594/3-1

Leopardi D, Gerdes A, Albert R, Gutzmer J, Lehmann B, and Burisch M (2024a) LA-ICP-MS U-Pb cassiterite age data of the Sadisdorf deposit link Sn-Li-(W-Cu) mineralization in the eastern Erzgebirge to the collapse of the Altenberg-Teplice Caldera: Geochemistry, p. 126038.

Leopardi D, Gutzmer J, Lehmann B, Burisch M (2024b) The Spatial and Temporal Evolution of the Sadisdorf Li-Sn-(W-Cu) Magmatic-Hydrothermal Greisen and Vein System, Eastern Erzgebirge, Germany. Econ Geol 119(4):771-803.

Li YJ, Zhang RQ, Ji H, Wang C, Tan J, Wei JH (2022) Chemistry and U–Pb geochronology of cassiterite in the Xiasai deposit, central Yidun Terrane (SW China): Link between Sn and Ag–Pb–Zn mineralisation. Ore Geol Rev 149

Li Y, Liu Z, Shao Y, Liu L, Chen K, Zhao H, You S, He M (2024) Garnet geochronology, major and trace element geochemistry of the Huanggangliang Fe-Sn polymetallic deposit, NE China. Ore Geol Rev 106048.

Liu L, Zhou T, Zhang D, Liu G, Zhao Z, Sun J, White NC (2021) Major and trace elements analyses of garnet from the Haobugao Zn-Fe-Sn polymetallic deposit, northeast China: Implications for skarn formation and hydrothermal fluid evolution. Ore Geol Rev 138:104337

Lorenz W (1974) Die lithostratigraphische Entwicklung der Paragneis-Glimmerschiefer-folge des mittleren und westlichen Erzgebirges.-unveröff. Diss. Bergakademie Freiberg, 203S.

Lorenz W (1979) Lithostratigraphie, Lithologie und Lithofazies metamorpher Komplexe. Z. Geol. Wiss., 7(3):405-418

Lu HZ, Liu Y, Wang C, Xu Y, Li H (2003) Mineralization and fluid inclusion study of the Shizhuyuan W-Sn-Bi-Mo-F skarn deposit, Hunan Province, China. Econ Geol 98:955-974

Makarevic̑ W, Fritsch E, Velickin W, Kargatev W, Ivanov I, Serov B, Nasarov WG, Lohrmann H (1976) Über die Ergebnisse der geologischen Erkundungsarbeiten im Bereich der Lagerstätte Geyer einschließlich der Vorratsberechnung auf Zinn mit Stand vom 1. Juli 1976. Internal report, SDAG Wismut Chemnitz.

van Marcke de Lummen G (1986) Tin-bearing epidote from skarn in the Land's End aureole, Cornwall, England. The Canadian Mineralogist:411–415

Meinert LD (1992) Skarns and Skarn deposits. Geosci Can 19:145–162

Meinert LD (1997) Application of skarn deposit zonation models to mineral exploration. Exploration and mining geology *6:*185-208.

Meinert LD, Dipple GM, Nicolescu S (2005) World skarn deposits. In: Hedenquist JW, Thompson JFH, Goldfarb RJ, Richards JP (eds) One Hundredth Anniversary Volume. Society of Economic Geologists, pp 299–336

Meyer N, Markl G, Gerdes A, Gutzmer J, Burisch M (2024a) Timing and origin of skarn-, greisen-, and vein-hosted tin mineralization at Geyer, Erzgebirge (Germany). Miner Deposita 59:1-22. https://doi. org/10.1007/s00126-023-01194-8

Meyer N, Burisch M, Gutzmer J, Krause J, Scheibert H, Markl G (2024). Mineral chemistry of the Geyer SW tin skarn deposit: understanding variable fluid/rock ratios and metal fluxes. Miner Deposita, 1-27.

Moscati RJ, Neymark LA (2020) U–Pb geochronology of tin deposits associated with the Cornubian Batholith of southwest England: Direct dating of cassiterite by in situ LA-ICPMS. Miner Deposita, 55(1):1-20.

Mrozek SA, Chang Z, Spandler C, Windle S, Raraz C, Paz A (2020) Classifying skarns and quantifying metasomatism at the Antamina deposit, Peru: Insights from whole-rock geochemistry: Economic Geology, v. 115, p. 177-188.

Ni P, Pan JY, Han L, Cui JM, Gao Y, Fan MS, Li WS, Chi Z, Zhang KH, Cheng ZL, Liu YP. (2023) The tungsten and tin deposits in South China: temporal and spatial distribution, metallogenic models and prospecting directions. Ore Geol Rev 157:105453

Pälchen, W., Walter, H. (2008). Geologie von Sachsen. Schweizerbart, Stuttgart

Pauliš P, Haake R (1991) Die Mineralien der Skarnlagerstätte Měděnec (Kupferberg) im Erzgebirge (ČSFR). Mineralien Welt 5:19-29.

Pauliš P, Vrtiška L, Sejkora J, Malíková R, Hloušek J, Dvořák Z, Gramblička R, Pour O, Ludvík, J (2015) Supergene mineralization of the skarn tin deposit Zlatý Kopec in the Krušné hory Mts. (Czech Republic). Bulletin Mineralogie Petrologie, 23(2):182-200.

Pfeiffer L, Schützel H (1969) Skarnparagenesen des Erzgebirges. – Freiberger Forsch.-H., C 266: 65-75, Leipzig.

Pokorný L, Zemánek V (1960) Erkundung der blinden Magnetitlagerstätten in den Skarnen yon Krusné hory (Erzgebirge). Geotechnica, svazek 29, 7 — 72, Praha 1960 (mit Deutscher Zusammenfassung

Ray, G. E. (2013). Skarns of the Canadian Cordillera: British Columbia Ministry of Energy and Mines. British Columbia Geological Survey Paper, 11, 112.

Ray GE, Webster ICL, Ballantyne SB, Kilby CE, Cornelius SB (2000) The geochemistry of three tin-bearing skarns and their related plutonic rocks, Atlin, Northern British Columbia. Econ Geol 95(6):1349-1365.

Reinhardt N, Frenzel M, Meinert LD, Gutzmer J, Kürschner T, Burisch M (2021) Mineralogy and fluid characteristics of the Waschleithe Zn skarn – a distal part of the Schwarzenberg mineral system, Erzgebirge Germany. Ore Geol Rev 131:104007. https://doi.org/10.1016/j.oregeorev.2021.104007

Reinhardt N, Gerdes A, Beranoaguirre A, Frenzel M, Meinert LD, Gutzmer J, Burisch M (2022) Timing of magmatic-hydrothermal activity in the Variscan orogenic belt: LA-ICP-MS U–Pb geochronology of skarn-related garnet from the Schwarzenberg District, Erzgebirge. Miner Deposita 57:1071–1087. https://doi.org/10. 1007/s00126-021-01084-x

Romer RL, Kroner U (2016) Phanerozoic tin and tungsten mineralization—tectonic controls on the distribution of enriched protoliths and heat sources for crustal melting. Gondwana Res 31:60–95. https://doi.org/10.1016/j.gr.2015.11.002

Romer RL, Cuney M (2018) Phanerozoic uranium mineralization in Variscan Europe–more than 400 Ma of tectonic, supergene, and climate-controlled uranium redistribution. Ore Geol Rev 102:474-504.

Romer RL, Thomas R, Stein HJ, Rhede D (2007) Dating multiply overprinted Sn-mineralized granites—examples from the Erzgebirge, Germany. Miner Deposita 42:337–359. https://doi.org/10.1007/s00126-006-0114-2

Romer RL, Förster HJ, Štemprok M (2010) Age constraints for the late-Variscan magmatism in the Altenberg-Teplice Caldera (Eastern Erzgebirge/Krusne hory). Neues Jahrbuch fur Mineralogie-Abhandlungen, 187(3):289.

Romer RL, Förster HJ, Glodny J (2022) Role of fractional crystallization, fluid-melt separation, and alteration on the Li and B isotopic composition of a highly evolved composite granite pluton: The case of the Eibenstock granite, Erzgebirge, Germany. Lithos, 422:106722.

Sächsisches Oberbergamt (2008): Der Bergbau in Sachsen. Bericht des Sächsischen Oberbergamtes und des Landesamtes für Umwelt, Landwirtschaft und Geologie (Referat Rohstoffgeologie) für das Jahr 2007. Available online ahttps://www.oba.sachsen.de/download/JB2007.pdf

Saxony Minerals & Exploration AG. Projekt Pöhla. https://smeag.de/index.php/de/profil/das-projekt. Accessed 12.12.2024

Saxore Bergbau GmbH (2024) Tellerhäuser Projekt. https://www.saxorebergbau.com/projekte/projekt-rittersgruen/geologischer-ueberblick/. Accessed 16.12.2024.

Schmädicke E, Mezger K, Cosca MA, Okrusch M (1995) Variscan Sm-Nd and Ar-Ar ages of eclogite facies rocks from the Erzgebirge, Bohemian Massif. J Metamorph Geol 13:537–552. https://doi.org/10.1111/j.1525-1314.1995.tb00241.x

Schwarz-Schampera U, Herzig PM (2000) Indium: geology, mineralogy and economics. Springer-Verlag, Berlin

Schuppan W, Hiller A (2012) Die Komplexlagerstätten Tellerhäuser und Hämmerlein: Uranbergbau und Zinnerkundung in der Grube Pöhla der SDAG Wismut. Bergbau in Sachsen, 17. Sächsisches Landesamt für Umwelt, Landwirtschaft und Geologie, Dresden.

Seifert T, Sandmann D (2006) Mineralogy and geochemistry of indium-bearing polymetallic vein-type deposits: implications for host minerals from the Freiberg district, eastern Erzgebirge, Germany. Ore Geol Rev 28(1):1–31. https://doi.org/10.1016/j.oregeorev.2005.04. 005

Seymore DB, Green GR, Calver CR (2006) The geology and mineral deposits of Tasmania: A summary. Department of Infrastructure, Energy and Resources p 29

Shail RK, Leveridge BE (2009) The Rhenohercynian passive margin of SW England: Development, inversion and extensional reactivation. Compt Rendus Geosci 341:140–155. https://doi.org/10.1016/j.crte.2008.11.002.

Simons B, Andersen JCØ, Shail RK, Jenner FE (2017) Fractionation of Li, Be, Ga, Nb, Ta, In, Sn, Sb, W and Bi in the paraluminous Early Permian Variscan granites of the Cornubian Batholith: precursor processes to magmatic-hydrothermal mineralization. Lithos 278:491–512

Solomovich LI, Trifonov BA, Sabelnikov SE (2012) Geology and mineralization of the Uchkoshkon tin deposit associated with a breccia pipe, Eastern Kyrgyzstan. Ore Geol Rev 44:59-69

Soloviev SG, Kryazhev SG, Dvurechenskaya SS (2019) Genesis of the Maikhura tungsten-tin skarn deposit, Tajik Tien Shan: Insights from petrology, mineralogy, and fluid inclusion study. Ore Geol Rev 104:561-588

Starý J, Mašek D, Gabriel Z, Němec M, Hodková T, Novák J, Kavina P (2024) Mineral commodity summaries of the Czech Republic 2023. Statistical data to 2022. Czech Geological Survey. 2023 yearbook -1, Prag.

Štemprok, M., 1967, Genetische Probleme der Zinn-Wolfram-Vererzung im Erzgebirge: Mineralium Deposita, v. 2, p. 102-118.

Štemprok M (1995) A comparison of the Krušné Hory-Erzgebirge (Czech Republic–Germany) and Cornish (UK) granites and their related mineralizations. Proc Ussher Soc 8:347-356.

Štemprok M (2016) Drill hole CS-1 penetrating the Cínovec/Zinnwald granite cupola (Czech Republic): an A-type granite with important hydrothermal mineralization. J Geosci:395–423. https://doi.org/10.3190/jgeosci.226

Štemprok M, Seifert T (2011) An overview of the association between lamprophyric intrusions and rare-metal mineralization: Mineralogia 42:121-162.

Štemprok M, Blecha V (2015) Variscan Sn–W–Mo metallogeny in the gravity picture of the Krušné hory/Erzgebirge granite batholith (Central Europe): Ore Geol Rev 69: 285-300.

Stober I, Bucher K (2005) The upper continental crust, an aquifer and its fluid: hydaulic and chemical data from 4 km depth in fractured crystalline basement rocks at the KTB test site. Geofluids *5*(1):8-19.

Swinkels, L. J., Schulz-Isenbeck, J., Frenzel, M., Gutzmer, J., and Burisch, M., 2021, Spatial and Temporal Evolution of the Freiberg Epithermal Ag-Pb-Zn District, Germany: Economic Geology, v. 116, p. 1649-1667

Tichomirowa M (2003) Die Gneise des Erzgebirges - hochmetamorphe Äquivalente von neoproterozoisch-frühpaläozoischen Grauwacken und Granitoiden der Cadomiden. Diss. Bergakademie Freiberg.

Tichomirowa M, Leonhardt D, (2010) New age determinations (Pb/Pb zircon evaporation, Rb/Sr) on the granites from Aue-Schwarzenberg and Eibenstock, Western Erzgebirge, Germany. Z. Geol. Wiss. 38 (2–3), 4, 99–123.

Tichomirowa M, Sergeev S, Berger H-J, Leonhardt D (2012) Inferring protoliths of high-grade metamorphic gneisses of the Erzgebirge using zirconology, geochemistry and comparison with lower-grade rocks from Lusatia (Saxothuringia, Germany). Contrib Mineral Petrol 164:375–396. https://doi.org/10.1007/s00410-012-0742-8

Tichomirowa M, Käßner A, Sperner B, Lapp M, Leonhardt D, Linnemann U, Münker C, Ovtcharova M, Pfänder JA, Schaltegger U, Sergeev S, von Quadt A, Whitehouse M (2019) Dating multiply overprinted granites: the effect of protracted magmatism and fluid flow on dating systems (zircon U-Pb: SHRIMP/SIMS, LAICP-MS, CA-ID-TIMS; and Rb–Sr, Ar–Ar) – granites from the Western Erzgebirge (Bohemian Massif, Germany). Chem Geol 519:11–38. https://doi.org/10.1016/j.chemgeo.2019.04.024

Tichomirowa M, Käßner A, Repstock A, Weber S, Gerdes A, Whitehouse M (2022) New CA-ID-TIMS U–Pb zircon ages for the Altenberg–Teplice Volcanic Complex (ATVC) document discrete and coeval pulses of Variscan magmatic activity in the Eastern Erzgebirge (Eastern Variscan Belt): International Journal of Earth Sciences 111:1885-1908.

Tichomirowa M., Käßner A, Burisch M, Weber S, Lehmann U, Görz I (2025) Diachronous pulses of Variscan magmatic activity in the Eastern and Western Erzgebirge (Germany and Czech Republic), their temporal geochemical evolution, and their relation to ore formation. International Journal of Earth Sciences, 1-21.

Thomas R (1994) Fluid evolution in relation to the emplacement of the Variscan granites in the Erzgebirge region: a review of the melt and fluid inclusion evidence. Metallogeny of collisional orogens, 70-81.

Thomas R, Baumann L (1980) Ergebnisse von thermometrischen und kryometrischen Untersuchungen an Kassiteriten des Erzgebirges: Zeitschrift für geologische Wissenschaften, v. 8, p. 1281-1299.

Tolksdorf JF, Hemker C, Schubert M (2020) Bronzezeitlicher Zinnseifenbergbau bei Schellerhau im östlichen Erzgebirge, Sachsen. Der Anschnitt, 71, 223-233.

Ulrych J, Dostal J, Adamovič J, Jelínek E, Špaček P, Hegner E, Balogh K (2011) Recurrent Cenozoic volcanic activity in the Bohemian Massif (Czech Republic): Lithos, v. 123, p. 133-144.

Vossen V (2018) Geochemical and mineralogical characterisation of polymetallic skarn mineralization in the Berggießhübel mining district, Saxony, Germany. Qualification work, Supervision: Th. Seifert, T. Petermann, A. Barth / Beak Consultants GmbH.

Wang X, Zhou R, Belousova E, Dhnaram C, Zhao J, He X, Patias D, von Gnielinski F, Lisitsin V (2024) Mineralization processes of the Mount Garnet Zinc deposit, NE Queensland (Australia): Insights from garnet geochemistry and U-Pb geochronology. Ore Geol Rev 105962

Warr LN (2021) IMA–CNMNC approved mineral symbols. Mineralogical Magazine *85*(3):291-320.

Weber S, Legler C, Kallmeier E, Schulz B, Burisch M (2023) Metamorphic origin of stratiform cassiterite mineralization in the Schwarzenberg-Aue district–Clues to the metamorphic history and pre-orogenic Sn enrichment of the Erzgebirge (Germany). Lithos, 454:107273.

Weinhold G (2002) Die Zinnerz-Lagerstätte Altenberg/Osterzgebirge. Bergbau in Sachsen, 9. Sächsisches Landesamt für Umwelt, Landwirtschaft und Geologie, Dresden.

Yuan J, Hou Q, Yang Z, Jiang H, Hu Z, Yu T (2018) Distribution and mobilization of Sn in silicate minerals from the Mesozoic Shizhuyuan W-dominated polymetallic deposit, South China. Ore Geol Rev, 101:595-608.

Zhao KD, Jiang SY (2007) Rare earth element and yttrium analyses of sulfides from the Dachang Sn-polymetallic ore field, Guangxi Province, China: Implication for ore genesis. Geochemica Journal 41:121-134

Zhao L, Zhang Y, Shao Y, Li H, Shah SA, Zhou W (2021) Using garnet geochemistry discriminating different skarn mineralization systems: Perspective from Huangshaping W-Mo-Sn-Cu polymetallic deposit, South China. Ore Geol Rev 138:104412

Zhou J, Feng C, Li D (2017) Geochemistry of the garnets in the Baiganhu W–Sn orefield, NW China. Ore Geol Rev 82:70–92

Ziegler PA (1990) Geological Atlas of Western and Central Europe: Den Haag, Netherlands, Shell Internat. Petroleum Maatschappij.

Ziegler PA, Dèzes P (2007) Cenozoic uplift of Variscan Massifs in the Alpine foreland: Timing and controlling mechanisms: Global and Planetary change, v. 58, p. 237-269.